Joana Bicker de Melo Alves Aparício

A Screening Strategy for Evaluation of Drug Transport across the Blood-Brain Barrier: Application to Catechol-*O*-methyltransferase Inhibitors, Dopamine β-hydroxylase Inhibitors and Dibenz[b,f]azepine-5-carboxamide Derivatives

Tese de Doutoramento em Ciências Farmacêuticas, ramo de Farmacologia e Farmacoterapia,
orientada pelo Professor Doutor Amílcar Celta Falcão Ramos Ferreira e pelo Professor Doutor Gilberto Lourenço Alves,
apresentada à Faculdade de Farmácia da Universidade de Coimbra.

Julho 2017

· U C ·

Universidade de Coimbra

Joana Bicker de Melo Alves Aparício

A Screening Strategy for Evaluation of Drug Transport across the Blood-Brain Barrier: Application to Catechol-*O*-methyltransferase Inhibitors, Dopamine β-hydroxylase Inhibitors and Dibenz[b,f]azepine-5-carboxamide Derivatives

Tese de Doutoramento em Ciências Farmacêuticas, ramo de Farmacologia e Farmacoterapia, orientada pelo Professor Doutor Amílcar Celta Falcão Ramos Ferreira e pelo Professor Doutor Gilberto Lourenço Alves, apresentada à Faculdade de Farmácia da Universidade de Coimbra.

Julho 2017

• U C •

FFUC FACULDADE DE FARMÁCIA
UNIVERSIDADE DE COIMBRA

The research work presented in this thesis was executed at the Laboratory of Pharmacology, Faculty of Pharmacy, University of Coimbra, under the supervision of Professor Amílcar Celta Falcão Ramos Ferreira and Professor Gilberto Lourenço Alves.

O trabalho de investigação apresentado nesta tese foi executado no Laboratório de Farmacologia da Faculdade de Farmácia da Universidade de Coimbra, sob a orientação do Professor Doutor Amílcar Celta Falcão Ramos Ferreira e do Professor Doutor Gilberto Lourenço Alves.

• U C •

FFUC FACULDADE DE FARMÁCIA
UNIVERSIDADE DE COIMBRA

CNC
CENTER FOR NEUROSCIENCE AND CELL BIOLOGY
UNIVERSITY OF COIMBRA, PORTUGAL

CICS-UBI
Centro de Investigação em Ciências da Saúde
Health Sciences Research Centre

The work underlying the present thesis was supported by Fundação para a Ciência e a Tecnologia, Portugal (SFRH/BD/78256/2011) through the POPH (Programa Operacional Potencial Humano) which is co-funded by FSE (Fundo Social Europeu), European Union, and by BIAL – Portela & Cª S.A., Portugal.

O trabalho subjacente à presente tese teve o apoio da Fundação para a Ciência e a Tecnologia, Portugal (SFRH/BD/78256/2011) através do Programa Operacional Potencial Humano (POPH) co-financiado pelo Fundo Social Europeu (FSE), União Europeia, e dos Laboratórios BIAL – Portela & Cª S.A., Portugal.

À minha mãe e à minha avó

Maria João e Maria de Fátima

AGRADECIMENTOS

Ao Professor Amílcar Falcão, meu orientador,

Gostaria de agradecer o convite que me fez para realização deste Doutoramento e pela oportunidade que me proporcionou de aprender mais e aprofundar a minha experiência em investigação científica. Agradeço ainda ter-me apontado a direcção em que deveria seguir quando estive incerta do rumo a dar ao trabalho mas, ao mesmo tempo, ter-me dado liberdade e autonomia para aprender a navegar. Por último, agradeço a confiança que depositou em mim e à qual espero corresponder.

Ao Professor Gilberto Alves, meu co-orientador,

Gostaria de agradecer o seu contributo para a execução deste trabalho, incluindo a partilha de conhecimentos e as sugestões importantes e construtivas que me foi dando durante este percurso. Agradeço também a sua disponibilidade, simpatia e todo o encorajamento que me permitiu chegar ao fim.

À Ana Fortuna,

Agradeço a disponibilidade que demonstrou para ir discutindo o trabalho ao longo da sua realização, e também o incentivo e a cooperação para que este se concretizasse, sacrificando parte do seu tempo profissional e pessoal.

Ao Professor Doutor Patrício Soares-da-Silva,

Director do Departamento de Investigação e Desenvolvimento dos Laboratórios BIAL, agradeço o apoio disponibilizado para a realização deste trabalho, o *feedback* que foi transmitindo e a possibilidade de poder trabalhar em colaboração com os Laboratórios BIAL.

Aos Laboratórios BIAL

Agradeço a cedência dos compostos em estudo para realização deste trabalho de investigação.

À Fundação para a Ciência e a Tecnologia,

Pela atribuição de uma Bolsa de Doutoramento que tornou exequível este trabalho.

À Ana Serralheiro, Joana Almeida e Sousa e Daniela Gonçalves,

"Queres ir rápido, vai sozinho. Queres ir longe, vai acompanhado". Vocês foram e serão sempre para mim, um exemplo a seguir, a todos os níveis; de profissionalismo, por procurarem trabalhar muito, mas também trabalhar bem; de companheirismo, por me terem tratado como igual, nunca terem menosprezado as minhas dúvidas e me terem transmitido tanto conhecimento, mesmo atrasando o vosso próprio trabalho; e de resiliência, pela atitude de coragem com que vos vi encarar e ultrapassar momentos muito difíceis das vossas vidas. Com vocês, cresci e aprendi muito. Obrigada pelas alegrias e tristezas que partilhámos e pela vossa amizade que me susteve diariamente. Espero que esta se prolongue durante muitos anos e que continuemos a estar presentes nas vidas umas das outras.

Aos outros colegas de investigação,

A todos os elementos do Nanolab, Filipa, Dulce, Sandra e Edna, agradeço a grande ajuda ao longo desta jornada, os conselhos que me deram e os convívios divertidos. Aos meus colegas de curso, de doutoramento e amigos, Marisa, Marlene e João, agradeço o vosso apoio, a enorme paciência com que me escutaram e o incentivo que foram dando em todas as etapas. Agradeço também à Carla e à Susana por me mostrarem que isto era possível, pela ajuda e por procurarem estar sempre presentes nas alturas especiais. E por último mas não menos importantes, agradeço à Raquel Pinho, à Ana Cláudia, à Joana Sequeira, à Célia, à Mariana, à Margarida e a outros elementos da Tecnologia Farmacêutica, o auxílio que me prestaram, a boa disposição e o carinho que me permitiram terminar este capítulo da minha vida.

À Sandra Barreto,

Pelo conhecimento que me transmitiu, sem o qual não teria sido possível realizar uma parte muito importante da minha tese. Agradeço também a amizade, os risos e os bons momentos que passámos juntas na sala de cultura de células.

Aos assistentes técnicos,

Um agradecimento muito especial à dona Gina por arranjar sempre tempo no seu trabalho para me ajudar quando precisei, mesmo não tendo qualquer obrigação de o fazer. Um agradecimento também ao senhor Pedro pela colaboração durante o trabalho experimental com os animais.

À minha mãe e à minha avó

A vocês, devo-vos tudo. Sem o vosso amor incondicional não teria sido capaz de percorrer o árduo caminho que me trouxe até aqui. Obrigada por darem significado a tudo o que de bom acontece na minha vida e por tentarem sempre proteger-me de todas as adversidades. Por me alimentarem o corpo e a alma, e por me ouvirem com atenção. Pela paciência, generosidade e ternura intermináveis. Por serem o meu porto de abrigo, por me darem força mesmo quando não têm, e por reconstruirem o que sobrou de mim no fim. Este trabalho é tão meu quanto vosso.

It's like in the great stories, Mr Frodo. (…) Those were the stories that stayed with you. That meant something, even if you were too small to understand why. But I think, Mr Frodo, I do understand. I know now. Folk in those stories had lots of chances of turning back, only they didn't. They kept going, because they were holding on to something."

J.R.R. TOLKIEN, THE LORD OF THE RINGS: THE TWO TOWERS

TABLE OF CONTENTS

INDEX OF FIGURES AND TABLES

FIGURES

TABLES

Appendix C

ABBREVIATIONS

A

AADC	Aromatic aminoacid decarboxylase
ABC	Adenosine triphosphate-binding cassette
ADME	Absorption, distribution, metabolism and excretion
AED	Antiepileptic drug
AJs	Adherens junctions
AMT	Adsorptive-mediated transcytosis
ANOVA	Analysis of variance
AP	Alkaline phosphatase
AP-BL	Apical to basolateral
AQP-1	Aquaporin-1
AQP-4	Aquaporin-4
ATP	Adenosine triphosphate
AUC	Area under the concentration-time curve
AUC_{extrap}	Extrapolated area under the concentration-time curve
$AUC_{0\text{-}inf}$	Area under the concentration-time curve from time zero to infinite
$AUC_{0\text{-}t}$	Area under the concentration-time curve from time zero to the last measurable concentration

B

BBB	Blood-brain barrier
BCRP	Breast cancer resistance protein
BCSFB	Blood-cerebrospinal fluid barrier
BHT	Butylated hydroxytoluene
BL-AP	Basolateral to apical

C

Caco-2	Human epithelial colorectal adenocarcinoma cell line
cAMP	3’,5’-Cyclic adenosine monophosphate
CEC	Cerebral endothelial cells
C_{last}	Last observed concentration

C_{max}	Maximum concentration
CNS	Central nervous system
COMT	Catechol-*O*-methyltransferase
CPT-cAMP	8-(4-Chlorophenylthio)-cAMP
CSF	Cerebrospinal fluid
CYP	Cytochrome P450

D

DAC	Dibenz[b,f]azepine-5-carboxamide
DAD	Diode-array detector
DBH	Dopamine β-hydroxylase
DDI	Drug-drug interaction
DMEM	Dulbecco's modified Eagle's medium
DMSO	Dimethyl sulfoxide
DOPAC	3,4-Dihydroxyphenylacetic acid

E

EMA	European Medicines Agency
ER	Efflux ratio

F

FBS	Fetal bovine serum
FDA	Food and Drug Administration
FITC	Fluorescein isothiocyanate
$f_{u,brain}$	Unbound drug fraction in the brain
$f_{u,brain,corrected}$	Unbound drug fraction in the brain corrected for pH partitioning
$f_{u,plasma}$	Unbound drug fraction in plasma

G

GFAP	Glial fibrillary acidic protein

H

HBSS	Hank's balanced salt solution
HPLC	High-performance liquid chromatography
HTS	High-throughput screening
HUVEC	Human umbilical vein endothelial cells

HVA	Homovanillic acid

I

ILAE	International League Against Epilepsy
iPSC	Induced pluripotent stem cells
ISF	Interstitial fluid
ITC	International Transporter Consortium

K

K_{el}	Apparent elimination rate constant
K_p	Ratio of total brain-to-plasma concentrations
$K_{p,uu}$	Ratio of unbound brain-to-plasma concentrations
$K_{p,uu,cell,pred}$	Predicted unbound drug intracellular-to-extracellular partitioning coefficient
$K_{p,uu,cyto,pred}$	Predicted unbound cytosolic-to-extracellular drug concentration ratio
$K_{p,uu,lyso,pred}$	Predicted lysosomic-to-cytosolic unbound drug concentration ratio

L

LAT1	L-type aminoacid transporter 1
LC/MS	Liquid chromatography/mass spectrometry
Log BB	Logarithm of the ratio of total brain-to-plasma concentrations
Log D	Octanol-water distribution coefficient
Log P	Octanol-water partition coefficient

M

MB-COMT	Membrane-bound catechol-*O*-methyltransferase
MDCK	Madin-Darby canine kidney cells
MRP	Multidrug resistance-associated protein
MRT	Mean residence time
MTT	3-(4,5-Dimethylthiazol-2-yl)-2,5-diphenyltetrazolium bromide

N

Na-F	Sodium fluorescein
NAT	N-acetyltransferase

O

OAPs	Orthogonal arrays of particles
OAT	Organic anion transporter
OCT	Organic cation transporter

P

PAMPA	Parallel artificial membrane permeability assay
Papp	Apparent permeability coefficient
PBL	Porcine brain lipid
PBS	Phosphate buffer saline
PD	Parkinson's disease
Pe	Effective permeability
PEG	Polyethylene glycol
PEPT2	Proton-coupled oligopeptide transporter
P-gp	P-glycoprotein
PML	pIon membrane lipid
POC	Proof of concept
POP	Proof of principle
PS	Permeability surface area product

R

R&D	Research and development
RMT	Receptor-mediated transcytosis

S

SAM	S-adenosyl-L-methionine
S-COMT	Soluble catechol-*O*-methyltransferase
SD	Standard deviation
SLC	Solute-carrier

T

$t_{1/2el}$	Apparent terminal elimination half-life
TEER	Transepithelial electrical resistance
TJs	Tight junctions
t_{last}	Time of the last observed concentration

t_{max}	Time to reach the maximum concentration
TPSA	Topological polar surface area

U

UWL	Unstirred water layer

V

VB-Caco-2	Vinblastine-treated Caco-2
$V_{u,brain}$	Volume of distribution of unbound drug in brain
$V_{u,brain,pred}$	Predicted volume of distribution of unbound drug in the brain

Z

ZO	Zonula-occludens

PUBLICATIONS

BICKER J. ET AL., Liquid chromatographic methods for the quantification of catecholamines and their metabolites in several biological samples - A review, Anal. Chim. Acta. 768 (2013) 12-34.

BICKER, J. ET AL., Blood-brain barrier models and their relevance for a successful development of CNS drug delivery systems: A review, Eur. J. Pharm. Biopharm. 87 (2014) 409–432.

BICKER, J. ET AL., A new PAMPA model using an *in-house* brain lipid extract for screening the blood–brain barrier permeability of drug candidates, Int. J. Pharm. 501 (2016) 102-111.

BICKER, J. ET AL., Elucidation of the impact of P-glycoprotein and Breast Cancer Resistance Protein on the brain distribution of catechol-*O*-methyltransferase inhibitors. (*Submitted*)

BICKER, J. ET AL., Assessment of the interactions of dopamine β-hydroxylase inhibitors with human P-glycoprotein and Breast Cancer Resistance Protein. (*In preparation*)

ABSTRACT

Despite the increasing incidence of central nervous system (CNS) diseases worldwide, there are several unmet clinical needs and a generalized failure in the discovery and development of innovative drugs to treat them. Indeed, the difficulty is such that several pharmaceutical companies are decreasing the investment made in this therapeutic area or even retreating completely from the field, in spite of the commercial opportunities that exist. This may aggravate and delay the development of much needed CNS drugs for the patients. Among the reasons for the lack of success are inconclusive pharmacokinetic data, due to misconceptions in the parameters used to describe and orientate brain penetration, as well as, insufficient exposure of the CNS to potential drugs because of the blood-brain barrier (BBB). Consequently, understanding the mechanisms that guide a compound into and out of the CNS is essential to improve CNS disease treatment and invert current trends. This evaluation also extends to peripherally-active drugs in order to reduce unwanted and potentially adverse CNS effects.

The rate, extent and intra-brain distribution are fundamental concepts to evaluate and select compounds during drug discovery and development programs. Given that the BBB is a highly complex and dynamic structure, it is not yet possible to completely recreate all of its features in a single laboratory model. Thus, to overcome this obstacle, it was decided that associating distinct models that encompass individual aspects of CNS penetration and combining the obtained data, would be a feasible approach.

The general purpose of the present thesis was to implement a screening strategy to characterize the passage of compounds across the BBB. This implied the optimization and validation of several experimental methods, including the parallel artificial membrane permeability assay (PAMPA), cell-based assays and *in vivo* studies.

The project began with the establishment of a PAMPA-BBB model using an *in-house* brain lipid extract. This method was applied to a set of test compounds, composed by catechol-*O*-methyltransferase inhibitors (BIA 9-1059, BIA 9-1079, entacapone, nebicapone, opicapone, tolcapone), dopamine β-hydroxylase inhibitors (etamicastat, nepicastat, zamicastat) and dibenz[b,f]azepine-5-carboxamide derivatives (eslicarbazepine acetate, *S*-licarbazepine). It demonstrated discriminatory capacity

between less and more permeable BBB compounds, as well as, physicochemical selectivity. In the subsequent stage of work, priority was given to catechol-*O*-methyltransferase and dopamine β-hydroxylase inhibitors.

Cell-based assays were performed to identify P-glycoprotein (P-gp) and breast cancer resistance protein (BCRP) inhibitors and/or substrates, since P-gp and BCRP are the two main efflux transporters of the BBB. Intracellular accumulation assays enabled the detection of concentration-dependent P-gp inhibitors (zamicastat) or BCRP inhibitors (BIA 9-1079, nebicapone, tolcapone, etamicastat, nepicastat, zamicastat). In bidirectional transport assays, three P-gp substrates (BIA 9-1079, etamicastat, nepicastat) and five BCRP substrates (BIA 9-1059, entacapone, nebicapone, opicapone, etamicastat) were identified. This required the previous validation of high performance liquid chromatography (HPLC) techniques for compound quantification.

Lastly, the extent of BBB penetration, given by the unbound ratio of brain-to-plasma concentrations ($K_{p,uu}$), was estimated during *in vivo* studies with Wistar rats for the catechol-*O*-methyltransferase inhibitors, BIA 9-1079 and tolcapone, applying validated HPLC techniques in plasma and brain homogenate. In order to determine the unbound fractions of BIA 9-1079 and tolcapone in plasma and brain homogenate, an ultrafiltration assay was applied. Intra-brain distribution was evaluated through the volume of distribution of unbound drug in the brain and the unbound drug intracellular-to-extracellular partitioning coefficient. $K_{p,uu}$ was below unity for both compounds, revealing a limited extent of brain penetration, particularly for BIA 9-1079, and the occurrence of efflux. This was confirmed through a significant increase of brain concentrations following the co-administration of a P-gp and BCRP inhibitor, elacridar.

Considering the obtained data, it can be concluded that the implemented strategy provides reliable information on the access of compounds to the CNS and that it can be applied in the future for the assessment of centrally-active compounds or other molecules intended for peripheral targets.

Keywords: Blood-brain barrier, bioanalysis, catechol-*O*-methyltransferase inhibitors, central nervous system, dibenz[b,f]azepine-5-carboxamide derivatives, dopamine β-hydroxylase inhibitors, pharmacokinetics.

RESUMO

Apesar do aumento da incidência de patologias do sistema nervoso central (SNC) a nível mundial, existem ainda várias necessidades terapêuticas a colmatar, bem como, uma falha generalizada na descoberta e desenvolvimento de fármacos inovadores para o tratamento dessas mesmas doenças. De facto, a dificuldade é tal que várias empresas do setor farmacêutico estão a diminuir ou a evitar por completo o investimento nesta área terapêutica, apesar das oportunidades comerciais existentes. Por sua vez, isso poderá contribuir para o agravamento e atraso do desenvolvimento de fármacos para o SNC. Entre os motivos para a falta de sucesso incluem-se dados farmacocinéticos inconclusivos, devido a uma interpretação errónea dos parâmetros utilizados para descrever a passagem para o cérebro, e a exposição insuficiente do SNC a potenciais fármacos, atribuída à presença da barreira hematoencefálica (BHE). Consequentemente, a compreensão dos mecanismos que definem o transporte de um composto para o SNC é essencial para melhorar o tratamento de doenças cerebrais e reverter as atuais tendências. Esta avaliação também se estende a fármacos de ação periférica, de forma a minimizar efeitos centrais indesejados e potencialmente adversos.

A velocidade, a extensão e a distribuição intra-cerebral são conceitos fundamentais para avaliar e selecionar compostos durante o processo de descoberta e desenvolvimento. Dado que a BHE é uma estrutura altamente complexa, não é ainda possível mimetizar todas as suas vertentes num só modelo laboratorial. Assim, considerou-se que a melhor abordagem seria associar modelos distintos que contemplam aspetos diferenciados da entrada no SNC e combinar a informação obtida.

O objetivo global da presente tese consistiu em implementar uma estratégia de *screening* para caraterizar a passagem dos fármacos através da BHE. Isso implicou a otimização e validação de vários métodos experimentais, incluindo o ensaio de permeabilidade em membranas artificiais paralelas (PAMPA), ensaios celulares e estudos *in vivo*. O projeto teve início com um modelo de PAMPA, utilizando um extrato lipídico de cérebro obtido *in-house*. Este método foi aplicado a um conjunto de compostos teste, constituído por inibidores da catecol-*O*-metiltransferase (BIA 9-1059, BIA 9-1079, entacapone, nebicapone, opicapone, tolcapone), inibidores da dopamina β-hidroxilase (etamicastat, nepicastat, zamicastat) e derivados dibenz[b,f]azepina-5-

carboxamida (acetato de eslicarbazepina, *S*-licarbazepina), tendo demonstrado capacidade discriminatória entre compostos menos e mais permeáveis através da BHE, assim como, seletividade físico-química. Na etapa seguinte do trabalho, foi dada prioridade a inibidores da catecol-*O*-metiltransferase e inibidores da dopamina β-hidroxilase.

A realização de ensaios celulares permitiu identificar inibidores e/ou substratos de glicoproteína-P (P-gp) ou de *breast cancer resistance protein* (BCRP), considerados os principais transportadores de efluxo da BHE. Em ensaios de acumulação intracelular foi possível detetar inhibidores concentração-dependentes de P-gp (zamicastat) ou BCRP (BIA 9-1079, nebicapone, tolcapone, etamicastat, nepicastat, zamicastat), enquanto em ensaios de transporte bidirecional foram identificados três substratos de P-gp (BIA 9-1079, etamicastat, nepicastat) e cinco substratos de BCRP (BIA 9-1059, entacapone, nebicapone, opicapone, etamicastat). Para poder proceder à quantificação, efectuou-se uma validação de técnicas de cromatografia líquida de elevada eficiência (HPLC).

A extensão de passagem através da BHE, dada pelo rácio de concentrações livres cérebro-plasma ($K_{p,uu}$), foi estimada durante estudos *in vivo* com ratos Wistar para dois inibidores da catecol-*O*-metiltransferase, BIA 9-1079 e tolcapone. Após a validação de técnicas de HPLC para a sua quantificação em plasma e cérebro, foi efetuado o ensaio de ultrafiltração para determinar as frações livres nessas mesmas matrizes biológicas. A distribuição intra-cerebral foi avaliada através do volume de distribuição de fármaco livre no cérebro e do coeficiente de partição intracelular-extracelular de fármaco livre. O valor de $K_{p,uu}$ foi inferior à unidade para ambos os compostos, revelando uma exposição cerebral limitada, em especial para o BIA 9-1079. A ocorrência de efluxo foi confirmada após co-administração de um inibidor de P-gp e BCRP, elacridar, o qual levou a um aumento significativo das concentrações cerebrais dos dois compostos.

Considerando os resultados obtidos, conclui-se que a estratégia implementada fornece informação fiável sobre o acesso dos compostos ao SNC e que poderá ser futuramente aplicada para a avaliação de compostos de ação central ou periférica.

Palavras-chave: Barreira hematoencefálica, bioanálise, derivados dibenz[b,f]azepina-5-carboxamida, farmacocinética, inibidores da catecol-*O*-metiltransferase, inibidores da dopamina β-hidroxilase, sistema nervoso central.

CHAPTER I

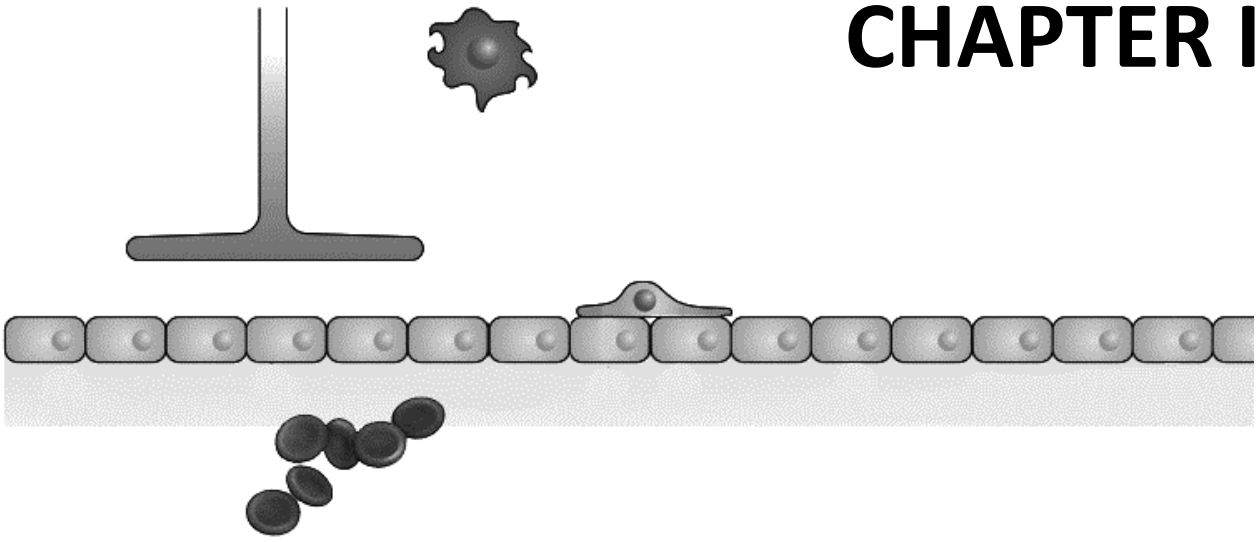

GENERAL INTRODUCTION

CHAPTER I. GENERAL INTRODUCTION

I.1. DRUG DISCOVERY AND DEVELOPMENT: STATE OF THE ART

Drug discovery programmes are initiated when there is a disease or clinical condition without a suitable and available medicinal product [1]. In the last years, pharmaceutical industries have been confronted with raising costs of research and development (R&D), high attrition rates and lack of first-in-class drugs. Despite the scientific discoveries and technological progresses such as modern molecular biology methods, structure-based drug design, high-throughput screening (HTS), combinatorial chemistry and the sequencing of the human genome, there has been no correspondence between the investment made in R&D and the number of new drugs that were effectively introduced in the market [2,3]. Consequently, without a dramatic increase in R&D productivity, the pharmaceutical industry may not be able to sustain sufficient innovation to replace the loss of revenues due to patent expirations by successful products [4]. These findings have forced pharmaceutical companies to re-think the conventional process of drug discovery and development.

Attrition and lack of innovation have been attributed, in part, to a poor and possibly biased target-selection at the start of the drug discovery process [5]. Since the beginning of the genomic era in the 80s, drug discovery has been focused on drug targets, usually proteins, with an important role in pathogenesis [2]. This hypothesis-based, rational and systematic method is called target-based approach and will be subsequently described in greater detail, as well as, the re-emerging alternative: phenotypic screening (Figure I.1).

In target-based drug discovery, the process starts with the identification and validation of the target, aiming to establish a link between a biological target and a human disease state [6]. The most important requirement for a target is to be *druggable*, i.e. accessible to a drug molecule, which, upon binding, will cause a measurable biological response [1]. Then, after the target has been selected and validated, HTS assays are developed and performed to allow the search for active and selective compounds. During HTS, compound libraries mainly generated by combinatorial chemistry are exposed to the purified target, in order to identify the molecules that engage the target and modulate the disease pathway - the initial actives

or *hits* [7]. *Hits* can be identified through various screening strategies but HTS has been the most frequently used approach, once it enables the analysis of millions of molecules in a fast, miniaturized and automatized format [1,8].

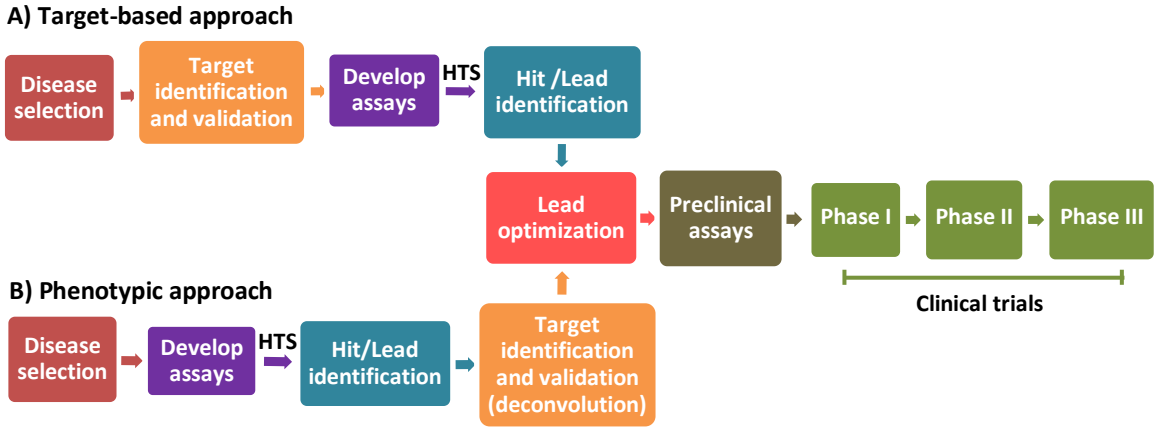

Figure I.1. Target-based (A) and phenotypic-based (B) drug discovery and development process. Post-marketing phase (Phase IV) is not depicted. HTS, high-throughput screening. Adapted from [9,10]

There is an on-going debate about the use of HTS for the identification of *hits* and *leads* in the pharmaceutical industry. Some authors blame the attrition rates and general lack of productivity on the limited success rate (45 - 55%) of the HTS methodologies, claiming that HTS assays fail to find *hits* for some targets or provide excessively lipophilic *hits* that cannot be turned into leads and subsequently to candidates. The composition and size of compound libraries is also pointed as a cause of failure of HTS in delivering high quality *hits* [11]. However, other authors do not share this point-of-view and state that the data generated by HTS have better quality and are more controlled than the data generated by low throughput assays. Indeed, most pharmaceutical companies regularly invest in the maintenance and improvement of compound libraries, by removing compounds with less *drug-like* or *lead-like* physicochemical properties. Hence, HTS remains an integral part of pharmaceutical research and is still often used for *hit* identification [12].

Typically, a large collection of *hits* is obtained and the most promising molecules are identified in the process of lead discovery and optimization [7]. The first step is to narrow down the number of *hits* and organize them into series, composed of

structurally-related compounds with the desired biological activity [6]. This reduction is achieved by submitting *hits* to a rigorous assessment of chemical integrity, synthetic accessibility, structure-activity relationships, toxicity, and absorption, distribution, metabolism and excretion (ADME) properties [8]. Converting *hits* into *leads* involves refining *hit* series to produce more potent and selective compounds with adequate pharmacokinetic properties [1].

At this stage, it also becomes essential to eliminate compounds likely to fail in clinical trials as early as possible, remembering to *"fail fast and cheap"* [13] because once a candidate reaches clinical stages, it becomes increasingly difficult to abort the project and public knowledge of this termination can contribute to a negative perception of the involved company [1]. Therefore, lead series with a superior profile in terms of selectivity, solubility, permeation and metabolic stability, i.e. with a better development potential, are prioritized [8]. Nonetheless, when the compounds are considered ready to advance for preclinical stages, the drug discovery team continues working and exploring potential back-up molecules, in case the preclinical and/or clinical characterization of the main compound of interest fails [1].

In summary, the target-based approach relies on manipulating a biological system, through the pharmacological modulation of a specific target [3]. In addition to enabling the application of molecular and chemical knowledge, the target is well-defined, which presupposes a good understanding of the disease and facilitates structure-based drug design and structure-activity relationships [2,14]. Nevertheless, there are also some limitations associated with this method, described in Table I.1.

Occasionally, when a specific target is activated or inhibited in an *in vivo* system, the system reroutes signalling pathways and triggers unpredictable compensatory mechanisms that bypass *in vitro* approaches. These adaptations are only detected later, as the molecule is tested in biological organisms, ultimately resulting in lack of efficacy. The same occurs with off-target liabilities, some of which are only detected in complex organisms and sometimes lead to adverse effects in clinical trials [14]. Thus, it can be very discouraging when highly targeted molecules fail to modify a disease or cause unanticipated toxicity, after substantial effort and investment was put into their optimization [15].

Table I.1. Main limitations of the target-based approach in drug discovery.

	Disadvantages	Ref.
Target-based approach	○ Restricted number of validated and druggable targets available for drug development;	[10]
	○ Starting from an already defined target prevents new targets from being discovered;	[14]
	○ The target of interest must be identified and validated before screening can begin;	
	○ The identified target may not be sufficiently relevant to the overall pathogenesis process, or provide sufficient therapeutic index (lack of efficacy);	[2]
	○ Off-target liabilities (lack of safety);	[14]

For these reasons, the interest in phenotypic screening recently resurfaced, given it was the method originally used before the target-based approach, when there was little knowledge of the molecular mechanisms behind a disease [2]. Phenotypic screening is not hypothesis-driven but a more holistic method that consists in testing a large number of compounds (in most cases randomly selected) in a system-based approach, using *in vitro* or *in vivo* assays that monitor phenotypic changes [3,16]. It is considered physiologically more relevant and less artificial, because intact cellular native environments, such as cell lines or induced pluripotent stem cells (iPSC), and organisms (e.g. *Caenorhabditis elegans, Drosophila melanogaster* or zebrafish) are used to identify *hits*, instead of testing them against a purified target protein. This can provide early toxicity and ADME data, as well as, efficacy data on relevant disease models; also, the most recent methodologies have been adapted to maintain the HTS format [10,15]. The concept of screening compound libraries by processing biological samples (individual cells, tissues or whole-organisms) to extract a visible readout, acquired by sophisticated and automated microscopy techniques, can be referred to as high-content screening [17,18].

Importantly, the phenotypic approach increases the chance of translating the leads and candidates to the patient, since the measured phenotype is normally relevant for the disease indication [16]. Furthermore, since several targets are screened at once, more opportunities are generated for compounds to engage the most biologically

relevant target in the used cell system [16]. This strategy contributes to the development of first-in-class drugs, i.e. drugs that modulate new targets or biological pathways, because the screening is unbiased with respect to mechanism of action, which does not need to be known beforehand [3,14]. Notwithstanding, phenotypic screening also has relevant drawbacks (Table I.2).

Table I.2. Main limitations of the phenotypic approach in drug discovery.

	Disadvantages	Ref.
Phenotypic approach	○ Difficult to optimize molecular properties due to lack of design parameters (hampered structure-based drug design)	[2]
	○ Integration of new screening technologies is more complicated	
	○ Challenging scalability of cellular reagents	[16]
	○ More difficult to define structure-activity relationships (requires target deconvolution)	[5]

In order to identify the molecular target and understand the cellular mechanisms behind the phenotypic changes, it is necessary to perform *target deconvolution*. Despite being time-consuming, complex and demanding a variety of different techniques (e.g. affinity chromatography, *in silico* methods), it is required to establish structure-activity relationships and aid the optimization of molecules [9,14,19].

Considering the characteristics of both approaches, their combination in a complementary mode seems to be the most promising strategy [3,15] or, in alternative, to select the approach that better fits the project in question. Hopefully, this will reverse the current trends and significantly decrease the verified attrition during clinical trials.

Clinical drug development is a process composed of several go/no-go decisions [13]. In phase I clinical trials, the safety and tolerability of an investigational drug are studied in a small number of healthy individuals, with the purpose of delineating safety margins and determining the maximum tolerated dose. Pharmacokinetic and pharmacodynamic features of the drug candidate are also strictly monitored, as the molecule is administered in single-dose or multiple-dose escalating mode. The generated data will be used to define the safe dose and dosing regimen that will be applied in phase II and

phase III. Although obtaining basic ADME information is an essential point at this stage, characterizing the safety profile of a candidate is also vital and constitutes a critical go/no-go step [6,20].

On the other hand, phase II clinical trials are generally designed to verify whether the clinical candidate possesses the desired biological effect, while safety studies proceed as well. The compound is tested on a larger number of individuals, specifically patients with the investigated pathology, and the therapeutic efficacy of the compound is evaluated, together with short-term side effects and possible risks. In spite of many candidates failing at this stage due to lack of efficacy or safety issues, an alarming number still reach phase III and cause late-stage failures [6,21].

In theory, the *"fail fast and cheap"* approach should prevent late-stage failures, but its application is often limited by a lack of appropriate experiments or fear of wrongly discarding a valuable candidate [22]. A proposed alternative has been to establish proof of principle (POP) and/or proof of concept (POC) as early as possible in the development chain, in order to reduce attrition in late phase II and III [4,23]. Thus, as soon as a candidate demonstrates reasonable safety and adequate ADME properties during phase I, a POP/POC trial is conducted in early stages of phase II or in the transition between phase I and phase II [24]. Although both terms (POP and POC) are sometimes used interchangeably, POP can be defined as the demonstration of the pharmacological principle in humans (healthy or patients) with help of a biomarker, whereas POC refers to the detection of early signs of efficacy, based on surrogate endpoints or clinical endpoints [22].

A biomarker is a characteristic that is objectively measured and evaluated as an indicator of normal biological processes, pathogenic processes, or pharmacologic responses to a therapeutic intervention [25]. When the link between a biomarker and a biological process or clinical endpoint has been scientifically proven, the biomarker is validated and attains the highest level of qualification, becoming a surrogate endpoint [21,26]. The number of accepted biomarkers as valid surrogate endpoints by regulatory authorities is small [27] but current research concerning biomarkers is very intensive, because their use has been associated with higher success rates during clinical development [28]. Among the advantages of using biomarkers as surrogate endpoints is the ability to provide researchers with early data and allow them to organize smaller and

more efficient studies, decreasing the number of individuals exposed to an experimental treatment [26]. Townsend and Arron [28] underlined the potential of biomarkers by referencing the four main reasons behind the failure of drug candidates: wrong target, meaning that despite having tested the compound preclinically, the target is not relevant to human disease; wrong molecule, due to an inadequate engagement of the target by the drug candidate; wrong outcome, caused by an insufficient understanding of the pathogenic relation between the molecular target and clinical manifestations; and lastly, a wrong enrolment of patients. Therefore, well-characterized biomarkers are important to establish POP/POC and make go/no-go decisions [4,27] nevertheless, if POP/POC biomarkers or surrogates do not adequately predict clinical outcomes, the candidate will fail in phase III confirmatory trials [22].

Phase III studies are typically randomized and controlled trials, aiming to test the effectiveness and safety of drug candidates in a large number of patients, at single-centre or multi-centre sites. These trials are conceived to collect information about the overall risk-benefit relationship of the candidate and take a long time to plan and organize, including coordinating the patient population to be selected, deciding the treatment administration, and the discussing the statistics and controls to be used. The time and investment depend on the clinical endpoint under evaluation, but the number of participants and complex design dictate that these trials are the most expensive of drug discovery and development [6,29,30].

Nonetheless, between 1998 and 2008, approximately 54% of all promising candidates that reached phase III failed to demonstrate clinical benefit or increased the risk of serious adverse events among participants [31]. Data from Thomson Reuters and Drugs of Today [32] point that specifically from 2013 to 2015, 48% of failures in phase II trials were caused by insufficient efficacy and 25% from lack of safety, whereas in phase III, the central reason of failure was 55% lack of efficacy, followed by 14% lack of safety and strategy, i.e. change in therapeutic area and/or merging companies. The increase in efficacy-related attrition from 48% in phase II to 55% in phase III shows that the "*fail fast and cheap"* strategy may not be completely working in this aspect. However, analysing the overall evolution trends from 2008 to 2015 in phase III trials, an 11% decrease of failures from insufficient efficacy was observed throughout the years, indicating that despite still being the principal cause of late stage failures, there is room for

improvement with better efficacy biomarkers, target selection, and understanding of disease biology [32].

In 2015, the 21th Century Cures Act was approved, which allows the Food and Drug Administration (FDA) to approve new drugs more quickly on the basis of biomarkers and surrogate endpoints of effectiveness, including alterations in laboratory tests or imaging studies. This, among other controversial measures, raised concerns that the FDA would lower approval standards for considering non-traditional study designs instead of randomized and controlled trials, reliant on clinical endpoints [33]. It was stated that biomarkers must be linked to patient health outcomes; otherwise patients may be exposed to ineffective or unsafe treatments. Notwithstanding, others claim that this new legislation provides a scientific framework for biomarkers in drug development and increases the feasibility and effectiveness of clinical trials, by enabling them to be more targeted [34].

I.2. THE CENTRAL NERVOUS SYSTEM IN DRUG DISCOVERY AND DEVELOPMENT

I.2.1. CNS exposure of peripherally-active drugs

Investigating the access of a molecule to the central nervous system (CNS) is always a fundamental step, regardless of whether the therapeutic target is located in the CNS or not. Therefore, CNS restriction can be interpreted as a challenge or an opportunity, depending on the specific purpose of the drug discovery and development program.

CNS exposure of drugs aimed at peripheral targets can be problematic and cause adverse effects in two situations; first, if the drug achieves sufficient concentrations in the CNS to result in off-target action; or if the modulated target is also located in the CNS, in which case, adverse effects will be an outcome of on-target engagement (right target/wrong tissue) [35]. Such effects can have nefarious consequences, namely project cancelation, regulatory rejection, product use restrictions, reduction of patient compliance and long-term toxicities [36]. An ideal pharmacological selectivity would be a solution to off-target liabilities nevertheless, when the target exists both peripherally and centrally, the key would be to design compounds with a limited access to the CNS. Furthermore, not all off-target liabilities can be detected in advance during preclinical

studies and CNS side-effects may contribute to a wrong interpretation of data at this stage [35,37].

A well-known case of right target/wrong tissue adverse effect is that of histamine-H1 receptor antagonists used for the treatment of allergic disorders such as rhinitis, atopic dermatitis and urticaria. First-generation antihistamines (diphenhydramine, hydroxyzine, promethazine, and doxylamine) reach the CNS and interact with H1 receptors located in brain parenchymal tissue, causing sedation and/or cognitive impairment. On the other hand, second-generation (cetirizine, loratadine) and third-generation (fexofenadine) antagonists, cause mild or little sedation at therapeutic doses and display better tolerability profiles, due to a more restricted access to the CNS [38,39]. Another example is the use of antimuscarinics for the treatment of overactive bladder. Some of them (olterodine and oxybutynin) interact with muscarinic receptors in the CNS, while others (trospium and fesoterodine) preferentially interact with peripheral muscarinic receptors in the bladder detrusor muscle and do not reveal central side-effects. Lastly, it is also important to mention the classic case of the antidiarrheal μ-opioid agonist loperamide, which is generally free of opioid-related side effects (e.g. sedation and respiratory depression) at high clinical doses [35]. Even though the lack of such side-effects may be related to poor intestinal absorption and low systemic exposure, it may be explained, in part, by a low degree of CNS penetration [37].

The CNS penetration of a compound depends on the equilibrium of passive and active movements across the blood-brain barrier (BBB). Peripheral selectivity is often associated with low passive permeability or affinity to efflux transporters at the BBB. Consequently, designing compounds with optimal physicochemical properties to generate an interaction with such transporters is a common strategy to maximize CNS restriction and avoid central side effects [37], although it should be noted that an efflux substrate can be centrally active at a given dose, provided it is sufficiently potent [40]. These aspects will be discussed in greater depth in following sections of this dissertation.

I.2.2. CNS exposure of centrally-active drugs

As previously mentioned, evaluating CNS exposure is important irrespectively of the location of the therapeutic target. Nevertheless, it is much more frequent to find

information in literature concerning brain exposure, when the aim of the research is to develop a drug for the treatment of a CNS disease. This approach to the topic is comprehensible, for the reasons that will be subsequently specified.

Despite intensive research, CNS disorders still affect hundreds of millions of people worldwide and the available drugs normally treat the symptoms instead of curing the disease [41]. The global burden of disease attributed to neurological disorders [e.g. Parkinson's disease (PD), epilepsy, depression] has been increasing from 2005 to 2015 together with total disability-adjusted life years, a parameter representing the lost years of healthy life, which augmented 17% [42]. Even so, data from 2005 to 2009 reveal that CNS drugs spend on average 8.1 years in clinical phase and 1.9 years in approval phase, which is superior to drugs from other therapeutic classes [43], as seen in Figure I.2.

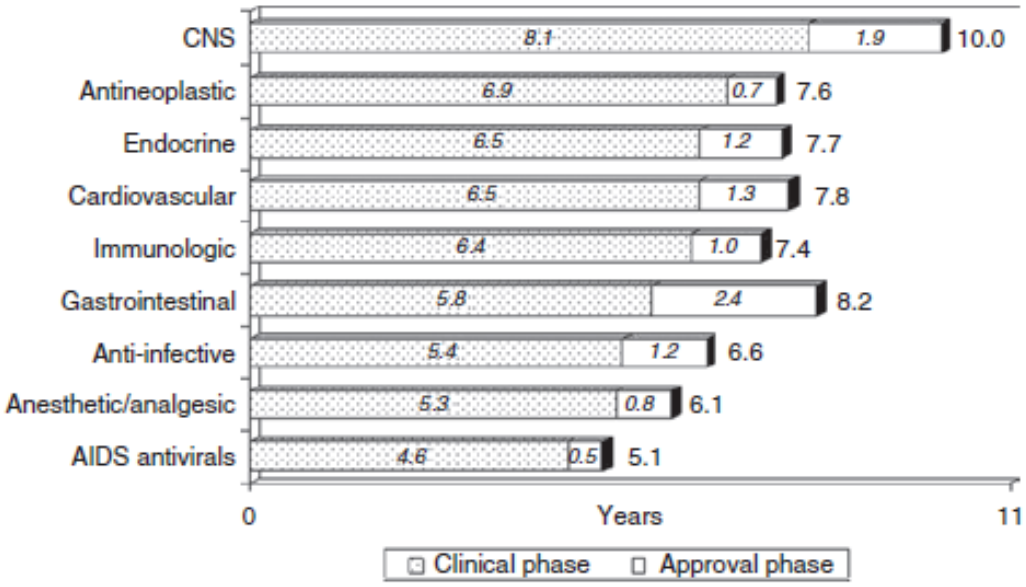

Figure I.2. Mean time of clinical and approval phases between 2005 and 2009, organized by therapeutic class. Adapted from [43].

In accordance to Thomson Reuters and Drugs of Today data, from 2013 to 2015, the therapeutic areas with a larger number of failures in phase II and III clinical trials were oncology and CNS diseases (Figure I.3A). While failures in oncology trials have been increasing from 23% in 2008-2010 to 32% in 2013-2015, attrition in CNS research remained mostly unaltered and consistently high (14-17%) during that 7-year period [32]. In parallel, data from the Pharmaprojects database [44] show that from 1990 to

2012, the number of new phase I trials for cancer drugs increased from 11% to 20%, whereas for CNS drugs there was a decrease from 11% to 7%, revealing that CNS drug development is slowing down (Figure I.3B).

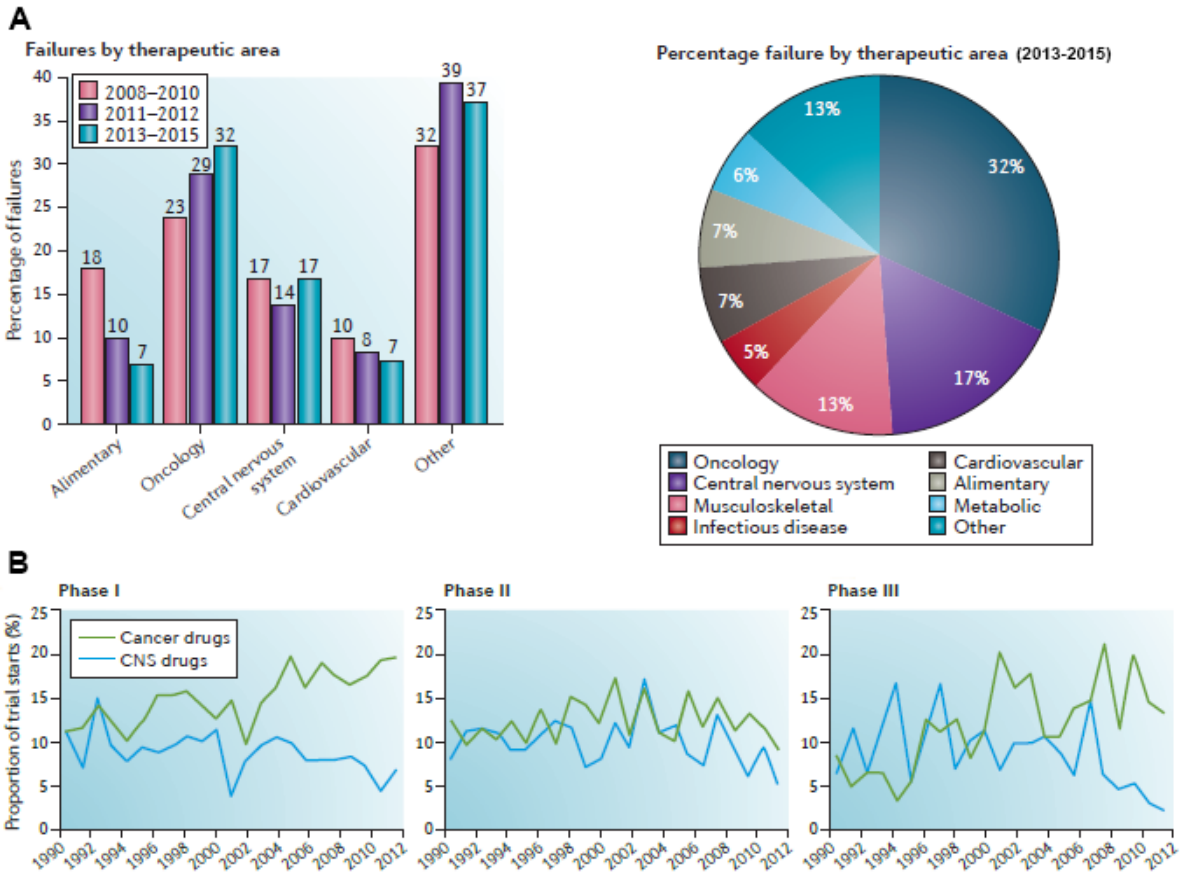

Figure I.3. Percentage of failures in phase II and phase III clinical trial by therapeutic area (A) and proportion of new phase I, phase II and phase III clinical trials starts (%) for cancer and central nervous system (CNS) drug candidates (B). Compiled and adapted from [32,44].

The graphics further demonstrate that although failures in phase III oncology trials are higher than CNS trials, the overall number of phase III oncology trials has also been increasing through the years, in contrast with CNS trials. Moreover, it was found that CNS drugs are 45% less likely to succeed in phase III than non-CNS drugs (not only cancer drugs). From 1990 to 2012, 46% of CNS trials were discontinued in phase III from lack of efficacy, while 11% were related to safety concerns [44]. Another interesting comparison between cancer and brain disorders is the disparity between costs and research funding. Despite being more costly than cancer, €798 *versus* €150-250 billion, CNS disorders received approximately the same amount of research funding in Europe in 2005, €4.1 *versus* €3.9 billion [45].

Butlen-Ducuing et al. [46] analysed the clinical development programs for CNS disorders of the European Medicines Agency (EMA) database and performed a distinction between applications for psychiatric and neurologic disorders. The outcomes of psychiatry applications were mostly affected by inadequate population selection in phase III, lack of clinical benefit, safety and insufficient justification for dose selection in phase I/II. Conversely, the main variables to affect neurology outcomes were failure to reach the primary endpoint (lack of efficacy) and lack of safety in phase III, as well as, concerns about pharmacokinetics and/or drug-drug interactions (DDIs) in early clinical stages (phase I and II).

In sum, to prevent the high levels of failure in phase III CNS clinical trials, it was recommended to improve preclinical models, upgrade the design of early-stage clinical trials and develop high quality and predictive clinical biomarkers. Moreover, it is necessary to continue the efforts in understanding the pathophysiological mechanisms behind CNS disorders, so as to proceed with the identification of new therapeutic targets [44,46].

This problematic lack of success in the research for novel treatments of neurological disorders and the expensive late stage failures caused large pharmaceutical companies to downscale their CNS development programmes (Table I.3) and smaller companies to simply abandon this therapeutic area [47]. From 2009 to 2014, the number of CNS drug discovery and development programmes by large companies decreased 52% [48] and it is estimated that only 9% of the compounds that enter phase I studies survive to launch [49]. In contrast, the interest of universities in CNS drug development, through the formation of academic drug discovery centres or public-private partnerships, is currently rising in several countries [48].

Go/no-go decisions in CNS drug development are particularly challenging due to a wide variety of reasons. In 2014, the Forum on Neuroscience and Nervous System Disorders organized by the American Institute of Medicine (current National Academy of Medicine) gathered participants from the pharmaceutical industry, government, academia and patient groups to discuss the main issues and propose alternatives to increase the efficiency of the development pipeline [50].

Table I.3. Central nervous system drug discovery and development programs in large pharmaceutical companies: 2009 versus 2014 [48].

Program	2009	2014	Percent decrease (%)
Bristol-Myers Squibb	12	2	83.3
Merck	32	7	78.1
Pfizer/Wyeth	46	15	67.4
AstraZeneca	21	7	66.7
GlaxoSmithKline	40	14	65.0
Sanofi/Genzyme	29	12	58.6
Lilly	16	9	43.8
Abbott/Abbvie	17	10	41.2
Johnson & Johnson	18	17	5.6
Roche/Genentech	22	21	4.5
Novartis	14	15	-7.1
Total	267	129	51.7

Some of the problems identified in this workshop and respective solutions are outlined below, together with recent views from other experts in the field:

1. **Unknown disease mechanisms**: the high complexity of the human CNS contributes to an insufficient understanding of brain disorders [51]. Hence, the aetiology and pathophysiology of many CNS disorders is unknown, making it difficult to develop targeted and validated therapies [50]. For instance, the mechanisms responsible for neurodegeneration are poorly understood, causing target-based drug discovery strategies to fail [14]. Phenotypic screening was pointed as a strategy capable of increasing the probability of success in this area, although it is necessary to continue the investigation of robust and disease-relevant cellular phenotypes with improved assay throughput [14,15]. It is expected that with phenotypic screening models capable of mimicking the human disease, more efficient clinical development and POC studies will be achieved [52].

2. **Translational difficulties**: the animal models used in early drug discovery lack predictive power to estimate efficacy [47,53]. Even though a particular aspect of the disease can be mimicked in an animal model, given that a relative number of complex

mechanisms and circuitries are shared between species at CNS level, an entire disorder can rarely be recapitulated [47,50]. Failures could be explained by a mismatch between the endpoints used in clinical trials and preclinical animal studies. Combining animal and non-animal (e.g. iPSCs, computational neuroscience) models of disease mechanisms may prevent failures in CNS development and improve target identification and validation [50].

3. Pharmacodynamic heterogeneity: inter- and intra-individual variability observed in humans, caused by disparities in genetic background, age, gender, diet, disease states and drug treatment. Hence, the same dose in different conditions may lead to different CNS effects [41]. This human heterogeneity consequently demands larger, more complex and more expensive clinical trials. Once again, the use of biomarkers was highlighted to demonstrate the modulation of the targeted pathway in humans, provide confidence that the therapeutic mechanism of action is adequately tested and facilitate the implementation of POC. The hindering factor at this stage is that the development and validation of biomarkers requires significant resources and tools from academic researchers and takes an excessively long time for industries, for which the priority is the development of the therapeutic molecule [50]. A possible solution to attain progress through collaboration and that is already being put to practice, are public-private partnerships.

4. Inconclusive pharmacokinetic data: lack of efficacy can be caused by insufficient exposure to the CNS target, therefore it is important to know the free concentration of a drug in brain extracellular or interstitial fluid (ISF) [51]. However, sometimes it is not reported if unbound or total concentration data referring to brain, plasma and intra-brain distribution were used [49]. To surpass this obstacle, Lange [41] elaborated the "Mastermind approach" which consists in investigating the pharmacokinetic-pharmacodynamic relationship of a CNS drug, by associating advanced preclinical models with mathematical calculations. It was proposed that microdialysis could be used in animal models to learn about the intracerebral distribution of drugs and CNS target site concentrations. These data could be, then, extrapolated to humans resorting to physiologically-based pharmacokinetic modelling, and consequently predict human CNS distribution and effects.

For all the aforementioned reasons, it becomes simple to understand why achieving *"the right drug, at the right time, at the right concentration, in the right place"* for CNS drugs is a very resource-consuming and time-consuming task.

I.3. CNS BARRIERS, COMPARTMENTS AND FLUIDS

In 1885, Paul Ehrlich conducted the first studies that evidenced the existence of a barrier between the brain and the blood. After injecting dyes intravenously to rats, it was observed that the dye was rapidly taken up by all organs except the brain. However, Ehrlich thought that the brain was made of a tissue to which the dye had no affinity for. Later in 1913, his associate Edwin Goldmann demonstrated that when dyes were injected directly into the CSF only the brain was stained, concluding that once within the CNS, the dyes were unable to access the blood circulation [54,55]. Therefore, Goldmann verified that there was a barrier between the brain and the blood, however the term *barrière hémato-encéphalique* only appeared for the first time in 1921, in reports by Stern and Gauthier, who expanded the concept by suggesting possible BBB functions and conducting pioneering experiments [56].

The molecular exchanges between the blood and the CNS or its fluid spaces are limited and regulated by several interfaces: the BBB, which will be discussed in section I.3.2; the epithelial cells of the choroid plexus that secrete the cerebrospinal fluid (CSF) into the cerebral ventricles; the epithelium of the arachnoid barrier that covers the outer brain surface above the layer of subarachnoid CSF; and the CSF-brain barrier formed by the separation of the ventricular system from the brain ISF, present only in the embryo during brain development [57–59]. The arachnoid barrier is a part of the blood-CSF barrier (BCSFB) in addition to the choroid plexus, given that the arachnoid membrane over the subarachnoid space and the choroid plexus invagination of the ventricles, are two major areas where the blood is near the CSF (Figure I.4) [57,60].

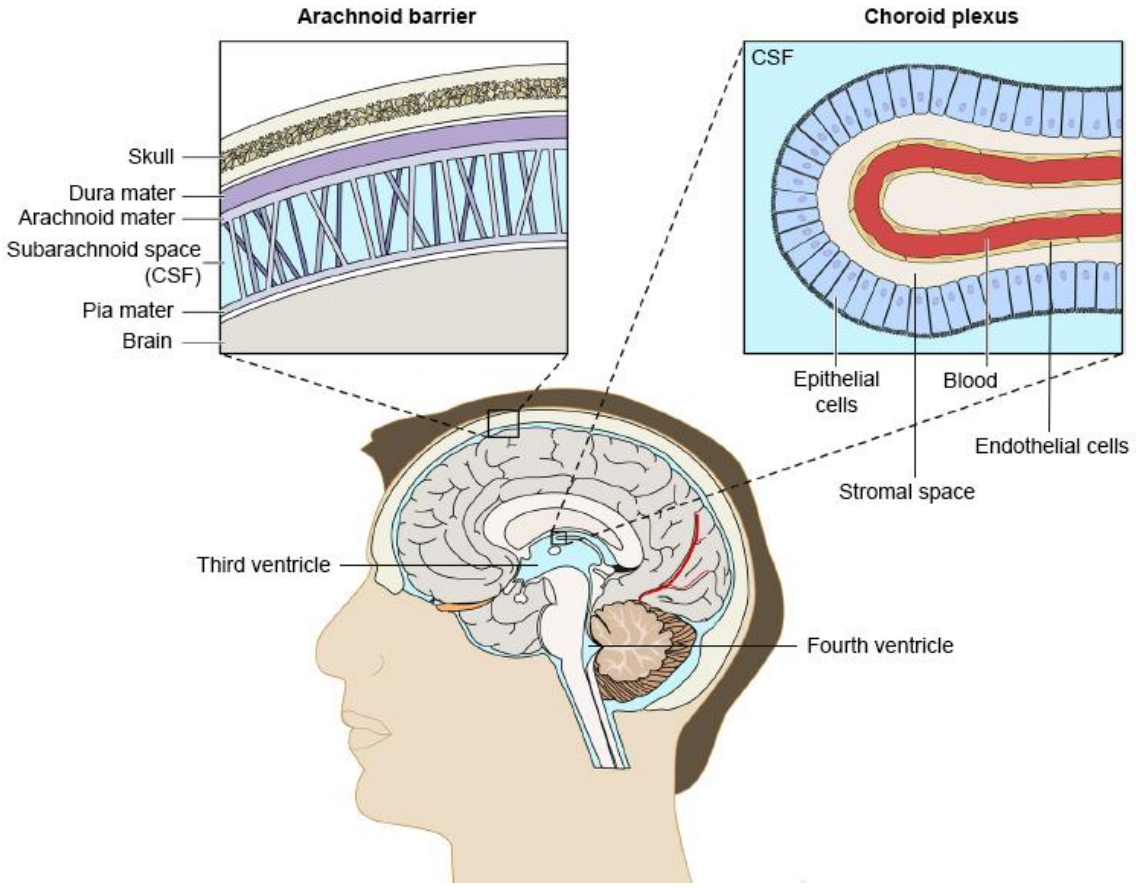

Figure I.4. The blood-cerebrospinal fluid (CSF) barrier, including the arachnoid barrier and the choroid plexus. In the choroid plexus, epithelial cells are united by tight junctions at the apical or CSF-facing surface and possess a brush border with microvilli and cilia. Adapted from [61,62].

These barriers prevent external influences from interfering with the microenvironment of the CNS due to being functionally tight and ensuring little diffusion by paracellular route between the blood, the CSF and the brain parenchyma [59]. The tightness is conferred by tight junctions (TJs) between cerebral endothelial cells (CECs) of the BBB and in the apical surface of the choroid epithelial cells of the BCSFB, which join cells in a belt-like fashion, severely hampering the passage of hydrophilic molecules. In the brain-CSF barrier there are strap junctions that surround cells from their ventricular surface, preventing the diffusion of solutes from the CSF to the fetal brain [58,59].

The choroid plexus in each ventricle is separated from the surrounding brain parenchyma by ependymal cells that line the ventricles [63]. In the adult, most of the

ependymal surface, with the exception of the choroid plexus, is not connected by TJs but by leakier gap junctions [64]. Moreover, the capillaries in the choroid plexus are fenestrated and separated from the epithelial cells by a thin layer of connective tissue called stroma (Figure I.4). Supposedly, the higher endothelial permeability of the basement membrane surrounding the choroidal capillary walls is caused by the absence of astrocytic processes, which in contrast are present at the BBB and contribute to its higher restrictiveness [60].

Besides possessing a large number of mitochondria that provide enough energy for secretory functions and transepithelial transport, choroid epithelial cells display well-developed microvilli projected into the CSF in the ventricular lumen, which increase the surface area for an effective delivery of the CSF and other transport functions [63]. Early literature data indicated that the surface area of the choroid plexus was only 0.021 m^2 or 0.1 % compared with 20 m^2 of the reported surface area of the BBB [65]. Nevertheless, this information has been rectified and more recently assessed data demonstrated a significant underestimation of the surface area of the human choroid plexus, pointing towards 2-5 m^2 [66]. Associated with the microvilli are epiplexus cells called Kolmer cells [60]. Kolmer cells, together with supraependymal cells and free-floating cells that move freely in the CSF form the group of intraventricular macrophages, allegedly derived from macrophages present in the stroma of choroid plexuses. These cells are not only involved in antigen-presentation, but also sequester iron in specific CNS pathologies that generate excessive iron levels [63].

Thus, about two-thirds of the CSF is secreted at high capacity by the four choroid plexuses in the lateral right, lateral left, third and fourth brain ventricles [67,68]. It is estimated that every day the CSF is replaced at least 3-4 times, since the CNS can accommodate 150 mL of CSF and the amount formed by choroid plexus in 24 h is approximately 500-600 mL [63]. The CSF circulates from the lateral to the third ventricle via the interventricular foramina and then to the fourth ventricle through the cerebral aqueduct. Afterwards, it flows down the central canal of the spinal cord and circulates in the subarachnoid space where it is reabsorbed by arachnoid villi or granulations, either to the systemic circulation or to regional and cervical lymph nodes [69]. Regular CSF flow is critical for balanced cerebral metabolism and propelled by several mechanisms, including arterial pulsations in the choroid plexus, a hydrostatic pressure gradient from

the CSF to venous blood and the movement of the ciliary processes that extend from the apical surfaces of ependymal cells [60]. The production, continuous flow and elimination of the CSF serve as a washout system, especially affecting hydrophilic and large molecules [70].

CSF formation encompasses two steps: first the passive filtration of plasma across the choroidal capillary endothelium and subsequently, a regulated active secretion process across the epithelium [68]. At the membranes of the epithelial cells there are transporters that take up ions by facilitating mechanisms at the basolateral membrane, releasing or actively secreting them into the ventricles on the apical side. Essentially, CSF secretion resides on the net translocation of Na^+, K^+, Cl^-, HCO_3^- and water. For instance, Na^+ is extruded by the Na^+/K^+-ATPase pump located in the apical membrane. This ion is especially important because it creates the driving force for CSF secretion. The Na^+/K^+-ATPase pump utilizes 3 Na^+ ions for the exchange of 2 K^+ ions forming an electrochemical gradient, explored by other transporters. Another pump that contributes to Na^+ secretion into the CSF, although to a lesser extent, is the electrogenic Na^+-HCO_3^- cotransporter 2 (NBCe2) which exchanges 1 Na^+ ion for 3 HCO_3^- ions. All this ion movement leads to the creation of an osmotic gradient, responsible for the passage of water by the aquaporin-1 (AQP-1) channel [63,65,68]. The expression of AQP-1 at the BCSFB has a close connection with the CSF formation rate, given that lower levels are present when CSF formation has not yet reached its peak (i.e. early fetal development) or when it is decreasing, at an advanced age [60]. In this context, ionic homeostasis is one of the main functions of the CNS barriers. The movement of ions and water creates fluid flow of the CSF and ISF, provides buffering against ion fluctuations in the blood and preserves an optimal ionic medium for neural function and signalling. In fact, it is believed that the advantage for animals with better CNS ion homeostasis was the chief selective pressure leading to the evolution of the CNS barriers [67].

The regulation of the exchanges between the blood and the CSF at the BCSFB is mediated by transporters that contribute to the maintenance of CNS homeostasis (Figure I.5).

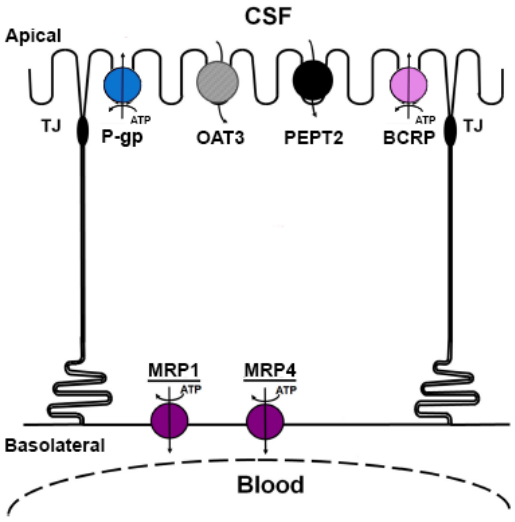

Figure I.5. Simplified representation of uptake and efflux transporters at the apical and basolateral surfaces of choroid plexus epithelial cells. CSF, cerebrospinal fluid; BCRP, breast cancer resistance protein; MRP, multidrug resistance-associated protein; OAT, organic anion transporter; PEPT2, proton-coupled oligopeptide transporter; P-gp, P-glycoprotein; TJ, tight junction. Adapted from [71,72].

These transporters belong to the solute-carrier (SLC) or adenosine triphosphate-binding cassette (ABC) super-families [73]. The first identified transporters of the choroid plexus were organic anion transporter (OAT) proteins at the brush-border membrane of the epithelial cells [63,74]. Typical substrates of OATs at the BCSFB encompass endogenous compounds such as neurotransmitter metabolites and the prostaglandins D2 and E2, involved in physiological sleep and neuroinflammation, which are cleared from the CSF through OAT3 (SLC22A8)-mediated uptake [74]. OAT-transported xenobiotics include β-lactam antibiotics, quinolones, non-steroidal inflammatory drugs, some antiepileptic drugs, cimetidine and anionic pesticides [73]. For instance, to achieve therapeutic efficacy in the treatment of meningitis, it would be necessary to administer antibiotics that are not removed from the CSF or in alternative, massive parenteral doses of penicillin that would saturate the removal mechanism mediated by OAT3, allowing more drug to remain in the CSF [66]. In resemblance to OATs, organic cation transporters (OCTs) are also located at the CSF-facing brush border. OCTs perform the uptake of monoamine neurotransmitters (e.g. dopamine) and xenobiotic cations from the CSF to the blood while protecting the CNS from cationic

neurotoxins, namely 1-methyl-4-phenylpyridinium [73,74]. The proton-coupled oligopeptide transporter PEPT2 (SLC15A2) was found at the apical membrane of BCSFB epithelial cells of rats, but not at the BBB. This transporter facilitates the mediation of neuropeptide homeostasis and neurotoxins from the brain, as well as, the clearance of antibiotics such as cephalosporins with an α-amino group [63,66,75].

Even though the role of ABC transporters at the BBB has been thoroughly investigated and will be discussed more extensively in following sections of this dissertation, their functional relevance at the BCSFB is not sufficiently understood. Initially, P-glycoprotein (P-gp, encoded by *ABCB1* or *MDR1*) was identified at the BBB but not at the choroid plexus [73], however in immunohistochemical and drug transport studies with cell lines from neonatal rats, P-gp was found at the apical or CSF-facing surface of choroidal epithelial cells, indicating that it engages in epithelial cell-to-CSF efflux and prevents the traffic of substrates out of the CSF. Interestingly, the traffic of substrates from the blood to the CSF is barred by multidrug resistance-associated proteins (MRP, encoded by *ABCC*), MRP1 and MRP4, located at the basolateral surface of choroidal epithelial cells [74,76]. Western blot studies revealed that in the adult rat brain, the levels of P-gp in choroid plexus are 0.5% of those found in brain microvessels, whereas MRP1 levels in brain microvessels are only 4% of those in the choroid plexus of the fourth ventricle. These differences were also confirmed in human samples. It has been speculated that P-gp at the BCSFB could impede the accumulation of neurotoxic lipophilic substances in the brain, while MRP1 is responsible for the basolateral efflux of drug conjugates formed in the choroid plexus [77].

Moreover, the choroid plexus possesses several drug-metabolizing enzymes with especially high activity, such as glucurono-, sulfo- or glutathione transferases, which demonstrated to influence drug concentrations in the brain. The association of metabolic reactions with the efflux of the formed conjugates, establishes yet another barrier that limits drug distribution into the CSF [70]. Lastly, in this regard, the breast cancer resistance protein (BCRP or MXR, encoded by *ABCG2*) has also been identified in the apical brush border of the choroid plexus of mice, rats and humans. An interesting work was recently published by Kaur and Badhan concerning the modulation of BCRP at the BCSFB by phytoestrogens [78].

Facilitated-transport carriers are additionally responsible for loading epithelial cells of the choroid plexus with micronutrients (e.g. vitamin C, folate), peptides and proteins transported from blood or synthetized in choroid plexus (e.g. transthyretin), growth factors and hormones, as well as, for maintaining those solutes in narrow concentration ranges within the CSF [60,79]. These substances reach the brain ISF from the CSF across the permeable ependyma and are fundamental for brain health [66]. In particular, transthyretin has been identified as a potential CSF biomarker because it is secreted almost exclusively by choroid plexuses and binds to amyloid-β, thereby contributing to its stabilization in soluble form. Ageing and Alzheimer's disease decrease transthyretin levels and CNS peptide toxicity may occur [68,80]. Currently, validated CSF biomarkers are beginning to be included in clinical trials for Alzheimer's disease but more research in this area is necessary for other neurodegenerative diseases, such as PD [81].

Hence, the stability of the brain ISF is strongly connected with the homeostatic transport mechanisms of the choroid plexuses [60]. The ISF occupies around 20% of brain volume and bathes neurons and glia. It has a similar ionic composition to plasma, although with more Mg^{2+}, less K^{+} and Ca^{2+} and very low protein content [57]. The communication between the CSF and the ISF is extensive and the CSF is regarded as a reservoir for ISF or the ultimate site of ISF waste products [82]. The ISF moves by bulk flow through low resistance pathways formed by perivascular spaces and axon tracts, draining into the CSF [83]. Thus, unnecessary metabolites from the ISF, like homovanillic acid (HVA) from dopamine metabolism, undergo CSF-mediated removal in order to ensure an efficient neuronal function. The CSF acts as a sink, lowering concentration gradients and taking substances to drainage sites for extrusion, namely at the arachnoidal-lymphatic-venous interfaces [68]. Nonetheless, it should be mentioned that molecules do not distribute only by passive diffusion or convection in the CNS, but can be actively pumped out of the ISF by BBB transporters and out of the CSF by BCSFB transporters [66]. As a result, the ISF and CSF can be considered parallel fluids in continuous flow, capable of mixing and with shared roles, but also with distinct and complementary functions [57].

CSF sampling has been highlighted as the best available method to estimate the unbound brain ISF concentrations in animals and humans [49]. Furthermore, a good

correlation was observed between the ratio of unbound concentrations in the CSF and the brain (r^2 = 0.88) [84]. Nevertheless, caution must be taken with P-gp and/or BCRP substrates because unbound ISF concentrations may be over-predicted by unbound CSF concentrations [40]. This has been justified by the different location and expression of these transporters at the BBB and BCSFB. Since at the BCSFB, P-gp is located in the apical surface of epithelial cells, drugs that are P-gp substrates would be pumped into the CSF, leading to higher CSF concentrations and to an overestimation of unbound ISF concentrations [85]. Another possible explanation is that P-gp at the BCSFB is less expressed and may be less efficient than P-gp at the BBB, indicating that the estimated CSF unbound concentration ratios would be higher than actual ISF concentrations, which would be decreased by P-gp efflux at the BBB [86].

I.3.1. PHARMACOKINETIC CONCEPTS OF CNS EXPOSURE

Drug movement into and out of the CSF and ISF depends on its physicochemical properties, protein binding and affinity for transporters of the BCSFB and BBB [66]. The main compartments and barriers of the brain parenchyma that influence drug distribution and pharmacokinetics in the CNS are illustrated in Figure I.6.

As previously referred in section I.2.2, inconclusive pharmacokinetic data is one of the causes of failure during the discovery and development of CNS drugs, due to inadequate methods for measuring brain exposure or incorrect data interpretation. This assessment also applies to peripherally-active compounds, for the reasons stated in section I.2.1. At this stage, it is important to emphasize that only unbound drug molecules are capable of moving across the compartments depicted in Figure I.6 and that brain exposure of drugs can be characterized according to rate, extent and intra-brain distribution [40].

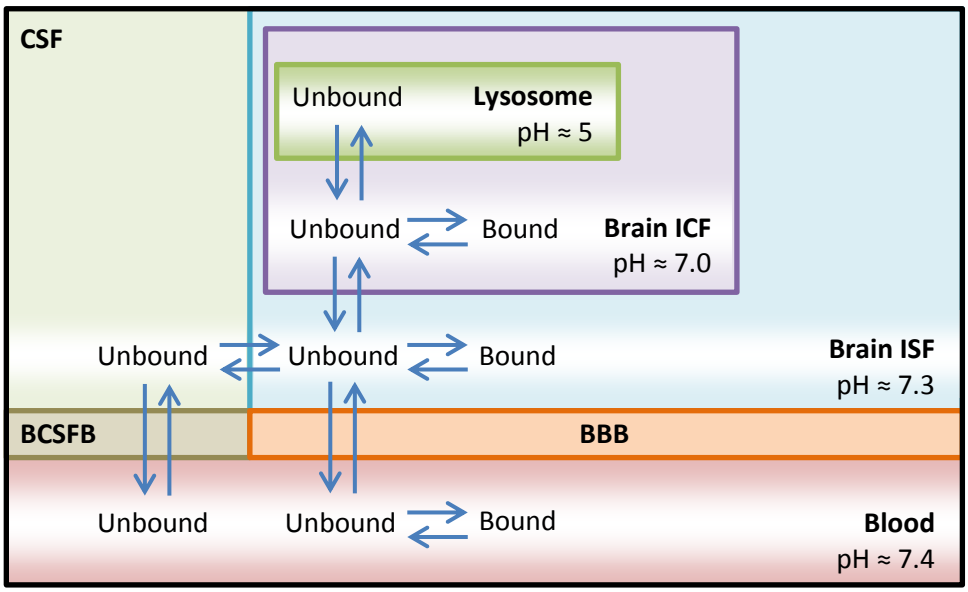

Figure I.6. Schematic representation of the main compartments and barriers of the central nervous system used to describe drug exchange and neuropharmacokinetics. BBB, blood-brain barrier; BCSFB, blood-cerebrospinal fluid barrier; CSF, cerebrospinal fluid; ICF, intracellular fluid; ISF, interstitial fluid. Adapted from [40,87].

The rate of CNS penetration is related to the speed at which a compound is capable of entering the ISF, independently of how much compound enters the CNS. It is influenced by the amount of drug delivered to the brain, controlled by the cerebral blood flow, and by the passive permeability of the compound across the BBB. The cerebral blood flow of rats (0.2-2 mL^{-1} min^{-1} g^{-1} brain) is faster than in humans (0.15 and 0.6 mL^{-1} min^{-1} g^{-1} brain for white and grey matter) [87]. For drugs that quickly enter the brain ISF, cerebral blood flow becomes rate-limiting and constitutes the upper limit of the rate of *in vivo* CNS penetration [41,87]. On the other hand, the passive permeability of a compound depends on the characteristics of the crossed membrane and on the physicochemical properties of the drug. Even though it describes the rate of passage across the BBB, a low passive permeability can limit the diffusion of a compound into the brain and thereby decrease the extent of CNS penetration. Conversely, a high passive permeability will enable the establishment of a fast equilibrium between plasma and the brain ISF but it does not imply that the compound will achieve high unbound concentrations in the CNS [85]. This parameter can be determined *in vitro* or *in vivo*, as it will be explored in sections I.3.4.1 and I.3.5 of this dissertation.

The extent of CNS penetration reflects the degree to which a compound enters the brain tissue [87]. It can be described by the ratio of total drug concentrations in brain and plasma (K_p) or its logarithm (log BB), or by the unbound concentration ratio between plasma and brain ISF ($K_{p,uu}$) [40]. For a long time, the development of compounds for CNS targets was based on the optimization of K_p or log BB, but this approach revealed to be misleading and counter-productive. Indeed, the compounds often demonstrated lack of efficacy, since high K_p values are associated with higher lipophilicity, meaning that the molecules rapidly cross the BBB but then exhibit a high degree of non-specific binding within the brain parenchyma, given that the brain has a relatively high lipid content [88].

In this context, the free-drug hypothesis postulates that the concentration of unbound drug is the driving force for all distribution processes [83]. It is the unbound concentration that distributes from the systemic circulation, across membranes, to tissues and exerts pharmacological activity. Since the CNS is an extravascular compartment, not directly accessed from the systemic circulation due to the BBB, the free concentration of compound in plasma must first cross the BBB and then undergo binding in the CNS [89]. Therefore, $K_{p,uu}$ gives a direct quantitative description of how the BBB manages the drug concerning passive transport and active influx/efflux. A $K_{p,uu}$ near 1 indicates dominant passive diffusion, whereas a $K_{p,uu}$ different from 1 suggests dominant active uptake to brain ($K_{p,uu} > 1$) or dominant efflux back into the blood ($K_{p,uu} < 1$) [83,87]. Notwithstanding, there is not a cut-off below which a drug is unsuitable for action within the CNS. Still, the lower $K_{p,uu}$ is, the higher will be the dose necessary to obtain pharmacologically relevant concentrations in the CNS, maintaining an unaltered potency [40].

$K_{p,uu}$ can be estimated directly resorting to an *in vivo* method such as microdialysis [49] or indirectly, by measuring and correcting K_p, using the unbound fractions in plasma ($f_{u,plasma}$) and brain ($f_{u,brain}$); these parameters are determined by *in vitro* methods, such as brain homogenates [89] or brain slices [90] (Table I.4). In spite of the need for two measurements, the indirect approach is more susceptible to screening and triaging compounds within the drug discovery setting. Extracting the brain tissue and homogenizing or slicing it, can be mastered by a wider range of scientists and technicians than the surgical expertise demanded for microdialysis [91].

However, significant discrepancies were noted between the data generated by the brain slice method and the brain homogenate method [91]. The brain slice method provides straightforward information concerning the volume of distribution of unbound-drug in brain ($V_{u,brain}$), which can be used to calculate $K_{p,uu}$ in combination with K_p and $f_{u,plasma}$. In contrast, the brain homogenate method allows the calculation of $f_{u,brain}$ that could be converted to $V_{u,brain}$ assuming that $V_{u,brain}$ = 1 / $f_{u,brain}$. Nevertheless this assumption is not always correct, as a result of distinct pH values in different brain compartments and the phenomena of *lysosomal trapping* or *lysosomotropism* [92].

Table I.4. Comparison of the advantages and disadvantages of the brain slice and brain homogenate methods used to estimate $K_{p,uu}$ from K_p.

	Brain slice	Ref.	Brain homogenate	Ref.
Advantages	Adaptable to high throughput format; Cost effective; Compatible with assay requirements in drug discovery;			[87]
	More physiological; Complex cellular structures are preserved;	[90]	Technical simplicity; General applicability;	[93]
	Cell-cell interactions and pH gradients are conserved.	[94]	The same equipment can be used for $f_{u,plasma}$	[40]
Limitations	Higher initial cost and effort to implement.	[95]	Sites that do not usually bind the drug *in vivo* are exposed;	[87]
			Loss of pH differences across cellular barriers.	[91]

The movement of weak acids and bases across cell membranes is guided by a pH gradient, since non-charged species are more likely to passively diffuse through membranes. This causes an accumulation of basic drugs in cells, because the intracellular pH is lower than the extracellular one, and particularly, in intracellular subcompartments called lysosomes with a pH of approximately 5 [95] as depicted in Figure I.6. Due to protonation inside the lysosomes, base compounds are unable to return to the cytosol. Despite the small physiological volume of lysosomes, intralysosomal concentrations of trapped compounds can reach high levels and

influence intra-brain distribution and pharmacokinetics. This process is saturable, energy-dependent and requires cellular integrity [92], which is lost during the brain homogenization technique. Therefore, $f_{u,brain}$ obtained with brain homogenates must be compensated for pH partitioning according to the pKa of the drug, thereby generating $f_{u,brain,corrected}$ values [95]. Then, $V_{u,brain}$ can be more accurately estimated as $V_{u,brain} = 1 / f_{u,brain,corrected}$. Data generated with the brain homogenate method corrected for pH partitioning revealed good correlation ($r^2 = 0.79$) with brain slice data [84]. Moreover, Di et al. [89] found no species differences in the $f_{u,brain}$ of 47 chemically-diverse compounds using the brain homogenate method.

In sum, applying the concepts of rate, extent and intra-brain distribution is essential to evaluate CNS exposure and lead to more successful drug development outcomes. Even though the CSF appears to be an appropriate sampling site to obtain preliminary knowledge of unbound brain concentrations [40], there are pitfalls associated with this approach, related to differences between the BCSFB and the BBB. Understanding the mechanisms that determine the net flux of drugs across the BBB and its properties is fundamental to assess CNS penetration during drug discovery [87].

I.3.2. THE BLOOD-BRAIN BARRIER AND THE NEUROVASCULAR UNIT

Although distinct interfaces form barrier layers between the CNS and the blood, the BBB, composed by CECs that delimit cerebral microvessels, is considered the major site of blood–CNS exchange and contributes to the maintenance of the homeostasis of the CNS [96,97]. The CECs, together with astrocytes, pericytes, microglia, neurons and the extracellular matrix (ECM), form the *neurovascular unit* (Figure I.7), a highly coordinated system that dynamically regulates the cerebral microvascular permeability and provides a basis for understanding the development and physiology of the BBB, including the mechanisms by which cerebral microvascular permeability can be influenced by drugs and disease [98–101].

Given the emerging interest in this modular organization and the fact that the specific features of the BBB must be considered for developing screening methods, it is important to firstly outline the structure and role of each associated cell type.

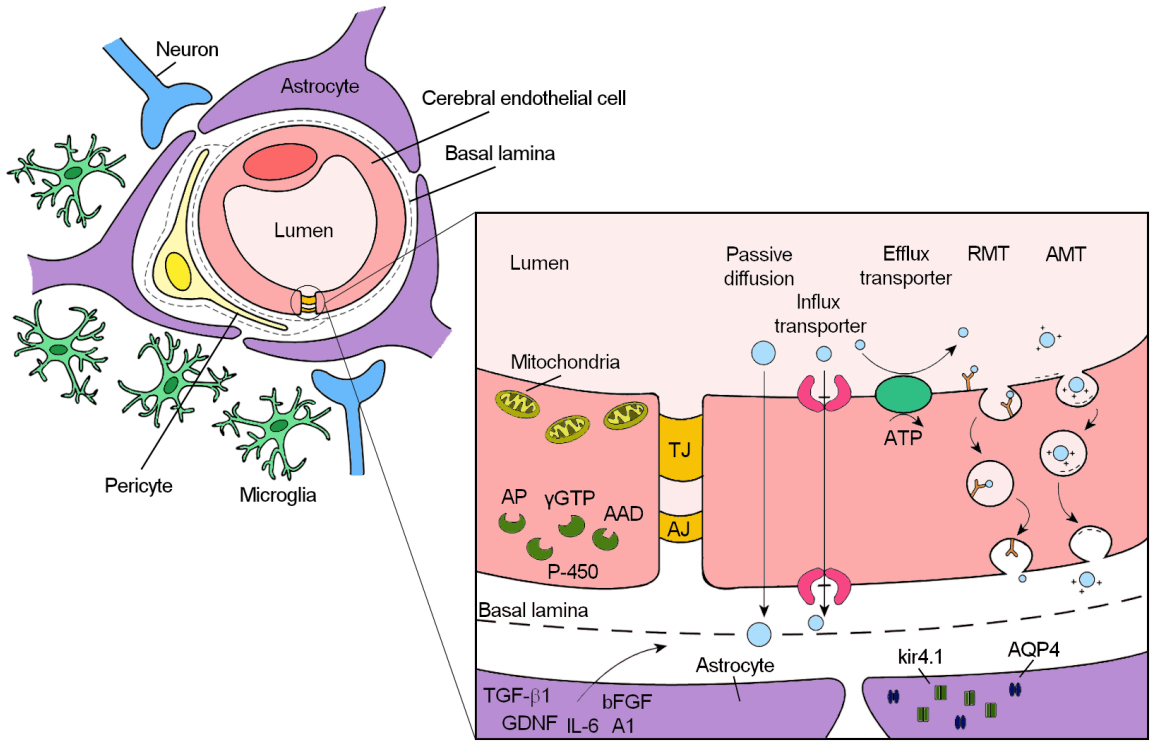

Figure I.7. Structural representation of the blood-brain barrier (BBB) and routes of transport. The BBB is a complex system composed by cerebral endothelial cells, separated from pericytes and astrocytic end-feet by the basal lamina. Microglia and neurons are also part of the neurovascular unit. The routes of transport across the BBB are shown in greater detail, as well as, several endothelial enzymes and regulatory factors released by astrocytes. The molecular organization of tight junctions and adherens junctions is not depicted. A1, angiopoietin 1; AAD, aromatic acid decarboxylase; AJ, adherens junction; AMT, adsorptive-mediated transcytosis; AP, alkaline phosphatase; AQP-4, aquaporin-4; ATP, adenosine triphosphate; bFGF, basic fibroblast growth factor; CYP, cytochrome P450; GDNF, glial-derived neurotrophic factor; γ-GTP, γ-glutamyl transpeptidase; IL-6, interleukin-6; Kir4.1, potassium channel; RMT, receptor-mediated transcytosis; TGF- β1, transforming growth factor-β1; TJ, tight junction. From [102] adapted from [96,99].

I.3.2.1. Cerebral endothelial cells

CECs constitute a selective barrier covering the inner surface of cerebral capillaries and therefore, heavily determine the BBB permeability of the vast majority of circulating compounds. Anatomically, CECs are different from peripheral endothelial cells as they

have no fenestrae, exhibit an extremely low pinocytotic activity [55] and possess a superior number of mitochondria, resulting in a more intense metabolic activity [97].

One of the most significant features of CECs is the presence of interconnections between adjacent cells, namely adherens junctions (AJs) and TJs [103]. In AJs, cadherin proteins in the intercellular cleft are connected to the cell cytoplasm by α-, β- and γ-catenins, mediating the adhesion of CECs to each other, the initiation of cell polarity and partially regulating the paracellular permeability [98]. Simultaneously, TJs occlude the intercellular cleft by forming a multi-protein complex composed by transmembrane proteins (claudins, occludin, junctional adhesion molecules) and cytoplasmic proteins [zonula-occludens (ZO)-1, ZO-2, ZO-3 and cingulin] linked to the actin cytoskeleton [55]. The loss of one of these proteins may severely compromise the integrity and functionality of the BBB [96]. TJs separate the apical and the basolateral domains causing cell polarization (fence function) and restricting the passage of ions, hydrophilic compounds and macromolecules through the paracellular pathway (gate function) [104,105]. The limited movement of small ions such as Na^+ and Cl^- leads to a considerably higher *in vivo* value of transepithelial electrical resistance (TEER) for brain endothelium than for peripheral capillaries (≈1000 Ω cm^2 *versus* 2–20 Ω cm^2) [96,99,103]. It was recently discovered that CECs have a more negatively charged membrane than other cells, making anionicity another determinant factor of BBB permeation [106].

Gaseous molecules and small lipophilic compounds can permeate the BBB by passive transcellular diffusion through the cellular membranes of CECs, while nutrients (e.g. glucose or amino acids) undergo carrier-mediated influx by SLC transporters. Large endogenous molecules, such as insulin or transferrin, cross the BBB by receptor-mediated transcytosis (RMT), whereas cationized proteins are usually carried by adsorptive-mediated transcytosis (AMT) [107,108]. A deeper knowledge of these influx transporters and of the regulation of brain endothelial transcytosis at a molecular level needs to be achieved, in order to use these mechanisms as targets to selectively facilitate CNS drug delivery, as it will be mentioned in section I.3.6. [109–111]. Another route of transport across the BBB which is currently being investigated, involves the migration of immune cells to the CNS and the surveillance role of the neurovascular unit [55,96,112] (Figure I.7).

It is important to highlight the relevance of the efflux carriers expressed by CECs, most of which belong to the ABC transporter family [67]. In opposition to the influx transporters aforementioned, ABC transporters are expressed in the apical or basolateral surface of CECs and mediate the efflux of lipophilic compounds which would otherwise easily diffuse across the BBB. P-gp is one of the best characterized ABC transporters because of its ubiquitous expression and broad substrate specificity, including a wide variety of structurally different drugs from distinct pharmacological groups [113]. Furthermore, the over-expression of P-gp is also subjacent to the pathophysiology of several neurological diseases and to the development of drug resistance phenomena [114]. Other members of the ABC protein family at the BBB include BCRP and MRP proteins [97]. In particular, the role of BCRP has been examined and it was found to cooperatively efflux compounds with P-gp [115]. Protein quantification studies inclusively demonstrated that BCRP has a higher expression in human brain microvessels than P-gp [116,117] and thus, screening BCRP as well as P-gp needs to be considered as a rational strategy for CNS drug development [74].

Lastly, CECs also form a metabolic barrier as they express a specialized set of enzymes such as alkaline phosphatase (AP), γ-glutamyltranspeptidase, aromatic acid decarboxylase and several cytochrome P450 (CYP) enzymes that metabolize numerous xenobiotics, including drugs (Figure I.7). Their expression in CECs is much higher than in non-neuronal capillaries [100], making them BBB markers [118]. Other markers include the von Willebrand factor VIII related antigen and the uptake of acetylated low density lipoproteins [103], which will be important to evaluate the endothelial properties of the different *in vitro* cell models.

I.3.2.2. Astrocytes

As represented in Figure I.7, astrocytes are glial cells that interact closely with CECs, ensuring the adequate neuronal function [100] and the control of the cerebral blood flow [119]. Astrocytic end-feet cover a large part of the basolateral surface of CECs and play an essential role in maintaining and up-regulating specific BBB characteristics, namely restrictive TJs, specialized enzyme systems and polarized transporter location

[104]. Indeed, the interaction between astrocytes and CECs determines the unique phenotype of CECs [100].

Other properties of astrocytes that influence the maturation of BBB are the expression of the intermediate filament glial fibrillary acidic protein (GFAP) and the presence of orthogonal arrays of particles (OAPs) [105]. The OAPs contain the potassium channel kir4.1 and the water channel aquaporin-4 (AQP-4) which mediates water movements between the intracellular, interstitial, vascular and ventricular compartments [97,120]. AQP-4 is also believed to influence cognition, learning and memory and has been implicated in several neurological disorders [121]. In addition to this, the OAP/AQP-4 polarity of astrocytes is related to the expression of agrin, a heparan sulphate proteoglycan of the basal lamina that separates astrocytes and pericytes from CECs. The accumulation of agrin occurs at the time of BBB tightening, suggesting that it is important for barrier integrity [99]. Further evidence that the components of the ECM contribute to the induction of BBB properties was given by the expression of matrix adhesion receptors on astrocytic end-feet, CECs, microglia and neurons [99,104] however this aspect will be explored in greater depth in section I.3.2.5.

Astrocytes also release regulatory factors that interfere with the BBB phenotype and the proper differentiation of CECs. Several molecules have been associated with this process, such as the glial-derived neurotrophic factor, transforming growth factor-β1, basic fibroblast growth factor, interleukin-6 and angiopoietin 1 [96,97,104].

I.3.2.3. Pericytes

Brain pericytes are mural cells separated from CECs by the basal lamina and associated with the stabilization of small vessels architecture, neovascularization and angiogenesis (Figure I.7). Despite being known that the loss of pericytes leads to an abnormal vascular morphogenesis, endothelial hyperplasia and increased permeability in the brain [122], there are only few specific data available concerning the functional role of pericytes on BBB properties [123,124]. This lack of information is partially justified by the difficulty of extracting pericytes from the surrounding basal lamina and also by the necessity of combining multiple markers to attain an unambiguous identification [55,125]. Nonetheless, it was currently revealed that pericytes regulate

specific BBB-gene expression patterns in CECs and induce the polarization of astrocytic end-feet, coordinating the bidirectional signalling between cells of the neurovascular unit [126]. Moreover, brain pericytes may be directly or indirectly involved in several CNS pathologies, making them increasingly considered as potential drug targets [111,124,127–129]. For instance, pericytes display marked alterations in ischemia and targeting pericyte responses may provide a new therapy for ischemic stroke [130].

I.3.2.4. Microglia and neurons

Microglia, also known as cerebral perivascular macrophages, are the resident immunocompetent cells of the brain [96,131]. They control innate and adaptive immune responses in the brain [104] and may modulate specific BBB properties by regulating TJs and consequently, the paracellular permeability [131].

Although few data are available on the effect of neurons on BBB properties [132], it was found in a co-culture cell model that neurons induce CECs to synthesize and sort occludin to the cell periphery [133]. This was later confirmed in a triple co-culture cell model with CECs, neurons and astrocytes, indicating a synergistic effect in the stabilization of TJs [134]. Therefore, the association of neurons with the cerebral vasculature is important during BBB development stages and also for its maintenance [135].

I.3.2.5. Extracellular matrix

The ECM is a non-cellular component of the neurovascular unit, fundamental for the maintenance of barrier properties and improvement of the integrity of the BBB [136]. It resembles a net-like structure that provides anatomical and biochemical support to the attached cells, by connecting and functionally separating CECs from astrocytes and pericytes [82,136]. The ECM is composed of glycosaminoglycans (e.g. hyaluronic acid, chondroitin sulfate, heparan sulfate), proteoglycans (e.g. chondroitin sulfate proteoglycans or lecticans, heparan sulfate proteoglycans), glycoproteins (e.g. laminin, fibronectin, tenascins) and collagen (collagen IV, XV, XVII) [82]. Essentially, three types of ECM prevail: perineuronal nets localized at neuronal bodies, axosomatic synapses and proximal dendrites; percapillary matrices, also known as basement membrane or basal

lamina, surrounding CECs; and the interstitial matrix of the stroma that binds cellular layers [55,82]. Interestingly, alterations in physiological conditions such as ageing, and psychiatric and neurological disorders modify ECM expression, indicating that ECM modifications may be an important part of pathophysiological changes in the brain [137].

Several functions have been attributed to the ECM, namely the induction of TJ biogenesis, an increased expression of AP and γ-glutamyltranspeptidase, P-gp regulation [138], neuron protection against pathological changes induced by amyloid-β and oxidative stress [137], storage of various proteins of the interstitial system like chemokines, neurogenesis guidance [82] and the coordination of cell physiology through the release of growth factors within the matrix [136]. Cell-cell and cell-matrix interactions of the BBB are mediated by two main receptors or adhesion molecules, dystroglycan and integrins. Dystroglycans are present in astrocytes, neurons and CECs while integrins are found in all cells involved in BBB formation. In addition to the management of signalling pathways that enable cell adaptations to the microenvironment, those matrix receptors form a link between the ECM and the cytoskeleton, which influences cell migration, proliferation, differentiation and survival [139].

The inclusion of ECM components in *in vitro* cell-based BBB models has greatly contributed to the improvement of the tightness and barrier integrity of those models [136], as referred in subsequent section I.3.4.2.2.

I.3.3. BBB EVOLUTION IN HEALTH AND DISEASE

The BBB is a dynamic interface that undergoes several physiological changes throughout life, from initial development to advanced age, as well as, alterations that result from pathological conditions.

BBB development begins with angiogenesis when endothelial progenitor cells invade the embryonic neuroectoderm and originate new vessels. This occurs because neuroectoderm cells release vascular endothelial growth factor, which directs vessel sprouting [140]. The next maturation steps of CECs in vascular sprouts involve a cross-talk with molecular elements of the forming CNS [141]. Neural progenitor cells secrete

molecular signals that cause the migration of endothelial cells into the embryonic neural tissue. Then, the endothelial cells are incorporated into nascent vessels and release platelet-derived growth factor-B, thereby promoting the recruitment of pericytes to immature vascular structures [141,142]. Initially, it was thought that astrocytes were responsible for the induction of post-natal BBB properties, but Daneman et al. [143] demonstrated that pericytes were recruited to nascent vessels a week prior to astrocyte generation. Thus, it was postulated that pericytes are more important for BBB formation during development, whereas astrocytes are required for BBB maintenance and response to neural function and disease. After adhering to CECs, pericytes deposit ECM components, leading to the formation of the basal lamina [140] and inhibit the expression of molecules that increase vascular permeability and CNS immune cell infiltration [143].

Interestingly, CECs already express TJ proteins such as occludin and claudin-5 during the CNS invasion. Nevertheless, these strands undergo full maturation during embryogenesis [142]. Interactions between CECs, pericytes and astrocytes contribute to the strengthening of the paracellular barrier and BBB tightening [140]. Moreover, BBB maturation also encompasses an increased expression of efflux transporters, which has been observed in the third post-natal week [142].

In addition to the modifications that take place during BBB development and maturation, other examples of physiological states that alter BBB characteristics include pregnancy, physical exercise and ageing. For instance, pregnancy has been associated with an increase of BBB permeability as a result of hemodynamic changes in the brain. It does not appear to be related with differences of TJ expression, but with a higher hydrostatic pressure on the BBB [144]. Similarly, moderate and high-intensity physical exercise on the treadmill led to an increase of BBB permeability in healthy men as consequence of higher oxidative stress, in opposition to low-intensity physical exercise [145]. In rats, it was observed that light treadmill exercise had protective effects on cognitive impairment derived from BBB disruption, as a result of chronic cerebral hypoperfusion [146].

Before examining BBB alterations underlying ageing, it is important to define physiological ageing as a deterioration of functions without cognitive decline or

dementia [147]. Briefly, the main age-related differences observed in humans encompass an increase in capillary wall thickness, accompanied by a decrease in number of CECs and respective mitochondria; a reduced expression of TJs and P-gp; accumulation of ECM components and an increase of the thickness of the basal lamina; production of neurotoxic pro-inflammatory mediators by microglia; degeneration and loss of pericytes; and deterioration of neuronal plasticity with increased apoptosis [147,148]. Reports on astrocytic modifications during ageing are varied. Some authors affirm that astrogliosis takes place with ageing, i.e. an augmented proliferation and reactivity of astrocytes characterized by a higher expression of GFAP, as a response to an inflammatory and oxidative state [149]. In parallel, other authors describe a loss of astrocytic end-feet contact with CECs in aged mice, caused by a depletion of AQP-4 [150] as well as, an accumulation of iron in astrocytes that can generate free radicals and harm cells [151]. Although there are controversial data, ageing has been associated with a higher permeability of the human BBB, according to a meta-analysis of 31 studies with 1953 individuals [152]. Indeed, albumin extravasion has been observed, together with increased brain leakage. It is believed that this leakiness may play a role in the development of age-related dementias [153]. There are several studies in literature concerning the effect of physiopathological conditions on the BBB, particularly in Alzheimer's disease and less in PD, but also in epilepsy, multiple sclerosis, schizophrenia, depression and hypertension [148,154].

To this day, very little is known about role of the BBB in PD. Initially, it was speculated that the BBB remained intact during PD due to the successful use of aromatic aminoacid decarboxylase (AADC) inhibitors, which will be analysed more methodically in section I.4.1 of this dissertation. AADC inhibitors like carbidopa and benserazide were developed to increase the availability of levodopa (L-DOPA, L-3,4-dihydroxyphenylalanine) to the brain by preventing its peripheral conversion to dopamine. This means that if the BBB was compromised, the AADC inhibitors would cause central inhibition and prevent the formation of dopamine in the brain, thereby reducing the potency of L-DOPA [155]. Notwithstanding, studies found that benserazide does inhibit central AADC in the rat at 10 mg kg^{-1} which, according to the authors, indicates BBB breakdown in PD [155,156]. Furthermore, modifications of [^{11}C]-verapamil brain uptake were also reported in patients with early-stage or advanced-stage PD, in

different brain regions. In early-stage PD, a lower uptake of [^{11}C]-verapamil was observed in midbrain and frontal regions, whereas in late-stage PD, a higher uptake was verified in frontal white matter regions. Therefore, it has been suggested that there may be a regional up-regulation of P-gp in early-stage PD and a down-regulation of P-gp in late-stage PD [157]. This P-gp dysfunction may be a part of PD pathogenesis by facilitating the entrance of neurotoxins to the brain [158]. Another possible cause that has been explored for PD pathogenesis is the passage of metals through the BBB, namely iron [151], explaining the current interest in iron-chelating therapies for PD [159].

In pharmacoresistant epilepsy, the overexpression of ABC transporters at the BBB is well-known [147]. Other epilepsy-related BBB modifications that have been investigated encompass a decrease in TJ expression, TJ opening and albumin extravasion [148], important indicators of BBB leakage. Indeed, cerebrovascular dysfunction is one of the mechanisms behind seizure activity and epilepsy perpetuation, however it is thought to extend beyond BBB breakdown and may also imply an impaired CSF-ISF circulation. Changes in CSF-ISF can affect the pharmacology of antiepileptic drugs through the impediment of drug distribution as a result of a reduced ISF flow, or through the potentiation of side-effects caused by decreased brain clearance. Therefore, BBB damage, an increased vascular permeability and pathological changes in ISF-CSF circulation can be synergistically involved in the pathogenesis of neurological diseases [160].

In fact, cerebrovascular dysfunction has not only been associated with epilepsy but is acknowledged to play a role in several neurological diseases [161]. Chronic hypertension is a common cause of BBB lesions, given that it impacts the structure of blood vessels and particularly the arterioles that deliver blood to central regions of the brain. The vascular remodelling caused by hypertension modifies not only the vessel wall but the surrounding ECM as well, leading to blood vessel fibrosis, vascular stiffening, cerebral blood flow impairment and ultimately, hypoperfusion and hypoxia. In turn, hypoxia triggers neuroinflammation, which activates the release of proteases by microglia that open the BBB by loosening TJs and breaking down the basal lamina [162]. Similar consequences have been found in rats with acute hypertension, namely BBB breakdown and an increase of brain microvascular permeability [163]. Another proposed

mechanism for BBB disruption in hypertension was the elevated circulating levels of angiotensin-II, which contribute to an exacerbated sympathoexcitation [164]. Nevertheless, in spite of the described neuroprotective effects of angiotensin-II blockers, inclusively of the BBB [165] a recently conducted study with candesartan (and ursodeoxycholic acid) failed to prevent the deterioration of BBB integrity and cognitive function in dietary-induced obese mice, even though blood pressure was successfully reduced [166].

I.3.4. *IN VITRO* BBB MODELS

Despite being well-known that no simple *in vitro* model can mimic all BBB functionalities [167], it is consensual that the model must possess at least the most relevant features of the BBB that interfere with the particular aim of the investigation. For instance, for an *in vitro* model to be appropriate for screening compounds according to their BBB permeability, it should possess low paracellular permeability and express key enzymes (e.g. AP) and carrier systems [e.g. L-type aminoacid transporter 1 (LAT1)] [99,168]. In general, *in vitro* models ought to gather as many BBB characteristics as possible, but remaining time practicable and feasible for high- to moderate-throughput screening [118]. Up to date, no specific *in vitro* BBB model has been adopted by pharmaceutical industries as the ‘‘gold standard’’ and therefore, developing more reliable models to test BBB permeation remains a current challenge [167]. Until then and whenever possible, combined approaches with distinct *in vitro* models should be applied for rationalizing and optimizing the evaluation of brain penetration during CNS drug discovery.

The principal advantages of the *in vitro* models, particularly in comparison with the *in vivo*, include the higher throughput capacity, the lower cost and lower amount of compound that is required, the ability of quantifying compounds directly in physiological buffer, the possible identification of early signs of cell toxicity and the lower number of necessary animals [169]. Importantly, *in vitro* BBB models also provide mechanistic information [67] by unravelling the complex molecular interactions that regulate the permeability of CECs under normal and pathological conditions [170]. Hence, these models can be used not only for permeability and transport assays, but also to elucidate

drug interactions at the BBB [171] and perform physiopathological [172], toxicological [173] and immunological studies [174].

I.3.4.1. Non-cell based surrogate models: parallel artificial membrane permeability assay

The parallel artificial membrane permeability assay (PAMPA) was firstly introduced by Kansy et al. [175] as a high throughput method able to predict the gastrointestinal absorption of drugs by transcellular passive diffusion. Since then, it has been adapted to mimic other biological membranes, including the BBB [176]. Succinctly, PAMPA uses a multi-well system in which the donor and the acceptor compartments are separated by a porous filter where a lipid artificial membrane is incorporated. During the incubation period, compounds move from the donor to the acceptor compartment by crossing the lipid membrane. Afterward, they are quantified in both compartments to determine the apparent (Papp) or effective permeability (Pe). Although the initial development of PAMPA targeted the evaluation of the intestinal permeability of compounds, modifications in the composition of the lipid solution resulted in PAMPA models capable of differentiating compounds that cross the BBB from those that do not [177]. The main characteristics of the PAMPA models that have been published for predicting the BBB permeability are summarized in Table I.5.

Di et al. [178] developed the first modified PAMPA model that adequately predicts the BBB permeation. A solution of porcine brain lipids (PBL) dissolved in dodecane was incorporated in the PAMPA filter to mimic the BBB. According to the experimentally determined Pe values, compounds were classified as CNS+ (high BBB permeation), CNS- (low BBB permeation) or CNS+/- (uncertain BBB permeation) and their Pe values were then plotted against literature data to identify false positives and false negatives. Few false positive and negative outliers were detected [178]. The false negatives were compounds transported by paracellular passive diffusion and substrates of influx transporters, whereas false positives were substances that undergo active efflux extrusion *in vivo* [179]. Interestingly, this PAMPA-PBL assay achieved better outcomes than the model using pIon membrane lipid (PML) (i.e. phosphatidylcholine in dodecane), because the PML model underestimated the permeability of three CNS+ compounds and

exhibited considerably more false negatives probably due to the cerebral origin of PBL, which mimics the lipid composition of CECs more closely [178].

Since then, several variations in this method have been developed to evaluate the BBB permeability properties of different drug candidates, which were mostly directed for the treatment of neurodegenerative diseases [180–189], obesity [190], stroke [191] and also spinal cord injury [192]. Recently, a PAMPA assay was adapted specifically to assess the BBB penetration of pharmacologically active natural products and plant extracts [193] and also natural and semi-synthetic ecdysteroids for the treatment of CNS tumours [194]. Apart from the lipid used to mimic the BBB, other experimental features have been changed throughout the development of those methodologies, particularly the solvent in which the lipid is dissolved, the composition of buffer solutions, the stirring conditions and the incubation time (Table I.5). It is noteworthy that nearly all studies were performed maintaining the pH of the donor and acceptor compartments at 7.4, which corresponds to the physiological pH of the blood, as initially defined by Di et al. [178].

Table I.5. Main characteristics of PAMPA models developed with the intention of predicting the blood-brain barrier permeability.

PAMPA	Donor compartment	Acceptor compartment	Lipid solution	Incubation time	Stirring	Predictive ability	Ref.
PAMPA-BBB	100 µM solution in PBS pH 7.4	PBS pH 7.4	10% (w/v) PBL in dodecane-hexane (3:1) (5 µL)	4 h	Yes	r^2 = 0.84 (*n* = 27)	[195]
PAMPA-BBB	100 µM solution in PBS pH 7.4	PBS pH 7.4	27 mg mL^{-1} PBL and 13 mg mL^{-1} cholesterol in dodecane (5 µL)	4 h	No	r^2 = 0.72 (*n* = 43)	[193]
PAMPA-BBB	250 µM solution in PBS pH 7.4	PBS pH 7.4	20 mg mL^{-1} PBL in dodecane 20 mg mL^{-1} phosphatidylcholine in dodecane (4 µL)	2 h / 5 h / 8 h / 16 h / 24 h	No	r^2 = 0.95 (*n* = 16) r^2 = 0.93 (*n* = 16)	[196]
PAMPA-BD PAMPA-BBB I PAMPA-BBB II	50-150 µM solution in NaOH-treated universal buffer	BSB pH 7.4 with scavenger BSB pH 7.4 BSB pH 7.4	4% (w/v) DOPC in hexadecane (1 µL) 10% (w/v) PBL in an alkane (1.5 µL) 10% (w/v) PBL in an alkane (3 µL)	30-60 min for lipophilic compounds 15 h for hydrophilic compounds	No Yes Yes	PAMPA-BBB II: r^2 = 0.84 (*n* = 85 weak base compounds)	[197]
PAMPA-BLM PAMPA-DS PAMPA-BBB PAMPA-BBB-UWL	90% of the TS of compounds in universal buffer pH 7.4	Universal buffer pH 7.4 Universal buffer pH 7.4 with surfactant Universal buffer pH 7.4 Universal buffer pH 7.4	2% (w/v) DOPC in dodecane 20% (w/v) soy lecithin in dodecane 20 mg mL^{-1} PBL in dodecane 20 mg mL^{-1} PBL in dodecane (4 µL)	18 h 4 h 18 h 1 h	No No No Yes	PAMPA-BLM: r^2 = 0.73 (*n* = 14) PAMPA-BBB: r^2 = 0.63 (*n* = 14)	[177]
PAMPA-BBB	500 µM solution in PBS pH 7.4	PBS pH 7.4	20 mg mL^{-1} PBL in dodecane-hexane (5 µL)	2 h	Yes	Validation: 26 compounds (26/34) correctly predicted.	[198]
PAMPA-BBB	1 mg mL^{-1} solution in PBS:ethanol (70:30) pH 7.4	PBS:ethanol (70:30) pH 7.4	20 mg mL^{-1} PBL in dodecane (4 µL)	2 h	No	r^2 = 0.97 (*n* = 10)	[190]
PAMPA-BBB PAMPA-PML	25 µg mL^{-1} solution in universal buffer pH 7.4	universal buffer pH 7.4	20 mg mL^{-1} PBL in dodecane 20 mg mL^{-1} phosphatidylcholine in dodecane (4 µL)	18 h	No	PAMPA-BBB: 31 compounds (31/33) correctly predicted. PAMPA-PML: 24 compounds (24/33) correctly predicted.	[178]

BBB, blood-brain barrier; BD, BD Biosciences; BLM, black lipid membrane; BSB, brain sink buffer; DOPC, dioleoylphosphatidylcholine; DS, double sink; PAMPA, parallel artificial membrane permeability assay; PBL, porcine brain lipids; PBS, phosphate buffer saline; PML, pIon membrane lipid; TS, thermodynamic solubility; UWL, unstirred water layer.

Notwithstanding, Tsinman et al. [197] varied the pH of the donor compartment in order to collect data under gradient conditions and characterize the contribution of the lipid membrane to permeability; however, this approach decreased the throughput of the PAMPA model and hence, it was recommended to conduct the assays at pH 7.4.

Moreover, the influence of the organic solvent in which the lipid is dissolved, on the permeability of PAMPA was evaluated by Carrara et al. [198] and it was noted that for borderline compounds with medium permeability, the dodecane-lipid ratio was able to shift CNS- compounds to CNS+.

In order to maximize the PAMPA throughput, the method should be as fast as possible, which can be achieved by reducing the incubation time. As depicted in Table I.5, the incubation time varies between 1 h and 24 h and depends on the lipophilicity of the compounds. An artifact that has been applied to attain this, particularly for lipophilic compounds, consists on stirring the PAMPA plates under constant agitation. Theoretically, this will decrease the thickness of the unstirred water layer (UWL), which hampers the transport of lipophilic molecules [199]. Indeed, Tsinman et al. [197] utilized vigorous stirring conditions for highly lipophilic compounds, to reduce the thickness of the UWL to 60 μm. However, this type of stirring is not recommended for less lipophilic compounds, because it may increase the aqueous channel porosity of the PBL membrane and allow some aqueous paramembrane diffusion of the compounds. This partially explains the lack of discrimination between BBB permeable or non-permeable compounds in the PAMPA-BBB-UWL model developed by Mensch et al. [177], in which all compounds, more or less lipophilic, were subjected to stirring. Similarly, Jhala et al. [196] studied the influence of the incubation time in two PAMPA-BBB models and did not observe differences in the permeability values after 5 h of incubation.

Overall, the predictive ability of PAMPA is reasonably good and in particular for compounds that cross the BBB by transcellular passive diffusion, considering that misclassified molecules are usually substrates of influx or efflux transporters such as P-gp or BCRP. In fact, the artificial lipid membranes used in PAMPA models do not include influx nor efflux transporters and particularly, the absence of efflux multidrug ABC transporters is one of the most significant limitations of PAMPA. This drawback may ultimately lead to the overestimation of the *in vivo* permeability of compounds that would otherwise be actively pumped out of the brain. Hence, PAMPA is considered a

high throughput, low cost and reproducible method that has a high power for predicting the *in vivo* BBB permeability of compounds that passively diffuse across the BBB [176–178]. To improve PAMPA results and overcome its limitations, cell-based models are often integrated as additional screening tools [200].

I.3.4.2. Cell-based models

Although the use of cell-based models for studying the BBB began with the isolation of brain capillaries [201], firstly from human and bovine brain [202] and then from rat brain, nowadays, brain microvessels can be obtained and purified from other species, including rabbit and pig [113]. Nevertheless, this technique is not suitable for permeability screening purposes [170]. In fact, the difficult access to the luminal surface of the vessels [203] makes the compounds reach the microvessels from the abluminal side, which is the opposite of the *in vivo* situation [204]. This limitation, along with the different expression and localization of transporters caused by the preparation procedures [113], led to the development of alternative approaches to mimic the BBB based on *in vitro* cell culture models.

In vitro cell culture models started to emerge just five years after the first isolation of cerebral microvessels, when it was found that CECs grew out of brain capillaries under adequate culture conditions [205]. As the accessibility of a drug from the blood into the brain is controlled by the drug permeation rate across the tight layer of CECs, several cell culture models have been developed to reconstitute the BBB *in vitro*. Interestingly, according to Tóth et al. [205], eight *in vitro* cell-based models of the BBB were patented between 1990 and 2010. These systems may incorporate cells of non-cerebral origin or CECs from primary cultures or cell lines, in monoculture, co-culture or triple co-culture configurations with other cells of the neurovascular unit, as further explored in the next sections.

Although *in vitro* culture models of BBB possess numerous advantages comparatively to *in vivo* studies such as cost-effectiveness, high to moderate throughput screening, versatility and the possibility to reproduce pathological abnormalities, there are serious drawbacks associated to the artificial environment under which the cells are cultured. The lack of exposure to physiological conditions may result in a different

expression of relevant cell biological transporters, ligands and enzymes [206]. Thus, cell culture models ought to fulfil certain criteria to be utilized for the screening of potential CNS drugs. Notwithstanding, *in vitro* findings must be firstly validated and compared with *in vivo* data to ensure their accuracy.

Briefly, *in vitro* permeability assays are carried out in multi-well plates, where two compartments simulating the blood (apical) and brain (basolateral) sides are separated by a microporous filter on which the cells are seeded, developing a cell monolayer that contacts with different culture media in each compartment (Figure I.8). The filters most frequently used include the Transwell™ polycarbonate or polyethylene terephthalate inserts. Polycarbonate inserts are suitable for permeability studies of hydrophilic and lipophilic molecules due to their low non-specific binding properties, whereas transparent polyethylene terephthalate inserts allow the microscopic observation of cell monolayers and have a very good biocompatibility [207,208].

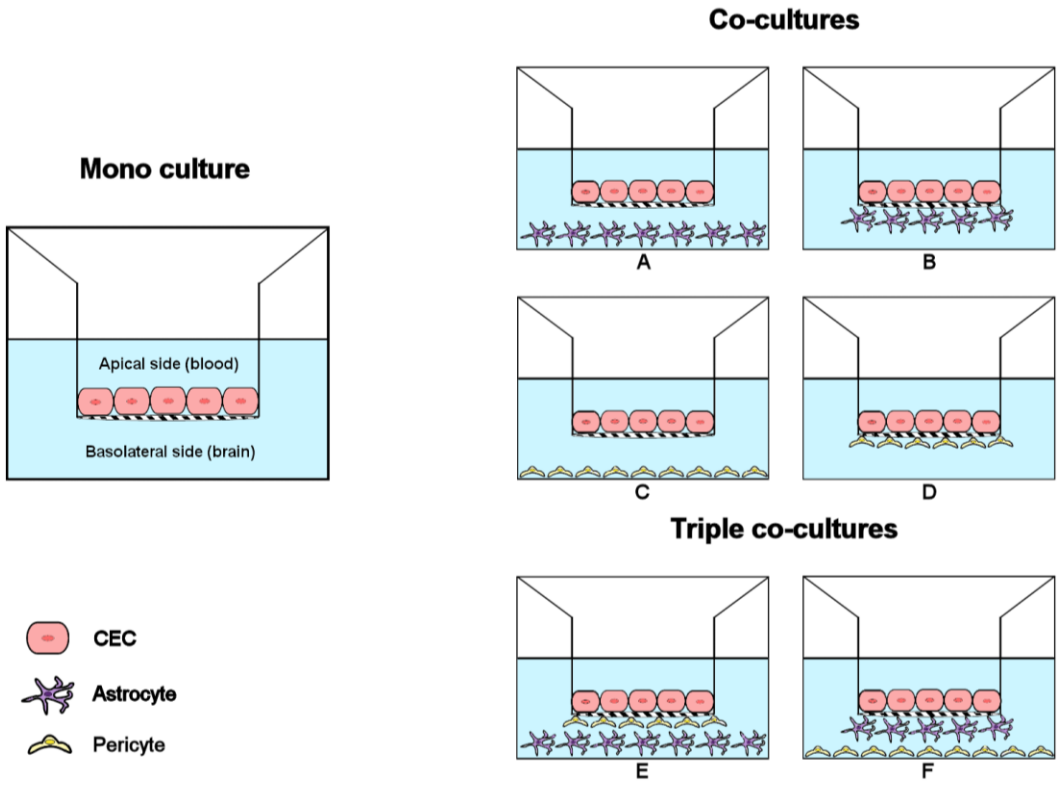

Figure I.8. *In vitro* cell-based blood–brain barrier models. Monocultures of cerebral endothelial cells (CECs) are being replaced by co-culture or triple co-culture systems, in which CECs are seeded with other elements of the neurovascular unit, such as astrocytes, pericytes or neurons, in a non-contact (A,C) or contact format (B, D). In triple co-culture systems, more than one cell type is seeded with CECs (E, F).

In *in vitro* models, the paracellular diffusion of compounds between endothelial cells must be limited by TJs in order to make the model discriminative. As it was mentioned in section I.3.2.1, TJs dictate the permeability by paracellular route and therefore, this feature should be assessed by measuring the TEER or evaluating the permeability of tracer hydrophilic substances with known molecular weight [103].

TEER is an indicator of the tightness of the CEC monolayer and, indirectly, of the paracellular permeability and BBB integrity. For a cell culture model to be considered adequate, the cell layer should display a sufficiently high TEER value and a low Papp for the specific molecules used as integrity markers [209]. To evaluate the TEER of the cell monolayer, a voltage-measuring electrode is placed in each compartment; the resistance data read in the apparatus are then corrected for blank filter resistance (cell free filter), multiplied by the filter surface area and expressed in $\Omega\ cm^2$ [123,210]. It is estimated that the *in vivo* TEER of brain microvessels exceeds 1000 $\Omega\ cm^2$ in frog and rat [211–213], but an *in vitro* TEER of at least 150–200 $\Omega\ cm^2$ has been considered sufficient for assessing solute and drug transport [132,168,205]. Nevertheless, some cell-based models may achieve superior values of TEER.

To be used as a marker of the paracellular transport, the tracer compound should not be a ligand for influx or efflux transporters, endothelial receptors or a substrate for endothelial enzymes [132]. Sodium fluorescein (Na-F) [172,214–216], lucifer yellow [217–219] and fluorescein isothiocyanate (FITC)-labelled substances, such as FITC inulin [220], FITC-dextrans [207] and FITC-bovine serum albumin [210] are frequently used as tracers, as well as, radiolabeled sucrose, inulin, albumin [221] and mannitol [222]. In contrast, propranolol is often utilized as a transcellular marker due to its lipophilic nature [223]. The *in vitro* transepithelial permeability coefficients ($cm\ s^{-1}$) of marker molecules should be determined before and after the permeability studies performed with the test compounds, in order to monitor the integrity of the monolayer and confirm that the test compound itself did not affect the barrier properties [123,220].

I.3.4.2.1. Primary cultures and immortalized cell lines of cerebral origin

Primary CECs provide the closest phenotypic resemblance to that of the *in vivo* BBB [170], because many of their characteristics are genetically programmed [102]. These

cells may be harvested from bovine [131,224,225], porcine [210,226–229], rat [215,230–233], mouse [234–237] or human [131,231,238,239] sources and are frequently utilized for the development and optimization of *in vitro* BBB models. Nevertheless, their generalized use is prevented by some important limitations depicted in Table I.6.

Table I.6. Advantages and disadvantages of the use of primary cultures and immortalized cell lines of cerebral endothelial cells as *in vitro* models of the blood-brain barrier.

	Sources	Advantages	Disadvantages		Refs.
Primary cultures	Bovine	Allow the isolation of a large amount of cells from a single brain.	Difficult to establish *in vitro-in vivo* correlations.	Complex, time consuming and labour intensive cell obtaining processes; Inconvenient for routine industrial use; High irreproducibility of the final characteristics of the cell population; Challenging to eliminate non-endothelial cells (e.g. pericytes, smooth muscle cells); Rapid *in vitro* de-differentiation or loss of phenotype.	[240]
	Porcine				
	Rat	Availability of BBB permeation data from *in vivo* pharmacokinetic studies.	Low yield; Require the sacrifice of multiple animals; Ethical and economic constraints.		[215,227,241]
	Mouse				[242]
	Human	Important tool for the study of the BBB at a cellular and molecular level, including BBB dysfunction.	Low yield; High costs; Difficult to obtain reliable sources of healthy tissue; Batch-to-batch variability.		[168,240,243]
Cell lines	Bovine: *t-BBEC-117*	Exhibits the formation of TJ-like structures; Expresses endothelial markers (acLDL uptake), influx (GLUT-1) and efflux transporters (P-gp) and functional endothelial - specific enzymes (AP).	Leaky; Not restrictive enough for permeability studies (i.e. low TEER values and high permeability of paracellular tracers); Difficult maintenance of transporter function and enzymatic activity; Require further characterization.		[244]
	Porcine: *PBMEC/C1-2*	Expresses endothelial markers (vWF), influx (GLUT-1) and functional efflux transporters (P-gp) and functional endothelial-specific enzymes (AP, γ-GTP)			[245–248]

Table I.6. *Continued*

Sources	Advantages	Disadvantages	Refs.
Rat: *RBE4* *RBE4.B*	Express TJ proteins (e.g. occludin), influx (GLUT-1, LAT1) and functional efflux transporters (P-gp) and functional endothelial-specific enzymes (AP, γ-GTP)		[133,203,248–250]
Mouse: *b.End3* *b.End5*	Express endothelial markers (vWF), TJ proteins (e.g. occludin, claudins -1,-5, ZO-1) functional influx (e.g. GLUT-1, LAT1) and efflux transporters (P-gp), and functional endothelial-specific enzymes (AP); Commercially available.		[251–257]
Human: *hCMEC/D3* *BB19* *NKIM-6* *TY08* *HBMEC/ciβ*	*hCMEC/D3:* Exhibits a non-transformed phenotype over several passages; Expresses endothelial markers, TJ proteins (e.g. claudin-5, ZO-1), functional efflux transporters (e.g. BCRP, P-gp) and CYP genes.		[243,258–265]
	BB19, NKIM-6, TY08, HBMEC/ciβ: Express endothelial markers (vWF), TJ proteins (e.g. ZO-1) and efflux transporters (BCRP, P-gp).	*NKIM-6*: low expression of occludin and does not express claudin-5.	[223,266–268]

BCRP, breast cancer resistance-associated protein; acLDL, acetylated low density lipoproteins; AP, alkaline phosphatase; BBB, blood-brain barrier; CECs, cerebral endothelial cells; CYP, cytochrome P450; GLUT-1, glucose transporter-1; γ-GTP, γ-glutamyltranspeptidase; LAT1, L-type aminoacid transporter 1; P-gp, P-glycoprotein; TEER, transendothelial electrical resistance; TJ, tight junction; vWF, von Willebrand factor VIII related antigen; ZO, zonula-occludens. The common disadvantages of primary cultures and immortalized cell lines were adapted from references [91,132,133,176,206,215,219,249].

In order to circumvent the disadvantages of primary cultures, several immortalized CEC lines were created with the potential to provide a stable source with high yield and homogeneity throughout numerous passages [251]. Commercially available cell lines are increasingly used to their reliability, since they are acquired from trusted sources; consistency, as the inter-batches variability is minimal; longevity, resulting from the fact that immortalized cell lines are specially treated by transfection processes so that their

specific characteristics do not disappear over the time; and efficiency, which is related to a reduced preparation time and cost [241]. However, immortalized CEC lines are generally leakier than primary cultures (Table I.6), which strongly limits their use for permeability screenings. Despite preserving basic cerebral endothelium-like features, the absence of other elements of the neurovascular unit, the lack of physiological stimuli and the immortalization process itself, affect the expression level of TJs, enzymes and transporters from the SLC and ABC families [258]. Nonetheless, they have proved useful for other applications, such as mechanistic and biochemical studies of the BBB under physiological or pathological conditions and for the design of CNS-targeted drug delivery systems [168,249].

Currently, there is an interest in the development of *in vitro* BBB models from human pluripotent stem cells, submitted to an endothelial and neural co-differentiation process [259,269,270]. Although further validation is recommended, it appears to be a promising alternative for drug permeability screening studies.

I.3.4.2.2. Induction of BBB properties in endothelial cells

Several strategies have been outlined throughout the years to achieve a better representation of the *in vivo* BBB and improve barrier function in cell culture, particularly with CECs. Among these advances is the development of co-culture and triple co-culture systems.

It was previously referred in section I.3.2.1 that all elements of the neurovascular unit strongly contribute to the development and maintenance of the BBB phenotype. Consequently, co-culture and triple co-culture systems have been implemented through the combination of primary or immortalized cell lines of CECs with astrocytes, astrocytic cell lines, C6 glioma cell lines, pericytes, mixed glial cells and/or cell-conditioned media (Table I.7 in Appendix A). Some co-culture models use cells from different species, while others, named syngeneic models, incorporate cells from the same species to avoid interspecific non-recognition problems [132,271]. Different co-culture systems and possible orientation formats are represented in Figure I.8.

In contact co-cultures, astrocytes or glial cells are seeded in close proximity with endothelial cells at the opposite site of the filter membrane, whereas in non-contact co-

cultures, these cells are seeded on the bottom of the wells [209]. At this point it is important to highlight that the properties of Transwell™ membranes such as thickness, pore size and density and filter coating determine whether the inter-cell contact occurs [236]. Wuest et al. [272] recently investigated the influence of pore size, membrane material and contact/non-contact orientations for a co-culture model with mice CECs and rat astrocytes. A higher TEER was obtained for cells seeded in a non-contact orientation and filters with a pore size of 0.4 µm. This pore size is also considered appropriate for restricting astrocyte cell bodies to the seeded side, while allowing astrocytic end-feet to pass through the pores and interact with endothelial cells seeded on the opposite side [273]. Interestingly, this corroborates previous results obtained in contact co-cultures, in which a lack of induction of BBB properties in CECs was observed, because the pores became clogged by astrocytic end-feet, and hence, blocked the passage of astrocytic soluble factors, promoting an incomplete extension of astrocyte foot processes to the endothelial side [236,271,274]. When 3.0 µm pores were applied, the entire cellular body reached the opposite side, promoting the astrocytes growth on both sides of the membrane [271,274].

Variations in TEER and responsiveness to astrocytes may additionally be caused by the coating substrate of the Transwell™ filters [174]. This substrate serves as a replacement of the ECM, which is involved in cell differentiation and the formation of a functional barrier [275], as stated in section I.3.2.5. Type IV collagen, fibronectin and laminin are major components of the basal lamina [276], however rat tail collagen type I is frequently used alone or in combination with type IV collagen (Table I.7 in Appendix A). The experimental results obtained with different combinations of these proteins are conflicting [240,277], which indicates a need for further research of this aspect.

It is well-known that astrocyte-derived soluble factors secreted into the culture medium are responsible for the induction of a BBB phenotype on endothelial cells [278–280]. Therefore, conditioned media, which include the astrocyte conditioned medium and the C6 conditioned medium, collected from growing astrocyte cultures and C6 glioma cultures, have been utilized to modulate TJ barrier properties regarding tightness and protein expression levels [245,278,281]. This artifact translates into higher TEER values [208,229,246,251,281], increased expression of ZO-1 [280], higher AP activity [240,244] and the induction of efflux transporters [208].

Upon cell confluence, growth medium is commonly replaced by differentiation, supplemented or assay mediums which are often serum-free in order to improve and preserve the differentiation of CECs (Table I.7 in Appendix A). Although serum is added to culture media to promote cell proliferation, a negative effect on the barrier properties of the endothelial monolayer was observed [282], probably due to serum-derived factors, such as vascular endothelial growth factor and lysophosphatidic acid, that inhibit the formation of TJs or/and open already established TJs [228]. The absence of serum leads to a displacement of TJ proteins from the cytoplasm to the cell borders and increases the tightness of the monolayer [253]. In fact, removing serum from the culture media in the basolateral compartment of the *in vitro* model will mimic the physiology of the BBB more closely, as the basolateral surface of the brain microvascular endothelium is exposed *in vivo* to serum-free ISF [283].

In addition to serum-free conditions, culture media are often supplemented with hydrocortisone to increase the tightness of the CEC monolayer. Nonetheless, the exact mechanism by which it stimulates the formation of barrier properties is unclear. Alternations in cell morphology and elasticity, namely the reorganization of the cytoskeleton of CECs and cell–cell contact zones have been demonstrated [234,235], however the up-regulation of TJ protein expression has also been reported [284,285]. Other proposed mechanisms of action of hydrocortisone include an anti-apoptotic effect [230,286] and a protective effect on the endothelial glycocalyx [287].

Interestingly, it was observed that rat CECs treated with corticosterone or hydrocortisone alone, attained lower TEER values than those treated with glucocorticoids and puromycin. Puromycin-treated monolayers respond more favourably to glucocorticoid treatment, because CECs tend to maintain confluence, whereas cultures lacking puromycin exhibit gaps in the monolayer, either devoid of cells or filled with pericytes [230]. This purification method is applied in earlier culture steps to selectively eliminate contaminating cells from primary cultures of CECs [215].

Since the TJ resistance of CECs is regulated by second messengers, particularly 3’,5’-cyclic adenosine monophosphate (cAMP) [278], supplementing the culture medium with cAMP modulators, such as the cell-permeable cAMP analogue, 8-(4-chlorophenylthio)-cAMP (CPT-cAMP) has been applied to obtain TEER values similar to those observed physiologically. Indeed, when associated with RO-20-1724, a phosphodiesterase

inhibitor, CPT-cAMP increased the values of TEER in a wide variety of BBB models (Table I.7 in Appendix A). RO-20-1724 elevates the endothelial levels of cAMP by preventing its rapid metabolization and is consequently combined with CPT-cAMP in culture media to decrease the paracellular permeability [132,207,214,216,218,236,254].

Lastly, it is important to emphasize the incorporation of shear stress into cell culture through the development of tridimensional or dynamic *in vitro* BBB models. Shear stress is the force generated by blood flow, to which the apical surface of endothelial cells is constantly exposed *in vivo* [288,289]. CECs respond to shear stress by structural and functional remodelling. On the one hand, shear stress promotes the differentiation of CECs into a BBB phenotype, but on the other hand it inhibits their cell cycle and prevents their growth in a multi-layer way system [290–292]. Moreover, BBB tightness is increased through the up-regulation of TJ and AJ proteins, which leads to higher values of TEER than those observed in static Transwell™ models (Table I.7 in Appendix A) and induce the expression of ABC transporters and CYP enzymes [292]. For these reasons, different types of dynamic BBB systems have been developed, some of which are based on coated hollow fiber tubes inside a sealed chamber. This system is known as the hollow fiber apparatus where the fiber tubes represent the capillaries and the sealed chamber represents the extraluminal space [288–290]. Briefly, CECs are seeded intraluminally, while glial cells are seeded on the extraluminal space surrounding the capillaries and culture medium is pumped at a controllable rate. Santaguida et al. [293] adapted this concept into a new platform composed by a hollow fiber cartridge with a TEER monitoring system, whereas Siddharthan et al. [280] utilized a distinct flow system with a transparent chamber and a snapwell insert. Recently, Cucullo et al. [294] expanded the BBB module by adding a venule segment, thereby reproducing the physiology of cerebrovascular network, which may contribute to the development of new CNS therapeutic strategies. Despite the referred advantages, these systems have some limitations that prevent their disseminated use: cell growth cannot be evaluated directly and is assessed through the consumption of glucose or production of lactate; TEER measurements require a hardware adaptation [288,290,293] and a longer time is needed to reach steady-state TEER values [295]. So far, the developed dynamic BBB models are not yet compatible with the high throughput requirements of the pharmaceutical industry due to their high technical demands.

I.3.4.2.3. Cell lines of non-cerebral origin

Given the difficulties inherent to the lack of the tightness required to make cerebral cell lines suitable for BBB permeability screens, epithelial cell lines of non-cerebral origin have been utilized by several CNS discovery groups. The Madin–Darby canine kidney (MDCK) cell line, the human epithelial colorectal adenocarcinoma cell line (Caco-2) and the human urinary bladder carcinoma cell line (ECV304) are the most widely used. However, since these cells are neither endothelial nor cerebral, they exhibit distinct morphological characteristics from those of CECs and express peripheral organ-specific sets of membrane proteins [219] which may compromise their use as BBB models [170].

One of the greatest advantages of MDCK cells is that they are easy to grow, because they only require few days of culture to be ready for assays [176]. They can be transfected with the *MDR1* or *ABCG2* gene in order to polarize the expression of P-gp or BCRP and subsequently study the influence of P-gp or BCRP efflux through the BBB [170,176,296–298]. In a study by Garberg et al. [250] the MDCK-MDR1 cell line correctly identified all passively transported compounds and nearly all the effluxed compounds tested and hence, it was considered more discriminatory than other *in vitro* models, including a primary bovine and human CEC line co-cultured with astrocytes, a rat and mouse immortalized CEC line and other non-cerebral cell line models. Wang et al. [299] also investigated MDCK-MDR1 monolayers and examined their ability to identify P-gp substrates by measuring the bidirectional transport of 28 reference molecules. TEER was between 1800 and 2200 Ω cm^2 and, although integrity to paracellular markers was not evaluated, the model was considered discriminative.

The Caco-2 line was developed and has been extensively used for the prediction of drug intestinal absorption and permeation across physiological barriers. Nevertheless, comparative studies between Caco-2 cells and a co-culture of bovine CECs and astrocytes to predict the *in vivo* BBB permeability of compounds revealed weak correlations between Caco-2 data and *in vivo* BBB transport data (r = 0.68) [169]. Similarly, Lohmann et al. [300] observed differences in the drug permeability of seven compounds in Caco-2 cell monolayers and a primary culture of porcine CECs. This results from the non-endothelial and non-cerebral origin of Caco-2, which leads to a different expression and activity of transporter proteins [169,300]. Moreover, Hakkarainen et al.

[224] predicted the permeability of nine reference drugs using three *in vitro* models (i.e. MDCK-MDR1, Caco-2 and a primary culture of bovine CECs) and correlated the results with an *in vivo* method. All correlation coefficients were high, but the best correlation was given, as expected, by the primary bovine CECs (r = 0.99), followed by the Caco-2 (r = 0.91) and MDCK-MDR1 (r = 0.85) cell lines.

Hellinger et al. [301] developed a novel vinblastine-treated Caco-2 cell line (VB-Caco-2) which is characterized by expressing higher levels of P-gp than native cells and, therefore, an improved ability to identify P-gp substrates. Recently, a triple co-culture model of rat CECs, astrocytes and pericytes was compared with a MDCK-MDR1 model, a Caco-2 model and a VB-Caco-2 model using a set of ten compounds. Overall, the results achieved with rat triple co-culture BBB model were those with higher correlation with *in vivo* permeability data (r^2 = 0.79), while the VB-Caco-2 and MDCK-MDR1 models recognized a higher number of P-gp substrates. Consequently, these models have been considered valid alternatives for screening drug candidates for efflux transport, although the rat BBB model had the highest predictive value [219].

The ECV304 cell line was initially reported by Takahashi et al. [302] as a result of the spontaneous transformation of human umbilical vein endothelial cells (HUVECs). It began to be evaluated as part of the co-culture BBB models with the rat C6 glioma cell line [303,304] a glial cell strain cloned from a rat glial tumour. Nevertheless, several differences between ECV304 cells and HUVECs were observed, in simultaneous with a genetic similarity between ECV304 cells and the human bladder carcinoma epithelial cell line T24 [305,306]. During the attempts to establish the ECV304 line from HUVECs, the culture was most likely cross-contaminated and overgrown with T24 cells. Even so, ECV304 cells continued being used in BBB models for TEER dependent drug transport studies, due to the induction of BBB properties by co-culture with astrocytes or C6 cells and to the higher TEER values achieved by ECV304 layers, when compared with other BBB cell lines [307]. Barar et al. [308] studied the barrier functionality and plasma membrane features of ECV304 cells to assess their potential as a cell model for drug permeability screening, but the cells failed to form a discriminative tight barrier, even in the presence of modulators and were not recommended for this kind of assay. Moreover, Rodriguez-Gaztelumendi et al. [309] investigated the utility of the ECV304/C6 co-culture to study the influence of potentially toxic substances upon BBB function. It

was concluded that this model is of limited usefulness for both pharmacological and toxicological studies.

I.3.4.2.4. The BBB in microfluidic systems

In the latest years, the interest in using organs-on-chips or human vascular constructs to mimic human physiology has been growing, including for studies that involve the evaluation of drug efficacy and toxicity [310]. Indeed, several microfluidic-based cerebrovascular models are being developed with the purpose of achieving more physiological models on a miniaturized scale [311]. Besides allowing a precise control over local microenvironment [312], these systems enable the incorporation of shear stress, require fewer cells and reagents and provide a non-destructive microscopy of cellular interactions [313]. Furthermore, these devices possess thinner membranes than dynamic BBB models, which reduce the distance between co-cultured cells, and smaller functional volumes for quicker media exchange and material conservation [295]. Most platforms involve a polydimethylsiloxane-glass interface with a porous membrane at the intersection of two microfluidic channels but the focus on three-dimensional (3D) models is rising (Table I.8).

One of the main advantages of using 3D culture is the capacity to reproduce the hierarchical biological makeup of brain microvessels and/or more complex neurovascular units [311]. The encapsulation and culture of cells inside matrices in 3D cell culture helps cells retain their native tissue specific functions and mimic spatiotemporal chemical gradients and mechanical microenvironments [314]. While two-dimensional models are able to recapitulate some important aspects of neurovascular function, they fail to address the 3D organization that is fundamental to several *in vivo* cellular processes [315]. Conversely, optimizing a matrix with an *in vivo*-like architecture is a very complex process. Reconstituted matrices from animal sources are prone to variability between lots, which decreases reproducibility and may introduce contaminants [311]. Therefore, these matrices were replaced by synthetic materials like hydrogels [315].

Nonetheless, the development and application of BBB microfluidic devices also encounters some challenges. One of the greatest obstacles to the wider implementation

of these systems is the lack of compatibility with already existing infrastructures, methodologies and standard culturing techniques, such as micropipetting, plate readers and automated handling systems. Moreover, some models use brain cells from animal sources (Table I.8) which are not inexhaustible and may generate issues of scalability and cross-species translation of results [312]. Another set-back is related with the high initial establishment costs and technological expertise that is required for the design and operation of the devices [313], thereby hindering their large-scale applicability and constraining them to an academic context [312]. Lastly, the diversity of device designs, selected cell types and readout protocols demonstrates versatility, but complicates comparisons between models. Thus, it is necessary to define common standards in order to quantitatively assess the functionality of BBB microfluidic systems [316]. For all the aforementioned reasons, microfluidic BBB devices are not yet adaptable for HTS.

Table I.8. Examples of microfluidic devices to modulate blood-brain barrier function and their main features.

Device composition	Cell types	Advantages	Disadvantages	Refs.
PDMS device with two central 3D hydrogel regions (neural tissues) flanked by two media channels (blood vessel wall)	HUVEC or hCMEC/D3 Astrocytes from P0-P2 rat cortical tissue Neurons from E-18 rat cortical tissue	Different cell types display specific morphological characteristics; Functional neurons and endothelial cell barrier.	No pericytes or microglia; No shear stress; No TEER measurements; Astrocytes and neurons of non-human origin.	[315]
VeroClear photopolymer layers with PC membrane (0.4 µm pores); Top chamber represents neuronal chamber and bottom microchannel represents blood vessels	hBMECs Rat primary astrocytes	Includes shear stress (low level); Expresses BBB characteristics; Access to luminal and abluminal compartments allows drug administration and sampling.	No pericytes, neurons or microglia; Astrocytes of non-human origin.	[317]
PDMS layers separated by a porous PDMS membrane (5 µm pores); Top and bottom layers represent blood vessels and the neural tissue	hBMECs hNT2-derived neuronal-glial cell population	Cell line hNT2 reproduces essential features of human neurons and astrocytes; User-friendly, convenient; Expresses BBB characteristics.	No shear stress.	[312]
Two PDMS sheets and a porous PC membrane (0.4 µm pores); Top layer represents blood vessels and bottom layer contains 3D-cultured nerve cells	hCMEC/D3 U251 glioma stem-like cells	Includes shear stress; Allows the evaluation of BBB permeability and anti-tumor activity of CNS drug candidates; Time and sample volume can be decreased due to microscale.	No TEER measurements.	[314]
Two PDMS micro molded channels separated by a PTFE or PE membrane (0.4 µm pores); Top layer represents blood vessels and bottom layer contains 3D-cultured astrocytes	b.End3 Astrocytes C8D1A	Includes shear stress; Co-cultures can be maintained for 14 days; Demonstrates cell viability and differentiation; PE and PTFE membranes allow phase contact imaging of cells.	No pericytes, neurons or microglia; No TEER measurements; Endothelial cells and astrocytes of non-human origin.	[318]

Table I.8. *Continued*

Device composition	Cell types	Advantages	Disadvantages	Refs.
Three PDMS layers and a PC membrane (0.2 µm pores) that divides the lower chamber (vascular) and top chamber (brain)	hBMECs Primary human astrocytes and pericytes Neurons differentiated from hiPSCs	Reduced media volume-to-cell ratio; Adjustable flow on both sides of barrier; Unit is self-contained, can operate in any orientation and includes shear stress; Differential delivery of drugs or nutrients to the vascular or the brain chamber.	Hydrophobic molecules may adsorb to the PDMS; Unknown extent of the region of the barrier being quantified for TEER.	[319]
PDMS chamber (neural parenchyma) separated from a vascular channel via a microporous PC membrane (8 µm pores)	RBE4 Neural cells isolated from E-18 rat cortical tissue (astrocytes, microglia, neurons)	Allows comparison with data from rodent experiments and has Tight neurovascular barrier and neurotransmitter synthesizing neurons; Low sample volumes; Channels allow perfusion of media and stimuli in a dynamic and physiological manner; Enables view of sub-cellular features.	Embryonic cells may not reproduce essential features of mature *in vivo* BBB; No pericytes and no shear stress; Neuron-astrocyte-microglial ratios do not reflect *in vivo* numbers; Assembly does not provide a tight seal for shear stress and is prone to contamination; Low correlation with human data.	[320]
PDMS two-layer membrane-based device with a PC membrane (0.4 µm pores); Top side of the membrane represents blood vessels;	hCMEC/D3	Includes shear stress; hCMEC/D3 could be cultured for up to 7 days and expressed BBB characteristics (ZO-1 staining).	No glial cells; Low TEER values.	[321]
PDMS microfluidic device with microholes (3-5 µm) that trap injected cells	HUVECs ACM	Includes shear stress and a shorter assay time; BBB permeability can be monitored over time.	Lacks three dimensional configuration of CECs, astrocytes, and pericytes; No glial cells;	[322]
Four PDMS substrates and a center PC membrane (0.4 µm pores); Top side of the membrane represents blood vessels and bottom side contains astrocytes	b.End3 Astrocytes C8D1A	Includes shear stress; Expresses key characteristics of a BBB model (TJ expression, selective permeability to tracers).	No pericytes, neurons or microglia; Endothelial cells and astrocytes of non-human origin.	[295]

ACM, astrocyte conditioned medium; BBB, blood-brain barrier; CEC, cerebral endothelial cell; hiPSC, human-induced pluripotent stem cell; hNT2, pluripotent human NTera2 clone D1; PC, polycarbonate; PDMS, polydimethylsiloxane; PE, polyester; PTFE, polytetrafluoroethylene; TEER, transepithelial electrical resistance; TJ, tight junction; ZO-1, Zonula-occludens-1.

I.3.5. *IN VIVO* AND *IN SITU* MODELS

Traditionally, the CNS-acting drug discovery programs assume that the chance of a new lead to be a successful drug improves as its rate and extent of brain penetration increase, however, understanding drug concentrations within the brain compartment is also important [323].

In vivo brain uptake techniques provide a reliable evaluation and characterization of drug BBB penetration [200]. Since these are methodologies with low throughput screening capacity, their application is mainly reported in more advanced phases of drug development programs. Notwithstanding, the results obtained *in vivo* are particularly important to optimize and validate the *in vitro* models aforementioned.

Among the several *in vivo* studies, the key concepts used for estimating the ability of a drug to overpass BBB include the rate of BBB permeation, the extent of equilibration of a compound across the BBB [324] and intra-brain distribution [40]. The rate of brain uptake of a drug at the initial state, also known as permeability surface area product (PS) or influx clearance, evaluates how fast compounds can cross the BBB *in vivo*. It is considered the best index of BBB permeability, because it is not compromised by drug metabolism, plasma protein binding or non-specific brain binding [176,325,326]. However, the PS product alone is a less relevant predictor of drug activity within the CNS than the extent of brain uptake [83]. The extent of brain distribution is given by K_p or log BB and was widely used in the pharmaceutical industry to evaluate and optimize brain penetration during drug discovery [327]. Nevertheless, since the extent of brain penetration is controlled by several parameters, namely influx and efflux transporters at the BBB, passive BBB permeability, non-specific binding to plasma and brain tissue and brain metabolism [325], it is important to reaffirm that a high K_p or log BB do not necessarily imply a high free drug concentration in the brain, responsible for the pharmacological activity, as mentioned in section I.3.1. The pharmacologically active drug component and its equilibration across the BBB are given by $K_{p,uu}$ [83].

Overall, the rate of BBB permeation, the extent of brain penetration and intra-brain distribution are important to identify CNS-acting drug candidates [83]. The extent of brain penetration can be studied in rodents, following an intraperitoneal, intravenous, oral or subcutaneous administration of the test compound. Plasma and brain are

sampled at variable time-points, submitted to sample pre-treatment procedures and the compound concentrations are determined, in most cases, by liquid chromatography-mass spectrometry (LC/MS) [200,324]. Then, $K_{p,uu}$ can be estimated combining total concentrations with $f_{u,plasma}$ and $f_{u,brain}$ or in alternative, obtained directly using microdialysis [40]. Other *in vivo* techniques that can be used to assess the rate of BBB permeation, the extent or intra-brain distribution are the brain uptake index technique, the *in situ* brain perfusion method, the intravenous injection technique, microdialysis and non-invasive techniques [83,200]. The technical procedures and the main advantages and disadvantages of each method are described in Table I.9.

Table I.9. Main characteristics of invasive and non-invasive *in situ* and *in vivo* blood-brain barrier models.

	Model	Procedure	Advantages	Limitations	Refs.
Invasive	*In situ* brain perfusion	The external carotid artery of the anesthetized animal is catheterized and all branches of the external and internal carotid artery are ligated; The reference and test compounds are perfused retrograde via the external into the internal carotid artery; The animal is decapitated, the brain is collected and the reference and test compounds are quantified.	Avoids systemic exposure and peripheral metabolism; Allows the study of multiple aspects of drug transport at the BBB (e.g. efflux mediated by P-gp or BCRP).	Cannot circumvent metabolism within the brain microcirculation; Does not measure free drug concentration within the brain; BBB integrity may be compromised during long-term perfusion; Requires specialized surgical skills; Labour intensive, time consuming, costly.	[113,200,325,328]
	Brain uptake index (BUI)	Bolus injection of radiolabeled test and reference substances into the common carotid artery of anesthetized animal; Animal is decapitated 5-15 seconds later to avoid potential efflux from the brain; Brain concentrations of the test and reference compounds are determined and related to the plasma concentrations to calculate the BUI.	Fast and flexible (i.e. allows modifications of the injectable composition)	Short brain exposure of the compound; Impossible to study slower uptake processes such as RMT and measure low values of PS; Possibility of systemic diffusion.	[118,200,221,329,330]
	Intravenous injection technique	A femoral vein or tail-vein of rats or mice is cannulated and the test compound is injected with a plasma volume marker (e.g. albumin); Blood is collected and concentrations in plasma are determined at various time points; Brain concentrations can be measured at pre-selected time points (if animals are sacrificed over time) or at the end of the experiment.	Simple to execute; Intact BBB physiology; Greater exposure to cerebral microvessels.	Peripheral metabolism.	[118,331,332]

Table I.9. *Continued*

Model	Procedure	Advantages	Limitations	Refs.
Intracerebral microdialysis	A microdialysis probe is inserted into a selected area of the brain and the probe is perfused with a physiological solution with a similar ionic composition of the extracellular cerebral fluid; The dialysate is continuously collected and the free or unbound concentration of the compound is measured.	No complex sample clean-up procedures; Unbound drug concentrations can be determined in different brain areas of freely moving animals; Reduced number of required animals for pharmacokinetic investigations.	Expensive and low throughput; Need to calculate *in vivo* recovery; Sample diluting effect; Technical difficulties with lipophilic compounds as they may bind to parts of the analytical apparatus.	[118,325,333–335]
Brain efflux index	The test and reference compounds are directly microinjected into the brain; The animal is decapitated, the brain is collected and the concentrations of the compounds are determined at selected time points; The ratios between the brain concentrations of the reference and test compound are established.	Allows an evaluation of the influence of efflux transporters in the passage through the BBB.	Needle tract injections may modify BBB properties; Large animal numbers are needed for multiple time-point analysis.	[113,118,332,336]
CSF sampling	Animals: CSF is collected by single puncture or, in case of continuous sampling, implantation of a cannula in the lateral ventricle or cisterna magna; Humans: CSF is collected by lumbar puncture or insertion of a cannula in the lumbar region.	Provides concentration-time profiles of unbound drugs in the CSF of individual animals	Cannot provide concentration-time profiles in humans (i.e. limited clinical application); Alters the CSF volume and affects pressure equilibrium; May be inaccurate in predicting unbound concentrations: P-gp substrates (free drug equilibrium is not fully established), slow rate of uptake or local metabolism; Timing and sampling site influence the results.	[64,91,325,333,335,337]

Table I.9. *Continued*

	Model	Procedure	Advantages	Limitations	Refs.
	Quantitative autoradiography	A radiolabelled compound is administered to an animal; Blood samples are collected, the brain is removed and radioactivity is measured.	Cheap; Easy to perform; Sensitive; High spatial resolution.	Cannot differentiate protein-bound and unbound compounds; Cannot differentiate between parent drug and metabolites; Time resolution cannot be achieved with one animal.	[113,118,333]
Non-invasive	Imaging (e.g. MRI, PET, SPECT)	MRI: a contrasting agent is injected intravenously and its brain distribution is measured. PET: a positron-emitting radionuclide or a compound labelled with a positron-emitting isotope is injected intravenously; The subject is placed in a counter that detects the emitted positrons. SPECT: a gamma-emitting compound is administered; Gamma scintigraphic images are acquired and the distribution of the compound throughout the body is observed.	Useful for assessing the permeability of the BBB in pathological conditions, performing transport studies, studying the function of efflux transporters at the BBB (e.g. P-gp) and validating *in vitro* results; Can be applied to both animals and humans.	Incompatible with routine screening; Expensive.	[118,200,338–343]

BBB, blood-brain barrier; BCRP, breast cancer resistance-associated protein; BUI, brain uptake index; CSF, cerebrospinal fluid; MRI, magnetic resonance imaging; PET, positron emission tomography; P-gp, P-glycoprotein; PS, permeability surface area product ; RMT, receptor-mediated transcytosis; SPECT, single photon emission computed tomography.

I.3.6. BBB MODELS AND DRUG DELIVERY TO THE CNS

The treatment of CNS-related disorders is a great challenge due to the difficulty of delivering molecules with therapeutic properties effectively and safely across the BBB. Neurodegenerative diseases [344,345], the human immunodeficiency virus [238,346], epilepsy [347] and CNS-based pain and brain cancer [348,349] are examples of pathologies that make the development of efficient brain-targeting drug delivery systems an urgent challenge. In this scope, an interesting review concerning the therapeutic impact of nanotechnology on CNS drug delivery was recently published [350].

Several strategies have been currently outlined to enhance brain drug delivery, namely BBB temporary disruption, drug chemical modifications, drug conjugation with a specific natural or artificial ligand and nanoscale drug delivery systems [107,351]. The disruption of the BBB causes a transient increase in the permeability of brain capillaries. It may be achieved through biological stimuli, such as TJ and AJ modulators capable of reversibly increasing paracellular transport [352]; physical stimuli such as ultrasound [353] or chemical stimuli such as the injection of a hyperosmolar solution of mannitol [351]. Even so, it is an invasive method with associated risks that requires a strict control of the extent of disruption [354] making the use of endogenous transport mechanisms, a safer entry route [355].

Chemical drug modifications usually involve masking the hydrophilic moieties of the drug structure in order to increase its lipophilicity [107,355]. This rationale strategy has been supported by the fact that, as mentioned in section I.3.2.1., the BBB has an anionic surface charge which increases the tendency of lipophilic cationic drugs to interact with it [106]. Nevertheless, these chemical alterations can result in a non-targeted delivery and lead to a widespread distribution of the drug in peripheral organs [348]. Moreover, the modified drug may lose affinity for the target receptor [356]. Therefore, instead of the standard approach that involved the passage of molecules with optimized characteristics (e.g. lipophilicity, molecular weight, hydrogen-bonding) by passive diffusion, improved drug delivery across the BBB has been accomplished by conjugating the molecule of interest with a natural or artificial ligand, able to interact with influx transporters or to avoid efflux carriers [104,357]. These conjugates are known as

molecular Trojan horses [356,358] and the ligands may be peptides, modified proteins or monoclonal antibodies (e.g. OX-26) that cross the BBB by RMT or AMT [354].

Nanoscale drug delivery systems such as liposomes, micelles and nanoparticles are often modified with ligands on their surface to increase the selectivity of the delivery. In fact, functionalized nanoparticles permit a highly specific transport of drugs across the BBB, as demonstrated by the incorporation of apolipoprotein-E, which enhances cell-uptake via the low density lipoprotein receptor through RMT [359–361].

The applications of *in vitro* or/and *in vivo* BBB models to evaluate the brain targeting efficacy and toxicity of these systems are presented in Table I.10. *In vitro* BBB models are commonly used to assess the mechanisms of cellular uptake, the internalization profiles of the nanocarriers as well as their cytotoxicity and permeability across cell monolayers. Exceptionally, Rempe et al. [362] utilized a porcine *in vitro* model to investigate the effect of poly(n-butylcyano-acrylate) nanoparticles on the BBB integrity through the monitorization of TEER and the permeability of paracellular markers.

The most commonly selected cell line for *in vitro* studies has been the b.End3, a cerebral endothelial line of mouse origin, probably because of its commercial availability, as referred in Table I.6. In opposition, MDCK and Caco-2 cells have been rarely used for studying drug delivery, due to the greater cellular and molecular similarity between primary cultures or immortalized lines of CECs and the *in vivo* BBB (Table I.10). It is interesting to highlight that non-cell based models have been also utilized for permeability assays [363]. PAMPA was chosen to examine the passive BBB permeation of *N*-methyl phenylalanine-rich peptides as BBB-shuttles and those with higher permeability were then evaluated in primary cultures of bovine CECs. The correlation between these two models was high ($r = 0.97$), when considering permeation by passive diffusion. The lipophilicity, hydrogen-bonding, membrane retention and permeability of the carriers was also determined by immobilized artificial membrane chromatography, a non-cell based BBB model with acceptable correlation with brain penetration for compounds that permeate by passive mechanisms [118,363].

Nonetheless, any conclusion obtained from *in vitro* assays should be confirmed *in vivo*. The main *in vivo* models used to analyse the pharmacokinetics and biodistribution of the nanocarriers are the intravenous injection method, due to its practical execution

and non-invasive imaging techniques (Table I.10). The results obtained *in vivo* are usually consistent with those *in vitro*, corroborating the need of using both types of models to attain a complete characterization of brain drug delivery systems.

Table I.10. Applications of *in vitro* and *in vivo* blood-brain barrier models for the development of central nervous system drug delivery systems.

Delivery system	***In vitro* model**	***In vitro* evaluation**	***In vivo* techniques**	**Refs.**
Glioma targeted liposomes [c(RGDyK)-pHA-PEG-DSPE-incorporated liposomes]	Primary rat CECs b.End 3 cells HUVECs U-87 glioblastoma cells	Cellular uptake Permeability Cytotoxicity	I.V injection	[364]
Antibody-modified chitosan nanoparticles [transferrin antibody and bradykinin B2 antibody]	hCMEC/D3 U138-MG glioblastoma cells	Cellular uptake Permeability Cytotoxicity	NR	[365]
Edavarone-encapsulated agonistic micelles	b.End 3 cells	Permeability	Imaging (MRI, NIR fluorescence)	[366]
Polysorbate 80-coated PLGA nanoparticles	RBE4 cells or primary rat CECs Primary rat astrocytes	Cellular uptake Permeability Cytotoxicity	I.V injection	[367]
Amyloid-β-targeting liposomes [Sphingomyelin/cholesterol, phosphatidic acid and anti-transferrin receptor antibody RI7217]	hCMEC/D3	Cellular uptake Permeability Cytotoxicity	NR	[368]
Aminosilane-coated iron oxide nanoparticles	b.End 3 cells Primary mouse astrocytes Primary mouse neurons	Cellular uptake Cytotoxicity	NR	[369]
Lactoferrin-conjugated PEGylated liposomes	b.End 3 cells	Cellular uptake	Imaging (SPECT)	[370]
P-aminophenyl-a-D-mannopyranoside liposomes	b.End3 cells C6 glioma cells	Cellular uptake	Imaging (NIR fluorescence)	[371]
Third-generation PAMAM dendrimer	Primary porcine CECs Caco-2 cells	Permeability Cytotoxicity	NR	[372]
TPGS-coated PS nanoparticles	MDCK cells	Cellular uptake	I.V injection	[373]

Table I.10. *Continued*

Delivery system	*In vitro* model	*In vitro* evaluation	*In vivo* techniques	Refs.
Penetratin functionalized PEG-PLA nanoparticles	MDCK-MDR1 cells	Cellular uptake Cytotoxicity	I.V injection	[374]
Immunopegylated nanoparticles [CD-71 / OX-26]	NR	NR	I.V injection Microdialysis	[375]
(G4-DOX-PEG-Tf-TAM) PAMAM dendrimer	Primary mouse CECs Co-culture of primary mouse CECs and C6 glioma cells	Cellular uptake Permeability Cytotoxicity	NR	[376]
Aptamer-peptide nanoparticles [AS1411-hsa]	Co-culture of b.End3 cells and C6 glioma cells	Cellular uptake Permeability	Imaging (Fluorescence)	[377]
Apolipoprotein-E HSA nanoparticles	b.End3 cells	Cellular uptake	I.V injection	[378,379]
gH625 polystyrene nanoparticles	b.End3 cells	Cellular uptake Permeability	NR	[380]
Alkylglyceryl-functionalized chitosan nanoparticles	b.End3 cells	Cellular uptake Cytotoxicity Permeability	NR	[381]
β-Cyclodextrin-poly(β-amino ester) nanoparticles	Primary bovine CECs	Cytotoxicity Permeability	NR	[382]
Bifunctional liposomes [Tf – poly-L-arginine]	b.End3 cells Primary glial cells	Cellular uptake Cytotoxicity Permeability	NR	[383]
Micelles [Stearic acid – grafted chitosan]	b.End3 cells	Cellular uptake Cytotoxicity	I.V injection Imaging (Fluorescence)	[384]
Magnetic nanoparticles	U-87 glioblastoma cells	Cellular uptake Cytotoxicity	I.V injection Imaging (MRI)	[349]
Bolaamphiphilic vesicles [GLH-19 / GLH-20]	b.End3 cells	Cellular uptake	I.V injection	[385]
p(HPMA)-co-p(LMA) copolymers	Immortalized human CECs	Permeability	NR	[386]
RMP-7 – MMA-SPM nanoparticles	Co-culture of primary human CECs and primary human astrocytes	Cellular uptake Permeability	NR	[346]
Solid-lipid nanoparticles	Primary rat astrocytes	Cytotoxicity	NR	[387]

Table I.10. *Continued*

Delivery system	*In vitro* model	*In vitro* evaluation	*In vivo* techniques	Refs.
PAMAM-PEG-WGA-Tf dendrimer	Co-culture of primary mouse CECs and C6 glioma cells	Cytotoxicity Permeability	NR	[388]
Liposomes [Apolipoprotein-E derived peptides]	RBE4 cells	Cellular uptake Cytotoxicity Permeability	NR	[389]
Immunoliposomes [Biotin – streptavidin – OX-26]	hCMEC/D3 cells	Cellular uptake Cytotoxicity Permeability	NR	[390]
PBCA nanoparticles	Primary porcine CECs	BBB disruption	Imaging (MRI)	[362,391]
Thermosensitive liposomes	Co-culture of ECV304 cells and primary rat astrocytes	Permeability	I.V injection	[392]
SiO_2 nanoparticles	hCMEC/D3 cells	Permeability	NR	[393]
N-methyl phenylalanine-rich peptide shuttles	PAMPA IAM chromatography Co-culture of primary bovine CECs and rat astrocytes	Permeability	NR	[363]
MAN-Tf liposomes	Co-culture of primary mouse CECs and C6 glioma cells	Cellular uptake Cytotoxicity Permeability	NR	[394]
Lactoferrin PEG-PLA nanoparticles	b.End3 cells	Cellular uptake Cytotoxicity	I.V injection	[395]
Polyether-copolyester dendrimers	b.End3 cells	Cellular uptake Cytotoxicity Permeability	NR	[396]
Chitosan nanoparticles	MDCK cells	Cytotoxicity Permeability	NR	[397]
PBCA nanoparticles MMA-SPM nanoparticles Solid lipid nanoparticles	Primary human CECs	Cellular uptake Cytotoxicity Permeability	NR	[238]
PEG-PHDCA nanoparticles	Co-culture of primary rat CECs and rat astrocytes	Cellular uptake Permeability	NR	[398]

Table I.10. *Continued*

Delivery system	*In vitro* model	*In vitro* evaluation	*In vivo* techniques	Refs.
CBSA nanoparticles	Co-culture of primary rat CECs and rat astrocytes	Cellular uptake Cytotoxicity Permeability	*In situ* brain perfusion	[399]

BBB, blood-brain barrier; Caco-2, human epithelial colorectal adenocarcinoma cell line; CBSA, cationic bovine serum albumin; CECs, cerebral endothelial cells; DOX, doxorubicin; DSPE, 1,2-distearoyl-sn-glycero-3-phosphoethanolamine; G4, fourth-generation; HPMA, N-(2-hydroxypropyl)-methacrylamide; HSA, human serum albumin; HUVEC, human umbilical vein endothelial cells; IAM, immobilized artificial membrane; I.V, intravenous; LMA, laurylmethacrylate; MAN, p-aminophenyl-α-D-mannopyranoside; MDCK, Madin-Darby canine kidney cells; MMA, methylmethacrylate; MRI, magnetic resonance imaging; NIR, near-infrared; NR, not reported; PAMPA, parallel artificial membrane permeability assay; PAMAM, polyamidoamine; PBCA, polybutylcyanoacrylate; PEG-PHDCA, poly(MePEG2000cyanoacrylate-co-hexadecylcyanoacrylate); PEG, polyethylene glycol; pHA, p-hydroxybenzoic acid; PLA, polylactic acid; PLGA, poly(lactic-co-glycolic acid); PS, polystyrene; RGD, arginylglycylaspartic acid; SPM, sulfopropylmethacrylate; TAM, tamoxifen; Tf, transferrin; TPGS, d-α-tocopheryl polyethylene glycol succinate; WGA, wheat germ agglutinin;

I.3.7. FINAL CONSIDERATIONS

The BBB is a highly organized interface in which cells with specialized functions interact in an interdependent way, forming a unique microenvironment. This *in vivo* complexity has not yet been achieved *in vitro*, since each model has limitations that prevent them from mimicking all properties of the *in vivo* BBB. Briefly, PAMPA models fail to identify active transport processes, while in cell-based models of cerebral origin, the cells are maintained under artificial conditions and out of the influence of neurovascular unit, which may compromise the application of these models. Furthermore, specifically regarding the previous model type, immortalized cell lines of cerebral origin do not form sufficiently tight monolayers *in vitro* for permeability screenings, whereas CECs from primary cultures are unsuitable for industrial uses and cannot be sub-cultured or stored for future use. On the other hand, cell lines of non-cerebral origin lack several properties of the *in vivo* brain endothelium.

In truth, the ideal *in vitro* model does not exist and each model must be suited and optimized for well-defined purposes. For permeability screenings, the challenge is to develop an *in vitro* model that is both faithful to critical aspects of the *in vivo* physiology and compatible with the high throughput requirements of the pharmaceutical industry. There is currently a great interest in the development of cell-based assays that are simultaneously less laborious and preserve fundamental BBB properties. In particular, cell lines of human origin are being investigated to avoid the difficulties found with the extrapolation of animal data to humans, possibly caused by inter-species differences in

the expression of BBB transporters. Moreover, the predictive power of *in vitro* models must be assessed using the reliable information provided by *in vivo* BBB models, in spite of their lower throughput and labour intensiveness. Therefore, the combination of both approaches will contribute to the design of more efficient and safer drug delivery systems, thereby improving the treatment of CNS-related pathologies.

I.4. CHEMICAL COMPOUNDS STUDIED IN THIS THESIS

The molecules used as test compounds in the scope of this thesis belonged to three main drug classes: catechol-*O*-methyltransferase (COMT) inhibitors, utilized for the treatment of PD; dopamine β-hydroxylase (DBH) inhibitors, developed for the treatment of hypertension and congestive heart failure; and dibenz[b,f]azepine-5-carboxamide (DAC) derivatives, applied for the treatment of epilepsy. In the subsequent sections, there will be a brief description of the pathology, available therapeutic options, and main pharmacodynamic and pharmacokinetic properties of the compounds in question.

I.4.1. CATECHOL-*O*-METHYLTRANSFERASE INHIBITORS

PD was first described in a medical context in 1817 by James Parkinson in *Essay of the Shaking Palsy*, but the term PD was proposed later by Jean-Martin Charcot who expanded the understanding of the disease [400]. Since then, numerous reports have been published about this progressive, disabling and neurodegenerative movement disorder [401]. It is the most common movement disorder and the second most common degenerative disease of the CNS. Although rare before 50 years of age, it is estimated that PD affects 1% of the population above 60 years and increases steadily with age, reaching a prevalence of 4% in the highest age groups [402]. Additionally, it is more often observed in men than women [403].

The clinical symptoms of PD progression vary with age. Usually, the diagnosis occurs with the onset of motor symptoms at age 50, but can be preceded by a prodromal phase of non-motor symptoms that tend to aggravate [404]. The main motor symptoms that characterize PD are bradykinesia (i.e. slowness of movements), rigidity and tremor at rest [405]. These are the cardinal criteria for PD diagnosis, recommended by the

International Parkinson and Movement Disorder Society. Even though gait impairment (flexed posture, freezing, and loss of postural reflexes) is a feature of PD, it often occurs in late-stage PD and its presence in early stages may suggest an alternative diagnosis [406]. Non-motor symptoms encompass neuropsychiatric symptoms (e.g. depression, anxiety, cognitive impairment), sleep disturbances, dysautonomic disorders (genitourinary, gastrointestinal, endocrine and cardiac) and others (e.g. pain) [405].

The main neuropathological characteristics of PD are the accentuated loss of dopaminergic neurons at the *substantia nigra pars compacta* and the cytosolic deposition of α-synuclein aggregates, termed Lewy bodies, in neurons of different brain regions and even in the peripheral nervous system [407,408]. The loss of dopaminergic neurons at the *substantia nigra* in early PD stages suggests that the degeneration in this region begins before the onset of motor symptoms and becomes more widespread as the disease advances [404]. Since dopaminergic neurons project to the striatum, composed by the caudate nucleus and putamen, the loss of *substantia nigra* cells will result in the depletion of striatal dopamine. In turn, this decrease of dopamine in the nigrostriatal system will increase the inhibitory output to the thalamus and indirectly to the cortex, repressing the initiation of movement [407]. Therefore, dopaminergic nigrostriatal loss is the core mechanism behind the cardinal motor manifestations of PD [404].

Up to this day, there is no cure for PD and current treatments are symptomatic, as there is no available therapy that slows down PD progression or prevents its manifestation. It usually encompasses pharmacotherapy, neurosurgery (deep brain stimulation) and supportive therapies such as physiotherapy, speech therapy and dietary measures [408]. The discovery of the dopaminergic deficit in PD patients led to pharmacological attempts to restore dopaminergic activity, i.e. dopamine-replacement therapy, using L-DOPA and dopamine receptor agonists that counteract the motor symptoms of the disorder [409].

L-DOPA was introduced in the late 1960s but despite the launch, over the years, of other drugs that boost dopamine levels, it continues to be the most effective agent in the treatment of PD and the gold standard therapy to which all other therapies are compared [401,409]. The clinical response to L-DOPA remains constant during 1-3 years of therapy named the honeymoon period, however in the following years, patients

experience a wearing-off effect (transition from ON-periods of response to therapy to OFF-periods with reappearance of motor symptoms) and dyskinesia (i.e. involuntary movements) in spite of stable plasma levels [408]. The mechanisms behind the long-term alterations in therapy are not completely clear, but may be associated with a deficient system of conversion, release and storage of dopamine caused by progressive neuronal loss, thereby making dopamine levels in synapses directly dependent on L-DOPA levels in the peripheral circulation. Alternatively, post-synaptic mechanisms have also been suggested [410]. Thus, to avoid motor fluctuations and reduce OFF-periods, it is important to provide sustained dopamine concentrations in the CNS, which can be improved by inhibiting the degrading enzymes of L-DOPA and/or dopamine (Figure I.9).

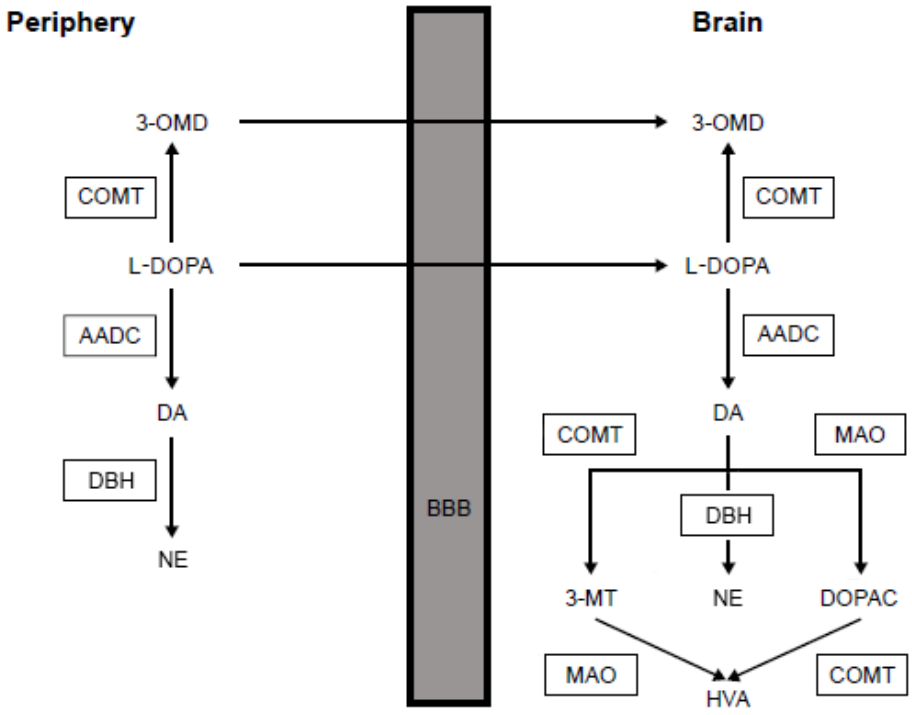

Figure I.9. Levodopa metabolism. AADC, aromatic aminoacid decarboxylase; BBB, blood-brain barrier; COMT, catechol-*O*-methyltransferase, DA, dopamine; DBH, dopamine β-hydroxylase; DOPAC, 3,4-dihydroxyphenylacetic acid; HVA, homovanillic acid; L-DOPA, levodopa; MAO, monoamine oxidase; 3-OMD, 3-*O*-methyldopa; 3-MT, 3-methoxytyramine; NE, norepinephrine. Adapted from [411].

In order to gain access to the CNS, L-DOPA is administered as a dopamine prodrug and undergoes uptake at the BBB by the LAT1 transporter subunit 4F2 heavy chain (4F2hc) [412]. Nevertheless, before reaching the CNS, L-DOPA is quickly and extensively

metabolized to dopamine by AADC and COMT enzymes present in extracerebral tissues like the gastrointestinal tract, liver and kidney. Indeed, it is estimated that approximately only 1% of an oral L-DOPA dose reaches the brain [413]. Consequently, to prevent the peripheral decarboxylation to dopamine, L-DOPA began to be co-administered with AADC inhibitors, carbidopa or benserazide, which improved its bioavailability, efficacy and tolerability. Furthermore, it enabled a substantial reduction of L-DOPA dosage, approximately 70-80%, and decreased peripheral side effects (e.g. nausea, vomiting, anorexia, hypotension). Notwithstanding, only 5–10% of an oral dose of L-DOPA reaches the CNS when co-administered with carbidopa. This occurs because the combination of L-DOPA with AADC inhibitors increases its conversion to 3-*O*-methyldopa by COMT, which competes with L-DOPA at the BBB for transport [410]. Therefore, the concomitant administration of L-DOPA/AADC inhibitor with a COMT inhibitor will prolong the plasma half-life of L-DOPA and increase its delivery to the CNS for dopamine biosynthesis [414].

COMT is a magnesium-dependent enzyme that catalyses the methylation of catechol substrates using S-adenosyl-L-methionine (SAM) as a methyl donor and yielding the *O*-methylated catechol and S-adenosyl-L-homocysteine as reaction products. Accordingly, its main physiological role is the elimination of biologically active or toxic catechols [415]. In mammals, COMT is ubiquitously distributed in almost all peripheral tissues as well as in the CNS, and may be present in different isoforms: membrane-bound COMT (MB-COMT) and soluble COMT (S-COMT). Nevertheless, the exact distribution of each isoform in tissues, particularly in the brain, is still controversial.

In peripheral tissues, COMT is more abundantly expressed in the liver and kidney, but can also be found in the intestine, stomach, heart and erythrocytes, for example [416]. S-COMT appears to be the main isoform of COMT in peripheral tissues, residing in the cytoplasm and nuclei of cells, whereas MB-COMT is the main isoform in the brain and more associated with the rough endoplasmic reticulum [417,418]. Moreover, COMT demonstrated substantial activity in glial cells, less activity in postsynaptic neurons and no activity in presynaptic dopaminergic neurons [419]. In contrast, Chen et al. [420] stated that MB-COMT can metabolize synaptic and extra synaptic dopamine on the surface of presynaptic and postsynaptic neurons. It was also mentioned that MB-COMT possesses a catalytic domain in the extracellular space, which goes against previous studies that reported MB-COMT as an intracellular protein, not associated with plasma

membranes [421]. Later, Schendzielorz et al. [422] confirmed that COMT was not present in presynaptic dopaminergic or noradrenergic neurons but is located instead, in postsynaptic GABAergic neurons in the striatum and cortex of rat brain. The conflicting data concerning COMT location may be caused by variations in the utilized experimental techniques or species-differences between mice [421], rats [420,422] and humans [418].

Following the first purification and characterization of COMT in the late 1950s, several classes of COMT inhibitors were identified. First-generation compounds possessed a catechol structure and were usually competitive [415]. Although several have been used *in vitro*, they showed little value as pharmacological agents due to their low potency, lack of selectivity and unacceptable toxicity [423]. Therefore, second-generation COMT inhibitors were synthetized in the late 1980s by independent laboratories. Most contained a key nitrocatechol structure and exhibited high potency, selectivity and oral activity [419]. Among them are nitecapone [3-(3,4-dihydroxy-5-nitrobenzylidine)-2,4-pentanedione; OR-462] and entacapone [2-cyano-N,N-diethyl-3-(3,4-dihydroxy-5-nitrophenyl)propenamide; OR-611], developed by Orion; tolcapone (3,4-dihydroxy-5'-methyl-5-nitrobenzophenone; Ro 40-7592), developed by Hoffmann-la Roche; and nebicapone [1-(3,4-dihydroxy-5-nitrophenyl)-2-phenylethanone; BIA 3-202], developed by BIAL-Portela & Ca., S.A. [416]. Nitrocatechols behave competitively with respect to the catechol substrate and uncompetitively with respect to the co-substrate SAM. Furthermore, these compounds are characterized as reversible tight-binding COMT inhibitors and display more affinity for COMT than for other enzymes implied in the metabolism of catecholamines, namely tyrosine hydroxylase, DBH, monoamine oxidase A or B and AADC [415].

Despite being chemically similar, tolcapone, entacapone, nebicapone and nitecapone have different pharmacodynamic and pharmacokinetic properties (Figure I.10).

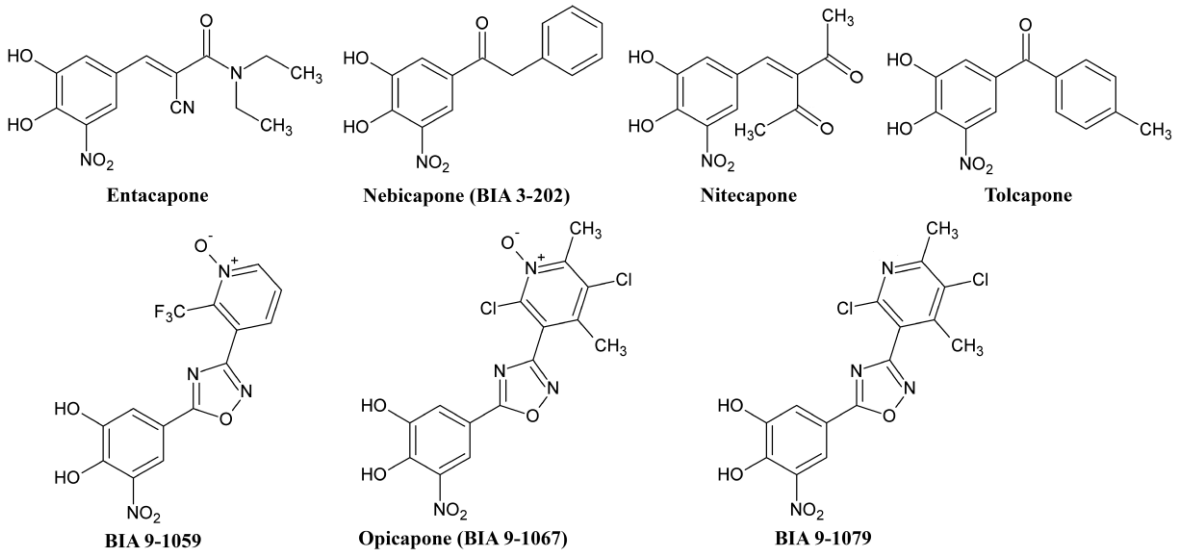

Figure I.10. Chemical structures of catechol-*O*-methyltransferase inhibitors: second-generation (entacapone, nebicapone, nitecapone, tolcapone), third-generation (BIA 9-1059, opicapone) and the active metabolite of opicapone, BIA 9-1079. All compounds were tested in this thesis, with the exception of nitecapone.

Attempting to compare potency parameters (IC_{50}, Ki, ED_{50}) found in literature and conclude about which compound is more potent in each biological matrix is often a difficult task, due to the wide variety of values found for the same parameter, compound and matrix. These discrepancies are not only explained by differences in experimental methods (e.g. protein concentrations), but also by different mathematical approaches [424], which prevent direct comparisons. Nonetheless, there is a generalized consensus that tolcapone is a potent inhibitor of central and peripheral COMT. According to Vieira-Coelho and Soares-da-Silva [425], tolcapone has more affinity for MB-COMT from brain and liver than for S-COMT *in vivo*. Furthermore, tolcapone is a potent inhibitor of brain COMT, while nebicapone is less potent at inhibiting cerebral COMT and entacapone failed to reach 50% inhibition level [426]. In the periphery, tolcapone and nebicapone demonstrated equivalent inhibition of liver COMT, while nebicapone is a stronger and longer inhibitor of liver COMT than entacapone [427]. Similarly, tolcapone also demonstrated a stronger and longer duration of action than entacapone [426]. When co-administered with L-DOPA and an AADC inhibitor, all COMT inhibitors tolcapone, nebicapone, entacapone and nitecapone caused a decrease of 3-*O*-methyldopa, as well as, an increase of L-DOPA levels in plasma and brain [428–431].

Some of the pharmacokinetic characteristics of entacapone, nebicapone, nitecapone and tolcapone are summarized in Table I.11.

Table I.11. Pharmacokinetic properties of second-generation (entacapone, nebicapone, nitecapone and tolcapone) and third-generation (opicapone) catechol-*O*-methyltransferase inhibitors after single-dose oral administration to humans.

	Dose (mg kg^{-1})	**t_{max}** (h)	**C_{max}** (µg mL^{-1})	**Oral bioavailability** (%)	**$AUC_{0\text{-}inf}$** (µg.h mL^{-1})	**$t_{1/2el}$** (h)	**PPB (%)**	**Ref.**
Entacapone (OR-611)	100	0.6	1.1	30 – 46 [432]	0.7	1.6	98	[431]
	200	0.7	1.8		1.6	3.4		
Nebicapone (BIA 3-202)	50	0.5	2.7	62.7 – 78.7 [413]	4.0*	2.4	99	[433]
	100	1.5	4.1		7.4*	2.9		
	200	2.0	5.9		16.0*	2.0		
Nitecapone (OR-462)	100	0.6	2.6	56	2.7	NR	97	[419]
Tolcapone (Ro 40-7592)	50	1.2	2.4	68 [434]	5.7	1.7	99	[435]
	100	1.7	4.6		12.2	2.0		
	200	1.8	2.3		18.5	2.1		
	200	1.7	4.9		16.8	1.6		[434]
Opicapone (BIA 9-1067)	50	3.5	0.5	NR	1.6	0.8	99	[436]
	100	1.8	0.9		2.3	1.2		
	200	2.0	1.3		3.9	1.3		

*$AUC_{0\text{-}t}$ is reported. $AUC_{0\text{-}inf}$, area under the concentration-time curve from time zero to infinite; C_{max}, maximum concentration; NR, not reported; PPB, plasma protein binding; $t_{1/2el}$, apparent terminal elimination half-life; t_{max}, time to achieve the maximum concentration.

Although these compounds are quickly absorbed after oral administration, first-pass metabolism limits their oral bioavailability, particularly for entacapone. Additionally, these COMT inhibitors undergo extensive metabolization in the liver, mostly through conjugation reactions, but a more detailed view of the metabolic pathways is given by Gonçalves et al. [413]. Lastly, their elimination is rapid, as revealed by the short apparent terminal elimination half-life ($t_{1/2el}$) and all nitrocatechols are highly bound to plasma proteins.

Due to the aforementioned reasons, all compounds appeared to be potential candidates for PD treatment but some did not advance in the R&D program. Even though nitecapone proceeded to phase I clinical trials, it was replaced by entacapone, which revealed to be a more effective clinical candidate. Identically, the development of

nebicapone was halted due to liver safety concerns [416]. As a result, among second-generation inhibitors, only entacapone (Comtan/Comtess®, 200 mg; Stalevo®: L-DOPA, carbidopa, entacapone) and tolcapone (Tasmar®, 100/200 mg) are currently available for therapy, although tolcapone has restricted use, being authorized only for patients that do not respond to other therapies, and requiring regular monitorization of liver enzymes. Due to descriptions of acute fulminant hepatitis, the marketing authorisation for tolcapone was initially suspended in the European Union and Canada [437] and later re-introduced in the European Union, under rigorous monitoring conditions [415]. Such effects were not observed for entacapone, however entacapone has a shorter half-life, a lower oral bioavailability and a lower potency than tolcapone, being concomitantly administrated with each dose of L-DOPA. Moreover, a wide inter-individual variation and elevated withdrawal rates have been reported [438]. Thus, there was an unmet need for the development of new COMT inhibitors, with a better therapeutic profile and more convenient dosage regimen [436].

In this sequence, heterocycle-based nitrocatechols were developed as long-acting and orally active COMT inhibitors, such as the preferentially peripheral BIA 9-1059 [3-(5-(3,4-dihydroxy-5-nitrophenyl)-1,2,4-oxadiazol-3-yl)-2-(trifluoromethyl)-pyridine 1-oxide] [439] and opicapone (2,5-dichloro-3-[5-(3,4-dihydroxy-5-nitrophenyl]-1,2,4-oxadiazol-3-yl)-4,6-dimethylpyridine 1-oxide; BIA 9-1067) [440] (Figure I.10). In particular, opicapone recently received a market authorisation by the Committee for Medicinal Products for Human Use of EMA (Ongentys®, 25/50mg) [441,442]. Through the incorporation of a pyridine *N*-oxide residue at position 3, it was possible to achieve a higher duration of inhibition and minimize toxicity [440] compared to entacapone and tolcapone. Opicapone provides a prolonged COMT inhibition [436], despite the low plasma exposure and short $t_{1/2el}$ of the compound in single-dose (Table I.11) or multiple-dose (1.0-1.4 h) [443]. With 200 mg, the maximal inhibition of S-COMT activity was 80% for tolcapone, 65% for entacapone and 80% for nebicapone, whereas a 93.8% inhibition could be achieved for opicapone with only 50 mg. Furthermore, S-COMT inhibition returned to baseline after 18 h with tolcapone, 8 h with entacapone and 16 h with nebicapone. In contrast, with 50 mg of opicapone there was still 53% inhibition after 24 h [436]. The sustained inhibition is justified by the slow dissociation rate and long residence time of the reversible COMT-opicapone complex, which constitutes an

appropriate pharmacodynamic profile for a once-daily administration [443], thereby contributing to patient compliance, over other COMT inhibitors that need to be taken in several times a day [438].

In preclinical studies with rats [438] and cynomolgus monkeys [444], opicapone was administered before L-DOPA/benserazide and increased the systemic exposure of L-DOPA, reducing 3-*O*-methyldopa levels. This was also observed in healthy humans [445] and PD patients [446] after administering L-DOPA/benserazide or L-DOPA/carbidopa, although the plasma L-DOPA levels were significantly higher with L-DOPA/benserazide than L-DOPA/carbidopa [445]. In PD patients with motor fluctuations, opicapone effectively increased the ON-time and reduced the OFF-time, positively contributing to the quality of life of the patient [446]. Moreover, it displayed a favourable risk-to-benefit ratio in the management of end-of-dose motor fluctuations in phase III studies [447]. Regarding safety, it has always been reported that opicapone possessed a good tolerability profile [436,443,445,446,448]. Sulphation is the main metabolic pathway of opicapone, originating the inactive metabolite BIA 9-1103, and the bile is probably the main route of excretion. Nevertheless, opicapone may also undergo methylation, glucuronidation or *N*-oxide reduction and originate the minor active metabolite BIA 9-1079 (Figure I.10). This metabolite represents less than 20% of opicapone systemic exposure and is therefore unlikely to contribute to the therapeutic effect [443]. BIA 9-1079 is considered the major animal metabolite, while BIA 9-1103 is the major human metabolite [442].

To conclude, it is worth to mention that opicapone exhibits peripheral selectivity, i.e. it preferentially inhibits peripheral COMT. This was demonstrated by Kiss et al. [440] in *in vitro* assays of COMT activity, based on the conversion of epinephrine to metanephrine by COMT. It was shown that opicapone (3 mg kg^{-1}; oral route) had no effect on central COMT activity in rats. Bonifácio et al. [444] conducted microdialysis experiments with cynomolgus monkeys (100 mg kg^{-1}, oral route) and did not observe a decrease in HVA levels in brain dialysate, which originates from the degradation of 3,4-dihydroxyphenylacetic acid (DOPAC) by COMT in the catecholamine pathways (Figure I.9). HVA levels also did not decrease in rat brain tissue after oral administration of opicapone (3 mg kg^{-1}) [438]. For instance, tolcapone decreased HVA and increased DOPAC brain levels in the rat (10 mg kg^{-1}, intraperitoneal route [449]; 30 mg kg^{-1}, oral

route [450]) whereas entacapone did not [449], confirming their preferentially central and/or peripheral COMT inhibition. It has been debated whether a COMT inhibitor to be used in PD therapy ought to present peripheral selectivity or not, but a limited access to the brain was generally considered advantageous, in order to avoid potentially undesired central side effects [415]. Recently, however, the interest in the development of centrally active COMT inhibitors resurfaced and non-nitrocatechols [450] and nitrocatechols [451] with improved safety profiles are being investigated.

All previously referred COMT inhibitors (BIA 9-1059, BIA 9-1079, entacapone, nebicapone, opicapone, tolcapone) were tested in the scope of this dissertation, with the exception of nitecapone.

I.4.2. DOPAMINE B-HYDROXYLASE INHIBITORS

The interest in the development of DBH inhibitors is based on the hypothesis that inhibition of this enzyme may provide clinical improvements in patients suffering from cardiovascular disorders such as hypertension and/or congestive heart failure [452].

For the last decades, the major focus in high blood pressure research has been the renin-angiotensin-aldosterone system, neglecting other pressure-raising systems, namely the sympathetic nervous system. Notwithstanding, there is now general agreement that the overactivity of the sympathetic nervous system initiates and sustains blood pressure elevation in patients with arterial hypertension [453]. Initially, it was noticed that there was a significant elevation of the levels of the sympathetic neurotransmitter norepinephrine in plasma of hypertensive patients compared with normotensive patients [454]. However, plasma levels are a rough indicator of sympathetic function, because less than 20% of norepinephrine released from nerve terminals appears in systemic circulation [455]. Consequently, other techniques were developed to assess regional sympathetic nervous system activity, namely microneurography, which measures sympathetic nerve firing rates to skeletal muscle and skin; and the norepinephrine spillover technique, which measures the release of neurotransmitter to plasma, from individual organs [456]. It was then verified that in borderline and established hypertension, nerve firing rates in postganglionic sympathetic fibers passing to skeletal muscle blood vessels are augmented, as well as,

the spillover of norepinephrine from the heart and kidneys, demonstrating that there is a high sympathetic outflow to these organs [457]. Indeed, an elevated activity of the sympathetic nervous system has been shown in younger patients (< 45 years old) and also in elderly patients with different clinical forms of hypertension [454,458].

The first evidence that the sympathetic nervous system is involved in congestive heart failure was the increased excretion of norepinephrine in urine [459]. Later, it was observed that increased rates of sympathetic firing in the failing heart lead to a downregulation of β1-adrenoreceptors in the myocardium, remodelling of the left ventricle, arrhythmias and necrosis, thereby compromising the functional integrity of the heart [460]. These modifications caused by sympathetic overdrive are known as *end-organ damage* and further encompass renal damage and arterial dysfunction. Other nefarious consequences include metabolic abnormalities such as insulin resistance and dyslipidaemias [458]. Moreover, in opposition to what was previously thought, there is no cardiac sympathetic denervation in patients with heart failure. In fact, the sympathetic outflow to the heart is preferentially stimulated in severe congestive heart failure and norepinephrine spillover from the heart to plasma can be 50 times higher than normal [453]. Therefore, activation of the sympathetic nervous system is an important pathophysiological feature of hypertension and heart failure, and constitutes a logical therapeutic target.

In this context, non-pharmacological methods may have a sympatholytic effect, but a large number of studies investigate sympathetic deactivation by pharmacological methods (i.e. antihypertensive drugs) [461] or more recently, surgical catheter-based procedures like renal denervation [462]. As a part of pharmacological methods, inhibition of sympathetic nerve function with adrenoreceptor antagonists (β-blockers) could be a therapeutic approach, however several patients do not tolerate the acute hemodynamic deterioration associated with β-blocker treatment, resultant from an abrupt withdrawal of sympathetic support [463]. Another alternative therapeutic approach would be the prevention of the biosynthesis of norepinephrine through the inhibition of DBH, a copper II ascorbate–dependent monooxygenase [464]. This enables a gradual sympathetic slowdown and increases the availability of dopamine, which can improve renal function by provoking renal vasodilatation and inducing diuresis and natriuresis [465]. First- and second-generation DBH inhibitors included cooper chelating

compounds such as disulfiram or fusaric acid, a phytotoxin [466], but these compounds exhibited low potency, poor selectivity for DBH and caused toxic side effects [467].

Afterwards, third-generation inhibitors were developed, specifically nepicastat [5-aminomethyl-1-(5,7-difluoro-1,2,3,4-tetrahydronaphth-2-yl)-1,3-dihydroimidazole-2-thione; RS-25560-197]. During *in vitro* assays with human and bovine DBH, Stanley et al. [460] verified that nepicastat produced a potent concentration-dependent DBH inhibition and had a negligible affinity for other enzymes. Additionally, nepicastat was administered to spontaneously hypertensive rats (3, 10, 30, 100 mg kg^{-1}, oral route) and dogs (0.1, 1, 3, 10 mg kg^{-1}, oral route). In both species, a decrease of noradrenaline, increase of dopamine and, consequently, an increase of dopamine-noradrenaline ratio were observed in the mesenteric/renal artery and left ventricle, at a dose of 3 mg kg^{-1} in the rat and 0.1 mg kg^{-1} in the dog. Interestingly, these alterations were also observed in the cerebral cortex but only at higher doses, 30 mg kg^{-1} in the rat and 1 mg kg^{-1} in the dog, with the exception of the ratio, equally altered at 0.1 mg kg^{-1} in the dog. Hence, in dogs, the magnitude of changes in catecholamine levels in cerebral cortex appears comparable to those in peripheral tissues, whereas in the rat, nepicastat (< 30 mg kg^{-1}) produced significant changes in catecholamine levels in peripheral tissues without affecting the cerebral cortex [460]. In another study with dogs, nepicastat prevented progressive left ventricular dysfunction and remodelling [468] and followed to early clinical trials [467]. Nevertheless, the fact that nepicastat could cause peripheral and central effects raised concerns related with potentially undesired and serious CNS side effects, and consequently the pursuit for a safer, more potent and peripherally selective DBH inhibitor continued.

Etamicastat [5-(2-aminoethyl)-1-(6,8-difluorochroman-3-yl)-1,3-dihydroimidazole-2-thione; BIA 5-453] was developed as a potent and reversible inhibitor of DBH for the treatment of hypertension and heart failure [469]. After being administered to mice (100 mg kg^{-1}, oral route), etamicastat decreased norepinephrine levels in the heart, but did not alter its levels in the frontal and parietal cortex. These findings suggest that etamicastat (Figure I.11) exerts its inhibitory DBH effects almost exclusively in the periphery and does not possess significant inhibitory effects in the brain [452].

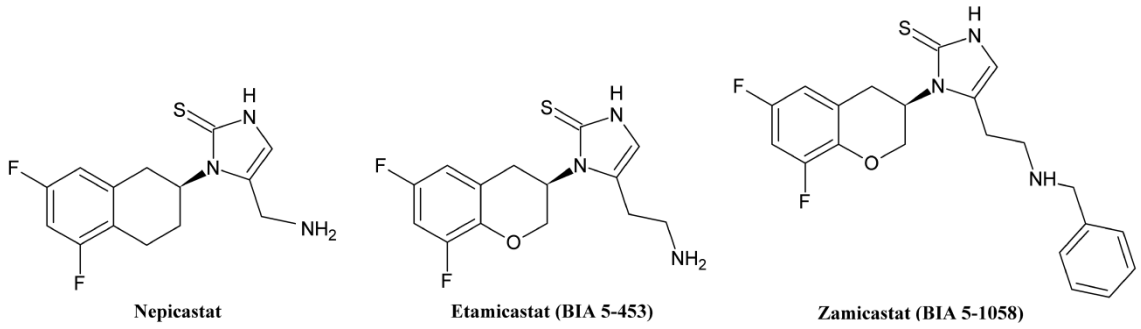

Figure I.11. Chemical structures of dopamine β-hydroxylase inhibitors: nepicastat, etamicastat and zamicastat.

In another investigation performed in mice, Loureiro et al. [470] compared etamicastat and nepicastat, observing that only trace amounts of etamicastat were detected in the brain (100 mg kg^{-1}, oral route; 10 mg kg^{-1}, intravenous route), in contrast to nepicastat, for which it was possible to determine a $K_{p,uu}$ of 0.03 (after oral administration) and 0.1 (after intravenous administration). This reveals that efflux might be involved in the passage across the BBB, an assumption that was confirmed for both compounds through a significant increase of brain levels after co-administering the inhibitor elacridar. Indeed, during *in vitro* cell-based assays, it was evidenced that etamicastat and nepicastat are P-gp substrates. Still, at 30 mg kg^{-1} by oral route, nepicastat was able to affect catecholamine levels in the brain and heart, while etamicastat reduced norepinephrine levels in the heart, without affecting the prefrontal and parietal cortices [470].

Other preclinical studies performed in rats reinforced that etamicastat revealed a limited transfer to brain tissues, through quantitative autoradiography, following a 50 mg kg^{-1} dose administration [471]; and through unaltered catecholamine levels in the brain cortex of spontaneously hypertensive rats, after 30 mg kg^{-1} by oral route [472]. Comparing renal denervation surgery with etamicastat administration in spontaneously hypertensive rats, Pires et al. [473] concluded that etamicastat promoted a more prolonged downregulation of sympathetic activity than renal denervation, achieving a sustained decrease in systolic and diastolic blood pressure.

In healthy humans, etamicastat did not modify pharmacodynamic variables in relation to placebo following the first dose (25-600 mg kg^{-1}), however after multiple dose administration (once-daily, 10 days), a significant decrease in diastolic blood pressure occurred at 100 and 200 mg kg^{-1} and there was a reduction of norepinephrine excretion in urine [469]. Identically, in patients with hypertension, etamicastat showed a reduction in systolic and diastolic blood pressure after 10 days of treatment [465]. Concerning pharmacokinetics, it is important to highlight that a relatively high interindividual variability in pharmacokinetic parameters has been observed. This is justified by the fact that *N*-acetylation mediated by *N*-acetyltransferase (NAT), specially the NAT2 phenotype, is the main metabolic pathway of etamicastat, leading to differences in systemic exposure between poor and rapid NAT2 acetylators [464,465,469]. The metabolite formed by *N*-acetylation is BIA 5-961 but etamicastat can also undergo other reactions such as glucuronidation, oxidation, oxidative deamination and desulfation [474]. Although the main metabolites inhibit DBH, catecholamine levels were not altered in mice after 100 mg kg^{-1} administration by intraperitoneal route and thus, only etamicastat demonstrates pharmacological effects [471]. Its absorption is quick (3-4 h) and it is mostly eliminated in urine (58.5%), unchanged (20%) or as BIA 5-961 (10.7%) [474].

To finalize, information about zamicastat [(R)-5-(2-(benzylamino)ethyl)-1-(6,8-difluorochroman-3-yl)-1H-imidazole-2(3H)-thione; BIA 5-1058] in literature is yet scarce. Zamicastat is a reversible DBH inhibitor that decreases norepinephrine levels in the periphery without effect in brain tissues [475]. It was demonstrated that zamicastat (Figure I.11) displays affinity for free DBH as well as for the complex enzyme-substrate, and does not affect DBH expression *in vivo* [476]. In spontaneously hypertensive rats, this compound decreased systolic and diastolic blood pressure without modifying heart rate (3, 30, 100 mg kg^{-1}, oral route). The combination of zamicastat at 30 mg kg^{-1} with other antihypertensive drugs from different groups (e.g. angiotensin converting enzyme inhibitors, angiotensin receptor antagonists, diuretics, calcium channel blockers) enabled a stronger and more prolonged blood pressure reduction than any of the other compounds alone [475]. Furthermore, in aged spontaneously hypertensive rats, zamicastat decreased systolic blood pressure, the heart/body weight ratio, plasma levels of inflammatory markers, triglycerides and free fatty acids after a 9 week treatment with

30 mg kg^{-1}. Thus, it presented cardiometabolic benefits and reduced end-organ damage [477].

All the aforementioned DBH inhibitors (etamicastat, nepicastat, zamicastat) were submitted to experimental assays described in this thesis.

I.4.3. DIBENZ[B,F]AZEPINE-5-CARBOXAMIDE DERIVATIVES

According to the World Health Organization, 50 million people in the world are estimated to have epilepsy, 80% of which live in low and middle income countries [478]. The exact definition of epilepsy has been changing over time. In 2006, the International League Against Epilepsy (ILAE) defined epilepsy as a brain disorder characterized by an enduring predisposition to generate epileptic seizures, and by the neurobiological, cognitive, psychological and social consequences of this condition. Later in 2014, the definition of epilepsy was updated as a disease of the brain defined by any of the following conditions: at least two unprovoked (or reflex) seizures occurring more than 24 h apart; one unprovoked (or reflex) seizure and a probability of further seizures similar to the general recurrence risk (at least 60%) after two unprovoked seizures, occurring over the next 10 years; diagnosis of an epilepsy syndrome. In turn, an epileptic seizure is generally accepted as the transient occurrence of signs and/or symptoms due to abnormal, excessive or synchronous neuronal activity in the brain [479]. In 1981, the ILAE classified seizures as partial, which could be subdivided into simple or complex, depending on whether there was consciousness impairment during the seizure; or generalized, when both brain hemispheres were involved. Generalized seizures could be subdivided into tonic and/or clonic, myoclonic, absences, atonic and epileptic spasms. Furthermore, in 1989, epilepsies and epileptic syndromes were categorized by etiology into two broad groups, idiopathic or symptomatic [480]. Nevertheless, these terminologies are regularly revised through the years, such as the ILAE 2017 amendments to seizure type classification that encompass seizures of focal, generalized or unknown onset [481].

Although methods such as surgery [482], vagal nerve stimulation and dietary adjustments (e.g. ketogenic diet) have been employed to treat epilepsy, antiepileptic drugs (AEDs) remain the most widely used treatment strategy [483]. The treatment of

epilepsy began with potassium bromide in 1857, which was found to effectively reduce the frequency of seizures, despite the absence of clinical controlled trials. The discovery of the anticonvulsant properties of phenobarbital occurred afterwards in 1912 and eventually surpassed bromide therapy. Still, the search for a less sedative compound continued, and a number of non-sedative phenyl compounds were developed, among which was phenytoin [484]. Phenytoin was the first AED to be discovered using a preclinical electroshock model that demonstrated its efficacy in preventing seizures. It received official FDA approval in 1953 [485]. Other first-generation AEDs encompass primidone (1954), ethosuximide (1960), carbamazepine (1974), valproic acid (1978) and benzodiazepines (e.g. clonazepam). These drugs have proven efficacy and remain in the current clinical use [486] but several CNS and non-CNS adverse effects influence their tolerability, like nausea, loss of coordination, vomiting, rash and motor disturbances [485].

Second- and third-generation AEDs emerged from the optimization of the pharmacokinetic properties and/or tolerability of first-generation AEDs [483]. The compounds were identified by rational drug design, structural modification of existing molecules and systematic screening against a range of seizure models in rodents [484]. Examples of second-generation AEDs are gabapentin, lamotrigine, levetiracetam, oxcarbazepine, pregabalin and topiramate, among others [486]. Particularly, oxcarbazepine is a second-generation drug to carbamazepine with action on the voltage-gated sodium channel [487]. In humans, carbamazepine undergoes oxidative metabolism to carbamazepine-10,11-epoxide, whereas oxcarbazepine is reduced to its pharmacologically active metabolite licarbazepine, thereby avoiding the formation of the toxic epoxides. In reality, oxcarbazepine acts as an achiral prodrug and undergoes a stereoselective biotransformation, given that licarbazepine appears in plasma as *S*-licarbazepine [eslicarbazepine; (10S)-10-hydroxy-10,11-dihydro-5H-dibenz(b,f)azepin-5-carboxamide; BIA 2-194] and *R*-licarbazepine in an approximately 4:1 enantiomeric ratio [488].

The favourable pharmacokinetic profile of *S*-licarbazepine was one of the incentives for the development of a new third-generation AED, eslicarbazepine acetate [(S)-10-acetoxy-10,11-dihydro-5H-dibenz(b,f)azepine-5-carboxamide; BIA 2-093] [487]. Eslicarbazepine acetate was designed to be a member of the dibenz[b,f]azepine family

represented by carbamazepine and oxcarbazepine, sharing with them the dibenzazepine nucleus with the 5-carboxamide substituent. However, it is structurally different at the 10,11-position, which results in differences in metabolism [489]. Unlike carbamazepine, eslicarbazepine acetate (Figure I.12) is not metabolized to carbamazepine-10,11-epoxide and unlike oxcarbazepine, it is not pre-systemically metabolized to *S*-licarbazepine and *R*-licarbazepine. Instead, eslicarbazepine acetate is rapidly and extensively biotransformed into the active entity *S*-licarbazepine following oral administration, and chiral inversion to *R*-licarbazepine (through oxidation to oxcarbazepine) is minor [487]. The *S*-licarbazepine-to-*R*-licarbazepine AUC ratio is approximately 19 with only 0.5% circulating oxcarbazepine. Therefore, exposure to *R*-licarbazepine and oxcarbazepine after oral administration of eslicarbazepine acetate is minimal [490].

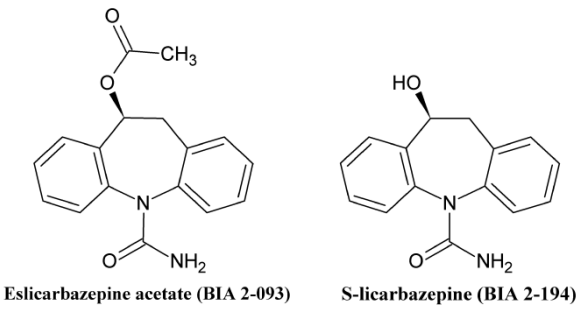

Figure I.12. Chemical structures of eslicarbazepine acetate and *S*-licarbazepine.

In 2009, eslicarbazepine acetate was approved by EMA as Zebinix® (200, 400, 600, 800 mg) and in 2013 by the FDA with brand name Aptiom®, as an adjunctive therapy in adults with partial-onset seizures with or without secondary generalization. Mechanistically, it not only interacts with voltage-gated sodium channels, enhancing their slow inactivation, but also blocks low and high-affinity inward currents of calcium channel $hCa_v3.2$ [491].

Regarding pharmacokinetics, following an oral administration of 600 mg eslicarbazepine acetate, *S*-licarbazepine levels achieved C_{max} in plasma after 2-3 h post-dose [492]. Bioavailability is considered high, given that the amount of metabolites recovered in urine corresponded to more than 90% of an eslicarbazepine acetate dose and *S*-licarbazepine was responsible for more than 95% of systemic exposure. Preclinical

studies are normally performed in species with the most similar metabolic pathways to humans, i.e. the mouse, the hamster and the rabbit [490]. Thus, preclinical studies conducted in adult male CD1 mice suggested that *S*-licarbazepine crosses the BBB in lesser extent than *R*-licarbazepine from the total $AUC_{0\text{-}inf}$ brain-plasma ratios, which were 0.39 and 0.23, respectively (350 mg kg^{-1}, oral route). This reveals a stereoselective brain disposition, as the brain-plasma ratio of *S*-licarbazepine is approximately 2 times greater than that of *R*-licarbazepine [493]. In another study with adult CD1 mice, *R*-licarbazepine once again revealed a smaller extent of brain distribution than *S*-licarbazepine and oxcarbazepine [494]. To assess the involvement of efflux transporters, mice were pretreated with verapamil or probenecid as P-gp or MRP inhibitors, but the brain-plasma ratio of *S*-licarbazepine was unaffected by both compounds. Conversely, verapamil, but not probenecid, increased the brain-plasma ratio of *R*-licarbazepine, revealing that *R*-licarbazepine is a P-gp substrate. Moreover, the brain-plasma ratio of *R*-licarbazepine with verapamil was similar to that of *S*-licarbazepine in vehicle-treated animals. These results were in agreement with previous findings reporting that the racemic (*R,S*)-licarbazepine appears to cross the BBB by P-gp mediated active transport, in alternative to simple passive diffusion [495].

Despite the variety of AEDs, seizures persist in a considerable proportion of epilepsy patients, approximately 30%, who are considered pharmacoresistant or refractory to treatment. These patients do not respond to any of two to three first line AEDs, even in an optimally monitored regimen. The basis of cellular resistance is not yet completely known, but may be related with modifications affecting AED targets [496] or the BBB, as previously referred in section I.3.3. In a study by Doeser et al. [497] *S*-licarbazepine potentially overcame a cellular resistance mechanism to conventional therapeutic antiepileptic drugs and simultaneously exhibited anticonvulsant and antiepileptogenic effects.

Both eslicarbazepine acetate and *S*-licarbazepine were tested in the experimental assays presented in this dissertation, specifically in the PAMPA-BBB model.

I.5. AIMS OF THIS THESIS

Evaluating the passage of compounds to the CNS is an essential step during any drug discovery and development program, whether the therapeutic target is peripheral or central. In order to perform this assessment, it is necessary to comprehend and apply the pharmacokinetic concepts of CNS exposure, including rate, extent and intra-brain distribution, as well as, to characterize the interactions of compounds with the main interface that separates the CNS from the peripheral environment, the BBB. Nevertheless, due to the reasons exposed in the general introduction of the present thesis, it is not yet possible to completely mimic all intricacies of the BBB in a laboratorial setting and, more specifically, in one sufficiently predictive model, while maintaining the high throughput requirements of drug screening stages.

Therefore, the main goal of the present thesis was to establish a viable screening strategy to describe the passage of compounds across the BBB, based on the association of complementary *in vitro* and *in vivo* models and on the combination of the data supplied by each model. The specific aims outlined for the implementation of this work were as follows:

- Development and optimization of an *in vitro* PAMPA-BBB model to estimate the passive transcellular permeability of compounds and the influence of their physicochemical properties on the rate of passage across the BBB.

This method was applied to COMT inhibitors, DBH inhibitors and DAC derivatives as test compounds.

- Development and optimization of *in vitro* cell-based assays to assess the effect of the two major efflux transporters of the BBB, P-gp and BCRP, on the CNS penetration of compounds. Potential P-gp and BCRP inhibitors were identified using intracellular accumulation assays while P-gp and BCRP substrates were identified resorting to validated bidirectional transport assays. The quantification of reference and test compounds in the previous assay implied the validation of high-performance liquid chromatography (HPLC) techniques beforehand.

These assays were applied to COMT inhibitors and DBH inhibitors as test compounds.

- Adaptation and execution of the assay of ultrafiltration with plasma and brain of Wistar rats to determine $f_{u,plasma}$ and $f_{u,brain}$.

These assays were performed with COMT inhibitors, tolcapone and BIA 9-1079.

- *In vivo* pharmacokinetic studies in plasma and brain of Wistar rats to determine the extent of CNS penetration, $K_{p,uu}$, and intra-brain distribution following an intravenous administration of compounds. The involvement of P-gp and BCRP on the *in vivo* brain disposition was investigated by co-administering the compounds with a P-gp and BCRP inhibitor. The quantification of the compounds in all biological samples implied the previous validation of HPLC techniques in plasma and brain rat matrices.

These studies were carried out with COMT inhibitors, tolcapone and BIA 9-1079.

CHAPTER II

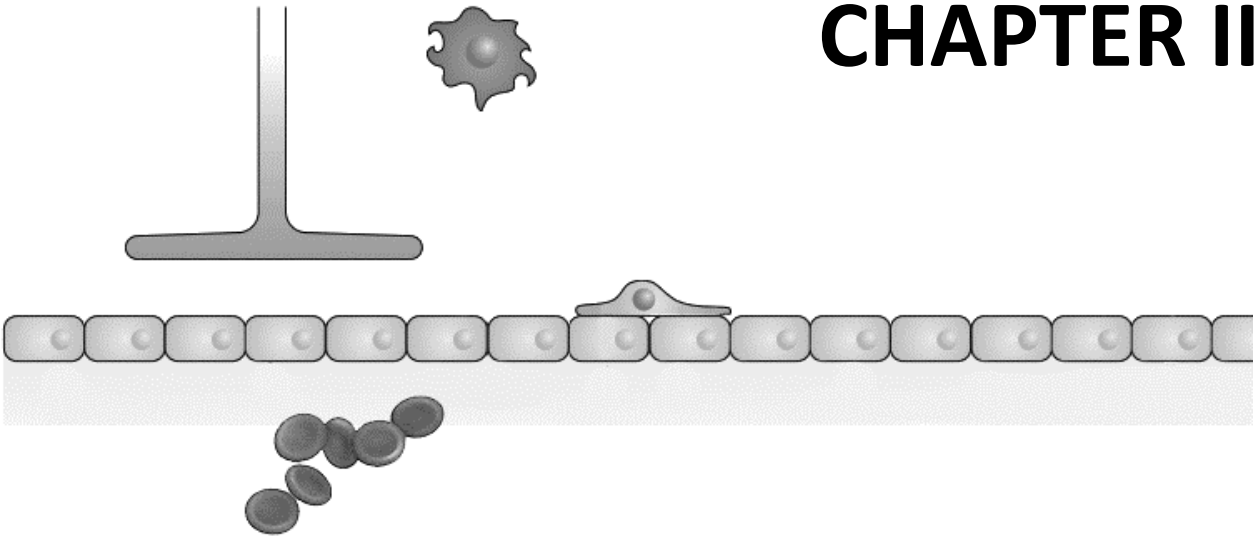

PASSIVE PERMEABILITY: PAMPA-BBB

CHAPTER II. PASSIVE PERMEABILITY: PAMPA-BBB

The PAMPA technique is an HTS assay applied to evaluate the passive transcellular permeability of compounds. Even though it was originally developed to determine gastrointestinal absorption, through the years it underwent modifications to predict the rate of passive permeation across other biological barriers such as the BBB.

In this chapter, a cost-effective and reproducible lipid extraction method was applied to obtain an *in-house* brain lipid extract capable of discriminating compounds according to their permeability across the BBB. Firstly, the lipid extraction technique was described, followed by the optimization steps of the PAMPA-BBB model. These optimization procedures were carried out using marketed drugs as reference compounds. Then, the relation between the physicochemical properties of reference molecules and their passive permeation was analysed, and the PAMPA-BBB technique was performed with a set of test compounds, encompassing COMT inhibitors, DBH inhibitors and DAC derivatives.

II.1. INTRODUCTION

The high attrition rate reported among the CNS drug discovery programs together with the unsatisfactory number of neurotherapeutics that currently reach the market represent a great challenge to the pharmaceutical industry [84,324]. Indeed, the passage through the BBB, which is the CNS barrier that mainly regulates drug permeability into the brain, is considered the bottleneck of a fast and successful development of CNS-acting drugs [67,498]. Therefore, an early screening of the BBB penetration potential of new chemical entities in drug discovery programs becomes crucial not only for CNS-compounds in order to evaluate if the therapeutic target is reached, but also for peripherally-active compounds whose penetration into the brain may cause adverse neurological side-effects. Since a great number of compounds must be simultaneously and quickly evaluated at the initial phases of drug discovery programs, several attempts have been undertaken to develop HTS *in vitro* assays that predict the penetration of new drug candidates through the BBB [102]. Among them is the *in vitro* PAMPA that emerged as a HTS tool, less costly and labour intensive than cell-based techniques and that can be easily applied at early drug discovery stages, in opposition to the *in vivo* methodologies. Since its introduction by Kansy et al. [175], PAMPA has been widely applied to predict the gastrointestinal absorption of drugs by transcellular passive diffusion. In this non-cell-based system, an artificial lipid membrane is impregnated into a porous filter and the compounds are screened according to their Papp through that membrane. Modifying the composition of the artificial membrane, PAMPA has been adapted to mimic other biological membranes, including the skin [499,500] and the BBB [178,179,197,198,501]. Despite the absence of active influx and efflux systems and enzymes, PAMPA is able to accurately measure the transcellular passive diffusion of compounds, which is the main entry pathway of compounds to the brain across the membrane of brain endothelial cells [85,176,200,502]. At the beginning of drug discovery programs this information is of great importance since the evaluation and interpretation of multiple mechanistic-type assays may be expensive, time-consuming and challenging.

The first successful PAMPA-BBB model consisted in coating the PAMPA filter with commercialized porcine polar brain lipid (PBL) and revealed an improved ability to

predict the BBB permeation when compared with phosphatidylcholine, which is mainly used to predict gastrointestinal absorption. Compounds with Papp lower than 2.0 x 10^{-6} cm s^{-1} were classified as non-BBB permeable (BBB^-) while those with Papp higher than 4.0 x 10^{-6} cm s^{-1} were considered BBB permeable (BBB^+) [178]. Although other models have been subsequently developed in an attempt to further improve the assessment of the BBB permeability, this pioneer model using PBL was breakthrough to accurately distinguish BBB^+ from BBB^- and hence, it is currently used to validate other PAMPA-BBB models [193]. Nonetheless, it is noteworthy that differences in experimental conditions affect the outcome of the PAMPA model using PBL, as recently demonstrated by Müller et al. [195]. These findings imply method optimization and validation in each laboratory before evaluating new drug candidates.

In the present work, an *in-house* brain lipid extract obtained by a modified Folch extraction procedure was tested as lipid barrier in a PAMPA-BBB model. The optimization of the experimental conditions of the model was carried using 18 commercially available compounds as reference molecules and the results were compared with those obtained with phosphatidylcholine and PBL. Phosphatidylcholine was used to confirm the differences in compound classification between using brain-specific lipid solutions and general lipid solutions [178], while PBL was used as it is regarded as the reference lipid membrane in PAMPA models to predict passive permeability across the BBB. The reference molecules are chemically and structurally diverse, belong to a wide range of pharmacological groups and are frequently used during the development of *in vitro* BBB models [178,197,198]. In order to demonstrate the discriminatory ability of the current PAMPA-BBB model to support drug discovery programs, the optimized experimental conditions were then applied to evaluate a set of 11 test molecules (Figure II.1), encompassing peripheral and/or central COMT inhibitors, DBH inhibitors and DAC derivatives. The aim of this study was to evaluate the reliability of the lipid extraction process in this context, as well as the discriminatory capacity of the *in-house* brain lipid extract between BBB^+ and BBB^- compounds and its applicability as lipid membrane in PAMPA. Furthermore, the physicochemical selectivity of the PAMPA model was estimated and *in vitro-in vivo* correlations were constructed to determine its predictive capacity.

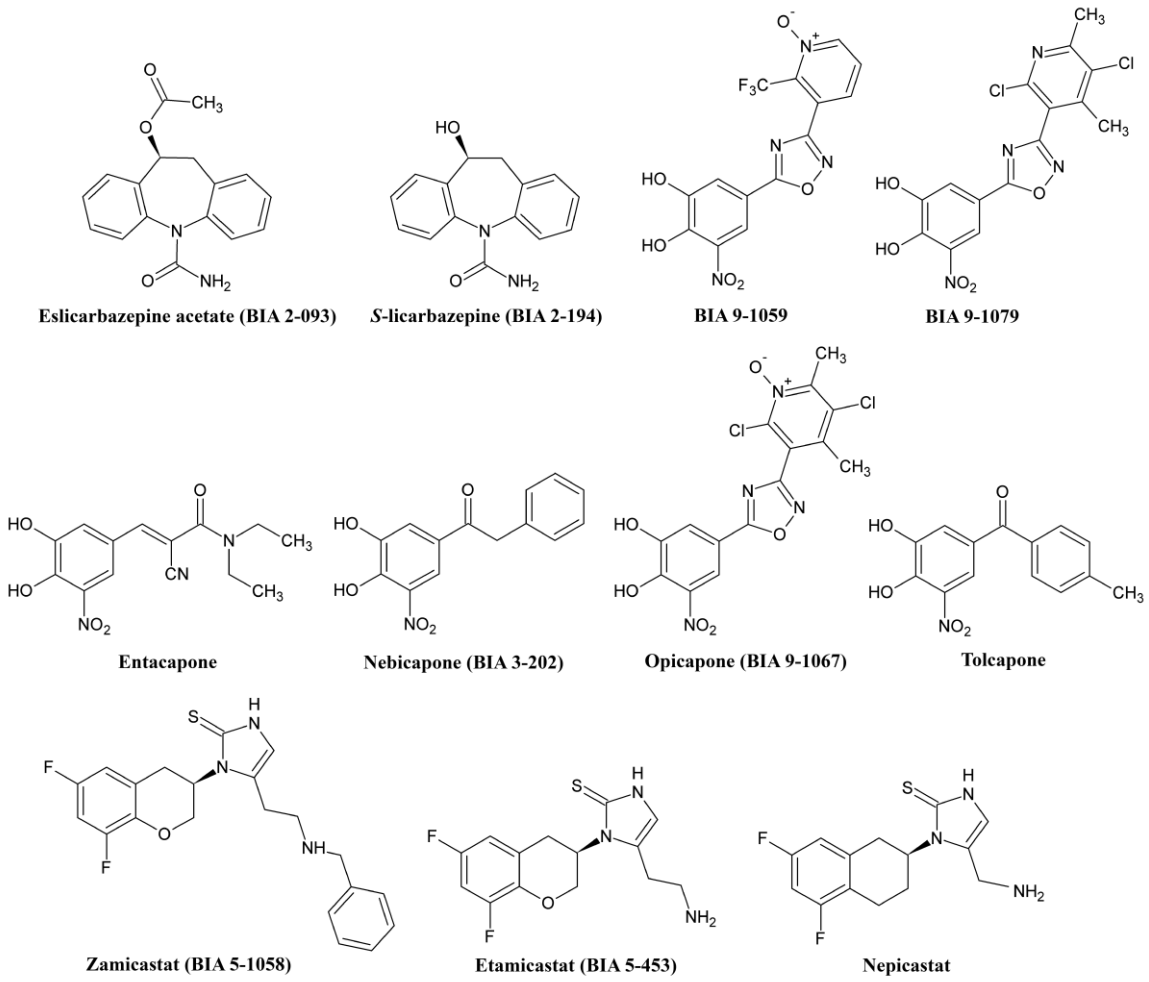

Figure II.1. Chemical structures of the 11 compounds used as test set in PAMPA models.

II.2. MATERIALS AND METHODS

II.2.1. CHEMICALS AND REAGENTS

Reference compounds including caffeine, carbamazepine, carbamazepine 10,11-epoxide, cimetidine, dopamine, furosemide, hydrocortisone, loperamide, norfloxacin, oxcarbazepine, propranolol, phenytoin, piroxicam, quinidine, sulfasalazine, trazodone and verapamil were obtained from Sigma–Aldrich (St., Louis, MO, USA). Atenolol was acquired from Acros Organics, ThermoFisher Scientific (MA, USA). Test compounds included tolcapone, entacapone, nebicapone (BIA 3-202), opicapone (BIA 9-1067), BIA 9-1059, BIA 9-1079, nepicastat, etamicastat (BIA 5-453), zamicastat (BIA 5-1058), eslicarbazepine acetate (BIA 2-093) and *S*-licarbazepine (BIA 2-194) that were kindly supplied by BIAL-Portela & Ca., S.A. (S. Mamede do Coronado, Portugal). Chloroform,

methanol (HPLC grade), ammonium acetate, ammonium molybdate, ascorbic acid, DMSO and 37% hydrochloric acid were purchased from Fisher Scientific (Leicestershire, UK). BHT was acquired from Acros Organics, Thermo Fisher Scientific (MA, USA), *n*-dodecane was acquired from Sigma–Aldrich (St. Louis, MO, USA) and 60% perchloric acid was purchased from Panreac (Barcelona, Spain). Monopotassium phosphate and disodium phosphate were acquired from Chem-Lab NV (Zedelgem, Belgium).

L-Phosphatidylcholine extracted from soybean (P5638) was purchased from Sigma–Aldrich (St., Louis, MO, USA) and PBL (no. 141101) from Avanti Polar Lipids, Inc. (Alabaster, AL).

II.2.2. LIPID EXTRACTION

The lipid extraction procedure was adapted from the traditional Folch extraction method [503–505]. 0.01% BHT was added to solvents as antioxidant and all protocol stages were performed with glass material. Firstly, fresh pig brain tissue (0.3 g) was homogenized in 2 mL of methanol using a glass-teflon homogenizer. Then, 4 mL of chloroform were added [chloroform:methanol (2:1, v/v)], ensuring a 20-fold dilution of the tissue weight. The homogenates were transferred to sealed amber vials and stored at -80 °C until extraction, or to test tubes for overnight rotation at 4 °C. Following the overnight rotation period, 1.5 mL of 0.15 M ammonium acetate were added in order to achieve the critical ratios between the solvents [chloroform:methanol:ammonium acetate (8:4:3, v/v/v)]. The sample was vortexed (15 s), centrifuged (2000 *g*/4 °C/10 min) and the lower chloroform phase was aspirated gently into a new test tube. Subsequently, 6 mL of chloroform:methanol (2:1, v/v) were added to the original homogenate, vortexed and centrifuged as above. The lower phase was combined with the first chloroform extract and a second phase extraction was initiated by adding 1.5 mL of 0.15 M ammonium acetate, vortexing and centrifuging as formerly stated. Lastly, the lower phase was transferred to a new test tube and evaporated under nitrogen at 37 °C. According to the weight of lipid residue, *n*-dodecane was added to redissolve the lipid in the final concentration (2% or 10%, w/v) and the lipid solution was applied in the PAMPA assay.

II.2.2.1. Phosphorus assay

The phosphorus assay was conducted to estimate the phospholipid concentration of the lipid extracts and evaluate the variations of the phospholipid content in extracts from different brain regions. The concentration of phosphorus in each *in-house* extract was determined by comparing the absorbance values of the sample extracts with a monopotassium phosphate reference curve (1–5 mg of phosphorus standards prepared from a 100 mg mL^{-1} stock solution). This assay was based on the colorimetric ascorbic acid technique proposed by Rouser et al. [506]. Lipid samples were dried completely under nitrogen at 45 °C, 0.65 mL of 60% perchloric acid were added to each tube and the tubes were placed in a heated-block at 180 °C for 45 min. After cooling, 3.3 mL of water, 0.5 mL of a 25 mg mL^{-1} ammonium molybdate solution and 0.5 mL of a 100 mg mL^{-1} ascorbic acid solution were added to the tubes, vortexing after each addition. The tubes were placed in a boiling water bath for 10 min and the absorbance of the cold samples was read at 800 nm.

The phospholipid content of the extracts was estimated according to the equation II.1 from Mitchell [505]:

$$\text{Phospholipid content} = \frac{\mu\text{g phosphorus} \times 780}{30.97} \qquad \text{(II.1)}$$

where 780 is the average mass of phospholipids (grams) and 30.97 is the molecular weight of phosphorus (grams).

Data were analysed for statistical significance using one-way analysis of variance (ANOVA) with a *post-hoc* Bonferroni test. Differences were considered significant when $p < 0.05$.

II.2.3. PAMPA-BBB PROCEDURE OPTIMIZATION

Stock solutions (10 mM) of each reference and test compounds were prepared by dissolving the corresponding amount of drug in DMSO and then diluted with phosphate buffer saline (PBS) pH 7.4 to obtain the donor drug solution at the final concentration of 500 µM (final DMSO concentration of 5%). This concentration was chosen for all drugs with the exception of zamicastat (tested at 100 µM due to compound precipitation) in order to allow the quantitation of all compounds at the acceptor compartment. There is

no risk of saturation given the absence of carrier-mediated transport processes at the artificial lipid membrane.

PAMPA optimization was based on the previously developed method by our research group for the prediction of human intestinal absorption and plasma protein binding [507]. To adapt the experimental conditions for the prediction of BBB permeability and compare the Papp obtained with the *in-house* lipid extract with those achieved with phosphatidylcholine and PBL, six assays were performed varying the lipid type of the artificial membrane (phosphatidylcholine, PBL or *in-house* extract) and its concentration. Thus, the artificial lipid membrane solutions were daily prepared by dissolving each lipid in *n*-dodecane at two different concentrations (2% or 10%, w/v) and the Papp of the reference compounds through each artificial membrane was evaluated. Therefore, the 96-well microfilter plates (MultiScreen1-IP, catalogue no. MAIPNTR10, Millipore Corporation, Bedford, MA, USA) and the 96-well microtiter plates (MultiScreen1-IP, catalogue no. MATRNPS50, Millipore Corporation, Bedford, MA, USA) were used as acceptor and donor compartments, respectively.

The PAMPA assay was initiated by adding 300 µL of each donor solution per well of the microtiter plate and coating the hydrophobic filter of each acceptor well with 6 mL of phosphatidylcholine, PBL or *in-house* brain lipid extract in *n*-dodecane. The volume of lipid solution was chosen to enhance method precision and prevent interferences in the spectrophotometric quantification of acceptor wells. Indeed, volumes lower than 5 µL compromised method precision with higher inter-well coefficient of variation values, whereas volumes higher than 6 µL impaired the spectrophotometric quantification. After applying the lipid, acceptor wells were filled with 150 µL of PBS (pH 7.4) containing the same content of DMSO as the donor solution, thereby avoiding co-solvent influence only in one of the compartments. The acceptor filter plate was then carefully placed onto the donor plate and the assembly was incubated for 3, 6 or 16 h at room temperature, under gentle stirring (50 rpm). After incubation, the plates were separated and the drug concentrations were determined by ultraviolet spectrophotometry. Equilibrium solutions were prepared in parallel, by diluting the stock solutions to the same concentration as that with no membrane barrier. All experiments were executed in triplicate and the Papp was reported as mean ± standard deviation (SD).

The Papp of each compound (cm s^{-1}) was calculated based on Sugano et al. [508] and applying the equation II.2:

$$Papp = -2.303 \times \frac{V_{dn}V_{ac}}{V_{dn}+V_{ac}} \times \frac{1}{S \times t} \times \log\left(1-\frac{flux\%}{100}\right)$$
$$Flux(\%) = \frac{OD_{ac}}{OD_{eq}} \quad \text{(II.2)}$$

where V_{dn} is the volume of the donor solution (0.3 mL), V_{ac} is the volume of the acceptor solution (0.15 mL), S is the surface area of the filter that separates both compartments (0.26 cm^2), t is the incubation time (s), OD_{ac} is the optical density of the solution in the acceptor compartment and OD_{eq} is the optical density of the equilibrium solution.

The PAMPA model using the *in-house* lipid extract was repeated two additional times, using lipid extracts from different brains in order to evaluate the interindividual reproducibility.

II.2.4. PAMPA AND PHYSICOCHEMICAL PROPERTIES AFFECTING BBB PERMEATION

Passive permeation of drugs through cell membranes is dependent not only on the chemical composition of the membrane but also on the physicochemical properties of the molecules, including the octanol-water partition coefficient (logP), the octanol-water distribution coefficient (logD) at pH 7.4, molecular weight, charge state, rotatable bonds, topological polar surface area (TPSA) and hydrogen bonding atoms, among other parameters [502,509–514]. Thus, in the scope of our work, the Papp values achieved using the PAMPA technique, were correlated with known physicochemical characteristics of the reference compounds (Table II.1) by simple linear regression analysis and the goodness of fit was assessed by the square of Pearson correlation coefficient (r^2).

Table II.1. Literature classification and measured and predicted physicochemical properties of the reference compounds used during the development of PAMPA models [86,515,516].

Reference compound	Literature classification	MW (Da)	pKa	Charge at pH 7.4	Log P	Log D (pH 7.4)	TPSA	HBA	HBD	THBC	RB
Caffeine	BBB+	194.1	10.4	0	- 0.07	-0.07	48.5	3	0	3	0
Carbamazepine	BBB+	236.2	9.3	0	2.45	2.45	46.81	1	1	2	0
Carbamazepine 10,11-epoxide	BBB+	252.3	NF	NF	1.3	0.69	55.61	1	1	2	0
Oxcarbazepine	BBB+	252.3	13.7; 10	NF	1.7	1.25	65.09	2	1	3	1
Phenytoin	BBB+	252.3	8.33	0	2.47	2.47	58.2	2	2	4	2
Propranolol	BBB+	259.3	9.45	+	3.48	1.2	46.24	3	2	5	6
Trazodone	BBB+	371.9	7.00	0	3.80	2.64	34.31	4	0	4	7
Verapamil	BBB+	491.1	8.92	+	3.79	2.51	56.29	6	0	6	14
Atenolol	BBB-	266.3	9.6	+	0.16	-1.03	92.48	5	3	8	8
Cimetidine	BBB-	252.3	7.1	+	0.40	0.33	81.67	6	3	9	6
Dopamine	BBB-	153.2	8.93	NF	-0.98	-0.8	66.5	3	3	6	2
Furosemide	BBB-	330.7	3.9	-	2.03	-1.54	130.02	5	3	8	5
Hydrocortisone	BBB-	362.4	NF	NF	1.61	1.37	104.22	5	3	8	2
Loperamide	BBB-	477.0	8.7	+	5.5	4.22	43.18	4	1	5	9
Norfloxacin	BBB-	319.3	8.7; 4.4	±	-1.03	-0.46	75.12	6	2	8	5
Piroxicam	BBB-	331.3	5.5; 1.9	±	3.06	0.2	104.05	5	2	7	2
Quinidine	BBB-	324.4	9.3	+	3.44	2.41	43.08	4	1	5	4
Sulfasalazine	BBB-	398.4	2.0	-	2.3	-0.78	148.16	8	3	11	6

BBB, blood-brain barrier; HBA, hydrogen bond acceptors; HBD, hydrogen bond donors; Log P, octanol-water partition coefficient; Log D, octanol-water distribution coefficient at pH 7.4; MW, molecular weight; pKa, ionization constant; NF, not found; RB, rotatable bonds; THBC, total hydrogen bonding capacity; TPSA, topological polar surface area. (+) positive charge, (-) negative charge, (0) neutral, (±) zwitterion.

II.3. RESULTS AND DISCUSSION

II.3.1. LIPID EXTRACTION

Results from the phosphorus assay following lipid extractions from distinct brain regions revealed statistically significant differences between the phospholipid content of extracts from frontal cortex, parietal cortex and whole-brain when compared to occipital cortex (Figure II.2). This finding indicated that in order to avoid variations of phospholipid content, it is recommendable to extract the lipid from a tissue pool instead of isolating it from a specific brain region. Moreover, the extraction procedure becomes

easier to perform and less laborious. Consequently, this procedure was adopted in all lipid extractions preceding PAMPA assays. In addition, the phospholipid content of lipid extracts from three different brains showed approximately 18.6 ± 4.61 μg phospholipids per mg wet brain weight (*n* = 2 extracts per brain), indicating a good reproducibility of the lipid extraction method.

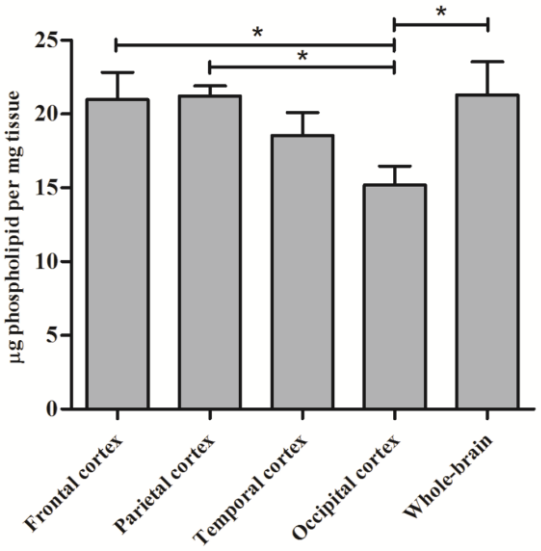

Figure II.2. Comparison of total phospholipid content (mg per mg tissue) in distinct brain areas and in whole-brain lipid extracts. Values are shown as mean ± standard deviation (*n* = 3 extracts per brain area). Statistically significant differences ($p < 0.05$) are marked with an asterisk (*).

II.3.2. PAMPA OPTIMIZATION

As previously stated in section II.2.3, initial experimental conditions were established based on a PAMPA method already developed by our research group [507] but further studies concerning the buffer solution (TRIS or PBS at pH 7.4), incubation time (3 h, 6 h or 16 h) and stirring were executed. All assays were conducted at pH 7.4 to mimic the physiological conditions in which the blood and the brain extracellular fluid are maintained. The conditions that allowed a better discrimination between BBB^- and BBB^+ compounds were selected for subsequent assays and included the use of PBS; a 16 h incubation period that improved the discrimination of low permeant compounds from one another; and a gentle stirring of 50 rpm. Indeed, stirring PAMPA plates leads to a reduction of the thickness of the unstirred water layer, which is nearly absent in vivo and

particularly in the BBB [517], thereby preventing a limited diffusion of lipophilic molecules.

The Papp values experimentally obtained for the reference compounds under the six distinct conditions are presented in Table II.2.

Table II.2. Experimental apparent permeability coefficient (Papp) values of the reference compounds under the six experimental conditions tested in PAMPA development. Results are expressed as mean (standard deviation), *n* = 3.

Lipid	**Phosphatidylcholine**		**PBL**		***In-house* lipid extract**	
Concentration (w/v)	2%	10%	2%	10%	2%	10%
Reference compound	Papp ($x10^{-6}$ cm s^{-1})					
Caffeine	2.18 (0.90)	2.01 (0.03)	1.56 (0.48)	1.69 (0.03)	1.88 (0.04)	1.59 (0.35)
Carbamazepine	7.66 (0.18)	8.16 (0.46)	9.30 (0.60)	13.2 (0.98)	9.58 (0.44)	9.48 (0.52)
Carbamazepine 10,11-epoxide	9.03 (4.81)	13.2 (4.72)	3.07 (0.14)	13.2 (3.98)	3.26 (0.19)	5.74 (0.70)
Oxcarbazepine	12.9 (1.82)	12.2 (0.50)	5.59 (0.22)	10.0 (0.67)	5.81 (0.05)	11.2 (2.73)
Phenytoin	17.3 (9.80)	8.32 (0.77)	9.93 (2.41)	15.3 (9.45)	7.94 (0.23)	7.78 (1.25)
Propranolol	10.8 (0.31)	4.80 (0.53)	21.3 (2.74)	10.5 (0.67)	11.6 (1.71)	2.17 (0.14)
Trazodone	7.55 (0.18)	4.25 (0.28)	18.4 (2.81)	8.74 (0.40)	8.84 (0.61)	3.07 (0.32)
Verapamil	9.49 (0.23)	6.02 (0.68)	12.1 (1.13)	13.9 (3.01)	14.1 (0.90)	5.39 (0.49)
Atenolol	0.54 (0.55)	0.61 (0.11)	0.10 (0.03)	0.67 (0.28)	0.47 (0.05)	1.35 (0.36)
Cimetidine	3.02 (0.37)	0.56 (0.06)	0.68 (0.20)	1.04 (0.36)	0.73 (0.06)	0.21 (0.29)
Dopamine	1.33 (0.02)	0.39 (0.02)	0.16 (0.11)	0.29 (0.04)	0.26 (0.05)	0.50 (0.05)
Furosemide	0.03 (0.03)	0.05 (0.003)	0.08 (0.009)	0.04 (0.01)	0.04 (0.004)	0.07 (0.002)
Hydrocortisone	5.27 (0.19)	25.9 (5.78)	0.25 (0.16)	13.9 (0.84)	1.27 (0.09)	3.30 (0.03)
Loperamide	4.51 (0.12)	4.62 (0.38)	12.8 (0.43)	11.3 (4.28)	5.39 (1.22)	6.50 (1.30)
Norfloxacin	0.55 (0.04)	0.48 (0.03)	0.28 (0.02)	0.45 (0.15)	0.12 (0.03)	0.18 (0.03)
Piroxicam	1.34 (0.04)	1.51 (0.09)	0.93 (0.09)	0.89 (0.03)	1.04 (0.04)	0.99 (0.05)
Quinidine	7.76 (0.41)	6.13 (0.64)	8.34 (0.15)	12.7 (1.28)	8.34 (0.15)	7.95 (0.18)
Sulfasalazine	0.04 (0.02)	0.01 (0.003)	0.01 (0.0005)	0.04 (0.005)	0.01 (0.006)	0.03 (0.005)

The reduced SD values found for the majority of the compounds suggest a good reproducibility of the methods. The effect of the qualitative and quantitative characteristics of the lipid artificial membrane is evidenced in Figure II.3.

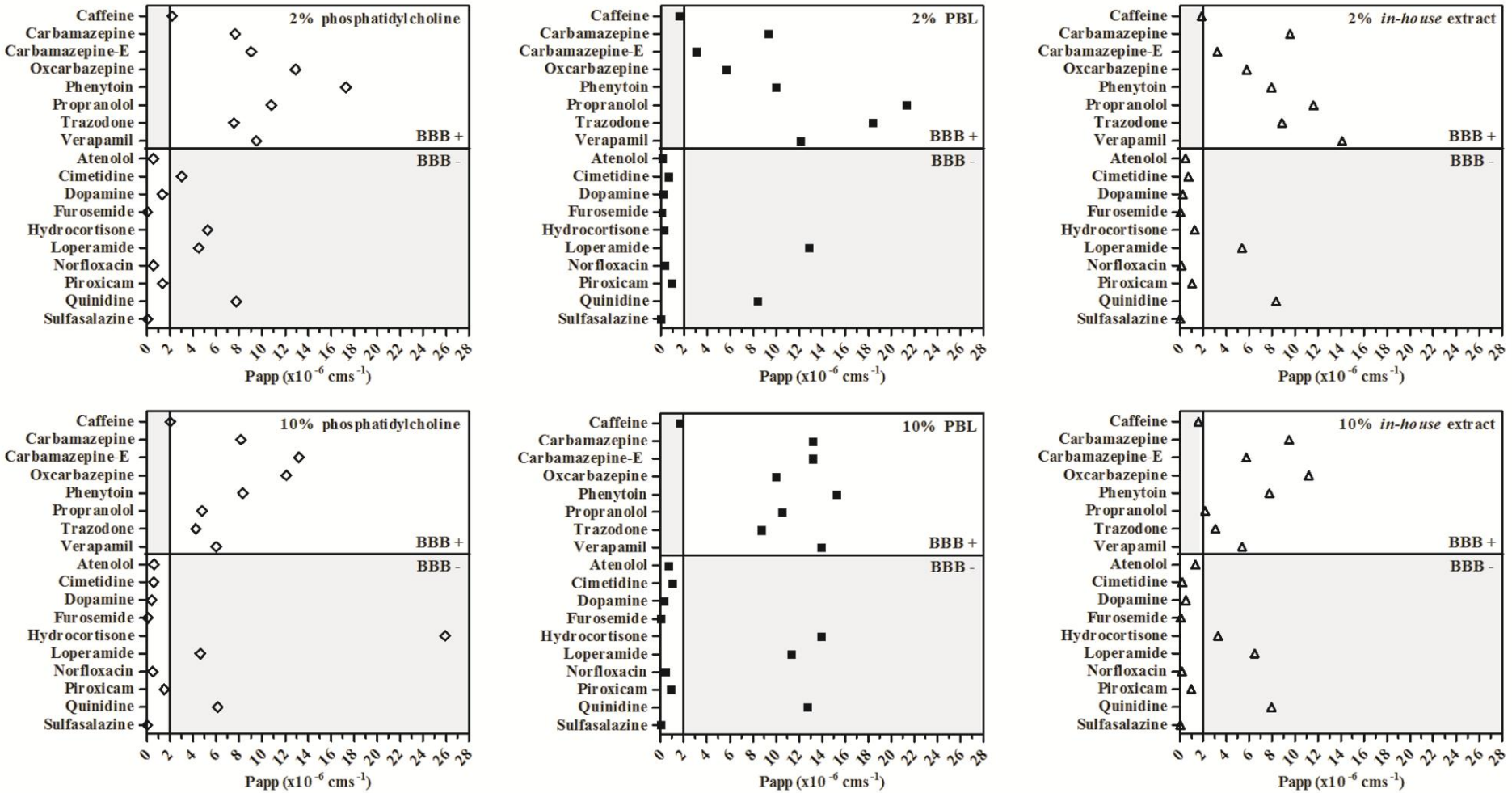

Figure II.3. Plot of the data from Table II.2 comparing the PAMPA models with 2% and 10% (w/v) phosphatidylcholine, porcine brain lipid (PBL) and *in-house* brain lipid extract for reference compounds. Compounds in grey areas were classified as false negative or false positive by the models. BBB, blood-brain barrier; carbamazepine-E, Carbamazepine 10,11-epoxide.

Accordingly, the arbitrary Papp cut-off value of 2.0 x 10^{-6} cm s^{-1} was defined to discriminate compounds possessing Papp values greater than 2.0 x 10^{-6} cm s^{-1} (considered BBB^+) and lower than 2.0 x 10^{-6} cm s^{-1} (considered BBB^-). The PAMPA models using the artificial membranes composed of 2% PBL and of 2% *in-house* lipid extract revealed one false negative (caffeine) and two false positives (quinidine and loperamide). Increasing the concentration of lipid extract to 10% resulted in one false negative (caffeine) and three false positives (hydrocortisone, loperamide and quinidine).

Based on the results of each experimental condition, *in vitro-in vivo* correlations were established between the *in vitro* rate of permeation, given by the Papp values of the reference compounds and the *in vivo* extent of brain penetration given by the respective log BB values reported in literature (Figure II.4).

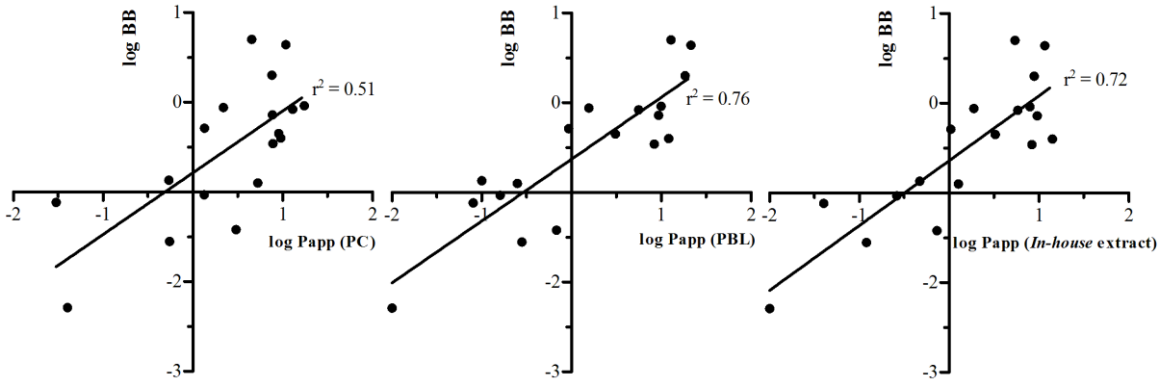

Figure II.4. Plot of the logarithmic apparent permeability coefficient (log Papp) values of reference compounds obtained with 2% (w/v) phosphatidylcholine (PC), porcine brain lipid (PBL) and *in-house* brain lipid extract against the corresponding logarithm value of total brain to total plasma drug concentration ratio (log BB). Log BB data were compiled from references [197,510,518].

Log BB is still often used in initial phases of drug discovery programs due to its easier experimental determination and data availability [92,519]. However, it describes the extent of brain permeation based on total drug concentrations which may reflect a high nonspecific binding to plasma proteins or brain tissue; in addition, it is heavily influenced by lipophilicity which generally favours passive permeation. Consequently, CNS drug discovery compounds should be optimized based on $K_{p,uu}$, although log BB

continues to be used with caution in the interpretation of its meaning [85,519]. From Figure II.4 it is evidenced that PAMPA models performed with 2% of PBL and 2% of the *in-house* lipid extract exhibit the highest correlation coefficients with log BB (r^2 = 0.76 and r^2 = 0.72, respectively) in opposition to 2% phosphatidylcholine which demonstrated a weak correlation of only r^2 = 0.51.

Therefore, from Figure II.3 and II.4, it is verified that the PAMPA assay performed with 2% of PBL preserved its predictive power as originally described by [178]. Importantly, the lipid extract herein proposed and tested as lipid artificial membrane revealed Papp values similar to those of 2% of PBL and predicted all the compounds in accordance with the standard methodology. The greater similarity in the classification of reference compounds between the *in-house* brain lipid extract and PBL is reflected by the strong Papp correlation (r^2 = 0.77), suggesting an equivalent discriminatory capacity for both lipids. In contrast, the correlation found between phosphatidylcholine and the *in-house* lipid extract was lower (r^2 = 0.56).

Furthermore, it is noteworthy that both false positives, loperamide and quinidine, and the false negative (caffeine) found with 2% of PBL and 2% *in-house* lipid extract were expected because in *in vivo* conditions these compounds are substrates of active transport processes of efflux or influx that are absent in PAMPA. In particular, loperamide and quinidine are known to undergo active efflux mediated by P-gp, whereas caffeine is transported not only by passive diffusion but also by carrier-mediated influx [178]. The influence of these transporters in compound access to the brain is more significant than the passive transcellular mechanism, justifying their misclassification in PAMPA models. Although other reference compounds such as cimetidine, hydrocortisone and sulfasalazine are efflux substrates, their intrinsic low passive permeability observed in the PAMPA model also hampers their access to the brain. These findings corroborate that the *in-house* lipid extract is a valid membrane to predict the passive diffusion of the compounds through BBB.

Importantly, to exclude interindividual variations, the *in-house* brain lipid extract was also prepared from two other distinct brains. The obtained Papp values were similar and all reference compounds were equally classified, thereby confirming that the applied extraction protocol is reproducible.

II.3.3. CORRELATION BETWEEN THE PHYSICOCHEMICAL CHARACTERISTICS AND EXPERIMENTAL APPARENT PERMEABILITY

The fact that PAMPA has been considered a versatile physicochemical screening tool for predicting drug permeability [175,193,501], prompted us to correlate the Papp values with the physicochemical properties of the reference compounds (Table II.1). Although these factors are not absolute indicators of *in vivo* CNS penetration, which is governed by complex biological processes [96,520], their knowledge can be used to optimize passive permeability and guide drug design during initial stages of drug discovery processes [521,522]. Hence, following the previous results, the Papp values achieved with 2% PBL and 2% *in-house* lipid extract were correlated with the physicochemical properties of the reference compounds described in Table II.1.

Despite a lack of agreement regarding exact values in literature, CNS compounds commonly possess a relatively low molecular weight (≤380 or <450 Da), logP (2–5) and logD pH 7.4 (1–3), small TPSA (60–70 $Å^2$ or <90 $Å^2$), low number of hydrogen bond donors (≤1) and acceptors (≤2) or less than 8 or 10 cumulative hydrogen bonds, and reduced molecular flexibility (<8 rotatable bonds) [51,510–512,519,523–525]. Although no correlation was achieved with the molecular weight, logP or rotatable bonds, strong correlations were accomplished with logD, a better lipophilicity index for BBB penetration and a better permeability predictor than logP [176,526], and with TPSA as well, while a moderate correlation was attained with total hydrogen bonding capacity (THBC) (Figure II.5). In this figure, it was verified that an increase of logD generally corresponds to an increase of Papp, in opposition to TPSA and THBC which display the reverse tendency. This coincides with recent studies suggesting that an increased H-bonding potential is associated with a lower passive permeability of a compound [502]. In particular, the Papp values of the reference molecules with 2% *in-house* lipid extract had a higher correlation with logD, the lipophilicity indicator, than 2% PBL, contrary to what was verified with TPSA and THBC, the polarity-related properties.

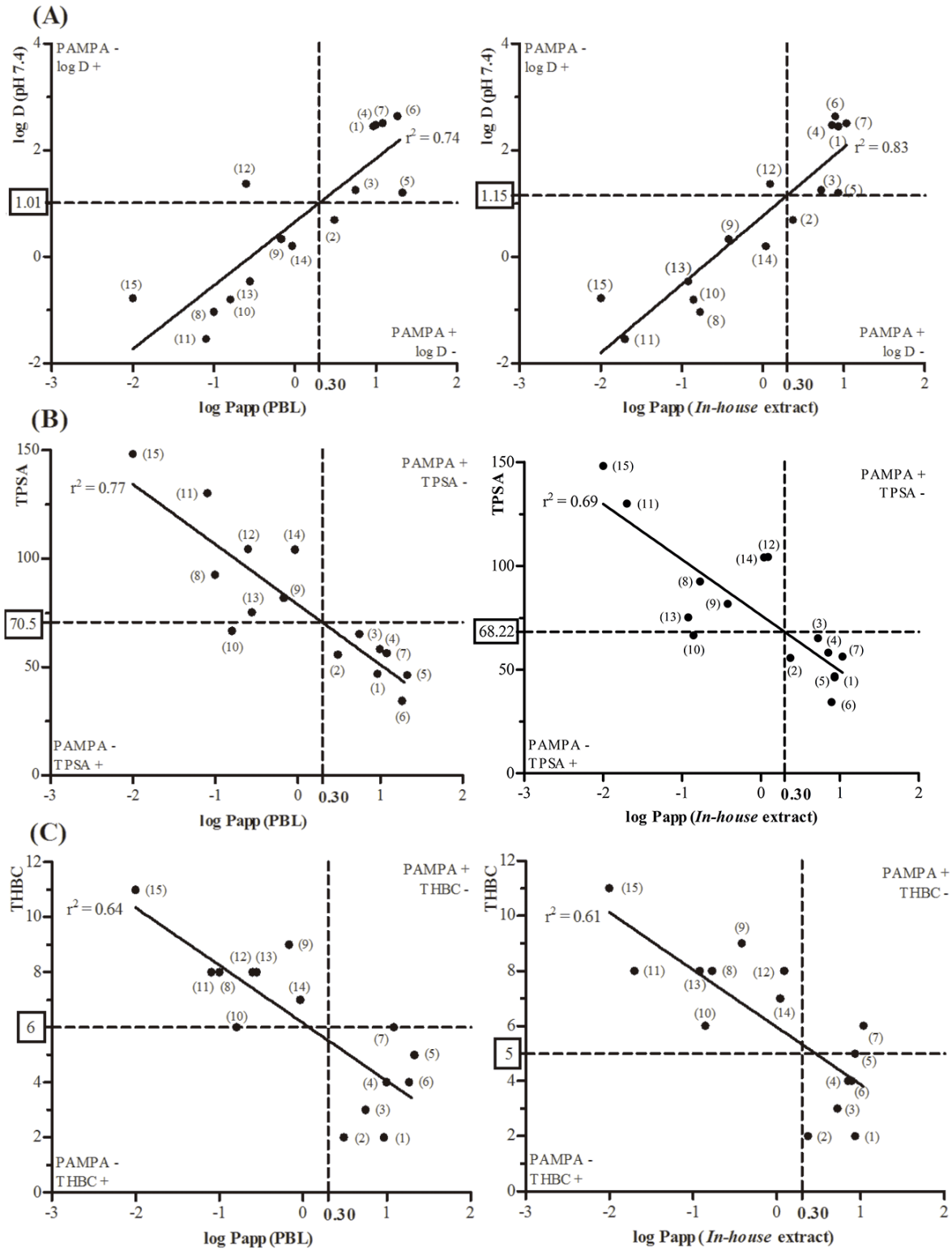

Figure II.5. Experimental logarithmic apparent permeability coefficient (log Papp) values of reference compounds obtained with 2% (w/v) porcine brain lipid (PBL) and *in-house* brain lipid extract versus their physicochemical properties, namely the (A) octanol-water distribution coefficient at pH 7.4 (log D pH 7.4), (B) topological polar surface area (TPSA) and (C) total hydrogen bonding capacity (THBC). The vertical dashed line represents the logarithm of the

predefined cut-off value of Papp (0.30) that separates blood-brain barrier (BBB) permeable (BBB^+) from non-permeable (BBB^-) compounds in the PAMPA models; the horizontal dashed line corresponds to the value of the physicochemical parameter that can be used to classify compounds as BBB^- or BBB^+ according to each correlation. Included reference compounds are (1) Carbamazepine, (2) Carbamazepine 10,11-epoxide, (3) Oxcarbazepine, (4) Phenytoin, (5) Propranolol, (6) Trazodone, (7) Verapamil, (8) Atenolol, (9) Cimetidine, (10) Dopamine, (11) Furosemide, (12) Hydrocortisone, (13) Norfloxacin, (14) Piroxicam, (15) Sulfasalazine. Caffeine, loperamide and quinidine were excluded from this analysis due to misclassification by both PAMPA models.

Observing Figure II.5 and interpolating logarithm of the previously established cut-off value to distinguish BBB^+ and BBB^- compounds (Papp = 2.0 x 10^{-6} cm s^{-1}), the PAMPA model performed with 2% of the *in-house* lipid extract revealed that BBB^+ compounds are molecules with a logD > 1.15, TPSA < 68.22 A^2 and THBC < 5. Considering the information in Table II.1, it is also noticeable that compounds classified as BBB^+ are neutral or basic molecules, which accords with the literature description [512,527].

Overall, it is important to note that the observed trends are in conformity with literature reports and the favourable values found for each physicochemical parameter coincide with those that other authors defined for CNS or non-CNS compounds. Therefore, the physicochemical selectivity of the proposed PAMPA model was confirmed and the values of each property that allow the discrimination between BBB^+ and BBB^- compounds were specified.

II.3.4. TEST SET COMPOUNDS

In agreement with the results obtained with reference compounds, 2% *in-house* brain lipid extract was chosen as lipid solution to evaluate the 11 test molecules (Table II.3 and Figure II.6). Once again, the PAMPA model with 2% PBL was used to compare the results.

The correlation between the Papp values of the test compounds in both PAMPA models was strong (r^2 = 0.94); only zamicastat was differently classified depending on

the used PAMPA lipid, with a classification given by 2% *in-house* brain lipid extract coincident with that found literature data (Table II.3).

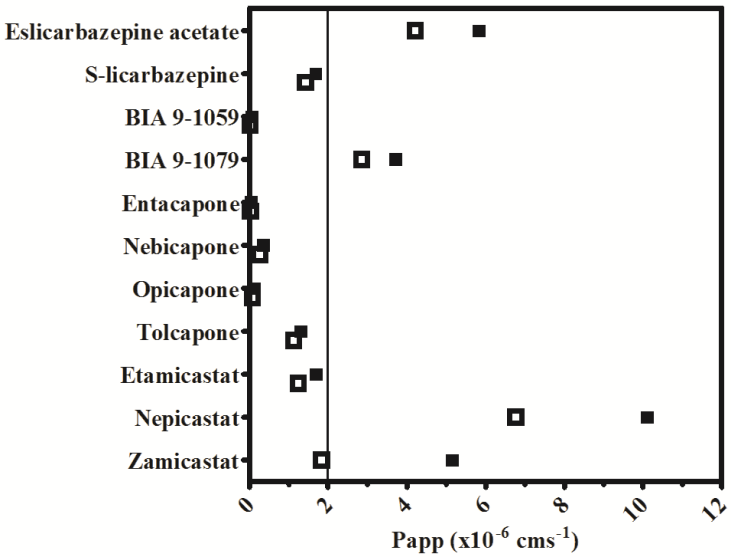

Figure II.6. Experimental apparent permeability coefficient (Papp) values obtained with PAMPA models with 2% (w/v) porcine brain lipid (full square) and *in-house* brain lipid extract (empty square) for the test compounds.

Both methods classified tolcapone, a peripheral and central COMT inhibitor [413,528–530] as BBB^- since its Papp was lower than 2.0 x 10^{-6} cm s^{-1}. This is in accordance with *in silico* predictions that classified tolcapone as unable to cross the BBB [531] and with the low logD value, high TPSA, negative charge state and high THBC of this compound, all unfavourable towards CNS penetration (Table II.3). In an *in vivo* microdialysis study performed by Hakkarainen et al. [224] it also demonstrated a low ability to enter the CNS ($K_{p,uu}$: 0.17), nevertheless *in vitro* cell-based assays revealed a high Papp, underlining that several assays should be performed to define the ability of compounds to reach the CNS, given that PAMPA only predicts passive diffusion. Likewise, *S*-licarbazepine was below the Papp cut-off value and classified as BBB^-, despite being well-known that *S*-licarbazepine reaches the CNS *in vivo* [488]. Notwithstanding, it was correctly ranked by both PAMPA models as the least permeable among other assessed antiepileptic drugs, specifically carbamazepine, oxcarbazepine, carbamazepine 10,11-epoxide and eslicarbazepine acetate, as demonstrated in *in vitro* studies [114,507] and *in vivo* by the brain/plasma ratios [494].

Table II.3. Physicochemical characteristics and apparent permeability coefficient (Papp) values obtained for the 11 test compounds in PAMPA models performed with 2% (w/v) porcine brain lipid (PBL) and *in-house* brain lipid extract. Physicochemical data were provided by BIAL-Portela & C.[a], S.A.

Test compounds	Literature classification	MW (Da)	pKa	Charge at pH 7.4	Log P	Log D (pH 7.4)	TPSA	HBA	HBD	THBC	RB	Papp ($x10^{-6}$ cm s^{-1}) Experimental Classification	
												PBL	*In-house* extract
Eslicarbazepine acetate (BIA 2-093)	BBB+ [114,507]	296.3	11.1	0	2.5	2.5	72.6	5	1	6	3	5.83 (0.65) BBB+	4.21 (0.64) BBB+
***S*-licarbazepine** (BIA 2-194)	BBB+ [488]	254.3	11.1	0	1.5	1.5	66.6	4	2	6	1	1.68 (0.11) BBB-	1.43 (0.49) BBB-
BIA 9-1059	BBB- [439]	384.2	10.0; 4.7	-	2.3	0.0	150.7	8	2	10	1	0.06 (0.003) BBB-	0.02 (0.002) BBB-
BIA 9-1079	BBB-	397.2	10.2; 4.9	-	4.2	1.7	138.1	8	2	10	0	3.71 (0.23) BBB+	2.86 (0.10) BBB+
Entacapone	BBB- [530]	305.3	10.0; 4.0	-	2.4	-0.7	130.4	7	2	9	3	0.04 (0.003) BBB-	0.03 (0.002) BBB-
Nebicapone (BIA 3-202)	BBB- [532]	273.2	10.2; 4.3	-	3.4	0.5	103.4	5	2	7	2	0.35 (0.007) BBB-	0.26 (0.02) BBB-
Opicapone (BIA 9-1067)	BBB- [444]	413.2	9.9; 4.9	-	2.4	0.1	150.7	8	2	10	0	0.13 (0.02) BBB-	0.08 (0.004) BBB-
Tolcapone	BBB+ [530]	273.3	9.9; 3.1	-	3.7	0.1	103.4	5	2	7	0	1.30 (0.02) BBB-	1.13 (0.13) BBB-
Etamicastat (BIA 5-453)	BBB- [470]	347.8	10.9; 9.4	+	1.9	0.4	56.0	2	2	4	3	1.69 (0.13) BBB-	1.24 (0.08) BBB-
Nepicastat	BBB+ [470]	331.8	11.3; 8.6	+	2.0	0.8	46.7	1	2	3	2	10.1 (1.32) BBB+	6.77 (0.47) BBB+
Zamicastat (BIA 5-1058)	BBB- [475]	401.5	10.9; 8.4	+	4.2	3.1	42.0	2	2	4	6	5.15 (0.39) BBB+	1.84 (0.36) BBB-

BBB, blood-brain barrier; HBA, hydrogen bond acceptor; HBD, hydrogen bond donor; log P, octanol-water partition coefficient; log D pH 7.4, octanol-water distribution coefficient at pH 7.4; MW, molecular weight; PBL, polar porcine brain lipid; pKa, ionization constant; THBC, total hydrogen bonding capacity; TPSA, topological polar surface area; RB, rotatable bonds. (+) positive charge, (-) negative charge, (0) neutral.

Recently, etamicastat was shown to have a very limited brain penetration in addition to being a P-gp substrate, whereas nepicastat is able to reach the CNS and cause a central and peripheral DBH inhibition, despite also being a P-gp substrate [470]. Interestingly, the influence of P-gp in the classification of these compounds was not decisive because the low passive permeability of etamicastat and the high passive permeability of nepicastat allowed an accurate classification by the PAMPA models. All other test compounds were correctly classified according to literature data.

These results corroborate the discriminatory capacity of the *in-house* brain lipid extract and validate the use of the applied lipid extraction process to attain viable lipid extracts.

II.4. FINAL CONSIDERATIONS

The *in-house* brain lipid extract incorporated as artificial barrier in PAMPA effectively differentiates BBB^- from BBB^+ compounds. Moreover, the implemented lipid extraction process proved to be reproducible, cost-effective since several extracts could be simultaneously obtained from a unique brain and reliable, because it provided lipid extracts with results comparable to the commercialized PBL. This process may be applied to attain brain lipid extracts from other sources or adapted to extract the lipid fraction of other biological tissues and evaluate the passive permeability across different physiological barriers.

In summary, the proposed PAMPA experimental model coupled to spectrophotometric drug quantification revealed to be a high throughput assay that can be used in early permeability screening stages of drug discovery, where thousands of compounds must be analysed in a short period of time.

Combining the information given by this assay and the physicochemical properties related to CNS exposure is advantageous because the BBB passive permeation potential of a compound can be rapidly estimated and optimized if necessary.

CHAPTER III

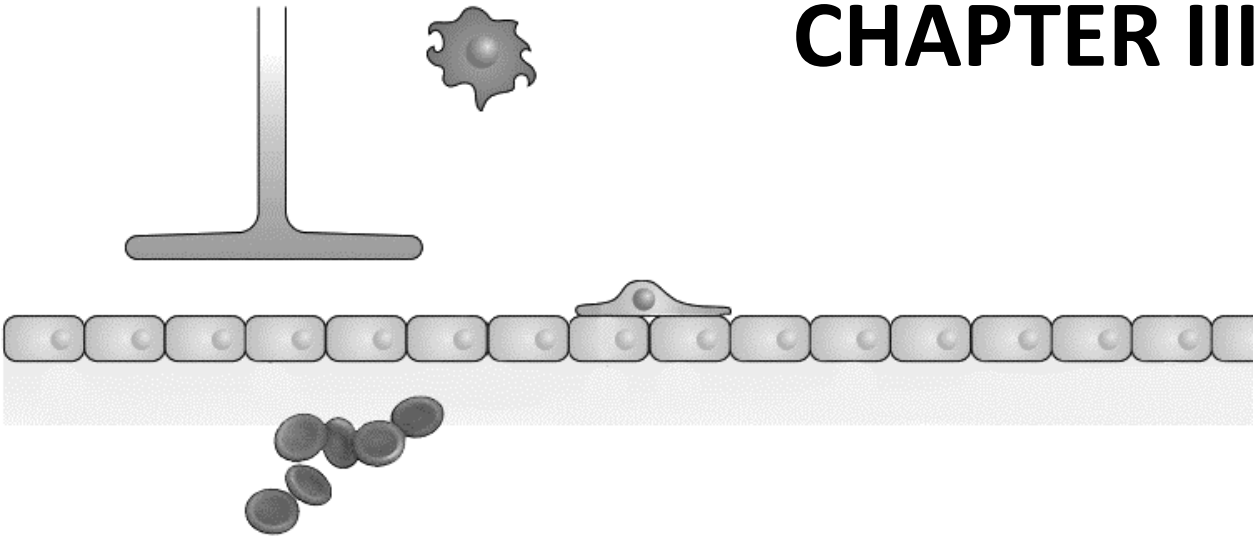

EFFLUX TRANSPORT AT THE BBB

CHAPTER III. EFFLUX TRANSPORT AT THE BBB

P-gp and BCRP form a potent efflux team at the BBB by limiting the entry of several drugs into the CNS. This chapter begins with a description of relevant P-gp and BCRP characteristics, namely their structure, localization and physiological functions; known substrates, inhibitors and inducers; polymorphisms; role in multidrug resistance; and DDIs.

Afterwards, the most widely applied *in vitro* transport assays in literature were briefly outlined, including membrane-based assays and cell-based assays.

To finalize, the experimental evaluation of P-gp and BCRP-mediated efflux in a cell-based BBB model was carried out, as well as, the identification of potential P-gp and/or BCRP inhibitors, among COMT and DBH inhibitors.

III.1. EFFLUX TRANSPORTERS: P-GLYCOPROTEIN AND BREAST CANCER RESISTANCE PROTEIN

The ABC superfamily is one of the largest, best characterized and most ubiquitously expressed families of efflux transporters. Within it there are 48 known genes, divided into seven subfamilies (from ABCA to ABCG) [533]. These transporters are normally membrane-bound proteins that contribute to homeostasis and participate in several physiological functions like the maintenance of lipid bilayers, peptide transport and sterol transport. Adenosine triphosphate (ATP) hydrolysis is required by ABC transporters as a source of energy for the active extrusion of substances across membranes, against the concentration gradient [534]. In addition to their direct contribution to the development of clinical drug resistance, ABC transporters regulate the absorption, distribution and elimination of several xenobiotics, including drugs and their metabolites [533]. While full ABC transporters display two transmembrane domains and two nucleotide binding domains, half ABC transporters only possess one transmembrane domain and one nucleotide binding domain, requiring homo- or heterodimerization to attain functionality [534] (Figure III.1).

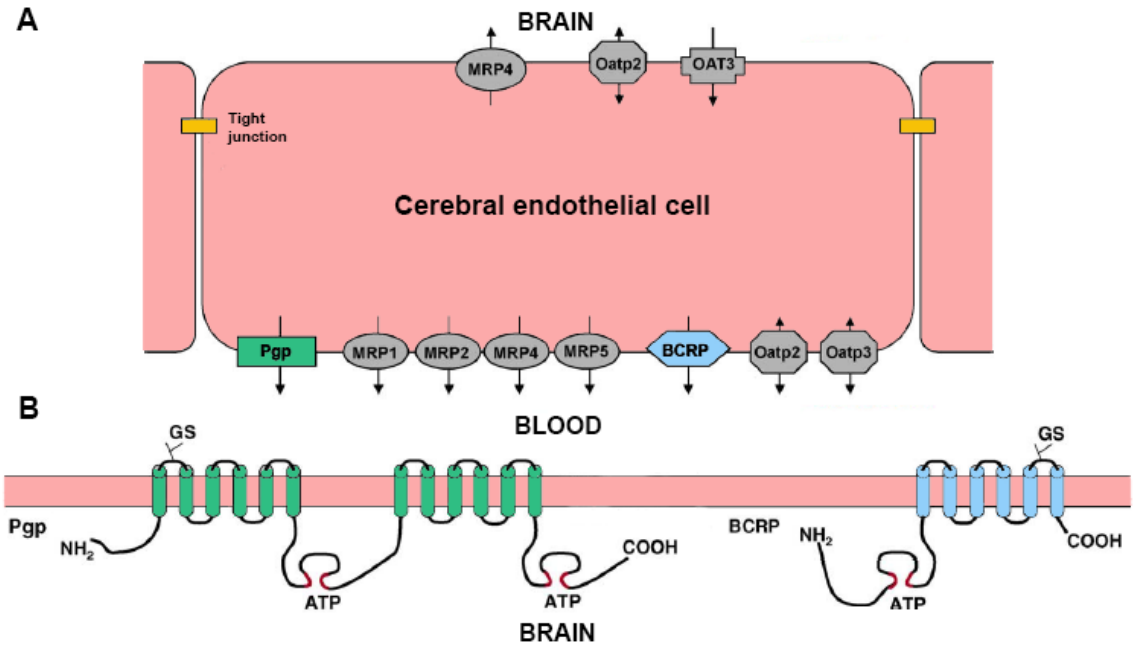

Figure III.1. Simplified distribution of efflux transporters across cerebral endothelial cells (A) and two-dimensional structural and topological models of P-glycoprotein (P-gp) and breast cancer resistance protein (BCRP) (B). P-gp has six transmembrane segments in two halves and two nucleotide binding domains, while BCRP has six transmembrane segments and only one

nucleotide binding domain. ATP, adenosine triphosphate; GS, glycosylation site. Adapted from [113,535].

III.1.1. P-gp

The ABCB subfamily is composed by 11 members responsible for the transport of various drugs, peptides, phosphatidylcholine and iron [534]. P-gp is one of the best known and most extensively studied members; it was originally identified in 1976 by Juliano and Ling as a 170-kDa transmembrane phosphorylated glycoprotein, in a colchicine-resistant Chinese hamster ovary cell line [536]. Structurally, P-gp is composed by 1276-1280 aminoacids with amino- and carboxy-termini located intracellularly [533]. It encompasses two homologous halves connected by a linker sequence, each containing six transmembrane sequences and one cytoplasmic nucleotide-binding domain, where binding and hydrolysis of ATP occurs (Figure III.1). Thus, nucleotide-binding domains are pivotal for transporter function [533,537] and contain three highly conserved sequences, the Walker A and B motifs, found in many ATP-binding proteins and the C motif, unique to this superfamily [538]. The linker sequence contains post-translational modification sites, specifically glycosylation and phosphorylation sites, needed for correct protein folding and trafficking [533].

There are two isoforms of human P-gp: type I, encoded by the *MDR1* gene; and type II, encoded by the *MDR2* gene. In rodents there are three isoforms, *mdr1a, mdr1b* and *mdr2*. The substrate specificity of *mdr1a* and *mdr1b* P-gp in rodents is different but partly overlapping and both are expressed in a similar manner to human P-gp, suggesting that the same functions are shared [113]. Indeed, only *MDR1* in humans and *mdr1a*/*mdr1b* in rodents appear to be responsible for drug resistance and efflux, whereas human *MDR2* and rodent *mdr2* are present in the canalicular membrane of hepatocytes and mediate the secretion of phosphatidylcholine into the bile [539].

Thus, P-gp is highly expressed in enterocytes, hepatocytes, kidney proximal tubules and the so-called drug sanctuary sites or blood-tissue barriers (BBB, blood-placenta barrier and blood-testis barrier) [535]. The precise location of P-gp at the BBB is still being discussed but most published data reveal that in mammals, including humans, P-gp is mainly expressed at the apical membrane of CECs [113], as represented in Figure

III.1. This observation is coherent with the increased brain penetration of P-gp substrates observed in knockout animal models or following the administration of a P-gp inhibitor. However, a study by Pardridge et al. [540] raised debate by suggesting that P-gp was located preferentially in astrocyte foot processes rather than in the apical membrane of CECs. This study was criticized for using only one P-gp antibody, which was considered insufficient for the obtainment of reliable results for the immunolocalization of P-gp [113]. Later, Schlachetzki and Pardrige [541] and Volk et al. [542] conducted further experiments in healthy rat and primate brain, concluding that P-gp is expressed in astrocytes, but at a lower level than in CECs. Other reports also mention the presence of P-gp in pericytes [543], microglia [544] and intracellularly [545]. This suggests that P-gp functions in the brain may be quite complex [113], requiring additional investigations.

On the other hand, it is unequivocal that P-gp displays a very wide substrate spectrum and participates in the extrusion of a variety of drugs from distinct drug classes. Among many examples are chemotherapeutic drugs, antiretroviral drugs, psychotropic drugs, antiepileptic drugs, immunosuppressants, antiarrhythmics, calcium-channel blockers, β-blockers, analgesics, antihistamines and antibiotics [546]. Its immense substrate profile makes it a formidable obstacle to CNS drug delivery [534]. Typically, P-gp substrates are lipophilic, weakly amphipathic, may differ considerably in molecular size ranging from 330 Da to 4000 Da [547] and often but not always, contain aromatic rings and positively charged nitrogen atoms [546]. From the perspective of pharmacological studies, the generally hydrophobic nature of P-gp substrates indicates that in theory, these compounds would passively diffuse across membranes and penetrate into tissues, if active transport was absent. Additionally, it means that the contribution of P-gp-mediated active transport will only have an impact in distribution, if the efflux is substantial comparatively to the passive diffusion rate. Otherwise, the activity of efflux pumps may be overwhelmed by the passive diffusion component [548].

Even though there are substantial functional data, the lack of a crystal structure of human P-gp has hampered rational drug design strategies. Notwithstanding, in recent years, structures began appearing for related proteins that can be used as templates for homology modelling [549]. In Figure III.2A is represented the structure of mouse P-gp model determined by Aller et al. [547] in an inward facing conformation with nucleotide binding domains far apart, resulting in an internal cavity open to the cytoplasm and to

the inner leaflet of the cellular membrane. Other crystal structures of P-gp homologues have been generated in bacteria and *Caenorhabditis elegans* but the mouse models display the best relation between sequence identity (87%) and resolution (3.8 Å) [549].

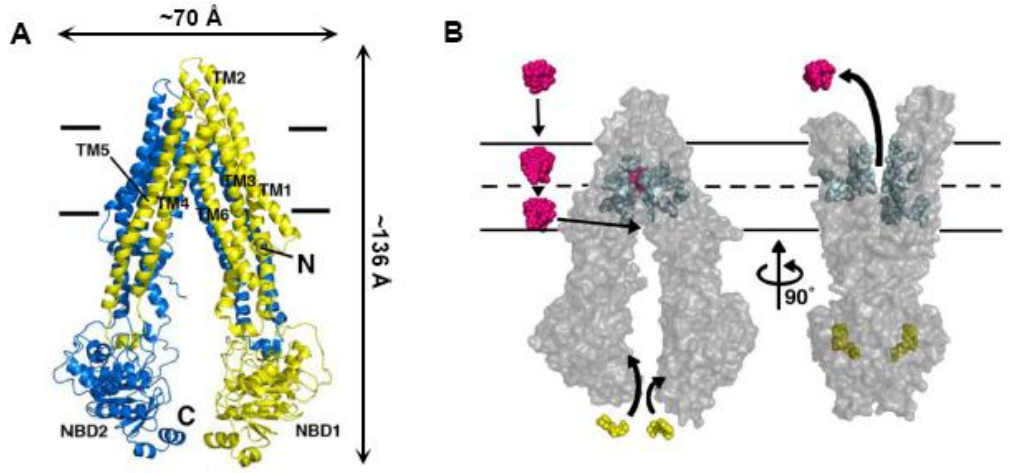

Figure III.2. Structural representation of the front stereo view of mouse P-glycoprotein (P-gp) (A) and model of substrate transport (B). X-ray crystal structures of mouse P-gp reveal an internal cavity with two nucleotide binding domains (NBDs) separated by approximately 30 Å. The structure of mouse P-gp has 87% sequence identity to human P-gp. The amino-terminal (N) half is in yellow and the carboxy-terminal (C) half is in blue. TM, transmembrane segments. Adapted from [547].

To this day, there is still controversy concerning the exact mechanism by which P-gp extrudes compounds out of cells [550] and the location of substrate binding sites on P-gp, relative to the cellular membrane [551]. It is believed that in a pre-transport state, P-gp presents an inward-facing structure and is unavailable for substrate binding from the extracellular space or from the outer leaflet of the cellular membrane. Substrate binding occurs to an internal cavity, open to the inner leaflet of the membrane or cytoplasm. This will supposedly trigger ATP binding, which in turn will induce dimerization of the nucleotide binding domains and a conformational change in P-gp, leading to an outward-facing structure (Figure III.2B). Then, the substrate is released due to a decrease of binding affinity or ATP hydrolysis, which disrupts the dimerization, resets the system back to inward-facing and reinitiates the transport cycle [547].

The broad substrate specificity of P-gp suggests the existence of multiple substrate binding sites within the active pocket, although the exact type and number of binding sites is unclear [550]. It has been proposed that P-gp possesses at least three possible cooperative binding sites, an H- and R-site, as well as, a third allosteric binding site with regulatory or modulatory functions, named M-site [552,553]. In theory, binding to one site will have a positive effect and stimulate binding to the other site [552]. Still, it is not yet known if the assignment of H- and R-sites is maintained during the efflux cycle and it is possible that the substrate binding sites may present different characteristics at different stages of the efflux mechanism [553]. Thus, in spite of the existing information concerning the polyspecificity of P-gp, the efflux mechanism is still far from being completely understood.

There are two main models describing the behaviour and handling of substrates by P-gp in the cell membrane. In one model it is advanced that P-gp behaves as a hydrophobic vacuum cleaner by interacting with lipophilic compounds accumulated within the cell membrane and extruding them to the extracellular aqueous phase. Before being effluxed, drugs partition into the membrane, spontaneously translocate to the cytoplasmic leaflet and there contact with P-gp binding pocket from within the bilayer interior. In the second model, P-gp is thought to act as a flippase, which means that after entering the membrane, substrates are moved from the inner to the outer leaflet of the membrane by P-gp and then passively diffuse to the extracellular aqueous phase, instead of being directly released [538]. In both models, P-gp is capable of preventing substrates from entering the cytosol and protects the cell from potentially harmful molecules. Nevertheless, the quick partitioning equilibrium complicates the distinction between flippase activity and direct transport [554].

Modulation of P-gp activity can be achieved by chemical modulation provoked by inhibitors of transport activity or inducers of expression, or genetic polymorphisms [551]. The most studied form of chemical modulation corresponds to transport inhibition, which has attracted the attention of the pharmaceutical industry as a means of improving the pharmacotherapy of compounds that are unable to reach the therapeutic target due to P-gp-mediated efflux [555]. Multidrug resistance is a frequent phenomenon in cancer cells responsible for chemotherapeutic failure or malignant tumour progression. One of the mechanisms subjacent to the resistance, is the

overexpression of ABC transporters that efflux both cytotoxic and targeted anticancer drugs. Therefore, it was hypothesized that the co-administration of an anticancer drug with an efflux inhibitor could overcome the resistance. Notwithstanding, the efforts so far have been unsuccessful and there is yet no effective treatment approved for a sensitization of malignant tumours to chemotherapeutic drugs without toxic effects [546]. Although a simple strategy to enhance the accumulation of anticancer drugs in tumour cells would be to increase the dose of the anticancer agent, this is not feasible due to systemic toxicity. Still, when a P-gp inhibitor is administered, it often inhibits P-gp not only at the target-site but also in tissues that would otherwise be protected of the P-gp substrate, or responsible for its elimination. Consequently, the systemic concentrations of P-gp substrate increase and the end-result is identical to that of dose escalation [551].

P-gp can be inhibited by blocking the drug binding site competitively, non-competitively or allosterically; by interfering with ATP hydrolysis or by altering the integrity of cell membrane lipids [556].

First-generation P-gp inhibitors (Table III.1) are pharmacologically active compounds, which were already in clinical use or under investigation for other therapeutic indications when the ability to inhibit P-gp was revealed [557].

Table III.1. Examples of P-glycoprotein (P-gp) inhibitors (first-, second- and third-generations) and inducers. From [555,557–561].

P-gp inhibitors			**P-gp inducers**
First-generation	Second-generation	Third-generation	
Verapamil, nifedipine, diltiazem, amiodarone, quinidine, prazosin, cyclosporine A, tacrolimus, erythromycin, tamoxifen, ibuprofen	Dexverapamil, MM36, valspodar, biricodar, toremifene	Zosuquidar (LY-335979), elacridar (GF120918), tariquidar (XR9576), laniquidar (R101933), ontogen (OC-144-093), HM30181	Dexamethasone, doxorubicin, vinblastine, rifampicin, reserpine, St John's wort

These include calcium-channel blockers (e.g. verapamil), immunosuppressants (e.g. cyclosporine A), antiarrhythmics (e.g. quinidine), antibiotics (e.g. erythromycin) and

antiestrogens (e.g. tamoxifen) [562]. Nevertheless, several of these compounds are substrates for other transporters and enzymes, leading to pharmacokinetic interactions in the presence of anticancer drugs, such as inhibition of CYP enzymes and reduced elimination of the anticancer agent with subsequent toxicity [535]. Furthermore, these compounds have low affinity for P-gp, demanding the use of high doses which, together with their non-selective activity, results in toxicity.

Second-generation P-gp inhibitors are analogues of first-generation inhibitors with improved efficacy, tolerability and potency due to structural modifications [535,562]. Indeed, these compounds are devoid of the pharmacological activity of first-generation inhibitors and possess a higher affinity for P-gp [562]. For instance, dexverapamil is an R-enantiomer of verapamil with no effect on the cardiovascular system. However, this generation of compounds caused complex and unpredictable DDIs by inhibiting two or more ABC transporters [556]. In sum, second-generation inhibitors have better pharmacological profiles than first-generation inhibitors but still retain some properties that limit their use as P-gp modulators [557].

Conversely, third-generation P-gp inhibitors have high potency for P-gp [535] with less drug interactions and toxicity [556]. These inhibitors were developed based on quantitative structure-activity relationships and combinatorial chemistry, which allowed the design of drugs with improved characteristics [557]. Even though tariquidar (Figure III.3) was initially described as a P-gp specific inhibitor, subsequent studies revealed that at concentrations above 100 nM it inhibits both P-gp and BCRP. Additionally, it was found that at lower concentrations tariquidar behaves as a BCRP substrate [563]. Further reports confirmed that tariquidar is a P-gp/BCRP inhibitor and BCRP substrate [342,564], but the experimental results on whether tariquidar is a P-gp substrate were conflicting. Weidner et al. [564] claimed that tariquidar does not behave as a P-gp substrate but Bankstahl et al. [342] and Bauer et al. [565] consider that tariquidar and elacridar are concentration-dependent P-gp and BCRP substrates and inhibitors.

Recently, a series of tariquidar analogues were synthesized to circumvent multidrug resistance, some of which inhibit P-gp and BCRP, while others were P-gp specific due to the presence of a sulphonamide group [566]. Nonetheless, the most specific third-generation P-gp inhibitors that have been developed so far are zosuquidar [567] and

laniquidar [557], although neurotoxicity was reported as a major side-effect for zosuquidar, as well as, potential DDIs with doxorubicin and vinorelbine [568].

Elacridar is another third-generation potent P-gp and BCRP inhibitor [569]. It is extensively used *in vitro* and *in vivo*, and has demonstrated to improve the BBB penetration of several compounds, including tyrosine kinase inhibitors developed for cancer treatment [570,571]. Furthermore, elacridar did not show a potent inhibition of human CYP enzymes *in vitro* [572], which constitutes an advantage compared to its predecessors [568]. On the other hand, it is an extremely lipophilic compound (log P = 5.67) with poor solubility, complicating the development of formulations [570].

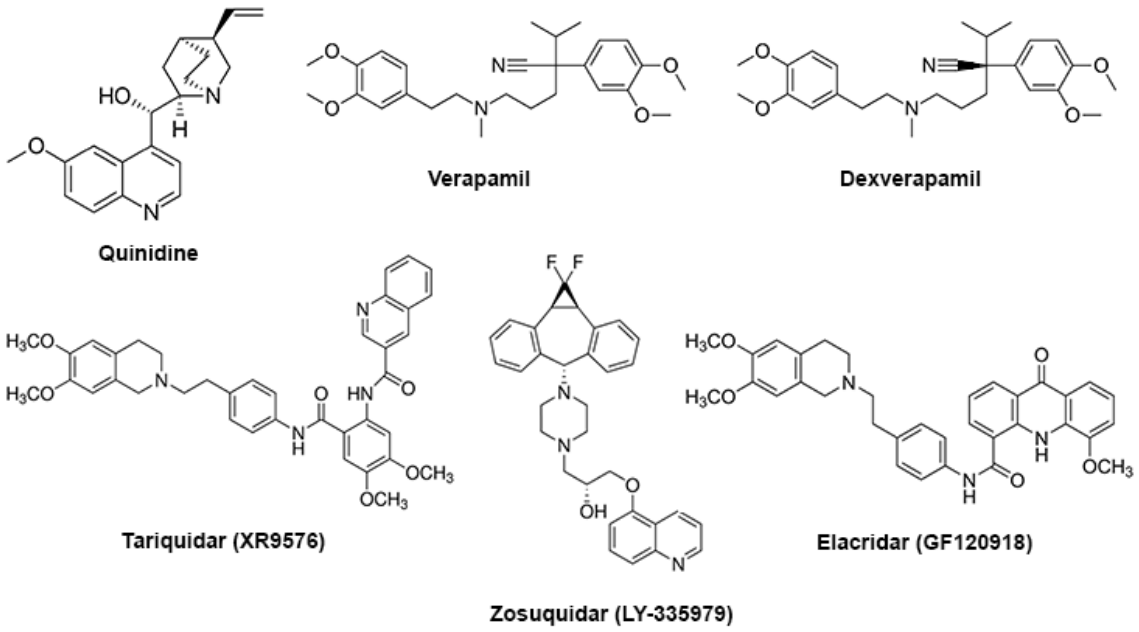

Figure III.3. First-generation (quinidine, verapamil), second-generation (dexverapamil) and third-generation (tariquidar, zosuquidar, elacridar) P-glycoprotein inhibitors. Tariquidar and elacridar have also been identified as breast cancer resistance protein inhibitors.

Montesinos et al. [573] attempted the co-administration of elacridar and tariquidar (1 mg kg^{-1}) with loperamide by single intravenous bolus in rats, and observed that the simultaneous use of both inhibitors increased loperamide levels in the brain more than the separate administration of each inhibitor. Thus, this combination was incorporated

into immunoliposomes to improve the solubility of elacridar and tariquidar, and modulate efflux at the BBB [574].

Notwithstanding, despite the progress and promising characteristics of third-generation inhibitors, these compounds are still far from being ideal modulators, capable of effectively and safely surpassing drug resistance in cancer cells or modulating efflux at the BBB. In truth, many inhibitors revealed unexpected toxicity or lack of efficacy in clinical trials [557]. Budge et al. [537] enumerated several reasons for the lack of clinical benefit, namely an inadequate preclinical evaluation; pharmacokinetic interactions between anticancer drugs and efflux inhibitors; multiple mechanisms of resistance and lack of pre-selection of patients; interactions between inhibitors and multiple ABC transporters; and high toxicity at non-target sites. Therefore, it has been recommended to shift the focus from identifying increasingly potent or specific inhibitors, to developing strategies for targeting the inhibitors to specific sites of action [551]. Another recent research trend that is being explored is the use of natural products as possible fourth-generation P-gp inhibitors [557,575].

P-gp induction has been significantly less studied that P-gp inhibition and consequently data are scarcer. This may be justified, in part, by the lack of adequate *in vitro* methods for the evaluation of transporter induction [558] but another reason is that at present, P-gp induction at human BBB does not appear to be clinically significant. For instance, after 11-29 days of treatment of healthy volunteers with rifampicin, a known P-gp inducer (Table III.1), there was no induction of P-gp at the BBB, using clinical doses that normally induce P-gp at the intestine. It has been explained that rifampicin may not achieve sufficient concentrations in CECs to induce P-gp, in contrast to the high concentrations attained in the intestine. Additionally, P-gp at the human BBB may already be maximally induced by environmental or endogenous factors, meaning that further induction may not be feasible [576].

Lastly, even though several human single-nucleotide polymorphisms have been identified in the *ABCB1/MDR1* gene that encodes P-gp, the vast majority of studies focused on their impact in pharmacokinetics, treatment response and drug-related toxicity have yielded conflicting results [551,577]. It is believed that if populations of humans homozygous for a null allele of *ABCB1* were present in high numbers, there would be many documented examples of adverse reactions to CNS-active P-gp

substrates. Nonetheless, this has not occurred, implying that *ABCB1* polymorphisms do not provide open CNS sensitivity to P-gp substrates in the broader population [578]. Still, despite the fact that clinical relevance appears to be limited, future research activities are being planned, involving new genomic methodologies and well-designed clinical studies [577].

III.1.2. BCRP

ABCG transporters, particularly BCRP, have been neglected in relation to P-gp, however the cooperative relationship between BCRP and P-gp at the BBB, referred in section I.3.2.1 and the role of BCRP in multidrug resistance, is bringing BCRP to the research spotlight. BCRP was discovered in 1998 in a human breast carcinoma cell line, when it was found to display resistance or reduced intracellular accumulation of anticancer drugs like mitoxantrone, daunorubicin and doxorubicin, in the absence of P-gp and MRP overexpression. Accordingly, the cells were sensitive to P-gp and/or MRP substrates like cisplatin, vincristine and paclitaxel, thereby revealing the presence of an additional transporter responsible for the resistance to the other tested drugs [579].

BCRP is a 72-kDa half-transporter, composed by 655 aminoacids and six transmembrane segments, four potential glycosylation sites and one nucleotide binding domain (Figure III.1) [580]. In opposition to P-gp, the nucleotide binding domain precedes the transmembrane segments and is closer to the amino-terminal than the carboxy-terminal, implying that BCRP may operate with a different transport mechanism, compared with P-gp [581]. It is known that in order to be functional, ABC transporters need two nucleotide binding domains and two membrane spanning domains. Thus, being a half-transporter, BCRP must dimerize to attain functionality. At the beginning, it was thought that BCRP operated only as a homodimer bridged by intermolecular disulphide bonds [582] but later experimental data pointed towards the formation of higher order homooligomers, such as tetramers [583]. Furthermore, BCRP function may be regulated by dynamic association/dissociation of BCRP monomers in the dimeric/oligomeric complex [583]. From this perspective, a deeper comprehension of the structural basis of oligomerization could be useful for the development of

molecules capable of disrupting the mechanism and consequently, inhibiting BCRP [583,584].

In 2015, Rosenberg et al. [585] determined the three-dimensional structure of human BCRP in a homodimer complex by cryo-electron microscopy and refined the homology-based structural model that had been previously developed (Figure III.4):

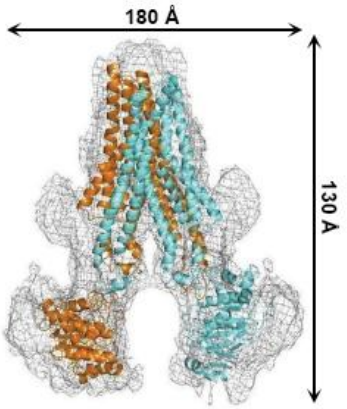

Figure III.4. Structural representation of breast cancer resistance protein. The homodimer has two nucleotide binding domains widely separated from each other. The two monomers are shown in different colours. Adapted from [585].

BCRP is expressed on the apical surface of placental syncytiotrophoblasts, liver canaliculi, colon and small intestine mucosal surface, cardiac muscle, pancreas, adrenal cortex, thyroid, parathyroid, ovaries, lactating mammary glands, stem cells, choroid plexus and CECs [558,580]. In mice and rats, the rodent homolog of BCRP, Bcrp1, has similar tissue localization to that in humans [581]. Nonetheless, BCRP protein levels in brain microvessels of human (8.14 fmol μg^{-1} protein) and cynomolgus monkey (14.2 fmol μg^{-1} protein) are 1.85- and 3.22-fold higher than BCRP levels in mice (4.41 fmol μg^{-1} protein), respectively. Conversely, mice express 2.56 and 3.29 times more P-gp than humans and monkeys [116,586,587]. Therefore, P-gp appears to be the main player in rodents, while BCRP is more predominant in humans and primates. Still, their functional contribution is yet to be completely understood [588]. Overall, it can be concluded that BCRP and P-gp are the dominant transporters maintaining CNS restriction [37].

Physiologically, BCRP contributes to tissue protection against potentially harmful endogenous compounds or xenobiotics [546]. For instance, it protects cells from

oxidative damage by reducing intracellular accumulation of porphyrins [581]. The expression of BCRP in the mammary gland mediates the secretion of drugs, carcinogens and toxins into the milk [589], which may seem to go against physiological functions for exposing suckling newborns to xenobiotics. Still, it could be important to stimulate and induce detoxification mechanisms in the infant. In addition, BCRP provides the milk with an essential nutrient, riboflavin (vitamin B_2) [590].

The broad substrate specificity of BCRP partially overlaps with P-gp substrates and when this occurs, P-gp and BCRP work synergistically in limiting drug penetration across the BBB [115,583]. BCRP is known to efflux structurally unrelated compounds, hydrophobic or hydrophilic, neutral, positively or negatively charged [591]. Among BCRP substrates are antitumor drugs (e.g. mitoxantrone, topotecan), antiretroviral drugs (e.g. zidovudine), antibiotics (e.g. ciprofloxacin), statins (e.g. rosuvastatin) and others (e.g. sulfasalazine, cimetidine) [580,592]. Moreover, BCRP transports sulphate and glucuronide conjugates, such as oestrone-sulphate or 17β-oestradiol-sulphate [593], but sulphated conjugates are generally better BCRP substrates than glucuronide conjugates [581]. It is important to mention that some BCRP substrates are only transported by mutant forms of BCRP found in cancer cell lines. Even if plasma membrane expression is not altered, these changes in aminoacid residues affect substrate specificity and/or overall transporter activity [583]. A common mutation involves the presence of threonine (R482T) or glycine (R482G) instead of arginine at the aminoacid 482 [580]. The protein with arginine in position 482 was obtained from healthy tissue and designated wild-type [594]. For instance, R482T and R482G transport daunorubicin and rhodamine-123, whereas wild-type BCRP does not. Conversely, methotrexate is only transported by wild-type BCRP but not by either mutant form [588]. It should be emphasized that although these mutations affect BCRP function in cancer cell lines, they have not yet been identified in human subjects or in samples from cancer patients [581]. Notwithstanding, the existence of these isoforms can contribute to confounding data in literature concerning the identification of BCRP substrates.

Identically to P-gp, it has been suggested that the vast substrate specificity of BCRP could be attributed to the multiple drug binding sites with distinct localizations and/or affinities within the binding pocket [588]. In a study conducted by Clark et al. [594] using

BCRP with the R482G isoform, three binding sites were identified, two of which displayed allosteric communication. Ejendal and Hrycyna also pointed towards the existence of multiple substrate binding sites using not only the R482G isoform, but also R482T and wild-type BCRP. Then, Giri et al. [595] performed transport studies and the obtained data supported the presence of multiple binding sites on the binding domain of BCRP. Thus, understanding the molecular interactions with this transporter is a fundamental step for the rational design of effective pharmacological inhibitors.

The development of BCRP inhibitors is sought after for the same reasons of P-gp inhibitors, i.e. enhancing target exposure to the drug [595]. Nevertheless, an indiscriminate blockage of BCRP in several tissues could prevent BCRP substrates from being eliminated from the organism and cause toxicity, in a similar manner to what was observed for P-gp inhibitors [596]. Some of the BCRP inhibitors discovered to this day are summarized in Table III.2.

Table III.2. Examples of breast cancer resistance protein (BCRP) inhibitors. From [580,581,597,598].

BCRP inhibitors
Fumitremorgin C and analogues (Ko143, Ko132, Ko134)
Novobiocin
Triclabendazole and metabolites
HIV protease inhibitors (nelfinavir, saquinavir, ritonavir)
Tyrosine kinase inhibitors (imatinib, nilotinib, apatinib)
Elacridar (GF120918), tariquidar (XR9576), tariquidar-derived BCRP inhibitors, HM30181-derived BCRP inhibitors
Tamoxifen and derivatives (TAG-11, TAG-139)
Dietary flavonoids (biochanin A, chrysin)

Produced by the fungi *Aspergillus fumigatus,* fumitremorgin C was the first selective BCRP inhibitor to be identified. Its widespread use *in vivo* was hampered by neurotoxicity, which gave rise to the development of safer and more potent analogues: Ko143, Ko132 and Ko134 [581]. Despite not being neurotoxic, Ko143 cannot be applied *in vivo* because it is an ester and therefore, susceptible to hydrolysis by plasma esterases. Furthermore, in concentrations above 1 μM, Ko143 loses BCRP specificity and

also inhibits P-gp and MRP1 [599]. As aforementioned, some of the third-generation P-gp inhibitors interact with BCRP, namely tariquidar and elacridar. Through structural modifications of tariquidar and HM30181, it was possible to develop potent tariquidar-derivatives [600] and HM30181-derivatives [597] with high BCRP selectivity. It is believed that such compounds could be useful to overcome multidrug resistance or modulate BCRP-mediated efflux at the BBB [600]. Even if translation into clinic does not occur, the existence of a specific, non-toxic and potent BCRP modulator will still allow the study of BCRP at a molecular level and expand the knowledge about its regulation, function and role in diseases [596].

Another aspect concerning BCRP that ought to be mentioned is the occurrence of genetic polymorphisms. In 2013, the International Transporter Consortium (ITC), a group of researchers from academia, industry and FDA [601], released a commentary addressing clinically relevant polymorphisms of membrane transporters, among which was BCRP (*ABCG2* c.421C>A, p.Q141K, rs2231142) [602]. The selection criteria were: having been significantly associated with the pharmacokinetics or pharmacodynamics of one or more drugs at genome-wide level; the existence of significant associations between the polymorphism and drug disposition, efficacy, or toxicity; and the exhibition of functional changes in *in vitro* studies. This polymorphism is observed most frequently in East Asians (26.6 – 35%), followed by Caucasians (7.4 – 11.1%) and sub-Saharan Africans (1.0%) [602]. In practice, it translates into reduced cell surface expression, lower efflux activities than wild-type BCRP [581] and increased plasma exposure of BCRP substrates [602].

Bauer et al. [603] conducted an interesting PET study comparing the brain distribution of radiolabeled [^{11}C]-tariquidar in non-carriers and heterozygous carriers of this polymorphism. Contrary to what was originally expected, no differences in brain distribution were observed for [^{11}C]-tariquidar between the subjects, despite the differences in BCRP expression. This result was attributed to the compensatory action of P-gp at the BBB, which could be masking the effect of the BCRP polymorphism. Under P-gp inhibition, the brain distribution of tariquidar was significantly greater in heterozygous carriers than in non-carriers, demonstrating an impaired BCRP function at the BBB of heterozygous carriers. This indicates that to significantly increase the

penetration of dual P-gp and BCRP substrates at the human BBB, it would be necessary to inhibit both transporters. Therefore, the risk of clinically relevant DDIs at the human BBB for dual substrates was not considered high, except in subjects with the c.421C>A polymorphism who may be more vulnerable to DDIs that involve P-gp, since BCRP will not be able to effectively exert a compensatory effect.

Indeed, in a world of ageing population that often requires polytherapy, it is fundamental to ensure that a compound can be introduced safely with co-medications, in order to avoid the occurrence of DDIs. The inhibiting drug is called *perpetrator*, while the drug whose exposure is altered is the *victim*. An increase in exposure can lead to adverse effects and toxicity, whereas a decrease in exposure can compromise drug efficacy [604]. BCRP and P-gp have been acknowledged by the FDA [558] and EMA [605] due to their importance in drug disposition, thereby recommending the *in vitro* identification of P-gp and BCRP substrates and/or inhibitors that could be involved in transporter-mediated DDIs. This evaluation posed a challenge for the pharmaceutical industry, particularly concerning BCRP, due to the lack of selective human BCRP inhibitors and established optimal clinical study designs [606].

Although DDIs in the intestine, liver and kidneys are more common, BBB drug-transporter interactions are rarer. For instance, Sadeque et al. [607] reported an interaction involving P-gp inhibition at the BBB of healthy volunteers, between loperamide (victim) and quinidine (perpetrator) that resulted in respiratory depression. Sasongko et al. [608] and Muzi et al. [609] also described P-gp inhibition at the BBB by cyclosporine A (perpetrator) with consequent increase of the CNS penetration of verapamil (victim). Notwithstanding, the concentrations of the perpetrators used in these studies were high and consequently, DDIs are unlikely to occur in therapeutic doses. Furthermore, the higher brain concentrations of the victim drug could be a result of higher plasma concentrations originated from a DDI in another place of the body [604]. The ITC considers that currently available drugs that are P-gp or BCRP inhibitors do not attain sufficient unbound concentrations in plasma to increase CNS exposure, meaning that the risk of DDIs at the human BBB is low [578].

III.2. *IN VITRO* ASSAYS FOR THE IDENTIFICATION OF P-GP AND BCRP SUBSTRATES AND/OR INHIBITORS

In vitro assays that assess transporter interactions are extremely important to determine whether a drug is a substrate or an inhibitor of a clinically relevant transporter [580]. In consequence of the needs of the pharmaceutical industry, these assays matured into routine tools over the past two decades and are extensively applied to predict *in vivo* and clinical situations [588]. Undoubtedly, the development and use of *in vitro* transporter assays has contributed to the comprehension of the role that transport mechanisms play in drug disposition and DDIs. This prompted the release of a white-paper by the ITC in 2013 with an overview of the experimental systems employed to conduct *in vitro* transporter studies [610]. The methods can be divided into membrane-based assays, including vesicular transport assays or ATPase assays; or cell-based assays, including accumulation or transport assays [580].

Membrane-based assays possess some benefits, namely ease of performance and adaptability to HTS mode. Additionally, these methods can be used to describe the xenobiotic effects on one specific efflux transporter [559] as the membranes are obtained from cells expressing the efflux transporter of interest [588]. However, cell-based assays are considered more instructive concerning drug-transporter interactions due to the preservation of cell structure [558]. There are also specific limitations associated with the application of membrane-based assays, as described below.

In vesicular transport assays (Figure III.5A) it is possible to distinguish efflux substrates from inhibitors, despite not being applicable for the identification of inducers [559]. Plasma membranes are obtained from transporter-expressing cells and utilized to form inside-out vesicles where substrates are effluxed into the vesicle, in the presence of ATP. Normally, experiments conducted with adenosine monophosphate provide a negative control for passive permeability [611]. The membranes are prepared under suitable conditions and can be obtained from different sources such as *Spodoptera frugiperda* insect cells (Sf9 or Sf21) infected with baculovirus containing the transporter complementary DNA; transfected or selected mammalian cell lines; transfected yeast cells; or artificial membrane vesicles [559]. Transported and non-transported molecules are separated by filtration with glass fiber or nitrocellulose membranes, since vesicles

with trapped molecules will be retained on the filters. Then, substrate molecules can be quantified by HPLC, LC/MS or liquid scintillation counting [588]. While efflux substrates demonstrate concentration- and ATP-dependent accumulation into the vesicles, inhibitors are detected by reduction in the concentration of probe substrate in the vesicles. Even though it is possible to prepare large batches of vesicles are cryopreserve them for late use [611], the preparation and purification protocols are complex. Notwithstanding, there are today commercially available sources of membrane vesicles expressing specific efflux transporters, as well as, vesicular transport kits [559]. The variability in transporter activity between batches or commercial sources may be problematic and should be taken into account, through the use of probe substrates and inhibitors [611]. Overall, this assay is suitable for compounds with low passive permeability and low non-specific binding, since the compound will not freely cross the membrane, but very lipophilic compounds can yield false negative results, due to high non-specific binding to the lipid membranes [580,612]. It has been validated for the identification of P-gp [613] and BCRP [614] substrates and/or inhibitors, and DDI assessment.

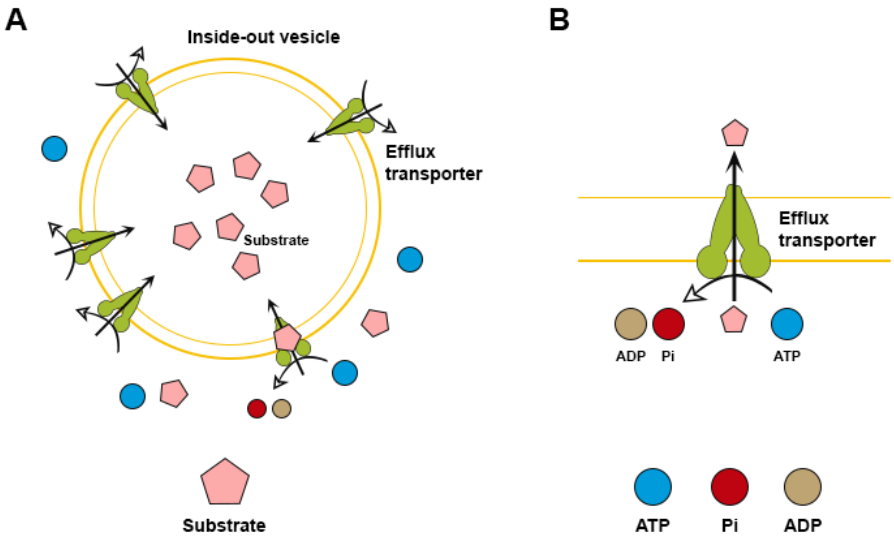

Figure III.5. Membrane-based assays: vesicular transport (A) and ATPase assays (B). ATP, adenoside triphosphate; ADP, adenosine diphosphate; Pi, inorganic phosphate. Adapted from [615].

The ATPase assay (Figure III.5B) is based on the concentration-dependent response of ATP cleavage to interacting compounds [588]. Experimental determinations can be performed in isolated membranes with the transporter of interest or in reconstituted ABC protein preparations [559]. Typically, activation of ATPase by compounds stimulates the hydrolysis of ATP to adenosine diphosphate and the release of inorganic phosphate which can be measured by colorimetric methods. The baseline levels of ATPase activation are monitored through the use of a vehicle control, and subtracted from test-compound data, in order to determine the real levels of ATPase activity [611]. Sodium orthovanadate, an inhibitor of ATPase activity in ABC proteins, is used as a control for complete inhibition and setting a reference point [588,611]. In practice, two protocols can be used: ATPase stimulation, during which the stimulation of basal ATPase activity is measured in the presence of the test compound; or ATPase inhibition, that requires the presence of a known substrate and a specific inhibitor. The latter does not give information on the nature of the interaction, because a decrease in the baseline transporter activity can be caused by inhibitors and/or slowly transported compounds that do not change ATPase activity [559].

Thus, this assay is easy to perform and amenable to HTS, however it is also susceptible to false positives and false negatives that arise from high intra- and inter-assay variability [611]. Moreover, the compounds should be evaluated at high and low concentrations in order to prevent the occurrence of false negative results, which can be verified when the ligand has low affinity and/or solubility [559]. It has been used to identify compounds that interact with P-gp and/or BCRP [559,580].

Cell-based assays provide clearer information regarding the interactions between compounds and ABC transporters. Furthermore, these assays are adaptable for HTS through automation and use of multi-well plates. In cellular accumulation assays (Figure III.6A), the cells are placed in contact with a fluorescent probe substrate, whose intracellular accumulation is inversely proportional to the ABC transporter activity [559]. This means that when an increased intracellular accumulation of the dye is observed in the presence of a test compound, compared with untreated control cells, the efflux transporter is being inhibited by the test compound [611]. Calcein-AM and rhodamine-

123 are commonly used P-gp probe substrates, whereas Hoescht 33342 (Figure III.6B) is usually selected as BCRP probe substrate [559]. This assay is simple, fast and cost-effective [611], but low permeability inhibitors may be underestimated due to insufficient interaction with the efflux transporter [580].

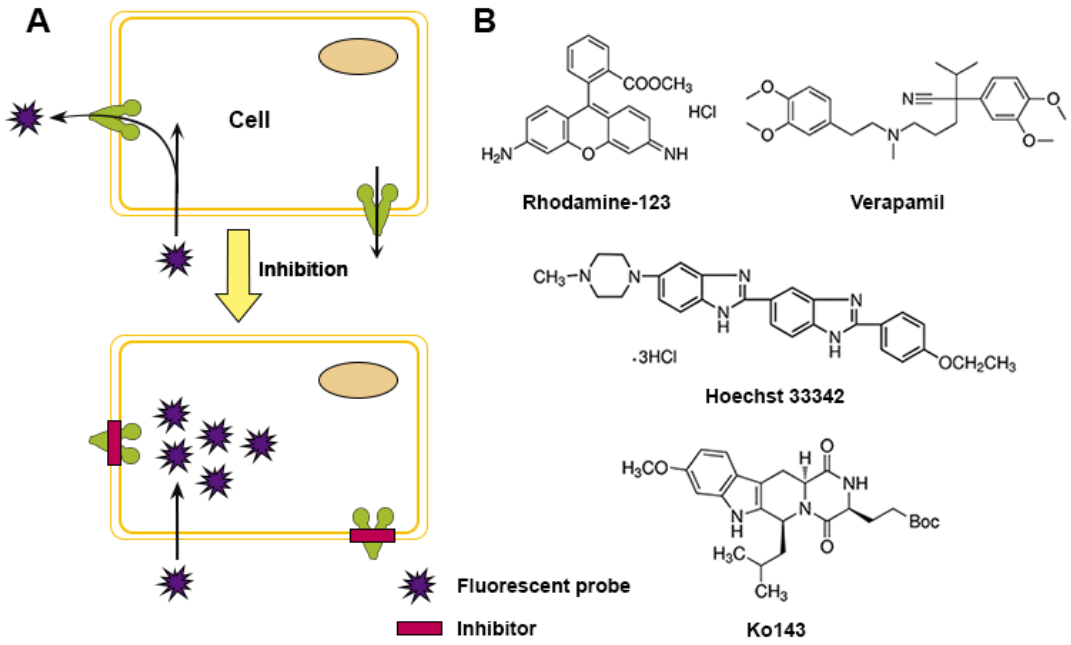

Figure III.6. Cell-based accumulation assay (A) and structure of common P-glycoprotein / breast cancer resistance protein fluorescent substrate probes (rhodamine-123 / Hoechst 33342) and respective inhibitors (verapamil / Ko143) (B). Adapted from [615].

Bidirectional transport assays using polarized cell monolayers are a classical approach to study the function of substrates and inhibitors [580]. The Transwell™ setup for these assays and their application as cell-based BBB models for permeability studies has already been described in section I.3.4.2. It is a sensitive method that determines the transport of test compounds [610], as it allows the evaluation of substrates and inhibitors. The preservation of the intact cell is advantageous for providing more information on compound permeability and interactions between compounds and transporters [559]. Notwithstanding, this method also has some limitations, such as, being more laborious than membrane-based assays [559] and requiring bioanalytical techniques for compound quantification. Besides, there is a risk of saturation of the efflux transporters and underestimation of the extrusion of compounds with rate-

limited diffusion [610]. Conversely, compounds with very high passive diffusion can give false negative results [580]. In addition, the expression of multiple transporters by a cell line, including endogenous transporters, can complicate the interpretation of results [559]. Nevertheless this may be corrected through background subtraction, e.g. comparing efflux between MDCK-MDR1 cells and the parent line MDCK II [219] and through the use of inhibitors. Feng et al. [616] conducted a study comparing the ATPase assay, the calcein-AM assay and the bidirectional transport assay to predict the interactions of CNS drugs with P-gp. It was observed that the bidirectional transport assay correlated better with *in vivo* results and represented a valuable *in vitro* tool to assess human P-gp interactions with compounds targeting the CNS. However, it was emphasized that other assays can serve as specialized methods to understand the kinetics and inhibition of CNS compounds, as well as, complement bidirectional transport studies to better comprehend and predict P-gp modulators *in vivo* [616].

While the FDA recommends the use of bidirectional assays for *in vitro* transporter studies [558], EMA refers that the choice of system can be justified by scientific literature and the physicochemical properties of the substance [605]. The ITC mentions that regardless of the selected experimental approach, it is fundamental that the system is well-characterized through the use of known substrates and inhibitors, and that appropriate controls should be included to confirm test results [617]. Moreover, it is considered that using validated probe substrates and inhibitors is critical to interpret transporter assay data [610] and create confidence in the results, so that the methodology can be successfully applied to determine whether a new compound is a substrate or an inhibitor of an efflux transporter [611].

III.3. EXPERIMENTAL EVALUATION OF HUMAN P-GP AND BCRP-MEDIATED TRANSPORT OF COMT AND DBH INHIBITORS

III.3.1. INTRODUCTION

During preclinical drug development stages, it is essential to characterize the brain pharmacokinetics of new drug candidates and determine the rate and extent at which these compounds are capable of crossing the BBB and reach the CNS. Indeed, substantial efforts are being conducted to improve CNS drug delivery in an attempt to reverse the lower clinical success rates observed for CNS drugs [618]; however this evaluation is also relevant for peripherally-active drugs, as potentially adverse side-effects can arise from an undesired brain exposure [36]. Hence, a greater knowledge of general drug distribution to the brain will contribute to the adoption of drug design strategies that increase or restrict access through the BBB, thereby minimizing the risk of late stage failures and enhancing preclinical and clinical success.

While reaching and sustaining sufficient concentrations of a CNS drug at the target-site within the brain is fundamental to ensure therapeutic action [84], maintaining a decreased drug transport across the BBB is important when targeting peripheral receptors. This may be achieved by combining the optimization of the intrinsic permeability of a compound with avoiding or targeting active efflux at the BBB. For instance, associating low passive permeability with affinity for efflux transporters has been used as a strategy to minimize brain penetration [85,619].

Often, the extrusion of xenobiotics, along with therapeutic compounds, is performed by transporters from the ABC family, including P-gp (also known as MDR1 or *ABCB1*), BCRP (*ABCG2*) and MRPs [113]. P-gp and BCRP are not only physiologically expressed in CECs but also in enterocytes, hepatocytes, heart endothelial cells, kidney proximal tubules, mammary tissue, testis and placenta [580,620–622]. At the BBB, it has been shown that P-gp and BCRP work cooperatively to restrict the brain penetration of several compounds, such as antitumor drugs [115] and the antiepileptic drug lamotrigine [623]. Their broad substrate specificity and strategic location at the luminal membrane of brain endothelial cells prevent drugs from entering the brain through efflux from the apical membrane and/or cytoplasm, back into the capillary lumen [37]. Recently, it was found that the expression of BCRP is more prominent in humans than

that of P-gp [117], whereas P-gp is more abundantly expressed in rodents [116,624]. This reinforces the need of screening both transporters during CNS drug development, by detecting P-gp and BCRP substrates and inhibitors which could cause DDIs. For these reasons, *in vitro* studies are recommended by the ITC, FDA and EMA to identify substrates or inhibitors of clinically relevant ABC transporters, including P-gp and BCRP, which are involved in drug disposition at brain endothelium [558,605,617].

The aim of the present work was to identify P-gp and BCRP substrates and/or inhibitors among COMT and DBH inhibitors and estimate the influence of these transporters on their CNS penetration. COMT inhibitors are used in combined therapy for the treatment of Parkinson's disease to improve the bioavailability and efficacy of L-DOPA [413,416], whereas DBH inhibitors are being developed for the treatment of hypertension associated with sympathetic nervous system overactivity [470,625]. At the present moment, there are three COMT inhibitors available in the market: entacapone; tolcapone, only used in patients unresponsive to other treatments and with monitoring of liver function; and opicapone, since its recent approval by EMA in June of 2016 [411,416]. The peripheral (BIA 9-1059, BIA 9-1079, entacapone, opicapone, etamicastat, zamicastat) and/or central (nebicapone, tolcapone, nepicastat) enzymatic inhibition displayed by these compounds justifies the investigation of the role that P-gp and/or BCRP may have in their access to the CNS. Given the lower throughput and high paracellular leakiness generally demonstrated by brain endothelial cell lines [102], cell-based assays were herein performed with MDCK type II cells as a surrogate model of the BBB [219,224,250,299,520,616,626–629]. In addition to fast growth and low metabolic activity [630], MDCK cells can form polarized monolayers with tight junctions when grown on semipermeable supports [631]; furthermore these cells can be stably transfected with the human *ABCB1* or *ABCG2* genes, leading to an overexpression of human P-gp or BCRP, respectively (MDCK-MDR1; MDCK-BCRP). Thus, in the present study, the effect on cellular viability and stability of the test compounds were studied in order to establish the experimental conditions for subsequent assays. Then, intracellular accumulation assays were performed to demonstrate transporter functionality and identify potential P-gp and BCRP inhibitors. Lastly, P-gp and BCRP substrates were investigated in bidirectional transport assays, previously validated using known

substrates and non-substrates as reference compounds, as required by international guidelines.

III.3.2. METHODS

III.3.2.1. Chemicals and reagents

Reference compounds (carbamazepine, propranolol, trazodone, cimetidine, quinidine, sulfasalazine) were obtained from Sigma-Aldrich (St. Louis, MO, USA) with the exception of atenolol which was acquired from Acros Organics, ThermoFisher Scientific (MA, USA). Test compounds (BIA 9-1059, BIA 9-1079, entacapone, nebicapone, opicapone, tolcapone, etamicastat, nepicastat, zamicastat) were kindly supplied by BIAL-Portela & Ca., S.A. (S. Mamede do Coronado, Portugal). Acetonitrile (HPLC gradient grade), methanol (HPLC gradient grade) and DMSO were acquired from Fisher Scientific (Leicestershire, UK). Formic acid (98–100%) and triethylamine were acquired from Merck KGaA (Darmstadt, Germany). All other chemicals were from Sigma-Aldrich (St. Louis, MO, USA) unless otherwise stated.

III.3.2.2. Cell culture

MDCK II parent cells and MDR1- and BCRP-transfected cells were purchased from the Netherlands Cancer Institute (NKI-AVL, Amsterdam, Netherlands). The cells were cultured in DMEM containing 0.04 M sodium bicarbonate and supplemented with 10% heat-inactivated FBS (Gibco Life Technologies, NY, USA), 100 μg mL^{-1} streptomycin and 100 IU mL^{-1} penicillin. Cells were grown in T-75 flasks (Orange-Scientific, Belgium), passaged twice a week using a 0.25% Trypsin-EDTA solution and cultured at 37 °C in 5% CO_2 and 95% relative humidity. All assays were performed with MDCK II cells from passage 5–14, MDCK-MDR1 from passage 6–23 and MDCK-BCRP from passage 4–13.

III.3.2.3. Cell viability studies

The influence of test compounds on cell viability was determined by the MTT [3-(4,5-dimethylthiazol-2-yl)-2,5-diphenyltetrazolium bromide] assay. MDCK II, MDCK-MDR1 and MDCK-BCRP cells were seeded into 96-well plates (Orange Scientific, Belgium) at a density of 1 x 10^4 cells per well and cultured for 24 h in a humidified

incubator at 37 °C in a 5% CO_2 atmosphere. After removing the culture medium, 200 µL of fresh medium without (control cells) or with each compound at different concentrations was added to the wells and the cells were incubated for 4 h (5 to 100 µM) or 30 min (only 100 µM). Thereafter, the wells were washed twice with PBS and the MTT solution (0.5 mg mL^{-1}) was added, followed by incubation for 2 h at 37 °C in 5% CO_2. Lastly, the MTT solution was removed and replaced with 100 µL of DMSO. Absorbance was measured at 570 nm (A_{570}) with a reference wavelength of 620 nm (A_{620}) on a Biotek Synergy HT microplate reader (Biotek Instruments®, VT, USA). Compound concentrations were not considered to compromise cell viability if it was maintained above 85% compared to control cells [632]. Cell viability was calculated according to the equation III.1:

$$\text{Cell viability (\%)} = \frac{(A_{570}\text{-}A_{620})_{\text{cells incubated with tested concentrations}}}{(A_{570}\text{-}A_{620})_{\text{control cells}}} \times 100 \qquad \text{(III.1)}$$

III.3.2.4. Stability studies

Prior to intracellular accumulation and bidirectional transport assays, the stability of COMT and DBH inhibitors was evaluated in order to ensure drug preservation during the experiments. Compound solutions were prepared in two concentrations corresponding to low (QC1) and high (QC3) quality control samples of the respective analytical calibration curve and data were compared before (reference sample) and after (stability sample) exposure to assay conditions (120 min maximum at 37 °C in Hank's balanced salt solution (HBSS) with 10 mM HEPES pH 7.4). Compounds were considered stable under such conditions when the percentage of the ratio between stability and reference samples was maintained between 85–115%.

III.3.2.5. Intracellular accumulation studies

To assess transporter functionality and identify P-gp and BCRP inhibitors, MDCK II, MDCK-MDR1 and MDCK-BCRP were seeded in 12-well plates (Corning Costar, NY, USA) at 3.0 x 10^5 cells per well for 48 h. The well-known P-gp or BCRP inhibitors, verapamil and Ko143 respectively, were used as positive controls. The assay was initiated by

washing the cells twice with pre-warmed HBSS with 10 mM HEPES pH 7.4, followed by an incubation of 30 min in the absence (negative control, no inhibitor) or presence of verapamil (100 µM), Ko143 (0.5 µM) or test compound (100 µM in 0.1% DMSO). Then, compound solutions were removed and the cells were incubated with 10 µM rhodamine-123 or Hoechst 33342 as P-gp or BCRP substrates, for 1 h at 37 °C. Cellular accumulation of rhodamine-123 or Hoechst 33342 was stopped by washing the cells thrice with ice-cold PBS and cell lysis was performed with Triton X-100 (0.1%, v/v) at room temperature during 30 min. An aliquot of cell lysate was used to measure the amount of accumulated rhodamine-123 or Hoechst 33342 utilizing the Biotek Synergy HT microplate reader (Biotek Instruments, VT, USA) in fluorescence mode (excitation and emission wavelengths of 485/528 nm for rhodamine-123; and 360/460 nm for Hoechst 33342). The protein content of cell lysates was also determined using the Bio-Rad Protein Assay Kit II (Bio-Rad Laboratories, California, USA) and cellular accumulation was normalized accordingly. When a significant P-gp or BCRP inhibition was observed ($p < 0.05$), additional concentrations of test compound were evaluated to verify whether the inhibition was concentration-dependent, generate dose-response curves and determine the concentration of test compound that inhibits accumulation of substrate by 50% (IC_{50}).

III.3.2.6. Bidirectional transport studies

For bidirectional transport studies MDCK II, MDCK-MDR1 and MDCK-BCRP were seeded in 12-well polycarbonate microporous Transwell™ inserts (1.12 cm^2, 0.4 µm pore size; Corning Costar®, NY, USA) at a density of 6.0 x 10^5 cells per well. Assays were conducted 7 days post-seeding and culture medium was changed every other day. The TEER of the polarized cell monolayer was monitored with the Evom® STX2 voltohmmeter (WPI, FL, USA). Na-F was used as a paracellular marker to attest the integrity of the cell monolayer during the transport assay and its fluorescence intensity was measured in a microplate reader as described in section III.3.2.5 for other fluorescent compounds.

Transport studies were performed from the apical to basolateral (AP-BL) and basolateral to apical (BL-AP) directions at 37 °C with gentle shaking (45 rpm) to minimize the impact of the unstirred water layer in the transport of lipophilic compounds. Firstly,

culture medium was replaced with pre-heated HBSS with 10 mM HEPES pH 7.4 and the cells were preincubated for 30 min at 37 °C. Then, the donor solution containing the reference or test compound (0.1% DMSO) was added to the apical (0.5 mL) or basolateral side (1.5 mL) and the receiver compartment was filled with fresh buffer. Aliquots (200 µL) were removed from the receiver side every 15 min during 60 min for higher permeability compounds or every 30 min during 120 min for lower permeability compounds. The removed volume was immediately replaced with fresh buffer to maintain compartment volumes and prevent the formation of a hydrostatic pressure gradient. At the end of the incubation period, aliquots were also withdrawn from the donor side to calculate mass balance.

The Papp of compounds was calculated following the equation III.2:

$$\text{Papp (cm s}^{-1}) = \frac{(dQ/dt)}{A \times C_0} \qquad \text{(III.2)}$$

where dQ/dt is the rate of permeation, A is the surface area of the membrane (cm^2) and C_0 is the initial drug concentration in the donor compartment [633].

The efflux ratio (ER) for the BL-AP and AP-BL directions was determined by the equation III.3:

$$ER = \frac{Papp_{BL\text{-}AP}}{Papp_{AP\text{-}BL}} \qquad \text{(III.3)}$$

Net flux ratios were calculated by dividing the ER obtained in transfected cells by the ER obtained with the parent line MDCK II [628]. If a net flux ratio over 2 was observed, verapamil (100 µM, 30 min) or Ko143 (0.5 µM, 1 h) were added to both sides of the cell monolayer before the donor solutions, to confirm the specificity of P-gp or BCRP-mediated efflux.

Mass balance of each compound was calculated according to the equation III.4:

$$\text{Mass balance} = \frac{C_f^D V^D + C_f^A V^A}{C_0^D V^D} \times 100 \qquad \text{(III.4)}$$

where C_f is the final compound concentration in the donor (C_f^D) or acceptor (C_f^A) compartment, C_0^D is the initial concentration in the donor compartment and V^D and V^A are the volumes of the donor and acceptor compartments, respectively [219].

III.3.2.7. Drug analysis

The concentration of reference and test compounds in samples collected from the bidirectional transport assay was determined by HPLC with a diode-array detector (DAD) in an integrated chromatograph model LC-2040C-3D (Shimadzu Corporation, Tokyo, Japan) using validated techniques. Chromatographic analysis was achieved in a LiChroCART® Purospher Star-C18 column (55 × 4 mm; 3 µm particle size from Merck KGaA, Darmstadt, Germany) by isocratic elution and samples were injected directly or following dilution with HBSS supplemented with 10 mM HEPES pH 7.4. Test compounds were quantified according to published methods [634,635] with minor alterations. Chromatographic conditions and validation parameters were summarized in Table III.3. Typical chromatograms of reference compounds can be found in Appendix B.

III.3.2.8. Data analysis

Data were processed using Graphpad Prism® 5.03 (San Diego, CA, USA) and expressed as mean ± SD. An unpaired two-tailed Student's t test was used to determine the differences of cell viability (%) compared with untreated control cells (100% cell viability) in the MTT assay and of rhodamine-123 or Hoechst 33342 accumulation compared with negative control cells (no inhibitor) in the intracellular accumulation assay. Differences were considered statistically significant when $p < 0.05$ (*), $p < 0.01$ (**) and $p < 0.001$ (***). IC_{50} values were calculated by non-linear regression by generating sigmoid dose-response curves with variable slope, with the fitting method of least-squares.

Table III.3. Chromatographic conditions and validation parameters obtained for the high performance liquid chromatography-diode array (HPLC-DAD) assays applied for the quantification of reference and test compounds in samples from the bidirectional transport assay.

	Mobile phase	Flow rate (mL min^{-1})	Detection wavelength (nm)	Injection volume (µL)	Retention time (min)	Calibration range (µM)	Coefficient of determination (r^2)	LLOQ (µM)	Precision (% CV)	Accuracy (% Bias)
Reference compounds										
Carbamazepine	H_2O/MeOH/ACN (60:30:10, v/v/v)	1.0	235	20	5.4	0.25 – 12	0.999	0.25	2.6	–2.8 to 3.5
Propranolol	H_2O/ACN/TCA (70:30:0.03, v/v/v; pH 2.5-2.6)		235		2.4	0.035 – 2	0.999	0.035	3.2	0.1 to 0.9
Trazodone	50 mM phosphate buffer/ACN/MeOH/TEA (70:25:5:0.3; v/v/v/v; pH 3.5)		249		1.6	0.1 – 4	0.996	0.1	0.6	–9.0 to –0.7
Atenolol	H_2O/MeOH/TEA (88:12:0.05, v/v/v; pH 3.0)		223		1.6	0.03 – 3	0.999	0.03	0.9	0.02 to 6.2
Cimetidine	H_2O/MeOH/TEA (86:14:0.05, v/v/v; pH 3.0)		220		1.4	0.01 – 0.4	0.999	0.01	2.6	–12.1 to –2.7
Quinidine	H_2O with 0.1% formic acid pH 3.0/ACN/MeOH (84:10:6, v/v/v)		249	50	3.8	0.02 – 1	0.999	0.02	4.6	–3.5 to 0.6
Sulfasalazine	50 mM phosphate buffer pH 2.5/ACN (70:30, v/v)		360		2.3	0.01 – 0.4	0.999	0.01	4.1	–4.0 to –2.3
Test compounds										
BIA 9-1059	50 mM phosphate buffer pH 2.45/ACN (63:37, v/v)	0.8	274	50	1.8	0.01 – 0.4	0.999	0.01	8.5	–5.9 to –0.7
Entacapone			305		2.5	0.014 – 0.7	0.999	0.014	6.4	–1.2 to 6.1
Opicapone			273		3.2	0.013 – 0.4	0.999	0.013	7.8	–7.4 to 1.5
BIA 9-1079	50 mM phosphate buffer pH 2.45/ACN (50:50, v/v)		280		4.7	0.04 – 2	0.999	0.04	4.3	–9.4 to -0.7
Nebicapone			276		1.7	0.02 – 0.1	0.999	0.02	8.6	–6.1 to 3.8
Tolcapone			271		2.0	0.018 – 1	0.999	0.018	8.8	–2.6 to –2.3
Etamicastat	50 mM phosphate buffer pH 2.45/ACN (75:25, v/v)	1.0	268		1.7	0.025 – 2	0.999	0.025	2.5	–0.6 to 3.9
Nepicastat			265		1.8	0.03 – 3	0.999	0.03	8.6	–1.1 to 2.3
Zamicastat	50 mM phosphate buffer pH 2.45/ACN (68:32, v/v)		269		2.3	0.05 – 2	0.999	0.05	7.8	–12.5 to –6.0

ACN, acetonitrile; Bias, deviation from nominal value; CV, coefficient of variation; LLOQ, lower limit of quantification; MeOH, methanol; TCA, trichloroacetic acid; TEA, triethylamine.

III.3.3. RESULTS

III.3.3.1. Cellular viability of MDCK II, MDCK-MDR1 and MDCK-BCRP cells

The MTT assay revealed a significant diminution on cell viability for some test compounds after a 4 h incubation period, particularly at 100 μM (Figure III.7). This was most evident for BIA 9-1079, for which a decrease of more than 15% cell viability was observed at concentrations higher than or equal to 20 μM in MDCK-MDR1 cells ($p < 0.01$), 50 μM in MDCK-MDR1 ($p < 0.001$) and MDCK-BCRP cells ($p < 0.01$) and at 80 and 100 μM in all cell lines ($p = 0.002$ for MDCK II at 80 μM or < 0.0001 in remaining cases). Hence, the incubation period with test compounds was shortened to 30 min, the duration of the incubation period in intracellular accumulation assays, and no significant loss of cell viability ($p > 0.05$) was verified at 100 μM, in all cell lines (Figure III.8). For studies exceeding 30 min (i.e. bidirectional transport assay) lower concentrations were selected for these test compounds, namely 10 μM (BIA 9-1079, nebicapone, tolcapone), 30 μM (nepicastat) and 60 μM (etamicastat), given that cell viability was not compromised during this period (Figure III.7).

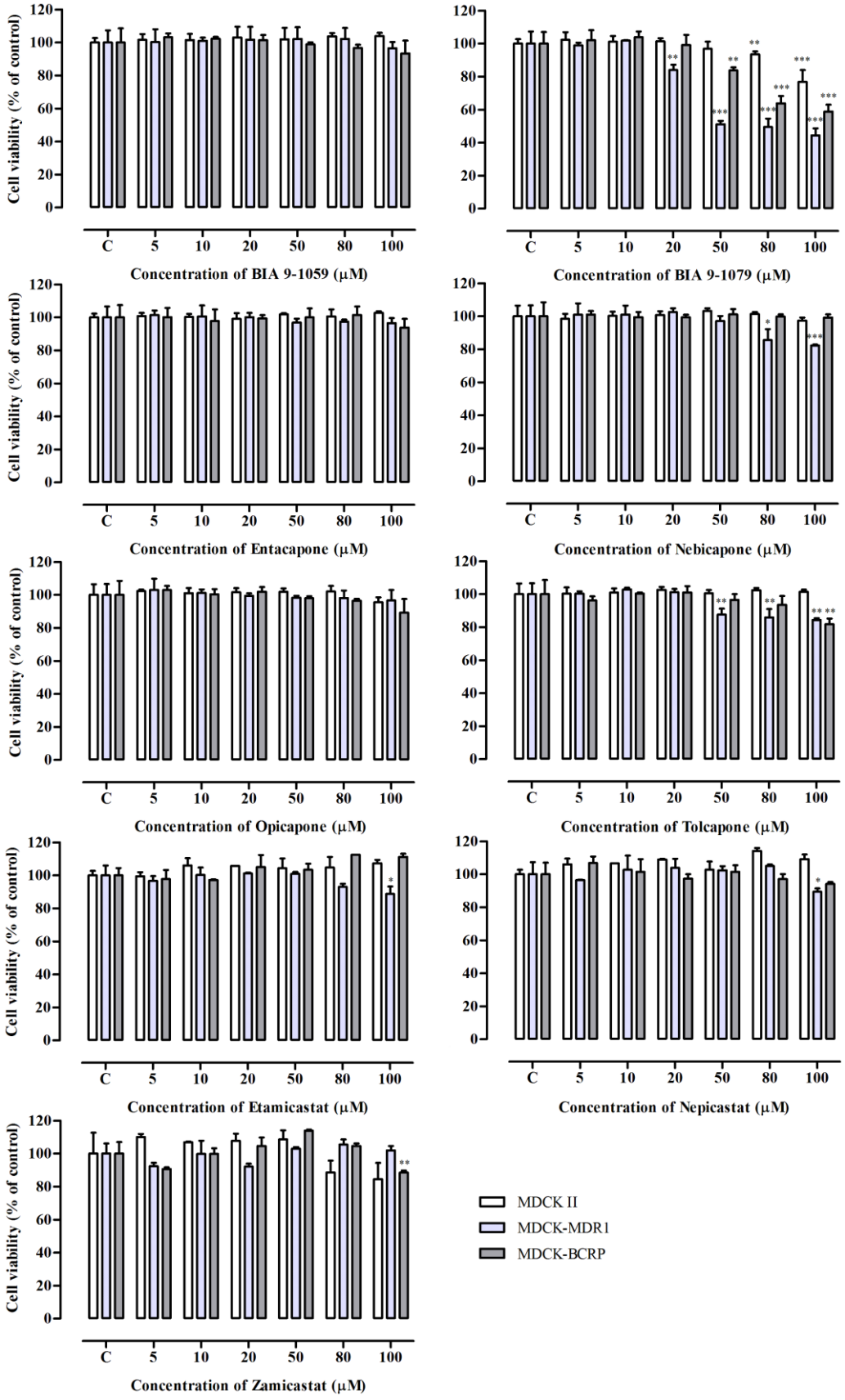

Figure III.7. Cell viability (%) of MDCK II (white bars), MDCK-MDR1 (light grey bars) and MDCK-BCRP (dark grey bars) cells after incubation with test compounds for 4 h (5, 10, 20, 50, 80, 100

µM). Data represented as mean ± standard deviation (n = 3). $p < 0.05$ (*), $p < 0.01$ (**) and $p < 0.001$ (***). C – control (100% cell viability).

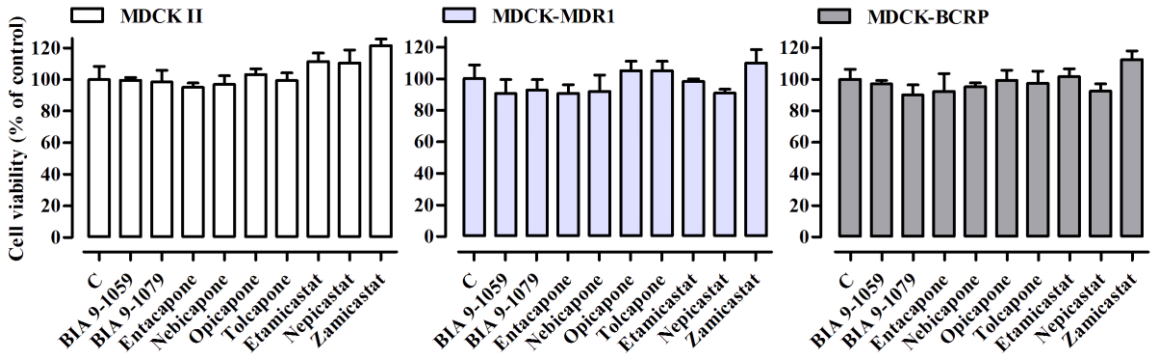

Figure III.8. Cell viability (%) of MDCK II (white bars), MDCK-MDR1 (light grey bars) and MDCK-BCRP (dark grey bars) cells after incubation with test compounds for 30 min at 100 µM. Data represented as mean ± standard deviation (n = 3). $p < 0.05$ (*), $p < 0.01$ (**) and $p < 0.001$ (***). C – control (100% cell viability).

III.3.3.2. Stability of COMT and DBH inhibitors

During 120 min, stability at 37 °C in HBSS with 10 mM HEPES pH 7.4 was kept in the range 85-115% for all compounds with the exception of BIA 9-1079, nepicastat and zamicastat (Table III.4). Significant reductions of average stability values under 85% were observed at lower concentrations (QC1) after 90 min for BIA 9-1079 and nepicastat and earlier for zamicastat at 60 min. These results were taken into consideration when defining the maximal duration of subsequent assays, in association with data from the MTT studies.

Table III.4. Stability (%) of catechol-*O*-methyltransferase and dopamine β-hydroxylase inhibitors in Hank's balanced salt solution (HBSS) with 10mM HEPES pH 7.4 under assay conditions (37 ° C for 120 min).

	Nominal concentration		Stability/reference analyte concentrations (%)			
	(µM)		30 min	60 min	90 min	120 min
BIA 9-1059	QC1	0.03	103.5 (2.20)	101.0 (2.43)	102.9 (1.22)	102.8 (3.94)
	QC3	0.35	100.0 (0.58)	100.8 (1.88)	101.6 (0.61)	100.4 (2.10)
BIA 9-1079	QC1	0.1	89.1 (2.26)	86.6 (4.97)	76.7 (2.67)	72.7 (6.14)
	QC3	1.6	96.8 (1.93)	95.4 (1.03)	93.1 (9.05)	96.3 (3.80)
Entacapone	QC1	0.04	100.6 (0.75)	99.3 (3.13)	100.2 (1.37)	99.9 (1.81)
	QC3	0.6	101.1 (1.57)	99.3 (2.60)	99.9 (1.15)	100.2 (1.42)
Nebicapone	QC1	0.06	95.0 (8.79)	96.4 (7.36)	95.7 (8.93)	95.6 (7.43)
	QC3	0.8	99.6 (1.08)	98.8 (0.60)	96.6 (1.16)	95.0 (1.73)
Opicapone	QC1	0.04	100.0 (5.65)	103.0 (4.73)	100.3 (1.61)	102.0 (7.63)
	QC3	0.32	97.7 (1.94)	97.5 (1.28)	95.4 (5.64)	96.2 (2.07)
Tolcapone	QC1	0.05	97.3 (2.85)	95.9 (1.41)	96.0 (1.51)	95.9 (3.60)
	QC3	0.8	101.9 (4.11)	99.2 (3.68)	98.4 (4.55)	96.4 (3.56)
Etamicastat	QC1	0.07	98.4 (0.89)	98.8 (2.57)	99.8 (5.63)	99.0 (4.84)
	QC3	1.6	99.1 (1.69)	99.0 (0.60)	97.9 (1.13)	97.9 (0.63)
Nepicastat	QC1	0.09	98.9 (8.99)	91.1 (4.59)	81.7 (6.84)	79.7 (3.71)
	QC3	2.4	101.0 (4.65)	94.9 (6.14)	94.3 (4.05)	92.8 (5.94)
Zamicastat	QC1	0.12	87.9 (2.83)	78.7 (3.81)	80.2 (7.10)	71.0 (3.02)
	QC3	1.6	93.2 (1.95)	92.9 (2.43)	91.8 (2.16)	86.3 (3.81)

Results are expressed as mean (SD) (*n* = 3). QC, quality control.

III.3.3.3. Intracellular accumulation of rhodamine-123 and Hoechst-33342 in MDCK II, MDCK-MDR1 and MDCK-BCRP cells

As presented in Figure III.9A-B, the functionality of P-gp and BCRP was confirmed through a significantly lower uptake of rhodamine-123 and Hoechst 33342 in MDCK-MDR1 and MDCK-BCRP cells compared with the parent line MDCK II. The addition of a P-gp (100 µM verapamil) or BCRP inhibitor (0.5 µM Ko143) reversed this tendency and led to an increased accumulation of classic substrates (rhodamine-123 and Hoechst 33342)

in both cases (by 3.0 and 4.2-fold, respectively). In contrast, no inhibitory effect was observed in MDCK II cells.

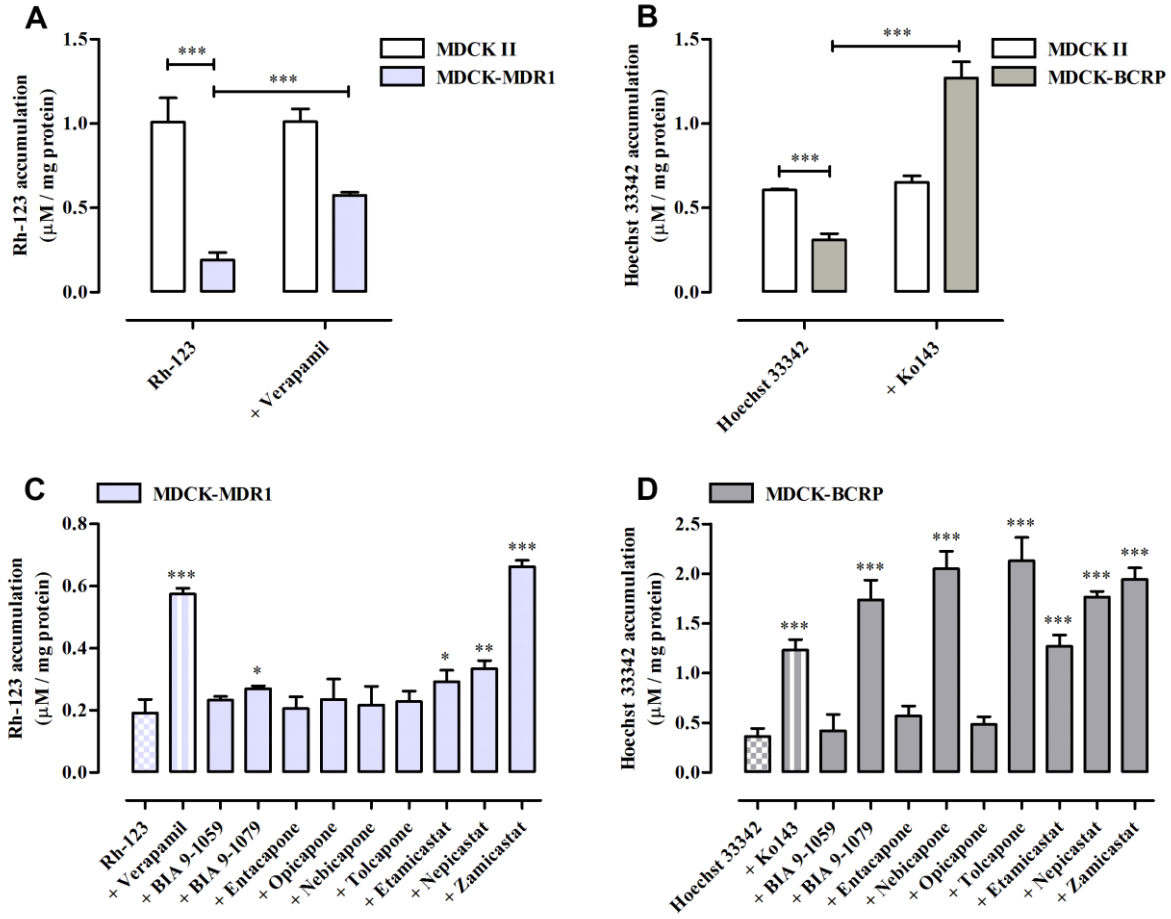

Figure III.9. Accumulation of rhodamine-123 (Rh-123) and Hoechst 33342 in P-glycoprotein (P-gp) and breast cancer resistance protein (BCRP)-transfected cells compared with parent MDCK II cells. Demonstration of P-gp and BCRP functionality after incubation with 100 µM verapamil or 0.5 µM Ko143 (A–B). Intracellular uptake observed following an incubation period with 100 µM test compounds (C–D). Data expressed as mean ± standard deviation (n = 3). $p < 0.05$ (*), $p < 0.01$ (**) and $p < 0.001$ (***).

Incubation of MDCK-MDR1 and MDCK-BCRP cells with 100 µM test compounds revealed a significant accumulation of rhodamine-123 or Hoechst 33342 for some compounds in relation to negative controls (no addition of inhibitor) (Figure III.9C-D). Since BIA 9-1079, etamicastat, nepicastat and zamicastat significantly inhibited P-gp in MDCK-MDR1 cells, other additional 6 concentrations were tested; nevertheless a concentration-dependent inhibition could only be demonstrated for zamicastat (Figure III.10A). The IC_{50} of the other compounds could not be experimentally determined

because it would be necessary to test concentrations over 100 µM to reach the top inhibition plateau, which would compromise solubility and the accuracy of the results. Indeed, when inhibitor potencies cannot be evaluated with full concentration-response curves due to restricted solubility, calculation of IC_{50} becomes erroneous and can lead to a wrong interpretation of relative potencies [636]. Consequently, the estimated IC_{50} of zamicastat in MDCK-MDR1 cells was 73.8 ± 7.2 µM.

Likewise, further concentrations of BIA 9-1079, nebicapone, tolcapone, etamicastat, nepicastat and zamicastat were tested in MDCK-BCRP cells (Figure III.10B-G) as a very significant BCRP inhibition was observed at 100 µM (Figure III.9D). The lowest IC_{50} values were obtained for BIA 9-1079 (IC_{50} = 3.85 ± 1.0 µM), followed by zamicastat (IC_{50} = 17.0 ± 2.7 µM) and nebicapone (IC_{50} = 18.4 ± 3.6 µM), and then by tolcapone (IC_{50} = 32.5 ± 3.3 µM), nepicastat (IC_{50} = 47.7 ± 1.8 µM) and etamicastat (IC_{50} = 59.2 ± 9.4 µM).

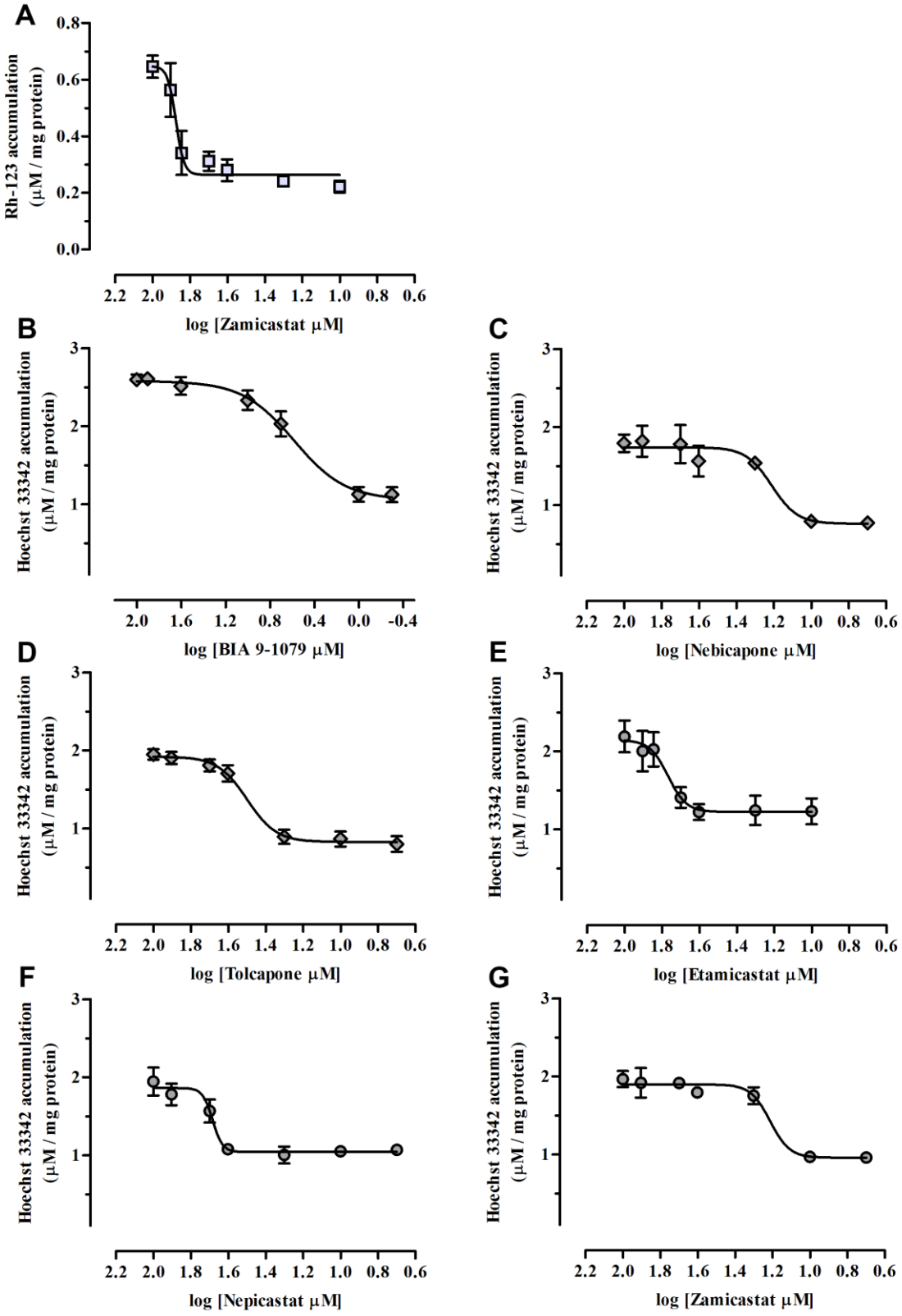

Figure III.10. Dose-dependent inhibition of P-glycoprotein and breast cancer resistance protein-mediated accumulation of rhodamine-123 (Rh-123) (A) and Hoechst 33342 (B–G) by catechol-*O*-methyltransferase and dopamine β-hydroxylase inhibitors in MDCK-MDR1 and MDCK-BCRP cells. Values represent mean ± standard deviation (*n* = 3).

III.3.3.4. Test compound transport across MDCK II, MDCK-MDR1 and MDCK-BCRP monolayers

The assessment of monolayer integrity was carried through the monitorization of TEER and Papp determination of the paracellular marker Na-F. Although registered TEER values were approximately 100 $\Omega.cm^2$ for all cell lines, which could be interpreted as an indicator of leaky monolayers, MDCK II cells are known to display low TEER values [637] due to ion movement through ion pores [219]. Moreover, the Papp of Na-F was inferior to $1.0x10^{-6}$ cm s^{-1} in MDCK II cells and $0.5x10^{-6}$ cm s^{-1} in MDCK-MDR1 and MDCK-BCRP cells (Table III.5), supporting the formation of a discriminatory cell monolayer.

Another estimated parameter in this assay was mass balance, which was between 80–100% for less lipophilic compounds and 70–80% for more lipophilic compounds. Due to very low mass balance (< 40%) in preliminary studies, this assay was not performed for zamicastat. Its high lipophilicity (logD pH 7.4 = 3.1) makes non-specific binding to assay plates or cellular retention probable causes of compound loss during the experiment. This is commonly observed in permeability assays with extremely lipophilic drugs and can lead to an underestimation of Papp values through a reduction of the concentrations in the donor (driving force) and receiver compartments [633,638]. Some solutions have been proposed in literature, such as washing plastic containers with organic solvents or adding serum proteins to the receiver compartment [638–640] but these approaches may interfere with analytical methods, membrane fluidity or transporter function.

The concentration of donor solutions and the sampling time of each reference and test compound were defined following preliminary assays and considering the sensitivity of the analytical methods, as well as the data from cell viability and stability studies. Prior to transport studies with COMT and DBH inhibitors, a set of seven chemically diversified commercial drugs was used to validate experimental conditions (Table III.5). This set included drugs with transcellular permeability (carbamazepine, propranolol and trazodone), paracellular permeability (atenolol), dual P-gp and BCRP substrates (cimetidine), P-gp–specific substrates (quinidine) and BCRP–specific substrates (sulfasalazine) [299,520,616,641,642]. Net flux ratios of respective P-gp and BCRP substrates were superior to 2 which verify a correct identification by the respective

transporter, and the obtained results were consistent with literature data, demonstrating that the applied method provides enough sensitivity for the identification of P-gp and BCRP substrates.

Among the tested COMT and DBH inhibitors, three compounds were identified as P-gp substrates, namely BIA 9-1079, etamicastat and nepicastat (Table III.6). Net flux ratios were reduced more than 50% in all cases by verapamil, approximately 78.7 ± 10.3% for BIA 9-1079, 86.1 ± 0.79% for etamicastat and 55.1 ± 1.98% for nepicastat, which attests the specificity of P-gp mediated efflux. This is in agreement with recently published data for etamicastat and nepicastat, which showed to be P-gp substrates in Caco-2 and MDCK-MDR1 cells [470]. In parallel, BIA 9-1059, entacapone, nebicapone, opicapone and etamicastat were for the first time identified as BCRP substrates. After pre-incubation with Ko143, a decrease in net flux ratio of 89.7 ± 2.18% was obtained for BIA 9-1059, 91.1 ± 2.47% for entacapone, 64.2 ± 3.96% for nebicapone, 91.2 ± 1.90% for opicapone and 52.8 ± 0.44% for etamicastat. The detection of net flux ratios > 2 together with a reduction of over 50% in the presence of an inhibitor, ascertain the identification of these COMT or DBH inhibitors as P-gp and/or BCRP substrates in accordance to the decision-trees provided by the ITC and FDA [558,617].

Table III.5. Bidirectional apparent permeability coefficient (Papp), efflux ratio (ER) and net flux ratio of reference compounds across MDCK II, MDCK-MDR1 and MDCK-BCRP cell monolayers. Papp values are indicated from the apical to basolateral (AP-BL) and basolateral-to-apical (BL-AP) compartments.

Reference compound	Transport	Donor solution (μM)	MDCK II			MDCK-MDR1			Net flux ratio		MDCK-BCRP			Net flux ratio	
			$Papp_{AP-BL}$ ($x10^{-6}$ cm s^{-1})	$Papp_{BL-AP}$ ($x10^{-6}$ cm s^{-1})	ER	$Papp_{AP-BL}$ ($x10^{-6}$ cm s^{-1})	$Papp_{BL-AP}$ ($x10^{-6}$ cm s^{-1})	ER	Without verapamil	With verapamil	$Papp_{AP-BL}$ ($x10^{-6}$ cm s^{-1})	$Papp_{BL-AP}$ ($x10^{-6}$ cm s^{-1})	ER	Without Ko143	With Ko143
Carbamazepine	PT	10	36.5 (1.93)	19.5 (0.60)	0.53	38.0 (2.54)	20.0 (5.53)	0.53	1.00	-	37.3 (5.60)	19.6 (3.85)	0.53	1.00	-
Propranolol	PT	10	19.6 (4.99)	20.0 (0.16)	1.02	23.8 (2.69)	20.8 (1.51)	0.87	0.85	-	25.4 (2.51)	22.4 (0.59)	0.88	0.86	-
Trazodone	PT	10	38.5 (3.30)	29.4 (1.31)	0.76	33.0 (2.58)	40.4 (3.14)	1.22	1.61	-	37.5 (5.03)	27.4 (2.91)	0.73	0.96	-
Atenolol	PP	100	0.22 (0.06)	0.28 (0.03)	1.27	0.35 (0.14)	0.24 (0.04)	0.69	0.54	-	0.14 (0.11)	0.20 (0.03)	1.43	1.13	-
Cimetidine	Efflux[a]	30	0.56 (0.14)	0.43 (0.03)	0.75	0.06 (0.02)	0.41 (0.05)	**6.40**	**8.50**	0.89	0.15 (0.04)	1.25 (0.08)	**8.34**	**11.1**	1.47
Quinidine	Efflux[b]	10	9.52 (2.53)	12.5 (2.49)	1.31	3.77 (0.91)	29.1 (1.37)	**7.73**	**5.90**	1.13	12.0 (3.48)	15.0 (0.48)	1.25	0.95	-
Sulfasalazine	Efflux[c]	60	0.81 (0.30)	0.28 (0.05)	0.34	0.30 (0.14)	0.17 (0.09)	0.56	1.64	-	0.13 (0.11)	0.30 (0.05)	**2.31**	**6.79**	0.92
Na-F	PP	100	0.48 (0.09)	-	-	0.09 (0.08)	-	-	-	-	0.11 (0.04)	-	-	-	-

[a]Efflux mediated by P-gp and BCRP, [b]P-gp, or [c]BCRP. Transport classification according to [299,520,616,641,642].

Na-F, sodium fluorescein; PT, passive transcellular; Passive paracellular. Efflux ratios (ER) and net flux ratios greater than 2 are marked in bold. Papp values are indicated from the apical to basolateral (AP-BL) and basolateral-to-apical (BL-AP) compartments and expressed as mean (SD) (n = 3).

Table III.6. Apparent permeability coefficient (Papp) values, efflux ratio (ER) and net flux ratio of catechol-*O*-methyltransferase and dopamine β-hydroxylase inhibitors across MDCK II, MDCK-MDR1 and MDCK-BCRP cell monolayers.

Test compound	Donor solution (μM)	MDCK II			MDCK-MDR1			Net flux ratio		MDCK-BCRP			Net flux ratio	
		$Papp_{AP-BL}$ ($x10^{-6}$ cm s^{-1})	$Papp_{BL-AP}$ ($x10^{-6}$ cm s^{-1})	ER	$Papp_{AP-BL}$ ($x10^{-6}$ cm s^{-1})	$Papp_{BL-AP}$ ($x10^{-6}$ cm s^{-1})	ER	Without verapamil	With verapamil	$Papp_{AP-BL}$ ($x10^{-6}$ cm s^{-1})	$Papp_{BL-AP}$ ($x10^{-6}$ cm s^{-1})	ER	Without Ko143	With Ko143
BIA 9-1059	60	1.29 (0.27)	1.47 (0.18)	1.14	1.22 (0.23)	0.35 (0.07)	0.29	0.25	-	0.24 (0.08)	1.69 (0.44)	**7.04**	**6.18**	0.64
BIA 9-1079	10	5.23 (2.75)	8.47 (0.91)	1.62	3.47 (1.77)	15.9 (4.19)	**4.58**	**2.83**	0.60	7.14 (4.63)	13.6 (1.74)	1.90	1.17	-
Entacapone	30	6.33 (0.37)	6.02 (0.39)	0.95	3.51 (1.33)	1.29 (0.36)	0.37	0.39	-	0.98 (0.19)	11.1 (0.92)	**11.3**	**11.9**	1.06
Nebicapone	10	24.6 (1.45)	17.6 (4.18)	0.72	23.9 (7.06)	14.3 (2.60)	0.60	0.83	-	5.40 (0.09)	11.6 (0.63)	**2.15**	**2.99**	1.07
Opicapone	30	4.72 (2.33)	6.08 (0.38)	1.29	2.56 (1.08)	2.50 (0.39)	0.98	0.76	-	0.42 (0.09)	9.73 (1.13)	**23.2**	**18.0**	1.58
Tolcapone	10	26.6 (5.07)	20.6 (3.87)	0.77	24.3 (2.84)	19.5 (3.37)	0.80	1.04	-	28.3 (2.93)	23.7 (1.65)	0.84	1.09	-
Etamicastat	60	0.58 (0.16)	0.52 (0.03)	0.90	0.34 (0.06)	1.79 (0.47)	**5.26**	**5.84**	0.82	0.33 (0.03)	1.06 (0.07)	**3.21**	**3.57**	1.68
Nepicastat	30	12.7 (0.98)	10.4 (1.01)	0.82	8.49 (1.05)	14.2 (1.47)	1.67	**2.04**	0.92	12.7 (2.05)	16.5 (1.13)	1.30	1.59	-

Efflux ratios (ER) and net flux ratios greater than 2 are marked in bold. Papp values are indicated from the apical to basolateral (AP-BL) and basolateral-to-apical (BL-AP) compartments and expressed as mean (SD) (*n* = 3).

III.3.4. DISCUSSION

The BBB is a dynamic interface responsible for the homeostasis of the CNS through the regulation of the molecular exchanges between the blood and the neural tissue. The conjugation of CECs with astrocytes, pericytes, microglia, neurons and extracellular matrix elements creates a severely restricted traffic of molecules into the CNS. While hydrophilic compounds are prevented from entering by paracellular route, smaller lipophilic compounds may undergo transcellular passive diffusion. There are also mechanisms of transcytosis, carrier-mediated influx and various efflux transporters, among which P-gp and BCRP have a prominent role. This complex microenvironment is extremely difficult to achieve *in vitro*, making the development of predictive, inexpensive, high throughput and BBB-specific *in vitro* models a very challenging task. Despite having different morphological and functional properties due to epithelial origin, MDCK cells and transfected subclones have been widely used to study permeability and efflux susceptibility across the BBB and are able to accurately distinguish passive from effluxed compounds [219,250]. Therefore, the MDCK II, MDCK-MDR1 and MDCK-BCRP cell lines were selected to determine the influence of P-gp and BCRP on the access of COMT and DBH inhibitors to the CNS. Additionally, it was investigated whether these compounds could inhibit the P-gp or BCRP-mediated efflux of known fluorescent probe substrates (rhodamine-123 and Hoechst 33342, respectively).

In the intracellular accumulation assay, reference P-gp (verapamil) and BCRP (Ko143) inhibitors successfully prevented the efflux of rhodamine-123 or Hoescht 33342 in MDCK-MDR1 and MDCK-BCRP cells, respectively. Care was taken to use Ko143 at 0.5 µM in all assays, due to the recently reported lack of BCRP specificity for concentrations above 1 µM [599]. Among COMT inhibitors, BIA 9-1079, nebicapone and tolcapone demonstrated a concentration-dependent inhibition of BCRP; on the other hand, the DBH inhibitors etamicastat and nepicastat inhibited BCRP with a slight effect on P-gp, while zamicastat clearly inhibited both BCRP and P-gp. There is a need to evaluate the inhibitory effect of circulating concentrations of zamicastat upon the fate of drugs that undergo combined human P-gp and BCRP efflux and for which BBB penetration may be drastically impaired.

Furthermore, IC_{50} values indicate that BIA 9-1079 was the most potent BCRP inhibitor among the test compounds. However, the observed inhibitory effect was not considered clinically relevant and a DDI risk at the BBB is low, as the circulating levels of this metabolite of opicapone are 30 times lower in plasma than the reported concentrations that result in inhibition of BCRP. In fact, according to Almeida et al. 2013 [436] the C_{max} obtained in plasma for BIA 9-1079 after a single therapeutic oral dose of 50 mg of opicapone was 51 ng mL^{-1} while the IC_{50} herein found was 3.85 µM (approximately 1530 ng mL^{-1}). So far, the most potent inhibitors capable of affecting efflux at the BBB in humans and non-human primates are tariquidar and elacridar [565,571,573], however these inhibitors are only available for research. For marketed drugs, modulation of efflux at the BBB is improbable because the unbound systemic concentrations attained for an inhibitor at therapeutic doses are low, meaning that major increases in brain uptake are not usually observed in the presence of clinically relevant doses of the inhibitor [578].

Transcellular permeability assays are frequently used in drug discovery programs to evaluate compounds as substrates of drug transporters. The rate of test compound transport across a cell monolayer is measured from the AP-BL direction or BL-AP direction, normally through quantification by HPLC, and the ER can be calculated to determine the asymmetry in flux caused by transporter activity [37]. Using validated experimental conditions with reference compounds, it was possible to identify three P-gp substrates (BIA 9-1079, etamicastat, and nepicastat) and five BCRP substrates (BIA 9-1059, entacapone, nebicapone, opicapone and etamicastat) among COMT and DBH inhibitors. Notwithstanding, the contribution of P-gp and BCRP-mediated efflux to the overall distribution of compounds across the BBB should be conjugated with information regarding other aspects that affect CNS exposure and/or activity. For example, BIA 9-1059, entacapone, opicapone and etamicastat are compounds with an intrinsically lower passive permeability (Table III.6; [643]) and therefore, efflux is an additional factor contributing to their peripheral selectivity. In particular, etamicastat was classified as a dual-substrate of P-gp and BCRP, making the synergic effect that both transporters have at the BBB another variable that determines its low brain penetration *in vivo*.

Conversely, nebicapone and nepicastat, which can cause peripheral and central COMT or DBH inhibition *in vivo*, were herein identified as BCRP or P-gp substrates,

respectively. It is noteworthy that for nebicapone the central inhibitory effect is dose-dependent, as a preferential peripheral selectivity was observed at 3 mg kg^{-1} and lost at 30 mg kg^{-1} in Wistar rats [644]. For nepicastat, the impairment of brain penetration by an efflux process is evidenced by its $K_{p,uu} < 1$ values (0.03 – oral administration; 0.1 – intravenous administration) but catecholamine levels in the brain were still altered due to DBH inhibition [470]. This reveals that even though P-gp and BCRP may limit access to the CNS, P-gp and BCRP substrates can be centrally active provided that the attained concentrations in the CNS are enough to cause a pharmacological response. In any case, there will be a disequilibrium in the brain and plasma distribution, which allied with the up- or down-regulation of transporter expression in several neuropathologies, will affect the rate and extent of BBB penetration of its substrates.

III.3.5. FINAL CONSIDERATIONS

Using intracellular accumulation assays and bidirectional transport studies with MDCK II, MDCK-MDR1 and MDCK-BCRP cells it was possible to successfully identify P-gp and BCRP inhibitors and substrates among COMT and DBH inhibitors. Given the translational difficulties reported in literature, there was herein the concern of performing these studies with P-gp and BCRP of human origin. To the best of our knowledge, there are no published *in vitro* studies characterizing the role of P-gp and BCRP on the BBB transport of the tested COMT and DBH inhibitors up to date, with the recent exception of P-gp in regard to etamicastat and nepicastat [470]. Our studies provide important information concerning the access of these compounds to the CNS, and may also improve the understanding of the mechanistic influence of these transporters on the absorption and distribution of the tested compounds across other biological barriers, where their expression can be a hindering factor to therapeutic efficacy.

CHAPTER IV

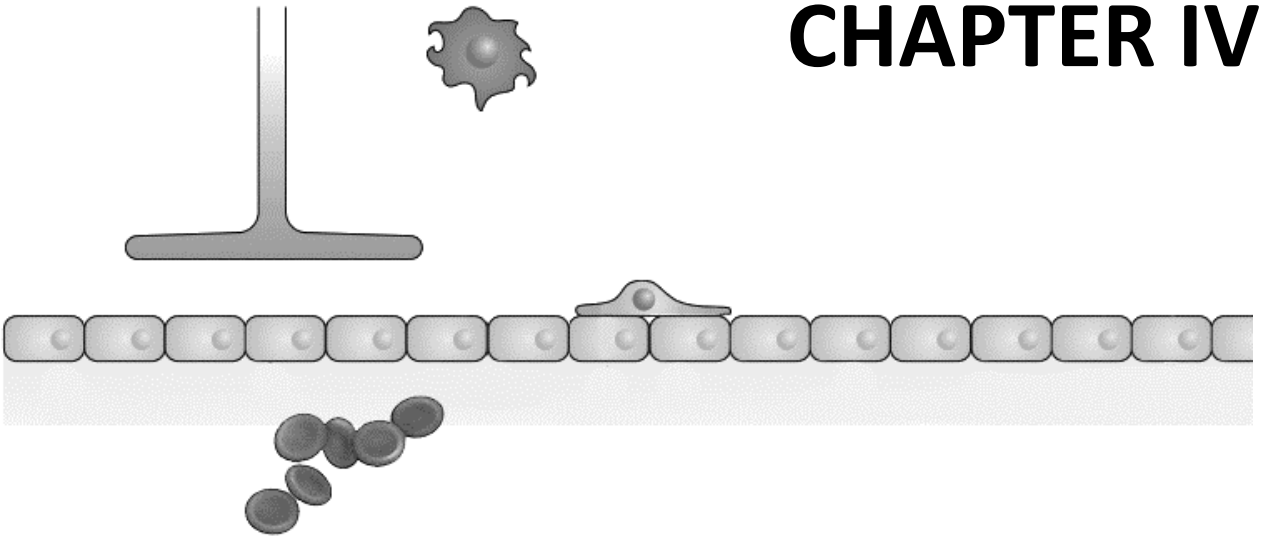

EXTENT OF BRAIN EXPOSURE: *IN VIVO* PHARMACOKINETIC STUDIES

CHAPTER IV. EXTENT OF BRAIN EXPOSURE: *IN VIVO* PHARMACOKINETIC STUDIES

Brain drug delivery is determined by several pharmacokinetic processes, including the rate of transport across the BBB into the brain, the extent of equilibration of unbound drug between the brain and plasma, and the degree of intra-brain distribution.

In this chapter, BIA 9-1079 and tolcapone were intravenously administered to Wistar rats, in order to determine their extent of brain penetration and intra-brain distribution. Plasma and brain samples were collected at pre-defined time points post-dosing by cardiac puncture, followed by intracardiac perfusion. All samples were pre-treated and analysed by HPLC-DAD using validated methods. Elacridar was included in the formulation to attest the involvement of P-gp and/or BCRP in the transport of BIA 9-1079 or tolcapone across the BBB. Moreover, $f_{u,plasma}$ and $f_{u,brain}$ were determined *in vitro* by ultrafiltration.

IV.1. INTRODUCTION

In order to comprehend and predict drug distribution into and within the CNS, it is important to integrate different concepts that define brain exposure and adequately interpret their meaning. Several parameters can be applied to characterize distinct aspects of brain penetration of drug candidates, but not all are critical for guiding drug design, lead optimization and candidate selection, and some should not be used as selection criteria for compound prioritization as they have little influence on *in vivo* CNS efficacy [85].

Up until recently, log BB or K_p were used to interpret the extent of distribution between brain and plasma, notwithstanding these parameters do not distinguish bound from unbound drug and can be potentially erroneous [148]. Researchers initially fell into the *lipidization trap*, which led to a mass production of CNS compounds with extremely high lipophilicity, an elevated K_p, and consequently high non-specific binding to brain tissue and low pharmacologically active unbound drug in the brain [92]. Instead, it is advisable to perform the assessment based on a more valuable parameter, $K_{p,uu}$, since it is reliably connected to pharmacodynamic effects and reflects the occurrence of active transport between brain ISF and plasma, when it differs from 1 [148]. Thus, $K_{p,uu}$ is not distorted by non-specific binding to brain tissue and represents the processes that determine the unbound drug levels in the key compartment of many CNS targets [604].

In truth, $K_{p,uu}$ informs about the relative magnitude of net influx and efflux clearances at the BBB, while describing the capacity of *in vivo* active transport, independently of which transporters are involved. For instance, the same drug can be exposed to several types of transport processes and ultimately it is the relationship between them, i.e. the dominant transport process, that will determine $K_{p,uu}$. If BBB transport is dominated by passive processes or active influx and efflux clearances are similar, $K_{p,uu}$ will be close to 1, whereas if elimination processes are more efficient (e.g. efflux transport), $K_{p,uu}$ will be below 1. Conversely, when $K_{p,uu}$ is above 1, influx processes at the BBB are quantitatively more efficient and the drug is actively transported from plasma to brain [40]. Nevertheless, the use of strict cut-offs for $K_{p,uu}$ to make go/no-go decisions is flawed, as there are known centrally-active compounds with $K_{p,uu} < 1$. In

alternative, is it advisable to deliberate about each compound in particular and associate $K_{p,uu}$ with pharmacodynamic potency data and target engagement [84].

Neuropharmacokinetic studies in rodents may be performed by taking brain and plasma samples at various time points and measuring total drug concentrations of samples. Then, the unbound drug concentrations can be derived through multiplication by $f_{u,plasma}$ and $f_{u,brain}$ [85]. Comparing $K_{p,uu}$ values obtained by single-dose administration with intravenous constant rate infusion, it was revealed that there was a good agreement between the approaches and that single-dose studies constitute an appropriate method [84].

In this context, *in vivo* studies were performed for BIA 9-1079, the preferentially peripheral active metabolite of opicapone in animals but minor in humans [442], and for tolcapone, a potent central and peripheral COMT inhibitor [530]. The purpose of this work was to compare and determine their extent of equilibration between plasma and brain and intra-brain distribution. Firstly, HPLC techniques for the quantification of BIA 9-1079 and tolcapone were adequately validated in plasma and brain matrices of Wistar rats. Afterwards, $f_{u,plasma}$ and $f_{u,brain}$ were determined by ultrafiltration for both compounds. Lastly, BIA 9-1079 and tolcapone were separately administered to Wistar rats by intravenous bolus injection. The concentration levels of the compounds were determined and the corresponding pharmacokinetic profiles were evaluated and compared. Elacridar, a third-generation potent P-gp and BCRP modulator, was also co-administered to assess the impact of efflux inhibition on the brain distribution of these compounds.

IV.2. METHODS

IV.2.1. Chemicals and reagents

BIA 9-1079, tolcapone and nebicapone were gently supplied by BIAL-Portela & Ca., S.A. (S. Mamede do Coronado, Portugal). Pentobarbital sodium salt, tamoxifen citrate salt, sodium dihydrogen phosphate dehydrate and hydrochloric acid (37%) were purchased from Sigma-Aldrich (St. Louis, MO, USA). Acetonitrile (HPLC gradient grade), ethyl acetate and DMSO were acquired from Fisher Scientific (Leicestershire, UK). *Ortho*-

phosphoric acid (85%) was purchased from Panreac (Barcelona, Spain). Polyethylene glycol (PEG) 400 was acquired from Merck Millipore (Darmstadt, Germany). Sodium chloride 0.9% solution and heparin-sodium 5.000 I.U mL^{-1} were purchased from B. Braun Medical (Queluz de Baixo, Portugal).

IV.2.2. Animals

Healthy male Wistar rats weighting 275–300 g were purchased from Charles River Laboratories (L'Arbresle, France). The animals were housed in a controlled environment (12 h light/dark cycle; temperature 20 ± 2 °C; relative humidity 55 ± 5%) for at least seven days prior to the beginning of the experiments, with *ad libitum* access to food and tap water. All experimental and care procedures were conducted in accordance with the European Directive (2010/63/EU) regarding the protection of laboratory animals used for scientific purposes and with the Portuguese law on animal welfare (Decreto-Lei 113/2013, 2013). The experimental procedures were reviewed and approved by the Portuguese National Authority for Animal Health, Phytosanitation and Food Safety (DGAV – Direção Geral de Alimentação e Veterinária).

IV.2.3. *In vitro* brain and plasma protein binding

The $f_{u,plasma}$ and $f_{u,brain}$ of tolcapone and BIA 9-1079 were estimated by ultrafiltration, according to [494] with minor alterations. An Amicon® Ultra-0.5 centrifugal filter device was used, with a low binding regenerated cellulose membrane and a 30 KDa cut-off (Merck Millipore, Darmstadt, Germany).

Blank plasma and homogenates of brain tissue collected from healthy Wistar rats (1 mL) were spiked with 10 µL of compound solution yielding a final concentration of 100 µM. Brain homogenates were prepared by dilution with 50 mM PBS pH 7.4 (1:4, w/v) using a Teflon® pestle tissue homogenizer (Thomas Scientific, Swedesboro, USA). At the beginning of the assay, 100 µL of plasma or brain homogenate were withdrawn to determine the initial compound concentration (C_1), while the remaining portion was incubated for 1 h at 37 °C in a shaking water bath. Following the incubation period, 100 µL were collected to determine the concentration of test compound not subjected to ultrafiltration (C_t) and 500 µL were transferred to the ultrafiltration device (n = 4) and

spun at 14000 g for 15 min at 37 °C. Then, the concentration of compound was analysed in the ultrafiltrate (C_f), in the concentrated sample at the top of the ultrafiltration device (C_c) and in the remaining sample volume at the end of the experiment (C_{37}) by HPLC. The unbound fractions (f_u) in plasma and brain were calculated considering equation IV.1 described by [494]:

$$f_u = 1 - \frac{C_t - C_f}{C_t} \quad \text{(IV.1)}$$

where C_t is the total concentration of compound not subjected to ultrafiltration and C_f is the ultrafiltrate free drug concentration.

In order to correct for the brain tissue dilution that occurs during homogenization, $f_{u,brain}$ was estimated according to equation IV.2 [40]:

$$f_{u,brain} = \frac{1/D}{((1/f_u) - 1) + 1/D} \quad \text{(IV.2)}$$

where f_u is the fraction of unbound drug in the diluted brain homogenate and D is the dilution factor of brain tissue.

The recovery and stability of plasma and brain samples were calculated following equations IV.3 and IV.4 [645]:

$$\% \text{ recovery} = \frac{(C_C \times V_C + C_f \times V_f)}{C_1 \times V_1} \times 100 \quad \text{(IV.3)}$$

$$\% \text{ stability} = \left(\frac{C_{37}}{C_1}\right) \times 100 \quad \text{(IV.4)}$$

where C_1 is the initial compound concentration at the beginning of the assay, V_1 is the volume of plasma or brain homogenate loaded to the ultrafiltration device, C_C and V_C are the drug concentration and volume of the sample on the top of the ultrafiltration device at the end of the centrifugation, C_f and V_f are the drug concentration and volume of the ultrafiltrate and C_{37} is the drug concentration at the end of the experiment.

IV.2.4. *In vivo* brain disposition of BIA 9-1079 and tolcapone

Rats were randomly distributed in two groups, each of which received either BIA 9-1079 (*n* = 30) or tolcapone (*n* = 27). On the day of the experiment, stock solutions of tolcapone and BIA 9-1079 were prepared in DMSO (40 mg mL^{-1}) and diluted 20-fold in a vehicle composed of PEG-NaCl 0.9% (50:50, v/v) to achieve a final concentration of 2

mg mL^{-1}. Prior to administration, the animals were anesthetized by intraperitoneal administration of sodium pentobarbital (60 mg kg^{-1}). Under anaesthesia, the formulation of tolcapone or BIA 9-1079 was administered by an intravenous bolus injection into the lateral tail vein, at the dose of 10 mg kg^{-1} with a total volume of administration of 5 mL kg^{-1}. For tolcapone, plasma and brain samples were collected immediately after its administration (0.03 h) and at 0.08, 0.25, 0.5, 0.75, 1, 3, 6 and 12 h post-dosing; for BIA 9-1079, an additional sample collection was performed at 24 h post-dosing.

The blood was collected from the left ventricle by cardiac puncture using heparinized syringes and immediately transferred to heparinized tubes for centrifugation at 1514 *g* for 10 min at 4 °C. Intracardiac perfusion with NaCl 0.9% was performed to remove residual blood from brain tissue. The brain was rapidly removed, carefully weighed and stored frozen at -80 °C until drug analysis.

To determine the influence of P-gp and/or BCRP in the transport of BIA 9-1079 and tolcapone, the rats were randomly divided into four groups (*n* = 8-12 animals per group), all of which received tolcapone or BIA 9-1079 in the same dose (10 mg kg^{-1}) of the previous study. In two of the groups, elacridar (2.5 mg kg^{-1}) was added to the formulation and co-administered with tolcapone or BIA 9-1079; on the other hand, the other two groups were co-administered with the vehicle [PEG-NaCl 0.9% (50:50, v/v)] instead of elacridar. The animals were sacrificed at 0.08, 0.25, 0.5 and 1 h post-dosing and the blood and brain were collected using the aforementioned procedures.

IV.2.5. Drug analysis

Samples collected from protein binding assays, as well as, plasma and brain samples from the *in vivo* studies were analysed by HPLC-DAD in an integrated chromatograph model LC-2040C-3D (Shimadzu Corporation, Tokyo, Japan) using validated techniques. Chromatographic analysis was achieved in a LiChroCART® Purospher Star-C18 column (55 × 4 mm; 3 µm particle size from Merck Millipore, Darmstadt, Germany) by gradient elution.

Plasma and brain samples of BIA 9-1079 and tolcapone were pre-treated according to published methods [634,635] with minor modifications. Briefly, sample pre-treatment encompassed two techniques, protein precipitation and liquid-liquid extraction. After

thawing at room temperature, rat plasma and brain homogenate samples were spun at at 13,400 rpm (12,045 *g*) for 2 min. Then, 100 µL (plasma) or 150 µL (brain homogenate supernatant) were spiked with 10 µL of internal standard working solution, tamoxifen (90 µg mL^{-1}) for plasma samples or nebicapone (35 µg mL^{-1}) for brain samples. Subsequently, protein precipitation was carried out by adding 400 µL of acetonitrile to samples, vortexing them for 30 s and centrifuging them at 13,400 rpm (12,045 *g*) for 10 min. The supernatant was collected and 200 µL of 2M hydrochloric acid were added and vortexed for 30 s. Then, liquid-liquid extraction was initiated by adding 500 µL of ethyl acetate. The mixture was vortexed for 2 min and centrifuged at 13,400 rpm (12,045 *g*) for 5 min. The upper organic layer was collected and placed in a clean glass tube, while the aqueous layer was re-submitted to liquid-liquid extraction using the same procedure. Organic phases were combined, completely evaporated under a nitrogen stream at 45 °C and the residue was reconstituted with 100 µL of 50 mM phosphate buffer pH 2.45: acetonitrile (50:50, v/v). Lastly, the reconstituted extract was spun for 2 min at 13,400 rpm (12,045 *g*) and 20 µL of the supernatant were injected into the HPLC system. Chromatographic conditions and main validation parameters are summarized in Table IV.1. Additional information on the bioanalytical techniques can be found in Appendix C.

Table IV.1. Chromatographic conditions and validation parameters of high performance liquid chromatography-diode array (HPLC-DAD) techniques applied for the quantification of BIA 9-1079 and tolcapone in samples from *in vivo* assays.

	BIA 9-1079		Tolcapone	
	Plasma	**Brain**	**Plasma**	**Brain**
Mobile phase	A: 50 mM phosphate buffer pH 2.45 B: ACN [33-60% (0-8 min); 60% (8-9 min); 60-33% (9-10 min); 33% (10-14 min)]			
Flow rate (mL min^{-1})	0.8			
Detection wavelength (nm)	280		271	
Injection volume (µL)	20			
Calibration range (µg mL^{-1})	0.04 – 6	0.02 – 4	0.04 – 6	0.02 – 4
Coefficient of determination (r^2)	0.998	0.996	0.998	0.997
LLOQ (µg mL^{-1})	0.04	0.02	0.04	0.02
Inter-day precision (% CV)	≤ 13.3	≤ 7.7	≤ 10.7	≤ 8.6
Inter-day accuracy (% Bias)	–6.9 to 4.6	–3.9 to 5.6	–6.1 to 9.3	–5.7 to 2.0

ACN, acetonitrile; Bias, deviation from nominal value; CV, coefficient of variation; LLOQ, lower limit of quantification.

IV.2.6. Pharmacokinetic data analysis

The C_{max} in plasma and brain of tolcapone and BIA 9-1079 and the corresponding time to reach C_{max} (t_{max}) were directly obtained from the experimental data. The remaining pharmacokinetic parameters were estimated from the mean concentration values determined at each time point by non-compartmental analysis using the WinNonlin® version 6.4 software. The pharmacokinetic parameters evaluated were the area under the drug concentration time-curve (AUC) from time zero to the time of the last measurable drug concentration (AUC_{0-t}) which was calculated by the linear trapezoidal rule; the AUC from time zero to infinite (AUC_{0-inf}) was calculated from AUC_{0-t} + (C_{last}/k_{el}), where C_{last} is the last observed concentration and k_{el} is the apparent elimination rate constant estimated by log-linear regression of the terminal segment of the concentration–time profile; the percentage of AUC extrapolated from t_{last} to infinity [AUC_{extrap}(%)], where t_{last} is the time of C_{last}; and the apparent terminal elimination half-life ($t_{1/2el}$) and mean residence time (MRT). $K_{p,uu}$ was calculated from the ratio of AUC_{0-t} for K_p, $f_{u,plasma}$ and $f_{u,brain}$, using equation IV.5 [84,95]:

$$K_{p,uu} = \frac{K_p}{\frac{1}{f_{u,brain\ corrected}} \times f_{u,plasma}} \quad \text{(IV.5)}$$

where $f_{u,brain,corrected}$ values are $f_{u,brain}$ values corrected for lysosomal trapping using the pH partitioning model proposed by [95]. Other parameters such as the predicted unbound cytosolic-to-extracellular drug concentration ratio ($K_{p,uu,cyto,pred}$), the predicted lysosomic-to-cytosolic unbound drug concentration ratio ($K_{p,uu,lyso,pred}$), the predicted unbound drug intracellular-to-extracellular partitioning coefficient ($K_{p,uu,cell,pred}$) and the predicted volume of distribution of unbound drug in the brain ($V_{u,brain,pred}$) were also estimated according to [95] and [84].

IV.3. RESULTS

IV.3.1. Binding of BIA 9-1079 and tolcapone to plasma and brain tissue

The obtained values of $f_{u,plasma}$ and $f_{u,brain}$ for BIA 9-1079 and tolcapone following ultrafiltration are indicated in Table IV.2. Both COMT inhibitors revealed high binding to plasma proteins in *in vitro* conditions, with recoveries ranging from 86.1 ± 1.8% (BIA 9-1079) to 96.0 ± 10.6% (tolcapone) and stability values of 105.9 ± 3.0% and 102.2 ± 2.5%. Uncorrected and corrected $f_{u,brain}$ values were lower for BIA 9-1079 than tolcapone with recoveries between 97.3 ± 3.1% for BIA 9-1079 and 91.9 ± 3.07% for tolcapone. Stability values were 100.2 ± 5.0% and 86.0 ± 1.4% for BIA 9-1079 and tolcapone, respectively.

IV.3.2. Plasma and brain pharmacokinetics of BIA 9-1079 and tolcapone

The mean concentration-time profiles of BIA 9-1079 and tolcapone in plasma and brain, after a single intravenous dose (10 mg kg^{-1}) to rats are depicted in Figure IV.1A-B. The main pharmacokinetic parameters estimated by non-compartmental analysis and other pharmacokinetic parameters relative to the extent and intra-brain distribution are presented in Table IV.2. Considering the pharmacokinetic profiles of both compounds in plasma (Figure IV.1A), it is visible that the systemic exposure of BIA 9-1079 is greater than that of tolcapone, as corroborated by the $AUC_{0\text{-}inf}$ which was 2.3-fold higher for BIA 9-1079. The 4.0-fold higher $t_{1/2el}$ (5.39 h vs. 1.36 h) demonstrates that BIA 9-1079 was more slowly eliminated and remained longer in plasma than tolcapone (2.46 h vs. 1.09 h).

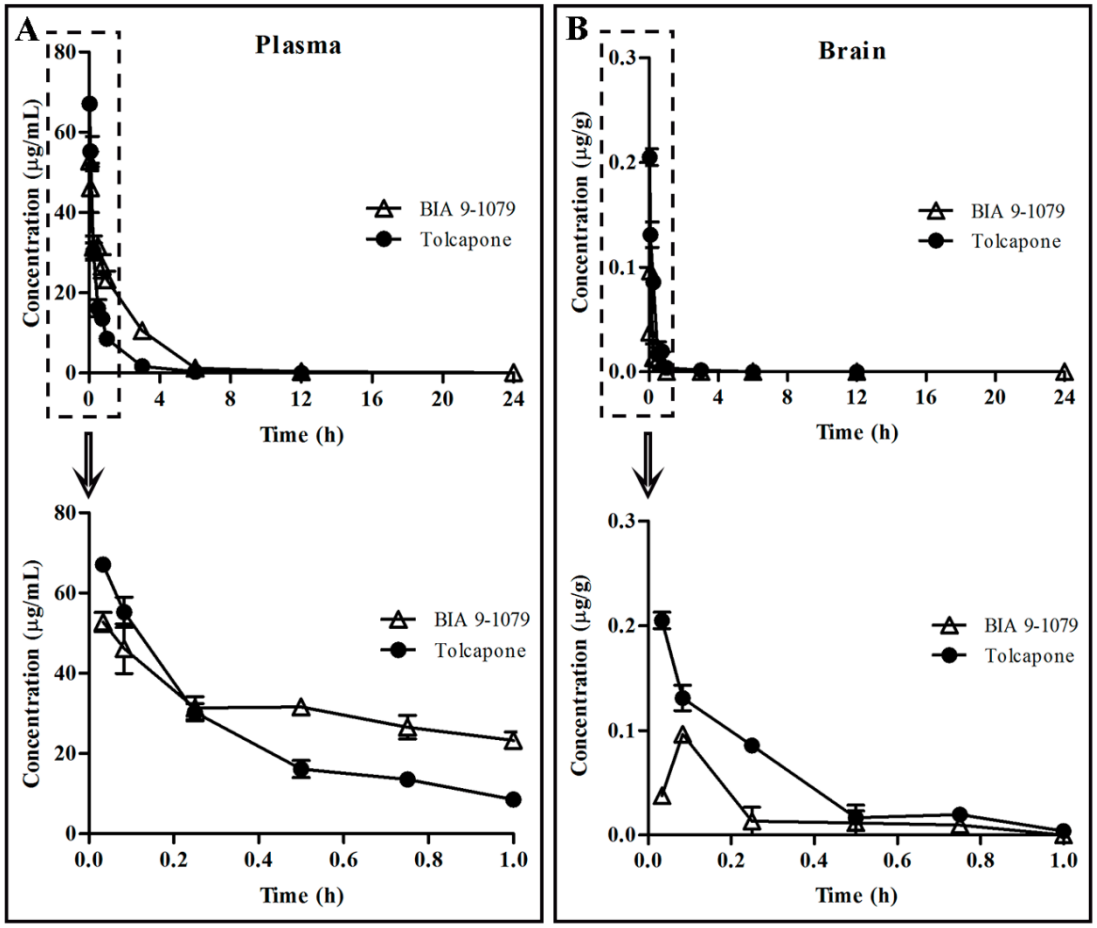

Figure IV.1. Mean concentration-time profiles of BIA 9-1079 and tolcapone in plasma (A) and brain (B) following 10 mg kg^{-1} intravenous administration to Wistar rats. Each data point is presented as mean ± standard error of the mean (*n* = 27 – 30 animals per group).

In opposition, brain exposure was 3.3-fold higher for tolcapone than for BIA 9-1079, considering the AUC_{0-t} values. The C_{max} in the brain was also 2.1-fold higher for tolcapone and reached almost immediately after administration (0.03 h). Nonetheless, the obtained $K_{p,uu}$ values were below unit for both compounds, indicating a restricted extent of brain penetration and dominant active efflux processes. As previously mentioned, this parameter was determined from K_p and *in vitro* $f_{u,brain}$ converted to $f_{u,brain,corrected}$ according to [95]. In order to determine $f_{u,brain,corrected}$, it was required to estimate $K_{p,uu,cell,pred}$ taking into account the pKa of the drug. Despite possessing two pKa values (4.9 and 10.2 for BIA 9-1079; 3.1 and 9.9 for tolcapone), both compounds were herein considered acids, due to the net negative charge displayed at pH 7.4. The observed $K_{p,uu,cell,pred}$ values (Table IV.2) reflect a low intracellular accumulation of the compounds and exclude trapping in lysosomes, as well as, uptake into cells.

Table IV.2. Pharmacokinetic parameters and binding data of BIA 9-1079 and tolcapone in plasma and brain after intravenous administration (10 mg kg^{-1}) to Wistar rats.

		t_{max} (h)	C_{max} (µg mL^{-1})	AUC_{0-t} (µg.h mL^{-1})	AUC_{0-inf} (µg.h mL^{-1})	AUC_{extrap} (%)	K_{el} (h^{-1})	$t_{1/2el}$ (h)	MRT (h)
BIA 9-1079	Plasma	0.03	52.78	84.08	84.94	1.02	0.13	5.39	2.46
	Brain	0.08	0.096	0.017	NC	NC	0.66	1.05	0.23
Tolcapone	Plasma	0.03	67.12	36.24	36.28	0.10	0.51	1.36	1.09
	Brain	0.03	0.205	0.056	0.057	1.79	1.53	0.45	0.38

	K_p	$f_{u,plasma}$	$f_{u,brain}$	$f_{u,brain,corrected}$	$V_{u,brain,pred}$ (mL g^{-1})	$K_{p,uu}$	$K_{p,uu,cyto,pred}$	$K_{p,uu,lyso,pred}$	$K_{p,uu,cell,pred}$
BIA 9-1079	0.0002	0.002 (0.001)	0.008 (0.001)	0.013	79.27	0.001	0.577	0.020	0.656
Tolcapone	0.0015	0.011 (0.003)	0.162 (0.028)	0.247	4.047	0.035	0.575	0.013	0.655

C_{max} is expressed in µg g^{-1} and AUC is expressed in µg.h g^{-1} in brain tissue; The presented $V_{u,brain,pred}$, $K_{p,uu,cyto,pred}$, $K_{p,uu,lyso,pred}$ and $K_{p,uu,cell,pred}$ values were predicted according to the pH partitioning theory. $f_{u,plasma}$ and $f_{u,brain}$ values are expressed as mean (SD), n = 4.

AUC_{extrap}, extrapolated area under the concentration-time curve; AUC_{0-inf}, area under the concentration-time curve from time zero to infinite; AUC_{0-t}, area under the concentration-time curve from time zero to the last measurable concentration; C_{max}, maximum concentration; $f_{u,plasma}$, unbound drug fraction in plasma; $f_{u,brain}$, unbound drug fraction in the brain; K_{el}, apparent elimination rate constant; K_p, ratio of total brain-to-plasma AUC_{0-t}; $K_{p,uu}$, unbound brain-to-plasma ratio; $K_{p,uu,cell,pred}$, predicted unbound drug intracellular-to-extracellular partitioning coefficient; $K_{p,uu,cyto,pred}$, predicted unbound cytosolic-to-extracellular drug concentration ratio; $K_{p,uu,lyso,pred}$, predicted lysosomic-to-cytosolic unbound drug concentration ratio; MRT, mean residence time; NC, not calculated; $t_{1/2el}$, apparent terminal elimination half-life; t_{max}, time to achieve the maximum concentration; $V_{u,brain,pred}$, predicted volume of distribution of unbound drug in the brain.

From $f_{u,brain,corrected}$ and $V_{u,brain,pred}$ (= $1/f_{u,brain,corrected}$) it is noticeable that both compounds reveal non-specific binding to brain parenchyma ($V_{u,brain,pred}$ > 0.8 mL g^{-1} brain), although this is more evident for BIA 9-1079 than tolcapone, because tolcapone displays a higher $f_{u,brain,corrected}$ (0.247) and it is therefore, more available for target engagement than BIA 9-1079. Brain tissue binding is also influenced by lipophilicity and even though both compounds are moderately lipophilic, BIA 9-1079 is more lipophilic (log D pH 7.4 = 1.7) than tolcapone (log D pH 7.4 = 0.1), originating a higher affinity of BIA 9-1079 to brain components.

The effect of the co-administration of elacridar on the plasma and brain concentration-time profiles of tolcapone and BIA 9-1079 are depicted in Figure IV.2A-D.

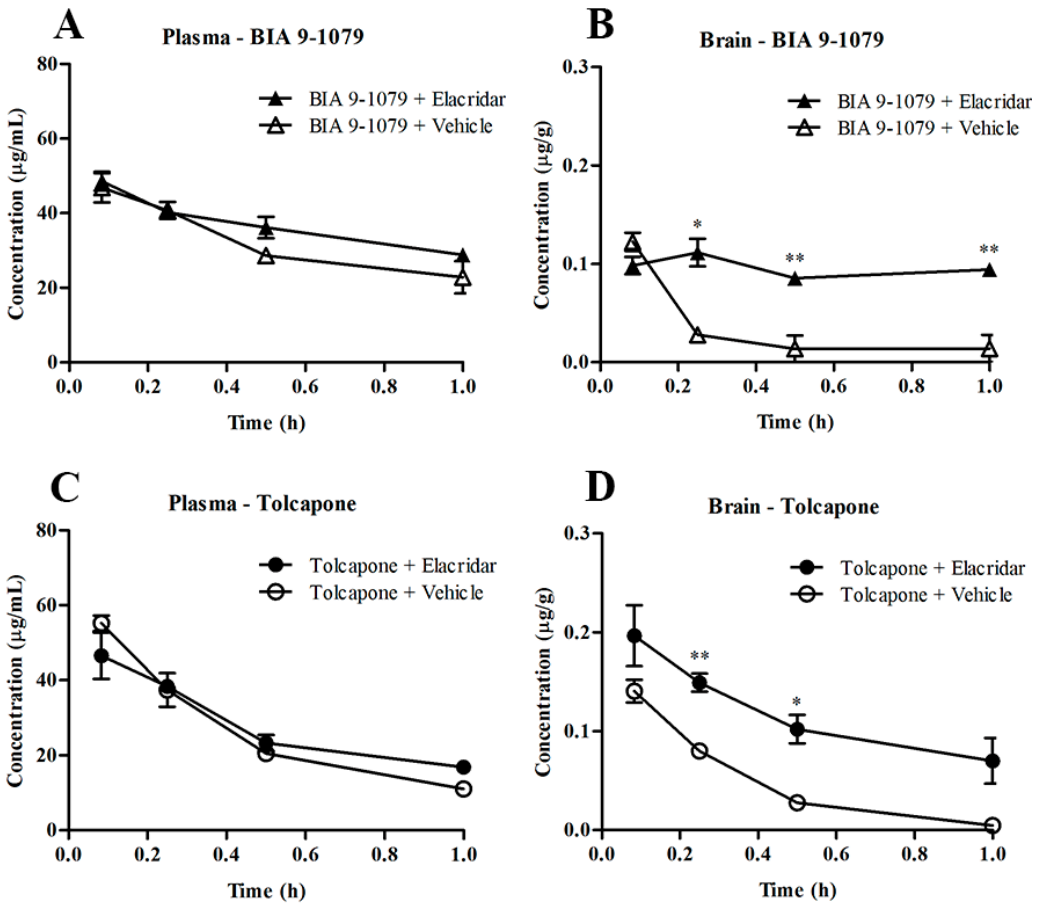

Figure IV.2. Mean concentration-time profiles of BIA 9-1079 and tolcapone in plasma and brain with and without the co-administration of elacridar (2.5 mg kg^{-1}) are depicted from A-D. Each data point is presented as mean ± standard error of the mean (*n* = 8 – 12 animals per group) and significant differences between group concentrations at specific time-points were calculated by two-tailed Student's t-test. $p < 0.05$ (*), $p < 0.01$ (**).

The proximity evidenced in Figure IV.2A and IV.2C between plasma concentrations after vehicle or elacridar administration and the AUC_{0-t} values of BIA 9-1079 or tolcapone with vehicle or with elacridar (Table IV.3), suggests that plasma exposure was not affected by the co-administration of elacridar. Nevertheless, statistically significant differences were found in brain concentrations of BIA 9-1079 and tolcapone between elacridar and vehicle-administered rats, namely at 0.25, 0.5 and 1 h post-dosing (Figure IV.2B / IV.2D). With elacridar, the brain AUC_{0-t} of BIA 9-1079 and tolcapone increased 2.57- and 2.38-fold, respectively. These results attest the contribution of P-gp and/or BCRP to the limited extent of brain distribution of these COMT inhibitors.

Table IV.3. Plasma and brain exposure of BIA 9-1079 and tolcapone after intravenous administration (10 mg kg^{-1}) to Wistar rats with or without co-administration of elacridar (2.5 mg kg^{-1}).

		AUC_{0-t} (μg.h mL^{-1})		**K_p**		**$K_{p,uu}$**	
		Vehicle	**Elacridar**	**Vehicle**	**Elacridar**	**Vehicle**	**Elacridar**
BIA 9-1079	Plasma	32.71	37.34	0.001	0.003	0.007	0.017
	Brain	0.037	0.095				
Tolcapone	Plasma	27.31	28.59	0.002	0.004	0.041	0.095
	Brain	0.050	0.119				

AUC is expressed in μg.h g^{-1} in brain tissue;

AUC_{0-t}, area under the concentration-time curve from time zero to the last measurable concentration; K_p, ratio of total brain-to-plasma AUC_{0-t}; $K_{p,uu}$, unbound brain-to-plasma ratio.

IV.4. DISCUSSION

BIA 9-1079 and tolcapone were administered to Wistar rats and the pharmacokinetic parameters obtained in the brain support that both compounds crossed the BBB quickly and soon achieved C_{max}. Still, the most clinically relevant parameter $K_{p,uu}$ revealed a low extent of brain penetration for both compounds, in particular for BIA 9-1079. These results were not surprising for BIA 9-1079 given that it had been identified as a P-gp substrate *in vitro*. Notwithstanding, tolcapone was not identified *in vitro* as P-gp or BCRP substrate, probably because its efflux was surpassed

by its very high permeability. In fact, this has also been observed for other high permeability efflux substrates, such as verapamil [219].

Additionally, the significant increase of brain exposure of BIA 9-1079 and tolcapone following the co-administration with elacridar confirms that P-gp and/or BCRP contribute to their limited access to the brain. Although other authors have reported low total or unbound brain-plasma ratios for tolcapone [224,419,529], this drug is a known peripheral and central COMT inhibitor, which could misleadingly convey that it crosses the BBB to great extent. In fact, 99% of brain COMT was inhibited after 0.5 h of an oral administration of tolcapone (30 mg kg^{-1}) to Wistar rats [426] probably due to its elevated potency, as evidenced by the very low IC_{50} values determined for membrane-bound (2 nM) and cytosolic (3 nM) brain COMT [425]. Hence, even though P-gp and BCRP severely hamper drug access to the CNS, efflux substrates can be centrally active if the administered dose is sufficient to result in pharmacologically active concentrations in the CNS.

Comparatively, BIA 9-1079 crossed the BBB in even less extent than tolcapone (35-fold lower $K_{p,uu}$), meaning that peripheral effects are favoured and CNS effects are much less probable. Indeed, the likelihood of CNS activity of a compound diminishes, as $K_{p,uu}$ decreases [646]. Furthermore, despite demonstrating peripheral selectivity and being a major metabolite of opicapone in animals, the contribution of BIA 9-1079 to the peripheral therapeutic effects of opicapone in humans is minor, given that BIA 9-1079 represents only 20% of its systemic exposure [443].

IV.5. FINAL CONSIDERATIONS

In vivo assays were performed for BIA 9-1079 and tolcapone, providing relevant information in regard to their extent of brain distribution and intra-brain tissue binding. Our studies are in line with the current notion that a conjugation of data from different parameters of CNS penetration is necessary to evaluate and explain brain drug transport.

CHAPTER V

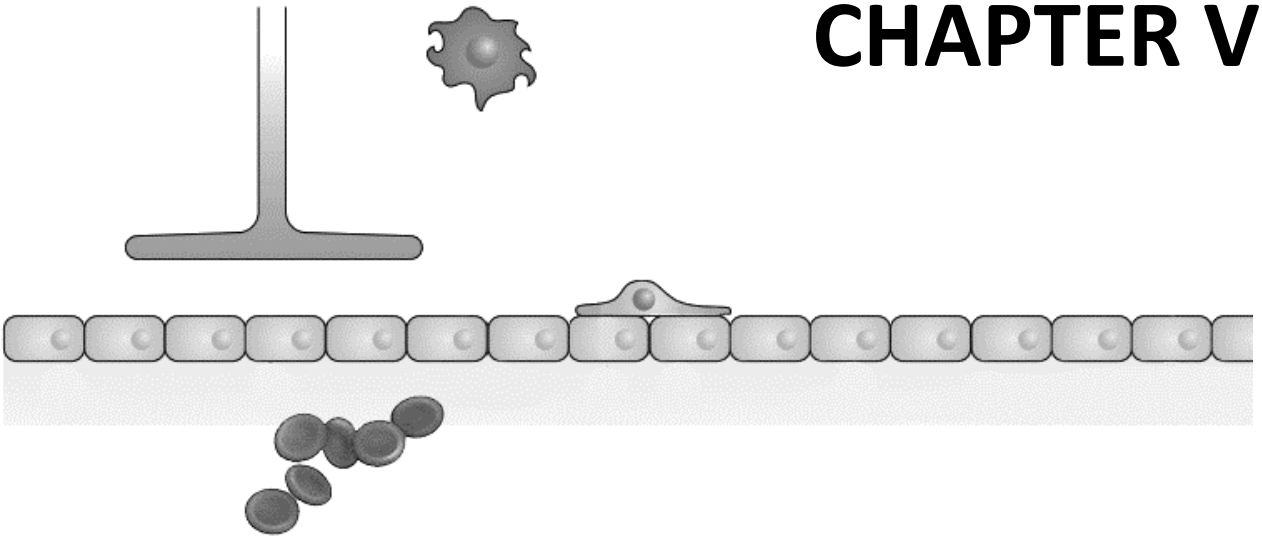

GENERAL DISCUSSION

CHAPTER V. GENERAL DISCUSSION

There is currently a large discrepancy between the necessity of more and improved drugs for the treatment of CNS diseases and the number of innovative compounds that is effectively reaching the market. Despite the diversity of CNS pathologies that affect millions of people worldwide, there has been a generalized decrease in the investment made in this therapeutic area, due to the disappointing results that many promising candidates yield during preclinical phases and even late-stage clinical phases. This trend caused researchers from the academy, pharmaceutical industry and regulatory agencies to re-think the overall development process and identify the reasons for such low success rates. In part, failure can be explained by the difficulties inherent to CNS drug delivery, since the CNS is considered a drug sanctuary protected from external influences by an extremely efficient system, the BBB. Given that much is yet unknown about the BBB both in physiological and pathological circumstances, it becomes difficult to develop and implement laboratory models capable of predicting how the BBB will handle a specific compound or a series of compounds, while remaining as simple, high throughput and economic as possible.

Furthermore, it is not only important to possess the appropriate *in vitro* and *in vivo* models, but also to accurately interpret the data provided by these models. This constitutes another struggle that had been hindering drug development in this field, since there were misleading definitions of pharmacokinetic concepts related to CNS exposure. For instance, too much emphasis was placed on the measurement of total brain and plasma concentrations instead of the free, unbound and pharmacologically available concentrations. In order to achieve optimal brain exposure, compounds were designed to be extremely lipophilic but this approach turned out to be counter-productive, because the molecules often revealed high non-specific binding and affinity for efflux transporters. Additionally, there were frequent misconceptions in literature involving other parameters of CNS penetration, namely: BBB permeability; unbound fractions in plasma and brain tissue; and the exact influence of transporters, or specifically, if during the development process for CNS targets it is advisable to advance or immediately reject substrates of efflux transporters. Consequently, it became urgent

to differentiate the processes that govern the pharmacokinetics of a compound in the CNS, namely the rate and extent of brain penetration and intra-brain distribution. These notions are also applicable when the purpose is to develop molecules for peripheral targets and avoid CNS side-effects. Even though the adopted strategies to minimize brain exposure during development are different from those to maximize it, the assessment of CNS penetration must always be performed for all compounds, regardless of the original intention.

So far, there is no consensus on the subject of the most appropriate screening strategy for determining the access of compounds to the CNS. In this context, the work underlying the present thesis relied on an integrative approach of data from *in vitro* and *in vivo* studies with the purpose of characterizing different aspects of CNS penetration. These models were optimized, validated, and then applied to diverse compound sets, including COMT inhibitors, DBH inhibitors and DAC derivatives.

In this section, the obtained information on the various topics covered within previous chapters will be combined and examined in greater detail. The usefulness of applying the developed *in vitro* and *in vivo* models for describing the passage of compounds to the CNS will be critically discussed, as well as, the advantages and disadvantages subjacent to each methodology. This complementary analysis will begin with the evaluation of passive permeability, followed by the investigation of possible interactions with the main efflux transporters of the BBB and the determination of unbound compound concentrations in plasma and brain biological samples.

The first aim of this thesis was to measure the passive permeability of compounds. Therefore, a PAMPA technique was developed and validated, as it is a high throughput, reproducible and robust method. In addition, PAMPA is widely used in early stages of drug discovery for the prediction of passive diffusion across phospholipid monolayers, and it has been adapted from the prediction of intestinal absorption to the BBB through the use of PBL [178]. Herein, a protocol that enables the obtainment of *in-house* brain lipid extracts was set by modifying the traditional Folch extraction method. The extracts were subsequently incorporated into the hydrophobic filters of the PAMPA plates and used as lipid membranes. Notwithstanding, it was firstly necessary to optimize and

validate the experimental conditions, resorting to 18 chemically diverse reference molecules with known BBB permeability. This implied the selection of an appropriate buffer solution, incubation period, stirring conditions, pH of donor and acceptor compartments, concentration of the lipid solution and a comparison with other lipid solutions, namely phosphatidylcholine and PBL. By applying the conditions that allowed a better classification of compounds with higher and lower BBB permeation, the *in-house* brain lipid extract revealed an equivalent discriminatory capacity to PBL (r^2 = 0.77) and superior to phosphatidylcholine (r^2 = 0.56). These observations supported its use for the prediction of passive diffusion across the BBB.

Moreover, the *in-house* brain lipid extract demonstrated physicochemical selectivity by achieving correlations with log D pH 7.4 (r^2 = 0.83), TPSA (r^2 = 0.69) and THBC (r^2 = 0.61). Interestingly, the observed values for each property, log D pH 7.4 = 1.15; TPSA = 68.22; THBC = 5, and the positive or negative slopes were in agreement with literature data, which indicate that passive diffusion is promoted by lipophilicity and limited by the hydrogen-bonding capacity of a drug.

The test compounds were also submitted to PAMPA with *in-house* brain lipid extract, once again obtaining similar results to those with PBL (r^2 = 0.94). Among them, eslicarbazepine acetate, BIA 9-1079 and nepicastat were classified as having high BBB permeation, whereas others fell under the defined cut-off value.

Herein, a comparison could be made between the Papp values obtained in PAMPA and the $Papp_{AP-BL}$ values estimated in the bidirectional transport assay with MDCK cells, for the tested COMT and DBH inhibitors. Both PAMPA and MDCK cells are routinely used by pharmaceutical companies for permeability measurements [647], but while some authors state that MDCK cells display BBB-like passive permeability [219], others believe that PAMPA is a more suitable model to determine passive permeability across the BBB, due to the distinct cytoarchitecture of MDCK cells [176]. In the bidirectional transport assay, BIA 9-1059, etamicastat, opicapone and entacapone were among the least permeable compounds, while nepicastat was among those with higher permeability. These results were identical to PAMPA notwithstanding, differences between the methods were more apparent for BIA 9-1079, tolcapone and nebicapone. With MDCK cells, BIA 9-1079 presented a lower passive permeability than in PAMPA, whereas tolcapone and nebicapone displayed a higher permeability. Taking into consideration

the physicochemical properties that were mentioned above, PAMPA provided an accurate classification, given that the most distinctive feature between the compounds, log D pH 7.4, is higher for BIA 9-1079, while TPSA and THBC are similar. Consequently, BIA 9-1079 was considered more permeable than nebicapone and tolcapone by the PAMPA model. Another possible explanation could be related to the fact that PAMPA reflects transcellular passive diffusion, while cell-based assays also contemplate paracellular passive diffusion and active transport. However, the hypothesis of paracellular diffusion for tolcapone and nebicapone in MDCK II cells seems unlikely, since the $Papp_{AP-BL}$ values obtained for the paracellular marker Na-F ($0.48x10^{-6}$ cm s^{-1}) and reference compound atenolol ($0.22x10^{-6}$ cm s^{-1}) were low, revealing a restricted paracellular pathway. Still, there are differences in the experimental conditions between the methods that may affect Papp values, such as incubation time (16 h *vs.* 60-120 min) or temperature (room temperature *vs.* 37 °C). For instance, a temperature increase generally leads to an increase in Papp, although not all compounds are affected and some are more affected than others [648]. Nevertheless, it is not consensual that conducting assays at 37 °C improves the predictivity of the model [195]. Therefore, it is important that Papp is compared when the applied conditions are similar, otherwise the agreeability between the models may be influenced by these variables.

Overall, the developed PAMPA method with *in-house* brain lipid extract effectively differentiated BBB permeable from less permeable compounds. The implemented lipid extraction process was reproducible, economical and is expected to have an extended applicability, for enabling the extraction of lipids from other biological sources.

Since the importance of efflux in the transport of several drugs across the BBB is unquestionable, the second aim of this dissertation was to establish a model that permitted the evaluation of the role of P-gp and BCRP, the two main efflux transporters of the BBB, on the access of compounds to the brain. To date, BCRP was not usually assessed, but recent developments point towards the synergy between this transporter and P-gp at the BBB. For this reason, there was the need to include BCRP-mediated efflux into the screening strategy.

Immortalized cell lines are appropriate for routine screening assays, since primary cell cultures are too laborious to prepare and maintain. However, BBB-specific immortalized cell lines do not form sufficiently restrictive tight junctions and are excessively leaky for transendothelial assays. Therefore, non-endothelial cell lines like Caco-2 or MDCK cells became widely used as surrogate models to study efflux at the BBB. Nonetheless, Caco-2 cells take approximately 21 days to be ready for assays due to a long differentiation time, making MDCK cells more advantageous. These cells can be stably transfected with the human *MDR1* or *ABCG2* genes, originating the MDCK-MDR1 and MDCK-BCRP lines that allow the identification of P-gp and BCRP inhibitors and substrates.

After performing cell viability and stability studies, potential P-gp and BCRP inhibitors were identified resorting to intracellular accumulation assays, using rhodamine-123 and Hoechst 33342 as fluorescent probe substrates for P-gp and BCRP, respectively, and verapamil and Ko143 as positive controls for inhibition. Initially, compounds were tested at a high concentration that did not compromise cell viability and when a significant decrease in the accumulation of probe substrate was observed, increasingly lower concentrations of test compound were used to verify concentration-dependency and calculate IC_{50}. Applying the established protocol, it was possible to identify one concentration-dependent P-gp and BCRP inhibitor (zamicastat) and five BCRP inhibitors (BIA 9-1079, nebicapone, tolcapone, etamicastat, nepicastat). IC_{50} values were in the micromolar range for all compounds, indicating that high unbound plasma concentrations would be necessary to achieve inhibition *in vivo*. Nevertheless, compounds that are dual P-gp and BCRP inhibitors may have a stronger impact on the brain exposure of drugs that go through combined efflux [604,649]. This suggests that in the future, the effect of circulating concentrations of zamicastat could be studied on synergistically effluxed drugs.

In addition to accumulation assays, a protocol was implemented for the identification of P-gp and BCRP substrates using the bidirectional transport assay. Despite being more arduous than the intracellular accumulation assay, this method reliably predicts efflux liabilities, correlates well with results from *in vivo* studies and is one of the most relevant to evaluate CNS distribution [616,650]. Setting up the experimental conditions for this technique revealed to be a demanding task, due to the

lack of consensus and standardization in literature regarding the conditions that provide the most predictive outcomes. Therefore, it was first necessary to ponder several experimental variables in order to ensure proper cell attachment and the formation of a restrictive monolayer, such as the type of Transwell™ membrane and pore size, well format, the cell density, the seeding and medium replacement techniques, and the number of days in culture before assays.

This assessment was performed through TEER measurements and through the evaluation of the Papp of the paracellular fluorescent marker, Na-F. Theoretically, in order to be free of leakiness, the TEER of the *in vitro* model should be high, while the penetrability of paracellular tracer molecules should be low. Nevertheless, low TEER values were registered throughout the culture period in the Transwell™ plates. Although this might be perceived as potentially problematic, it can be explained by the kidney origin of MDCK II cells, where ionic reabsorption is a physiological function. Consequently, these cells possess ion pores that contribute to ion movement and decrease TEER [219]. Indeed, MDCK type II cells normally display low TEER values due to the presence of pore-forming claudins, like claudin-2 [637]. Besides, TEER values are affected by several factors such as temperature or cell culture medium composition [651], causing variations in read-outs between laboratories. Therefore, the estimation of the Papp of Na-F was seen as a more reliable tool to monitor the integrity of the cell monolayers. The experimental conditions that yielded the lowest Papp for Na-F in all cell lines (under $1.0x10^{-6}$ cm s^{-1} in MDCK II cells and $0.5x10^{-6}$ cm s^{-1} in MDCK-MDR1 and MDCK-BCRP cells), indicating the generation of discriminatory monolayers, were chosen for following assays with reference molecules.

Independently of the selected experimental approach, it is important to apply a well-characterized system with known substrates and inhibitors, and to utilize adequate controls to confirm test results [617]. The reference molecules used to validate this assay were not randomly selected; in truth, a deliberate choice was made to include chemically diverse compounds with known mechanisms of transport. Some compounds were not efflux substrates, whereas others had low paracellular permeability or were P-gp-only substrates, BCRP-only substrates or P-gp and BCRP substrates. Nevertheless, before proceeding with the assays, it was required to validate HPLC techniques for

compound quantification. There was the concern to apply sensitive analytical methods, particularly for less permeable compounds, which could be more difficult to quantify in the acceptor compartment and especially in the first sampling times. Indeed, the sampling times and the concentration of donor solutions were defined in preliminary studies. The selected donor concentrations for each compound were always the lowest possible, taking into account the sensitivity of the applied analytical technique. Furthermore, the assays were performed with a protein-free buffer solution, thereby allowing the injection of samples directly into the HPLC apparatus without the need of pre-treatment steps, which together with short run-times (< 6 min), contributed to an increased overall throughput. This constitutes a significant advantage because when the three cell lines (MDCK II, MDCK-MDR1, MDCK-BCRP), compounds (reference and test molecules), time-points (four time-points) and sampling directions ($Papp_{AP-BL}$ and $Papp_{BL-AP}$) are considered, the final number of samples to analyse is quite large. Additionally, in order to minimize the impact of the replacement of growth medium by transport buffer, care was taken to equilibrate or pre-incubate the cells for 30 min before starting the transport study.

Following the recommended criteria [558,605,617], all reference compounds described as effluxed substrates in literature were correctly identified in the respective cell lines for exhibiting net flux ratios superior to 2. Moreover, after a pre-incubation with verapamil or Ko143, net flux ratios were reduced more than 50% in all cases, confirming that no other efflux transporters were responsible for the observed data. Therefore, the assay was deemed as appropriately validated, and the conditions were applied to COMT and DBH inhibitors.

In addition to the determination of Papp, efflux ratios and net flux ratios, the mass balance or recovery was estimated for reference and test compounds. This is a relevant parameter because when recoveries are too low, the obtained Papp becomes unreliable. It is more problematic for highly lipophilic compounds that can be adsorbed on the plastic or membrane support, preventing meaningful and reproducible permeability studies [633,652]. In our studies, mass balance was above 70% for all compounds, normally used as cut-off [610] except for zamicastat, which revealed a low recovery (< 40%) in preliminary assays. This is understandable, given that zamicastat is the most lipophilic of all test compounds, considering log D pH 7.4 values. Thus, no further

bidirectional transport assays were performed for this compound, because the obtained results would not be reliable or reproducible.

According to the same criteria as above, BIA 9-1079, etamicastat and nepicastat were identified as P-gp substrates in MDCK-MDR1 cells, whereas BIA 9-1059, entacapone, nebicapone, opicapone and etamicastat were identified as BCRP substrates in MDCK-BCRP cells. As a dual substrate, etamicastat will display a significantly impaired brain penetration, due to the cooperative effect of the two transporters in eliminating drugs from the brain. This was in agreement with recent literature data for etamicastat and nepicastat, which were identified as P-gp substrates [470].

In sum, through optimized and validated *in vitro* cell-based assays, new information was obtained concerning the interactions of COMT and DBH inhibitors with human P-gp and BCRP. Using intracellular accumulation and bidirectional transport assays with MDCK II, MDCK-MDR1 and MDCK-BCRP cells, P-gp and BCRP substrates and/or inhibitors were identified, thereby contributing to the comprehension of the mechanisms that control the access of the tested compounds to the CNS.

Another aim of the present dissertation was to evaluate the extent of CNS penetration ($K_{p,uu}$) and intra-brain distribution of two COMT inhibitors: BIA 9-1079, the major animal metabolite of opicapone, herein identified as a P-gp substrate; and tolcapone, a known inhibitor of central and peripheral COMT, that did not reveal to be an efflux substrate in bidirectional transport assays. To achieve this goal, *in vivo* pharmacokinetic studies were performed in male Wistar rats. The rat was chosen as animal model because it is the most commonly selected species for pharmacokinetic studies to assess COMT inhibitors [424,429,438,449,529,653]. Male rats were specifically used to prevent possible interferences from the female hormonal cycle. Moreover, BIA 9-1079 and tolcapone were administered by intravenous route in order to circumvent oral absorption and guarantee complete bioavailability.

Once again, before beginning these studies, bioanalytical techniques were validated to quantify BIA 9-1079 and tolcapone in rat plasma and brain. Although there were published techniques concerning the quantification of opicapone and BIA 9-1079 in rat plasma, kidney and liver [635], quantification in brain was not contemplated, nor of

tolcapone. Thus, adjustments were made to the chromatographic conditions of the previous technique, allowing the accurate, precise and reproducible determination of tolcapone and BIA 9-1079 in the biological matrices of interest.

The next step concerned the definition of the dose and formulation. The dose settled in preliminary studies and applied in literature [654] was 10 mg kg^{-1}. Considering the good practice administration volume in the rat of 5 mL kg^{-1} by intravenous bolus injection [655], formulations of 2 mg mL^{-1} were prepared in PEG-NaCl 0.9% (50:50, v/v), ensuring the complete solubilisation of tolcapone and BIA 9-1079. PEG 400 is among the safest organic co-solvents, commonly applied in preclinical *in vivo* pharmacokinetic studies due to its very effective solubilizing capability and safety [656] at a concentration of 50% for intravenous administration [657,658]. Sampling-points were also defined in preliminary studies, and extended for BIA 9-1079 up to 24 h post-dosing due to a slower elimination from plasma. Importantly, it was established that blood should be collected by cardiac puncture followed by intracardiac perfusion with NaCl 0.9%. This prevented contamination of brain samples with blood, which could lead to an overestimation of drug concentrations in brain tissue. Indeed, this correction is most important when blood concentration is large, e.g. after bolus intravenous injection, and parenchymal brain concentrations are small [659]. Furthermore, the existence of residual blood in brain homogenates has been demonstrated to affect the determination of $f_{u,brain}$ due to the presence of serum albumin [660]. For these reasons, the aforementioned procedures were adopted throughout all *in vivo* studies and for *in vitro* assessments of $f_{u,brain}$.

Following the conclusion of *in vivo* studies, the K_p of BIA 9-1079 and tolcapone was obtained. However, as previously referred in this dissertation, K_p not only reflects the passage of compounds across the BBB, but also non-specific binding to brain tissue and plasma proteins. In contrast, $K_{p,uu}$ is a more relevant parameter that provides an estimation of the extent of equilibration of unbound drug between plasma and brain ISF. Consequently, to calculate $K_{p,uu}$ from K_p, it was necessary to measure the $f_{u,plasma}$ and $f_{u,brain}$ of BIA 9-1079 and tolcapone. Several *in vitro* methods are available in literature for this purpose but some of the most widely applied are equilibrium dialysis and ultrafiltration. Equilibrium dialysis is a well-known technique nevertheless, it involves long equilibration times (4-6 h) at 37 °C, which may interfere with compound stability in

plasma and brain homogenate [92]. Conversely, ultrafiltration increases assay throughput, as it is much less time-consuming (1 h). Its greatest drawback is non-specific binding to the filter membrane and plastic device [661,662]. Thus, ultrafiltration was selected to estimate $f_{u,plasma}$ and $f_{u,brain}$ for BIA 9-1079 and tolcapone, with recoveries ranging between 86 – 97%. In addition to this, stabilities were calculated and stood between 86 – 105 %.

After correcting $f_{u,brain}$ values for lysosomal trapping according to the pH partitioning model, a $K_{p,uu}$ of 0.001 was obtained for BIA 9-1079 and 0.035 for tolcapone. Although the $K_{p,uu}$ of tolcapone was 35-fold higher than BIA 9-1079, indicating a much more impaired brain penetration for BIA 9-1079, both values were inferior to 1, which pointed towards the existence of active efflux transport. This result was expected for BIA 9-1079, but tolcapone had not been identified as efflux substrate in neither MDCK-MDR1 nor MDCK-BCRP cells, which could imply that it was effluxed by a BBB transporter other than P-gp or BCRP *in vivo*, or that *in vitro* the high passive permeability was masking efflux in the bidirectional transport assay. Indeed, there were other reports suggesting tolcapone as a possible efflux substrate, but the responsible transporter is not mentioned [88,224]. Therefore, elacridar, a dual P-gp and BCRP modulator, was added to the formulation at 2.5 mg kg^{-1} and co-administered with BIA 9-1079 or tolcapone, in order to attest the involvement of these transporters. This led to a significant increase in brain concentrations at 0.25, 0.5 and 1 h post-dosing and also to an increase in $K_{p,uu}$ of 2.43-fold for BIA 9-1079 and 2.32-fold for tolcapone, comparing to vehicle-treated rats. In opposition, no significant alterations were observed in plasma levels. These results confirmed that P-gp and/or BCRP were responsible for the low $K_{p,uu}$ values and limited extent of brain penetration of these compounds. The fact that tolcapone was not identified in Transwell™ assays as P-gp or BCRP substrate, as a consequence of its high permeability, reflects an unavoidable limitation of the method that had been previously addressed in this thesis.

Although efflux causes disequilibrium in the distribution between brain and plasma, it is important not to prematurely exclude efflux substrates from being CNS drug-candidates without analysing their intra-brain distribution. The extent of cellular barrier transport given by $K_{p,uu,cell,pred}$ was below 1 for BIA 9-1079 and tolcapone, indicating that

these compounds do not display a tendency to accumulate intracellularly, in agreement with literature data for nitrocatechols [419]. Likewise, the ratios of intracellular distribution into the cytosol and acidic organelles ($K_{p,uu,cyto,pred}$ and $K_{p,uu,lyso,pred}$) were also lower than 1. Furthermore, $V_{u,brain,pred}$ values were superior to 0.8 mL g^{-1} brain, particularly for BIA 9-1079, revealing a higher non-specific binding to brain tissue [324] for this compound.

To finalize, it is advisable to conjugate pharmacokinetic parameters with pharmacodynamic data for the assessment and selection of CNS and non-CNS compounds [84]. Pharmacodynamic studies were not performed in the scope of this dissertation, nevertheless, it is known that as $K_{p,uu}$ decreases, the likelihood of peripheral effects and avoidance of central side-effects increases. This means that central effects are more favourable for tolcapone than BIA 9-1079 given the 35-fold higher $K_{p,uu}$ of tolcapone. Additionally, tolcapone has been described in literature as a potent COMT inhibitor [530], indicating that the contribution of efflux transporters to decrease $K_{p,uu}$ may not necessarily prevent a compound from being centrally active.

In sum, through the association of several experimental models it was possible to characterize different features of CNS penetration, including the rate, extent and intra-brain distribution. The methods were optimized, validated and tested resorting to appropriate reference and test molecules.

Hopefully, the application of combined or integrative screening strategies will positively contribute to an improvement of the drug development process and facilitate the evaluation of the brain access of drugs directed at CNS and non-CNS pathologies.

CHAPTER VI

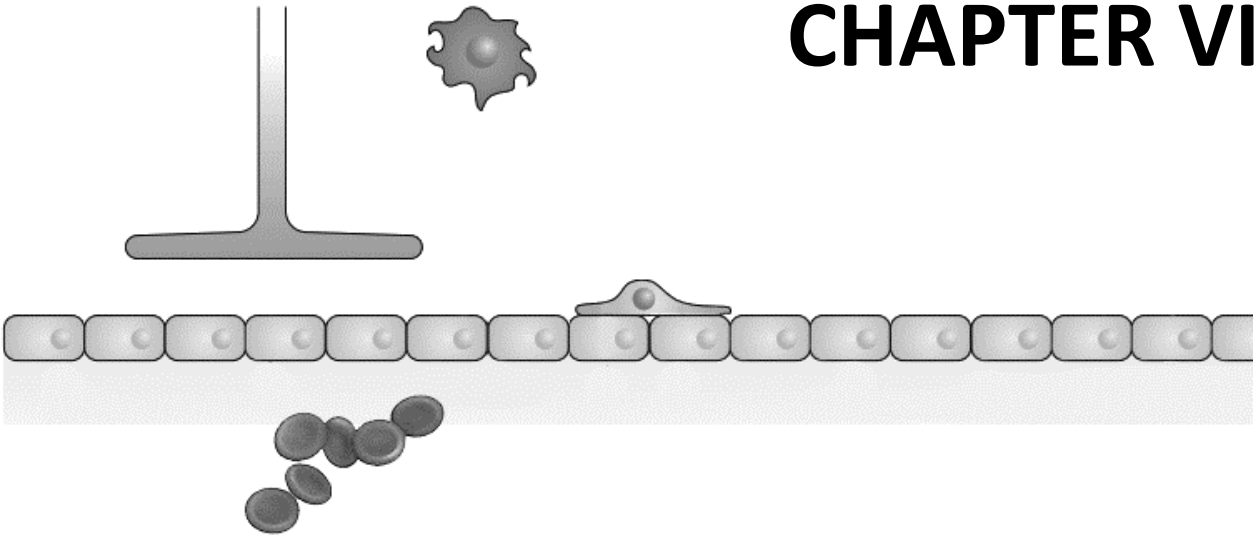

CONCLUSIONS AND FUTURE PERSPECTIVES

CHAPTER VI. CONCLUSIONS AND FUTURE PERSPECTIVES

The work developed in this dissertation encompasses a series of *in vitro* and *in vivo* methods, implemented with the purpose of describing the passage of compounds across the BBB. Due to its physiological complexity, the BBB cannot be fully mimicked in laboratorial setting. Therefore, the adopted strategy was to apply more than one model and combine the data provided by each model to attain a more complete overview of the main pharmacokinetic processes that govern the entry of compounds into and out of the CNS. This implied the study of the rate, extent and intra-brain distribution of compounds, including passive permeation, active transport processes, plasma protein binding and brain tissue binding.

Briefly, the main achievements of the research conducted in the context of the present thesis are the following:

- Application of a lipid extraction method to obtain *in-house* brain lipid extracts for the establishment of a discriminative PAMPA-BBB model. This model was validated resorting to 18 reference molecules, successfully distinguished more permeable from less permeable compounds and demonstrated physicochemical selectivity. It constitutes an economic and reproducible alternative for the assessment of passive permeability across the BBB.

- Identification of human P-gp and BCRP substrates and/or inhibitors in cell-based assays using MDCK II, MDCK-MDR1 and MDCK-BCRP cells. First, the determination of cellular viability was carried out through the MTT assay for all molecules, while compound stability was analysed before advancing for subsequent studies. Then, intracellular accumulation assays were executed, confirming transporter functionality and enabling the identification of concentration-dependent P-gp and/or BCRP inhibitors, as well as, their respective IC_{50} values. One P-gp and BCRP inhibitor (zamicastat) and five BCRP inhibitors (BIA 9-1079, nebicapone, tolcapone, etamicastat, and nepicastat) were identified.

- Bidirectional transport assays were performed in all cell lines for the identification of P-gp and/or BCRP substrates, through the estimation of their net flux ratios. Monolayer integrity was ensured through the careful optimization of experimental conditions and attested by the low Papp values of paracellular marker Na-F. Recoveries were verified to guarantee reliable Papp values, while net flux ratios were confirmed by pre-incubation with well-known P-gp or BCRP inhibitors. This assay additionally implied a previous validation of analytical HPLC techniques for the quantification of all compounds in samples, including reference and test molecules. Seven reference molecules were used to validate this method, including passively transported compounds by transcellular or paracellular route, P-gp-only and BCRP-only substrates, and dual P-gp and BCRP substrates. Applying the established conditions, all were correctly classified, according to literature data. Among test compounds, three P-gp substrates (BIA 9-1079, etamicastat, nepicastat) and five BCRP substrates (BIA 9-1059, entacapone, nebicapone, opicapone and etamicastat) were identified.

- Adaptation and validation of an HPLC-DAD technique for the quantification of BIA 9-1079 and tolcapone in plasma and brain homogenate samples from Wistar rats. This technique demonstrated sensitivity, precision and accuracy, with appropriate run-times and high absolute recovery values. It was used to support *in vitro* ultrafiltration assays, as well as, *in vivo* studies with these compounds.

- The ultrafiltration method was applied for a rapid and efficient estimate of $f_{u,plasma}$ and $f_{u,brain}$ of BIA 9-1079 and tolcapone. The recoveries and stability of these compounds were evaluated throughout the process, providing confidence in the reliability of the obtained results. BIA 9-1079 revealed lower $f_{u,plasma}$ and much lower $f_{u,brain}$ than tolcapone.

- The most important parameter of the extent of brain penetration, $K_{p,uu}$, was determined following *in vivo* pharmacokinetic studies with Wistar rats. Specific procedures were adopted during the practical execution of all studies in order to prevent the contamination of brain homogenate samples with blood, namely cardiac puncture and intracardiac perfusion. Systemic exposure was higher for BIA 9-1079, whereas brain exposure was superior for tolcapone, although limited for both compounds. $K_{p,uu}$ was below unity for both BIA 9-1079 and tolcapone, but especially for BIA 9-1079, demonstrating the involvement of efflux transporters in the limited extent of CNS access of these compounds. Furthermore, intra-brain distribution parameters revealed a low tendency of intracellular accumulation ($K_{p,uu,cell} < 1$) and also high non-specific binding to brain tissue, particularly for BIA 9-1079 ($V_{u,brain} > 0.8$ mg mL g^{-1} brain).

- Additional *in vivo* assays were carried out through the co-administration of elacridar, a potent P-gp and BCRP inhibitor. This led to a significant increase in brain concentrations and $K_{p,uu}$ of BIA 9-1079 and tolcapone, thereby confirming the role of P-gp and/or BCRP in hampering their passage to the CNS.

Developing methods to determine CNS exposure is a challenging but compelling research area. It must always be certified that these tools provide trustworthy information that benefits drug research. Taking into consideration the results achieved during this work, it can be concluded that associating different experimental models (PAMPA-BBB, cell-based assays and *in vivo* studies) is a viable approach for the study of rate, extent and intra-brain distribution of compounds, intended for CNS or peripheral therapeutic targets.

In the future, pharmacodynamic assays could be conducted to assess the relationship between the estimated pharmacokinetic parameters and pharmacological potency. Moreover, given that disease states alter BBB properties, it would also be interesting to investigate if and how different pathologies contribute to the modification of $K_{p,uu}$, in comparison with healthy models.

APPENDIX

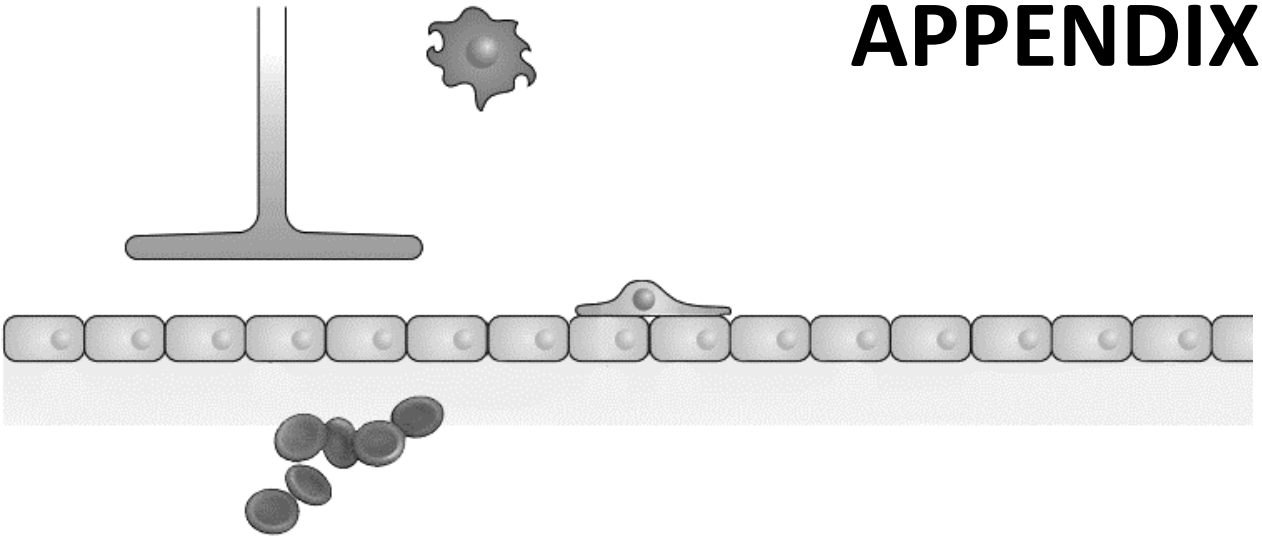

Table I.7. Co-culture and triple co-culture cell models of the blood-brain barrier [102].

Endothelial cells	Co-cultured cells	Culture medium	Filter coating solution	Cell density (cell cm^{-2}) [filter pore size]	Maximum TEER ($\Omega.cm^2$) day*	Permeability tracers P_e ($x10^{-6}$ cm s^{-1})	Static / dynamic	Ref.
Porcine CECs	Rat CTX-TNA2 astrocytes [non-contact]	*Growth medium* [10% PDS, 100U mL^{-1} penicillin, 100mg mL^{-1} streptomycin, 125mg mL^{-1} heparin , 2mg mL^{-1} L-glutamine in DMEM:ACM (1:1)] *Supplemented medium* [100U mL^{-1} penicillin, 2mg mL^{-1} streptomycin, 125mg mL^{-1} heparin, 312.5µmol L^{-1} CPT-cAMP, 17.5µmol L^{-1} RO-20-1724, 55µmol L^{-1} hydrocortisone, 2mg mL^{-1} L-glutamine in DMEM]	Rat tail collagen type I, human fibronectin (NR)	$8.0x10^4$ NR [0.4µm]	1700 – 2200 (day 7)	Lucifer yellow: 0.57	Static	[218]
Porcine CECs	Porcine pericytes [contact]	*Pericyte medium* [10% NBCS, 100U mL^{-1} penicillin, 100µg mL^{-1} gentamicin, 100µg mL^{-1} streptomycin, 2mM L-glutamine in DMEM / Ham's F12] *Differentiation medium* [20ng mL^{-1} bFGF or 4ng mL^{-1} TGF-β in serum-free pericyte medium]	Rat tail collagen type I (0.54 mg mL^{-1})	$2.5x10^5$ $5.0x10^3$ [0.4µm]	[bFGF-treated pericytes]: 542.27 - 797.28 (day 13)	NR	Static	[663]
Porcine CECs	Porcine astrocytes [contact]	*Primary growth medium* [15% HS, 100µg mL^{-1} heparin, 50µg mL^{-1} ECGS, 50µg mL^{-1} gentamicin, 5µg mL^{-1} amphotericin B in MEM] *Secondary growth medium* [2% FBS, 13% HS, 100µg mL^{-1} heparin, 50µg mL^{-1} ECGS, 50µg mL^{-1} gentamicin, 5µg mL^{-1} amphotericin B in MEM] *Astrocyte medium* [10% FBS, 50µg mL^{-1} gentamicin, 5µg mL^{-1} amphotericin B in MEM]	Fibronectin (20 µg mL^{-1})	$5.0x10^4$ $5.0x10^4$ [0.4µm]	NR	NR	Static	[664]
Porcine (or bovine) CECs	Rat C6 glioma cells [non-contact]	*Assay medium* [100U mL^{-1} penicillin, 100µg mL^{-1} streptomycin, 550nM hydrocortisone in DMEM / Ham's F12]	Rat tail collagen type I (5 µg cm^{-2})	$5.0x10^4$ $5.0x10^4$ [0.4µm]	[porcine]: 546 [bovine]: 507 (day 6)	Mannitol [porcine]: 2.31 [bovine]: 5.18	Static	[665]

Table I.7. *Continued*

Endothelial cells	Co-cultured cells	Culture medium	Filter coating solution	Cell density (cell cm^{-2}) [filter pore size]	Maximum TEER ($\Omega.cm^2$) day*	Permeability tracers P_e ($x10^{-6}$ cm s^{-1})	Static / dynamic	Ref.
Porcine CECs	Rat glial cells [contact / non-contact]	*Growth medium* [10% FCS, 0.25mg mL^{-1} gentamicin, 1mM pyruvate, 2mM L-glutamine in DMEM] *Plating medium* [10% NBCS, 0.1mg mL^{-1} gentamicin, 100U mL^{-1} penicillin, 0.1mg mL^{-1} streptomycin, 2mM L-glutamine in M199] *Assay medium* [0.1mg mL^{-1} gentamicin, penicillin/ streptomycin, 550nM hydrocortisone, 2mM L-glutamine in DMEM / Ham's F12]	Rat tail collagen type I (27 µg mL^{-1})	$2.5x10^5$ NR [0.4µm]	[contact]: 1112 [non-contact]: 680 (day 4)	Sucrose [contact]: 0.19	Static	[209]
Porcine CECs	Rat C6 glioma cells [non-contact]	*Endothelial medium* [10% heat-inactivated HS, 100U mL^{-1} penicillin, 100µg mL^{-1} streptomycin in M199] *Endothelial switch medium* [550nM hydrocortisone in M199] *C6 medium* [10% heat-inactivated FBS, 100U mL^{-1} penicillin, 100µg mL^{-1} streptomycin in M199] *ACM* [50% culture medium (10% heat-inactivated FBS, 100U mL^{-1} penicillin, 100µg mL^{-1} streptomycin in M199) + 50% C6 medium] *Astrocyte conditioned switch medium* [50% culture medium (550nM hydrocortisone in DMEM / Ham's F12) + 50% C6 medium]	Rat tail collagen type I (5 µg cm^{-2})	$1.0x10^5$ $1.0x10^4$ [0.4µm]	[endothelial switch medium]: 834 (day 6)	Sucrose: 1.6	Static	[240]
PBMEC/C1-2 cells	Rat C6 glioma cells [non-contact]	*Growth medium* [7.5% NBS, 100U mL^{-1} penicillin, 100µg mL^{-1} streptomycin, 5µg mL^{-1} heparin, 5µg mL^{-1} bovine transferrin, 7mM L-glutamine in IMDM:Ham's F12 (1:1)]	Rat tail collagen type I (4.88 µg cm^{-2}), human fibronectin (2.33 µg cm^{-2})	$8.0x10^4$ $2.1x10^4$ [1.0µm]	NR	NR	Static	[246]
Porcine CECs	Porcine astrocytes [contact]	*Primary endothelial medium* [15% HS, bicarbonate, 50µg mL^{-1} ECGS, 50µg mL^{-1} gentamicin, 100µg mL^{-1} heparin, 5µg mL^{-1} amphotericin B in MEM] *Secondary endothelial medium* [Primary endothelial medium, 2% FBS] *Astrocyte medium* [10% FBS, bicarbonate, 50µg mL^{-1} gentamicin, 5µg mL^{-1} amphotericin B in MEM]	Collagen type 1 (NR)	$5x10^4$ $5x10^4$ [0.4µm]	139 (day 5)	Inulin: NR	Static	[666]

Table I.7. *Continued*

Endothelial cells	Co-cultured cells	Culture medium	Filter coating solution	Cell density (cell cm^{-2}) [filter pore size]	Maximum TEER ($\Omega.cm^2$) day*	Permeability tracers P_e ($x10^{-6}$ cm s^{-1})	Static / dynamic	Ref.
Porcine CECs	Rat C6 glioma cells [non-contact]	*Endothelial medium* [10% FBS, 100U mL^{-1} penicillin, 100U mL^{-1} streptomycin in DMEM] *Endothelial switch medium*[50nM hydrocortisone in serum-free DMEM / Ham's F12]	Rat tail collagen type I (5 µg cm^{-2})	$0.2\text{-}0.25x10^6$ $1.0x10^5$ [0.4µm]	800 (day 6)	Sucrose: 3.3	Static	[254]
Bovine CECs	Rat astrocytes [contact]	*Growth medium* [125µg mL^{-1} heparin in DMEM:ACM (1:1)] *Supplemented medium* [312.5µM CPT-cAMP, 0.5µM dexamethasone, 17.5µM RO-20-1724, 50mM TES in DMEM without $NaHCO_3$]	Collagen type IV, fibronectin (NR)	$1.0x10^5$ $1.3x10^5$ [0.4µm]	1014 (day 6)	Mannitol: 0.88	Static	[222]
Bovine CECs	Rat C6 glioma cells [contact / non-contact]	*Endothelial medium* [10% HS, 50µg mL^{-1} gentamicin, 50µg mL^{-1} amphotericin-B, 50µg mL^{-1} polymixin-B, 10mM HEPES, 13mM $NaHCO_3$ in 45% MEM and 45% Ham's F12] *C6 medium* [2.5% FBS, 10% HS, 50µg mL^{-1} gentamicin, 7.5mg mL^{-1} EGCS, 10mM HEPES, 13mM $NaHCO_3$ in 45% MEM and 45% Ham's F12]	Collagen type IV (50µg mL^{-1}), fibronectin (40 µg mL^{-1})	$5.0x10^4$ $4.0x10^4$ [0.4µm]	NR	NR	Static	[667]
Bovine CECs	Rat glial cells [non-contact]	*Growth medium* [10% heat-inactivated NBCS, 10% heat-inactivated HS, 1ng mL^{-1} bFGF, 50µg mL^{-1} gentamicin, 2mM L-glutamine in DMEM]	Rat tail collagen type I (NR)	$4.0x10^5$ NR [0.4µm]	NR	Lucifer yellow: 7 Sucrose: 5.83	Static	[217]
Bovine CECs	Rat C6 glioma cells [non-contact]	*Growth medium* [50U mL^{-1} penicillin, 50 µg mL^{-1} streptomycin, 3µg mL^{-1} heparin, 3ng mL^{-1} hFGF in high-glucose DMEM with or without 10% FCS]	NR	$1.0x10^4$ $1.0x10^4$ [0.4µm]	Without / with serum: ≈ 45 / 60 (day 5-7)	Sucrose: NR	Static	[283]
Bovine aortic ECs	Rat C6 glioma cells [contact]	*Growth medium* [10% FBS, 100U mL^{-1} penicillin, 100µg mL^{-1} streptomycin, 25mM HEPES buffer, L-glutamine in DMEM]	Fibronectin (3 µg cm^{-2}), poly-D-lysine (3 µg cm^{-2})	[Static]: $1x10^5$ $1.5x10^5$ [0.4µm]	[Static]: 57.2 [Dynamic]: 650.7 (day 21)	Sucrose [Static]: 8.08 [Dynamic]: 5.34	Static Dynamic	[293]
Bovine CECs	Rat glial cells [non-contact]	*Growth medium* [10% heat-inactivated calf serum, 10% heat-inactivated HS, 50mg mL^{-1} gentamicin, 1ng mL^{-1} bFGF, 2mM L-glutamine in DMEM]	Rat tail collagen solution (NR) [668]	$4x10^5$ $2.5x10^4$ [0.4µm]	358 (day 12)	Sucrose: 5 FITC-inulin: 1.83	Static	[220]
	Rat C6 glioma cells [non-contact]				239 (day 12)	Sucrose: 11.5 FITC-inulin: 4.3		

Table I.7. *Continued*

Endothelial cells	Co-cultured cells	Culture medium	Filter coating solution	Cell density (cell cm^{-2}) [filter pore size]	Maximum TEER ($\Omega.cm^2$) day*	Permeability tracers P_e ($x10^{-6}$ cm s^{-1})	Static / dynamic	Ref.
Bovine CECs	Rat astrocytes [non-contact]	*Growth medium* [10% FCS, 10% HS, 50µg mL^{-1} gentamicin, 1ng mL^{-1} BFGF, 2mM L-glutamine in DMEM]	Rat tail collagen type I (NR)	$4.0x10^5$ $1.25x10^5$ [3.0µm]	500-800 (day 5)	Inulin: 0.7 Sucrose: 4.0	Static	[250]
Bovine CECs	Rat astrocytes [non-contact]	*Growth medium* [10% heat-inactivated NBCS, 10% heat-inactivated HS, 50µg mL^{-1} gentamicin, 1ng mL^{-1} BFGF, 2mM L-glutamine in DMEM]	Rat tail collagen type I (NR)	$4.0x10^5$ $1.2x10^5$ [0.4µm]	NR	Inulin: 4.0 Sucrose: 17.5	Static	[669]
Bovine aortic ECs	Rat C6 glioma cells [contact]	*Growth medium* [10% FBS, 1% pentomycin-streptomicin-fungizone in DMEM]	Fibronectin (30 µg mL^{-1})	$1.5x10^6$-$2.0x10^6$ [0.64µm]	500 (day 20)	NR	Dynamic	[290]
Bovine CECs	Rat astrocytes [contact]	*Growth medium* [125µg mL^{-1} heparin in DMEM+S:ACM (50:50)] *Differentiation medium* [5µg mL^{-1} apo-transferrin, 8µg mL^{-1} putrescine, 2.5ng mL^{-1} sodium selenite, 312.5µM CPT-cAMP, 17.5µM RO-20-1724, 1µM *trans*-retinoic acid in DMEM+S]	Collagen type IV (NR)	$3.0x10^4$ $4.5x10^4$ [0.4µm]	857 (day 9-10)	Na-F: 6.0 FITC-dextran: 1.5	Static	[214]
Bovine CECs	Rat astrocytes [contact]	*Complete medium* [10% heat-inactivated FCS, 3.7g L^{-1} $NaHCO_3$, 25mM HEPES, 4.5g L^{-1} glucose, 100U mL^{-1} penicillin, 100mg L^{-1} streptomycin, non-essential aminoacids, 2mM L-glutamine in DMEM] *Growth medium* [125µg mL^{-1} heparin in complete medium:ACM (50:50)]	Collagen type IV (NR)	$1.35x10^5$ $1x10^5$ [0.4µm]	293 (day 9)	NR	Static	[670]
Bovine CECs	Rat astrocytes [non-contact]	*Growth medium* [15% calf serum, 1ng mL^{-1} BFGF, 50µg mL^{-1} gentamicin, 2mM L-glutamine in DMEM]	Matrigel / human fibronectin / mouse laminin / commercial or prepared rat tail collagen I solution (NR)	$4x10^5$ $2.5x10^5$ [0.4µm]	661 (day 7)	Inulin: 12.5 Sucrose: 6.17	Static	[668, 671, 672]

Table I.7. *Continued*

Endothelial cells	Co-cultured cells	Culture medium	Filter coating solution	Cell density (cell cm^{-2}) [filter pore size]	Maximum TEER ($\Omega.cm^2$) day*	Permeability tracers P_e ($x10^{-6}$ cm s^{-1})	Static / dynamic	Ref.
Bovine aortic ECs	Rat astrocytes [contact]	*Growth medium* [10% FBS, 1.8g L^{-1} glucose, 10mM HEPES, MEM essential vitamine mixture, 100mM non-essential aminoacids, 1mM Na pyruvate, 100U mL^{-1} penicillin, 100µg mL^{-1} streptomycin, 0.25µg mL^{-1} fungizone, 2mM glutamine in DMEM]	Pronectin-F (NR)	$10x10^6$-$20x10^6$ [0.5µm]	736 (3-4 weeks)	Sucrose: 5	Dynamic	[288]
Rat CECs	Rat astrocytes [contact] and neurons [non-contact]	*Growth medium* [20% FBS, 100U mL^{-1} penicillin, 100mg mL^{-1} streptomycin, 0.6mg mL^{-1} glutamine in DMEM / Ham's F12]	Gelatine (30mg mL^{-1}), poly-D-lysine (10mg mL^{-1})	$1.0x10^5$ $1.5x10^5$ $0.5x10^5$ [NR]	365 (day 11)	HRP: NR Na-F: NR	Static	[673]
Rat CECs	Rat astrocytes [non-contact]	*Growth and differentiation medium* [20% bovine PDS, 80µg mL^{-1} heparin, 100U mL^{-1} penicillin, 100µg mL^{-1} streptomycin, 5µg mL^{-1} vitamin C, 5ng mL^{-1} selenium, 5µg mL^{-1} insulin, 5µg mL^{-1} transferrin, 325µg mL^{-1} glutathione, 1ng mL^{-1} bFGF, 500ng mL^{-1} hydrocortisone, 2mM glutamine in DMEM]	Rat tail collagen solution (0.33 mg mL^{-1}) [240], fibronectin (0.05 mg mL^{-1})	NR [0.4µm]	600 (day 5-7)	NR	Static	[674]
Rat CECs	Rat astrocytes [contact]	*Endothelial medium* [10% FBS, 5ng mL^{-1} VEGF, 2ng mL^{-1} bFGF, penicillin / streptomycin in DMEM] *Astrocyte medium* [20% FBS, penicillin / streptomycin in DMEM]	NR	$2.5x10^5$ $2.0x10^5$ NR	283.78 (day 24)	Na-F: 10.36 Albumin: 6	Static	[675]
Rat CECs	Rat neuronal parenchyma [non-contact]	*Growth medium* [10% FBS, 10ng mL^{-1} bFGF, 10mM glucose, 100U mL^{-1} penicillin, 100µg mL^{-1} streptomycin, 2mM L-glutamine in DMEM]	Rat tail collagen solution (NR) [222]	$5.0x10^5$ $1.0x10^6$ [0.4µm]	289.71 (day 7)	Na-F: NR FITC-BSA: NR	Static	[172]
Rat CECs	Rat astrocytes [non-contact]	*Endothelial medium* [20% HS, 50µg mL^{-1} gentamicin, 1ng mL^{-1} bFGF, 2mM L-glutamine in DMEM] *Astrocyte medium* [20% FCS, 52.4mM $NaHCO_3$, 250U mL^{-1} penicillin, 0.5% streptomycin, 7.5mM glucose, 2x aminoacids, 4x vitamins, 2mM L-glutamine in MEM]	Collagen type IV (0.33 mg mL^{-1}), bovine fibronectin (20 µg mL^{-1})	NR [0.4µm]	NR	NR	Static	[676, 677]

Table I.7. *Continued*

Endothelial cells	Co-cultured cells	Culture medium	Filter coating solution	Cell density (cell cm^{-2}) [filter pore size]	Maximum TEER ($\Omega.cm^2$) day*	Permeability tracers P_e ($x10^{-6}$ cm s^{-1})	Static / dynamic	Ref.
Rat CECs	Rat astrocytes [contact / non-contact] Rat pericytes [contact / non-contact] Rat astrocytes [contact] and pericytes [non-contact] Rat astrocytes [non-contact] and pericytes [contact]	*Supplemented endothelial medium* [10% PDS, 1.5ng mL^{-1} bFGF, 100µg mL^{-1} heparin, 5µg mL^{-1} insulin, 5µg mL^{-1} transferrin, 5ng mL^{-1} sodium selenite, 50µg mL^{-1} gentamicin, 500nM hydrocortisone in DMEM / Ham's F12]	Collagen (NR)	$1.5x10^5$ $1.5x10^4$ $1.5x10^4$ NR	Rat astrocytes [non-contact] and pericytes [contact]: 354 (day 4)	Na-F Rat astrocytes [non-contact] and pericytes [contact]: 3.9	Static	[123]
Rat CECs	Rat astrocytes [non-contact]	*Assay medium* [1.4µM hydrocortisone, 250µmol L^{-1} CPT-cAMP, 17µmol L^{-1} RO-20-1724 in EBM-2]	Collagen type IV (0.1 mg mL^{-1}), bovine fibronectin (0.05 mg mL^{-1})	$5.0x10^4$ $8.0x10^4$ [0.4µm]	270 (day 6)	Sucrose: 1.43	Static	[207]
Rat CECs	Rat astrocytes [non-contact]	*Growth medium* [5% FBS in EBM-2 MV]	Collagen type IV (NR)	$1.0x10^5$ $5.0x10^4$ [3.0µm]	220-300 (day 13)	Inulin: 1.28 Sucrose: 1.72	Static	[398]
Rat CECs	Rat astrocytes [non-contact]	*Growth medium* [20% bovine PDS, 100U mL^{-1} penicillin, 10µg mL^{-1} streptomycin, 1ng mL^{-1} bFGF, 250µmol L^{-1} CPT-cAMP, 17.5µmol L^{-1} RO-20-1724, 500ng mL^{-1} hydrocortisone in EBM]	Collagen type IV (12 µg cm^{-2}), bovine fibronectin (6 µg cm^{-2})	$5.0x10^4$ $8.0x10^4$ NR	508 (day 6)	Na-F: 0.75	Static	[215]
Rat CECs	Rat astrocytes [contact]	*Growth medium* [20% FBS in DMEM]	NR	$1.6x10^5$ $1.2x10^6$ [1.0µm]	313 (day 10-12)	Sucrose: 16	Static	[399]
SV40 rat CECs	SV40 rat astrocytes [non-contact]	*Endothelial medium* [10% FBS, 0.25% peptone, 0.9% glucose, BME aminoacids, BME vitamins, antibiotic / antimycotic in M199 medium] *Astrocyte medium* [10% FBS, high glucose, antibiotic / antimycotic in DMEM]	Rat tail collagen type I (60 µg mL^{-1})	$8.0x10^4$ NR [1.0µm]	50-70 (day 6-7)	Inulin: 5.3 Sucrose: 8.6	Static	[250]

Table I.7. *Continued*

Endothelial cells	Co-cultured cells	Culture medium	Filter coating solution	Cell density (cell cm^{-2}) [filter pore size]	Maximum TEER ($\Omega.cm^2$) day*	Permeability tracers P_e ($x10^{-6}$ cm s^{-1})	Static / dynamic	Ref.
RBE4.B cells	Rat astrocytes [contact] and neurons [non-contact]	*RBE4.B / Astrocyte medium* [10% heat-inactivated FCS in DMEM:Ham's F12 (2:1)] *Neuron medium* [serum-free Maat medium]	Collagen type IV (3.5 µg mL^{-1}), fibronectin (2.5 µg mL^{-1})	NR [0.4µm]	NR	Sucrose: NR	Static	[678]
Rat CECs	Rat astrocytes [contact]	*Growth medium* [200ml L^{-1} PDS, 100U mL^{-1} penicillin, 100µg mL^{-1} streptomycin in DMEM / Ham's F12]	Rat tail collagen type I, matrigel solution (NR)	NR [1.0µm]	438 (day 15-18)	NR	Static	[271]
RBE4.B cells	Rat neurons [non-contact]	*RBE4.B medium* [10% heat-inactivated FCS, 300µg mL^{-1} geneticin, 1ng mL^{-1} bFGF, 2mM L-glutamine in DMEM:Ham's F12 (2:1)] *Neuron medium* [serum-free Maat medium]	Collagen type IV (5 µg cm^{-2})	NR [0.4µm]	NR	NR	Static	[133]
Mice CECs	Mice astrocytes [contact / non-contact]	*Growth medium* [20% bovine PDS, 4µg mL^{-1} puromycin, 1ng mL^{-1} hFGF, 1µg mL^{-1} heparin, 100U mL^{-1} penicillin, 100µg mL^{-1}streptomycin, 0.25µg mL^{-1} amphotericin, 2mM L-glutamine in DMEM] *Supplemented medium* [5µg mL^{-1} insulin, 5µg mL^{-1} transferrin, 5ng mL^{-1} sodium selenite, 100U mL^{-1} penicillin, 100µg mL^{-1} streptomycin, 0.25µg mL^{-1}amphotericin, 1µM retinoic acid, 312.4µM cAMP, 17.5µM phosphodiesterase inhibitor, 550nM hydrocortisone, 2mM L-glutamine in DMEM / Ham's F12]	Collagen type IV (40%), human fibronectin (10%)	$4x10^5$ $4x10^5$ [0.4 / 1.0 / 3.0 / 8.0µm]	[non-contact / 0.4µm]: 212 (day 5)	Na-F [non-contact / 0.4µm]: 3.39	Static	[272]
Mice CECs	Mice astrocytes [contact]	*Growth medium* [20% FBS, 100mg mL^{-1} heparin, 5ng mL^{-1} FGF, 100U mL^{-1} penicillin, 100U mL^{-1} streptomycin in astrocyte specific medium]	NR	$3.0x10^5$ $2.0x10^5$ NR	NR	NR	Static	[679]
b.End3 cells	Rat glial cells [contact]	*Growth medium* [20% FBS, 1% penicillin / streptomycin / fungizone in DMEM]	Collagen (NR)	$1.5x10^6$ $1.5x10^4$ [0.4µm]	315 (day 7)	Na-F: 3	Static	[383]

Table I.7. *Continued*

Endothelial cells	Co-cultured cells	Culture medium	Filter coating solution	Cell density (cell cm^{-2}) [filter pore size]	Maximum TEER ($\Omega.cm^2$) day*	Permeability tracers P_e ($x10^{-6}$ cm s^{-1})	Static / dynamic	Ref.
Mice CECS	Mice astrocytes [non-contact]	*Growth medium* [20% bovine PDS, 4µg mL^{-1} puromycin, 1ng mL^{-1} hFGF, 1µg mL^{-1} heparin, 100U mL^{-1} penicillin, 100µg mL^{-1}streptomycin, 0.25µg mL^{-1} amphotericin, 2mM L-glutamine in DMEM] *Supplemented medium* [5µg mL^{-1} insulin, 5µg mL^{-1} transferrin, 5ng mL^{-1} sodium selenite, 100U mL^{-1} penicillin, 100µg mL^{-1} streptomycin, 0.25µg mL^{-1}amphotericin, 1µM retinoic acid, 312.4µM cAMP, 17.5µM phosphodiesterase inhibitor, 550nM hydrocortisone, 2mM L-glutamine in DMEM / Ham's F12]	Collagen type IV (40%), human fibronectin (10%)	$4x10^5$ $4x10^4$ [0.4µm]	195 (day 5)	Na-F: 1.25	Static	[216]
Mice CECs	Rat astrocytes [contact / non-contact]	*Endothelial medium* [5µg mL^{-1} insulin, 5µg mL^{-1} transferrin, 5ng mL^{-1} sodium selenite, 100U mL^{-1} penicillin, 100µg mL^{-1} streptomycin, 0.25µg mL^{-1}amphotericin, 1µM retinoic acid, 312.4µM cAMP, 17.5µM phosphodiesterase inhibitor, 550nM hydrocortisone, 2mM L-glutamine in DMEM / Ham's F12]	Collagen type IV, human fibronectin (NR)	$3.0x10^5$ $8.0x10^4$ [0.4µm]	190 (day 6)	Na-F [non-contact]: 3.5	Static	[236]
Mice CECs	Rat astrocytes [contact]	*Growth medium* [10% FBS, 1% penicillin-streptomycin in DMEM]	Collagen type I and III (NR)	$1.0x10^4$ $5.0x10^3$ [0.4µm]	350 (day 7)	Calcein: 1.33	Static	[241]
b.End3 cells	Rat astrocytes [non-contact]	*b.End3 medium* [10% FBS, 1% penicillin-streptomycin, 3mM L-glutamine in DMEM] *Astrocyte medium* [10% FBS, 1% penicillin-streptomycin in DMEM]	Matrigel (476 µg mL^{-1}), collagen type I and collagen type IV mixture (0.5 mg mL^{-1}, 40:60 v/v)	$6.6x10^4$ $2.75x10^4$ [0.4µm]	30.3 (day 3-4)	TAMRA: 5.9 Dextran 10k: 0.78 Dextran 70k: 0.16	Static	[252]
b.End3 cells	Rat C6 glioma cells [non-contact]	*b.End3 medium* [10% FBS, 100U mL^{-1} penicillin, 100µg mL^{-1} streptomycin, 1% non-essential aminoacids, 5µM 2-mercaptoethanol, 1mM sodium pyruvate, 250µM CPT-cAMP, 20µM RO-20-1724, 2mM L-glutamine in DMEM] *C6 medium* [10% heat-inactivated FBS, 100U mL^{-1} penicillin, 100µg mL^{-1} streptomycin in M199]	Rat tail collagen type I (5 µg cm^{-2})	$0.5x10^4$ $1.0x10^5$ [0.4µm]	130 (day 6)	Sucrose: 16.4-19.4	Static	[254]
hCMEC/D3 cells	Human astrocytes [non-contact]	*Growth medium* [5% FBS, 5µg mL^{-1} ascorbic acid, 1% lipid concentrate, 10mM HEPES, 1% penicillin-steptomycin in EBM-2]	Cultrex® rat collagen I (NR)	$1x10^5$ $1x10^5$ [3.0µm]	140 (day 8)	NR	Static	[174]

Table I.7. *Continued*

Endothelial cells	Co-cultured cells	Culture medium	Filter coating solution	Cell density (cell cm^{-2}) [filter pore size]	Maximum TEER ($\Omega.cm^2$) day*	Permeability tracers P_e ($x10^{-6}$ cm s^{-1})	Static / dynamic	Ref.
Human CECs	Human astrocytes [non-contact]	*Growth medium* [20% heat-inactivated FCS, 5mg mL^{-1} peptone, 25% glucose, 1% vitamins, 1% aminoacids, 1% antibiotic / antimycotic, 2mM L-glutamine in DMEM]	NR	$2x10^4$ $2x10^4$ [2.0µm]	130 (day 7)	NR	Static	[680]
Human CECs	Human astrocytes [contact]	*Endothelial medium* [5% FBS, 1% ECGS, 1% penicillin / streptomycin in endothelial cell medium] *Astrocyte medium* [2% FBS, 1% AGS, 1% penicillin / streptomycin in astrocyte medium]	NR	$4x10^5$ $4x10^5$ [1.0µm]	230 (day 14)	PI: 4	Static	[346]
hCMEC/D3 cells	Human astrocytes [contact] Human pericytes [contact] Human astrocytes [contact] and pericytes Human astrocytes and pericytes[contact]	*Endothelial medium* [2% human serum in EBM-2] *Astrocyte medium* [10% human serum in DMEM] *Pericyte medium* [2% human serum, 1% penicillin/ streptomycin, PGS]	Fibronectin (4 µg cm^{-2})	$2x10^5$ $5x10^3$ [8.0µm]	60 46 44 42 (day 10)	NR	Static	[681]
Human CECs	Human astrocytes [contact]	*Endothelial medium* [10% FBS, 15mg 100mL^{-1} ECGS, 100U mL^{-1} penicillin, 100µg mL^{-1} streptomycin, 800 U mL^{-1} heparin in 1.5g 100 mL^{-1} MCDB 105] *Astrocyte medium* [5% FBS, 100U mL^{-1} penicillin, 100µg mL^{-1} streptomycin, 2mM glutamine in DMEM / Ham's F12]	Fibronectin (3 µg cm^{-2}), poly-D-lysine (3 µg cm^{-2})	$4x10^6$ $6x10^6$ [0.5µm]	1100 (day 15)	Sucrose: 0.39	Dynamic	[682]
Human CECs	Human fetal astrocytes [non-contact]	*Endothelial medium* [10% heat-inactivated FBS, 10% Nu serum, 100U mL^{-1} penicillin, 100µg mL^{-1} streptomycin in M199] *Astrocyte medium* [10% FBS, 2mM L-glutamine, 100U mL^{-1} penicillin, 100µg mL^{-1} streptomycin in MEM]	[Static]: pronectin-F (10µg mL^{-1}) [Dynamic]: collagen (NR)	[Static]: 2x10 2x10 [0.5µm]	[Static]: 500 (day 5)	PI: NR Dextran: NR	Static Dynamic	[280]

Human CECs	Human astrocytes [non-contact]	*Endothelial medium* [5% FBS, 0.1% gentamicin, 0.1% hEGF, 0.04% hydrocortisone, 4% hFGF, 0.1% VEGF, 0.1% hRIGF, 0.1% ascorbic acid, 0.1% amphotericin-B in EBM-2] *Astrocyte medium* [5% FBS, 50mg mL^{-1} gentamicin, 10µg mL^{-1} hEGF, 10mg mL^{-1} insulin, 25µg mL^{-1} progesterone, 50mg mL^{-1} transferrin, 50µg mL^{-1} amphotericin-B in astrocyte growth medium]	Collagen (NR)	NR [0.4µm]	NR	Inulin: 12 Sucrose: 22	Static	[250]
Human CECs	Human astrocytes [contact]	*Endothelial medium* [5% FBS, 0.1% hEGF, 4% hFGF with heparin, 1% VEGF, 0.1% hRIGF, 0.1% ascorbic acid, 0.1% gentamicin, 0.1% amphotericin-B, 0.04% hydrocortisone in EBM-2] *Astrocyte medium* [5% FBS, 10µg mL^{-1} hEGF, 10mg mL^{-1} insulin, 25µg mL^{-1} progesterone, 50mg mL^{-1} transferrin, 50mg mL^{-1} gentamicin, 50µg mL^{-1} amphotericin-B in astrocyte growth medium]	Collagen (NR)	$5x10^4$ $5x10^4$ [0.4µm]	260 (day 15)	Sucrose: 16.7	Static	[683]

* Day on which TEER is maximum; ACM, astrocyte conditioned medium; AGS, astrocyte growth supplement; AP, alkaline phosphatase; bFGF, basic fibroblast growth factor; BFGF, bovine fibroblast growth factor; BMDR, brain multidrug resistance protein; BME, basal medium Eagle; CAA, cationic aminoacid transporter; CECs, cerebral endothelial cells; CPT-cAMP, 8-(4-chlorophenylthio)-3',5'-cyclic adenosine monophosphate; DMEM, Dulbecco's modified Eagle's medium; EAAT, excitatory aminoacid transporter; EBM, endothelial basal medium; ECs, endothelial cells; ECGS, endothelial cell growth supplement; FBS, fetal bovine serum; FCS, fetal calf serum; FITC-BSA, fluorescein isothiocyanate labelled bovine serum albumin; GFAP, glial fibrillary acidic protein; GLUT, glucose transporter; γ-GTP, γ-glutamyl transpeptidase; hEGF, human recombinant epidermal growth factor; HEPES, 4-(2-hydroxyethyl) -1-piperazineethanesulfonic acid; hFGF, human fibroblast growth factor; hRIGF, human recombinant insulin-like growth factor; HS, horse serum; ICAM, intercellular adhesion molecule; IMDM, Iscove's modified Dulbecco's medium; JAM, junctional adhesion molecule; LDL, low density lipoprotein; MAO, monoamine oxidase; MAP, microtubule associated protein; MCT, monocarboxylic acid transporter; MEM, Eagle's minimum essential medium; MMP, matrix metalloproteinases; MRP, multidrug resistance associated protein; NAA, neutral aminoacid transporter; Na-F, sodium fluorescein; NBCS, new-born calf serum; NBS, new-born bovine serum; NR, not reported; NT, nucleoside transporter; OAT, organic anion transporter; OATP, organic anion-transporting polypeptide; OCT, organic cation transporter; PDS, plasma-derived serum; P-gp, P-glycoprotein; PGS, pericyte growth supplement; PI, propidium iodine; α-SMA, α-smooth muscle actin; TAMRA, tetramethyl-6-carboxyrhodamine; TES, N-[Tris(hydroxymethyl)-methyl]-2-aminoethanesulfonic acid; TGF-β, transforming growth factor-beta; VCAM, vascular cell adhesion molecule; VEGF, vascular endothelial growth factor; ZO, zonula-occludens.

Appendix B

Figure B.1. Typical high performance liquid chromatography-diode array (HPLC-DAD) chromatograms of reference compounds (carbamazepine, propranolol, trazodone, atenolol, cimetidine, quinidine, sulfasalazine) used in bidirectional transport assays. Blank chromatograms are represented by the transport buffer Hank's balanced salt solution (HBSS) with 10mM HEPES pH 7.4 and compound chromatograms correspond to the third calibration standard of the respective analytical calibration range. Chromatographic conditions are described in Table III.3.

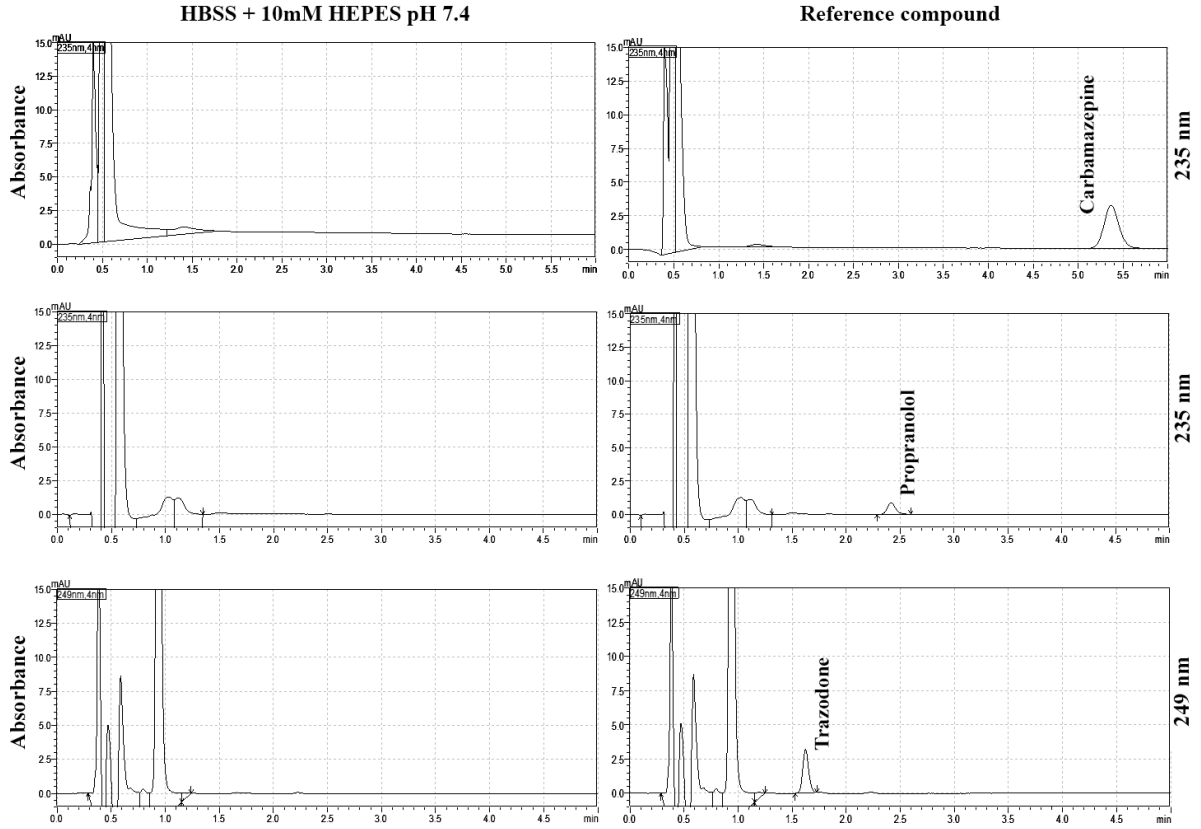

Figure B.1. *Continued*

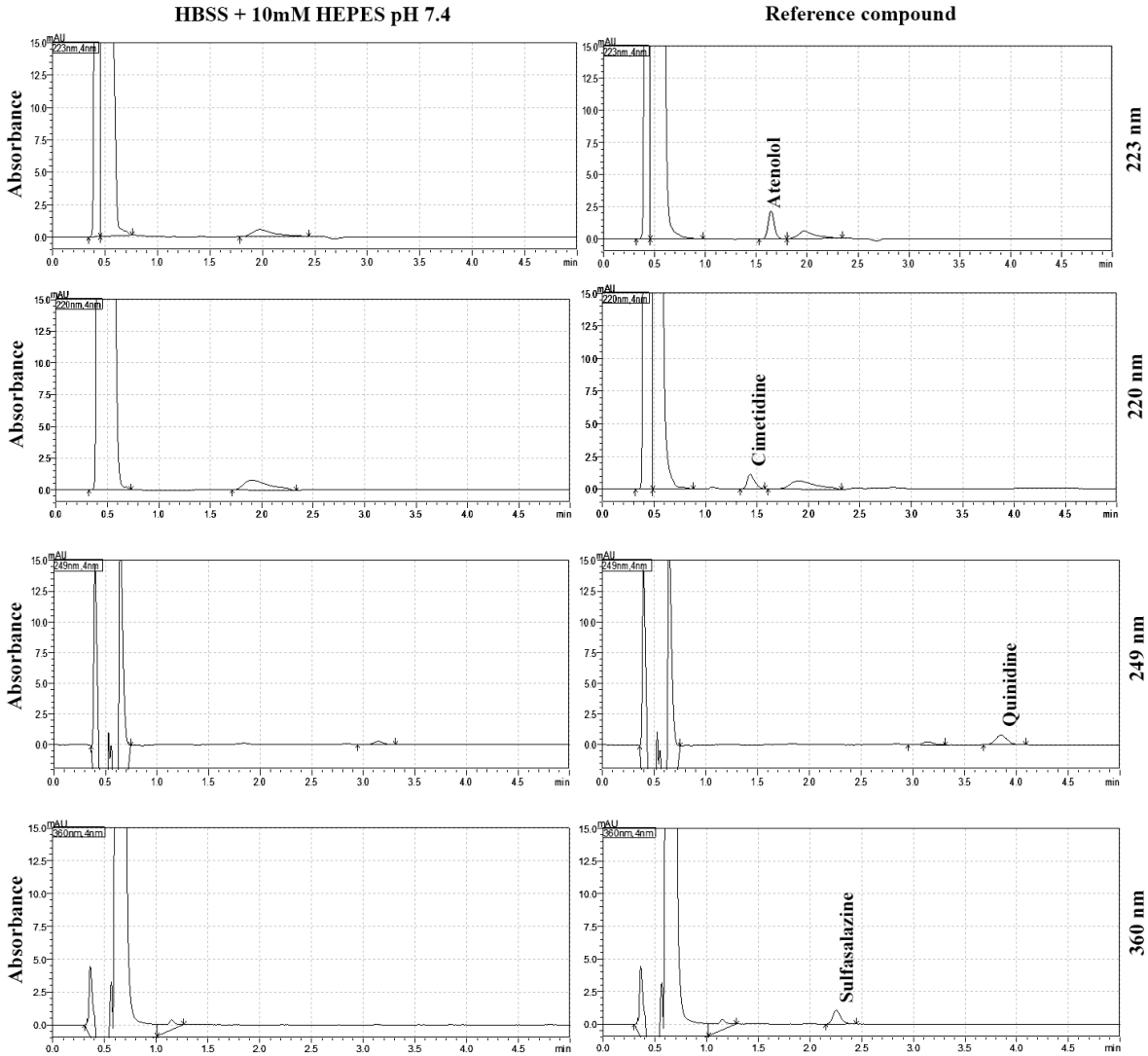

Figure B.2. Typical high performance liquid chromatography-diode array (HPLC-DAD) chromatograms of test compounds (BIA 9-1059, BIA 9-1079, entacapone, nebicapone, opicapone, tolcapone; etamicastat, nepicastat, zamicastat) tested in bidirectional transport assays. Blank chromatograms (A,B,C,D) are represented by the transport buffer Hank's balanced salt solution (HBSS) with 10mM HEPES pH 7.4 and compound chromatograms correspond to the third calibration standard of the respective analytical calibration range. Chromatographic conditions are described in Table III.3.

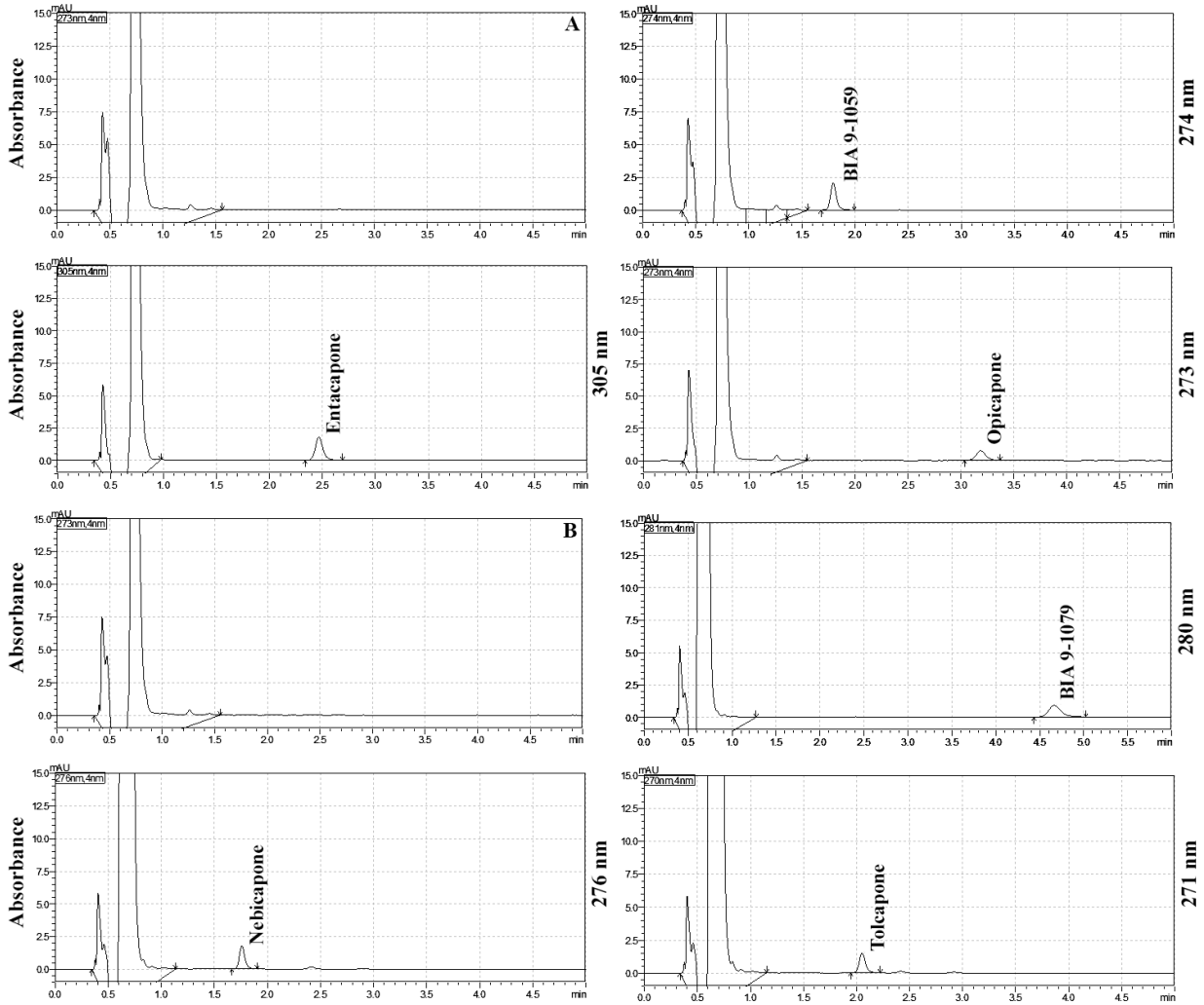

Figure B.2. *Continued*

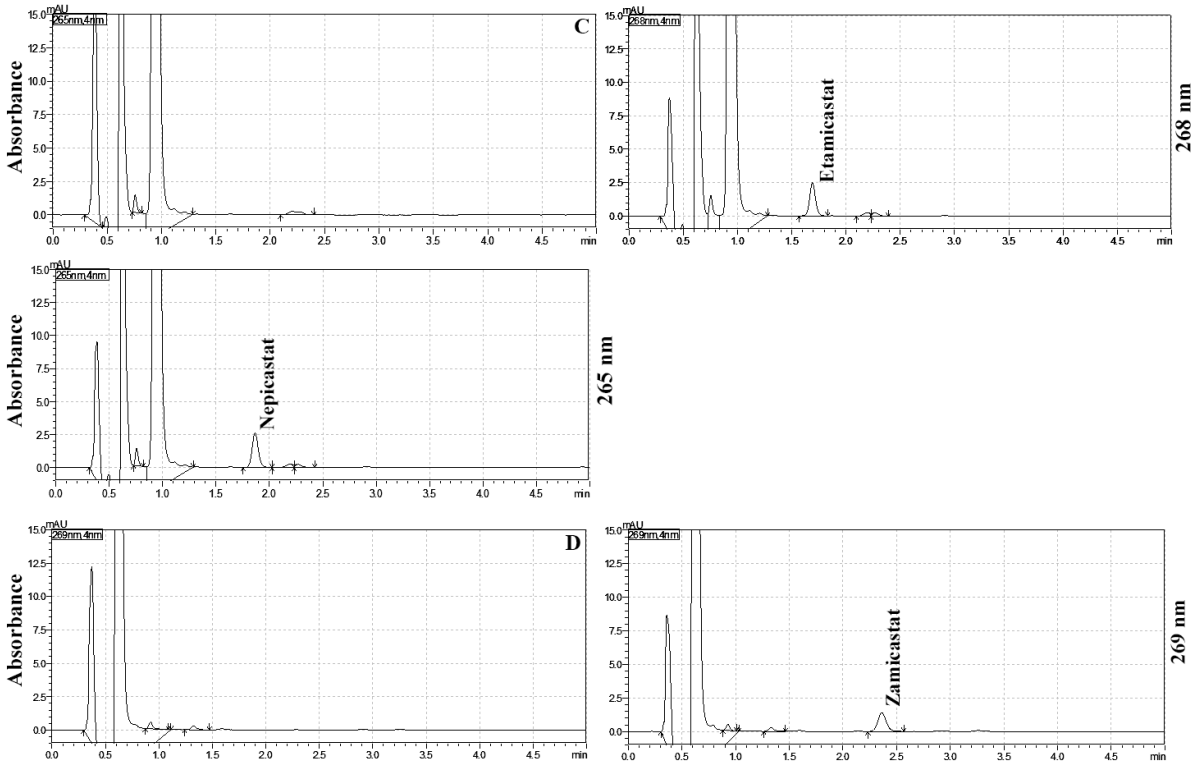

Appendix C

Table C.1. Main criteria necessary for the full validation of bioanalytical methods according to the Food and Drug Administration and European Medicines Agency guidelines [684,685].

Validation parameter	Regulatory requirements
Selectivity	- Proved using at least 6 individual sources of black matrix, which are then individually analysed and evaluated for interferences; - Interferences must be less than 20% of the analyte LLOQ and 5% of the internal standard.
Calibration curve	- Calibration standards should be prepared in the same biological matrix as the matrix of the intended study; - Minimum of three calibration curves during validation; - Minimum of six calibration concentration levels; - Concentrations of calibration standards should be within ± 15% of the nominal value, except for the LLOQ (± 20%).
Accuracy	- Represented by % of Bias; - Assessed on a minimum of three QC samples spiked independently from calibration standards. Concentrations are compared with nominal value and reported as % of nominal value; - Should be determined intra- and inter-daily with at least five determinations per concentration; - Mean value should be within 15% of nominal value except for the LLOQ (< 20%).
Precision	- Represented by coefficient of variation; - Demonstrated for LLOQ, low, medium and high QC samples with at least five replicates per concentration; - Should be determined intra- and inter-daily; - Should not exceed 15% of the CV except for the LLOQ, (< 20%).
Recovery	- Executed by comparing analytical results from low, medium and high extracted samples with unextracted samples that represent 100% recovery; - Does not need to be 100% but should be consistent, precise and reproducible.
Dilution integrity	- Demonstrated by spiking the matrix with an analyte concentration above the ULOQ and diluting with blank matrix; - At least five determinations per dilution factor; - Accuracy and precision should be within ± 15%
Stability	- Evaluated using low and high QC samples analysed after preparation and after storage conditions; - The obtained concentrations are compared to the nominal concentrations; - Mean should be within ± 15% of the nominal concentration.

Bias, deviation from nominal value; CV, coefficient of variation; LLOQ, lower limit of quantification; QC, quality control; ULOQ, upper limit of quantification.

Figure C.1. Typical high performance liquid chromatography-diode array (HPLC-DAD) chromatograms of extracted rat samples at 271 nm (A,C,E,G) and 280 nm (B,D,F,H): blank plasma (A,B); plasma spiked with tamoxifen as internal standard (IS) and analytes BIA 9-1079 and tolcapone (0.3 μg mL^{-1}) (C,D); blank brain homogenate supernatant (E,F); brain homogenate supernatant spiked with nebicapone as IS and analytes (0.2 μg mL^{-1}) (G,H).

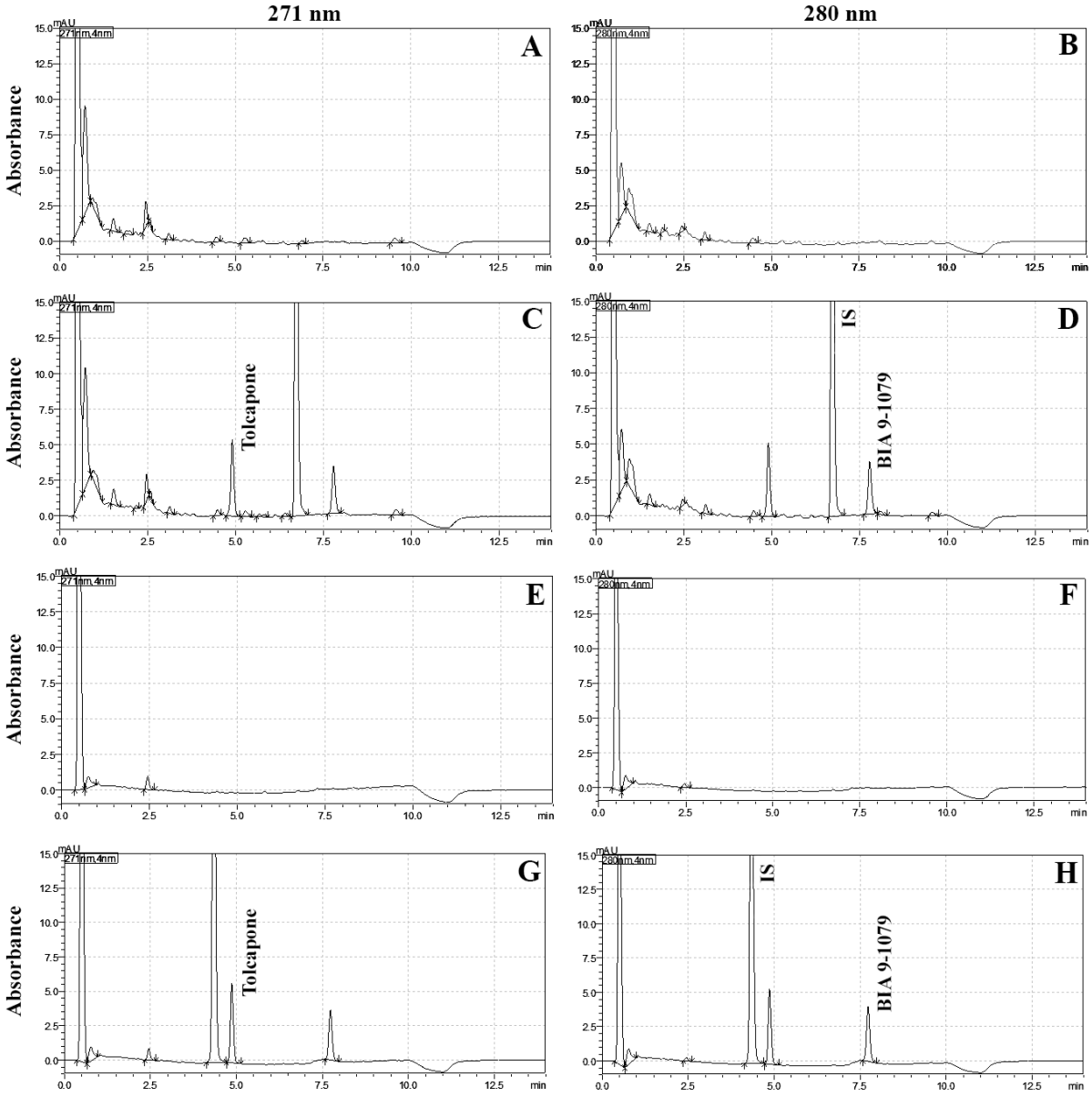

Table C.2. Intra- and inter-day precision (CV) and accuracy (bias) achieved during the determination of BIA 9-1079 and tolcapone in rat plasma and brain at the concentration of the lower limit of quantification (LLOQ), at low, middle and high concentrations of the calibration range, and following a sample dilution (Dil) (*n* = 5).

	Intra-day			Inter-day		
Nominal concentration (μg mL^{-1})	**Experimental concentration (μg mL^{-1})**	**CV (%)**	**BIAS (%)**	**Experimental concentration (μg mL^{-1})**	**CV (%)**	**BIAS (%)**
Plasma						
BIA 9-1079						
0.04 (LLOQ)	0.042 ± 0.004	10.65	3.82	0.042 ± 0.004	13.28	4.61
0.12	0.115 ± 0.005	4.77	-3.87	0.121 ± 0.014	12.10	1.12
3	2.942 ± 0.069	2.36	-1.92	3.022 ± 0.235	7.82	0.73
5.4	5.304 ± 0.092	1.73	-1.78	5.365 ± 0.417	7.79	-0.64
20 (Dil)	19.485 ± 0.585	3.01	-2.58	18.607 ± 2.144	11.55	-6.97
Tolcapone						
0.04 (LLOQ)	0.039 ± 0.001	1.63	-1.39	0.043 ± 0.004	9.26	8.46
0.12	0.128 ± 0.005	3.72	6.96	0.131 ± 0.008	6.17	9.25
3	3.043 ± 0.025	0.83	1.43	2.980 ± 0.210	7.05	-0.68
5.4	5.257 ± 0.084	1.60	-2.66	5.263 ± 0.391	7.43	-2.54
20 (Dil)	19.624 ± 0.458	2.34	-1.88	18.773 ± 2.012	10.73	-6.14
Brain						
BIA 9-1079						
0.02 (LLOQ)	0.019 ± 0.001	5.40	-3.62	0.021 ± 0.001	5.08	4.19
0.06	0.056 ± 0.004	7.82	-7.45	0.059 ± 0.004	7.73	-1.14
2	1.918 ± 0.015	0.77	-4.08	2.079 ± 0.059	2.83	3.96
3.6	3.753 ± 0.072	1.92	4.25	3.800 ± 0.107	2.81	5.55
13.3 (Dil)	12.900 ± 0.282	2.19	-3.23	12.816 ± 0.433	3.38	-3.86
Tolcapone						
0.02 (LLOQ)	0.020 ± 0.001	6.43	-2.08	0.020 ± 0.002	8.63	-0.08
0.06	0.056 ± 0.001	1.52	-6.42	0.058 ± 0.003	4.35	-2.82
2	1.997 ± 0.012	0.59	-0.15	2.010 ± 0.036	1.79	0.50
3.6	3.679 ± 0.035	0.95	2.19	3.673 ± 0.063	1.71	2.03
13.3 (Dil)	12.688 ± 0.307	2.42	-4.81	12.575 ± 0.367	2.92	-5.66

Table C.3. Absolute recovery of BIA 9-1079 and tolcapone from rat plasma and brain (%) using the applied sample pre-treatment procedures. Low, medium and high quality control samples were used (*n* = 5).

Matrix / analyte	Nominal concentration (μg mL^{-1})	Recovery (%)	
		Mean ± SD	CV (%)
Plasma			
BIA 9-1079	0.12	82.76 ± 5.87	7.09
	3	80.54 ± 2.40	2.98
	5.4	79.34 ± 1.57	1.98
Tolcapone	0.12	90.27 ± 3.06	3.39
	3	85.70 ± 0.23	0.27
	5.4	81.06 ± 1.63	2.01
Brain			
BIA 9-1079	0.06	87.76 ± 7.12	8.12
	2	90.85 ± 2.02	2.22
	3.6	90.01 ± 3.08	3.42
Tolcapone	0.06	80.36 ± 2.14	2.66
	2	93.38 ± 1.34	1.43
	3.6	92.17 ± 2.61	2.83

CV, coefficient of variation; SD, standard deviation.

Table C.4. Stability (%) of BIA 9-1079 and tolcapone in rat plasma and brain (*n* = 5) under the conditions that mimic sample handling and storage.

Stability conditions	Stability / reference analyte conditions (%)			
	BIA 9-1079		Tolcapone	
	Nominal concentration (μg mL^{-1})		Nominal concentration (μg mL^{-1})	
Plasma	**0.12**	**5.4**	**0.12**	**5.4**
Room temperature (4 h)	96.61	96.76	98.74	99.67
4 °C (24 h)	88.75	91.64	89.22	96.61
-80 °C (30 days)	86.27	94.85	97.26	97.07
Brain	**0.06**	**3.6**	**0.06**	**3.6**
Room temperature (4 h)	89.52	96.76	88.40	97.09
4 °C (24 h)	92.41	95.17	85.23	95.39
-80 °C (30 days)	94.98	100.36	100.16	99.38

REFERENCES

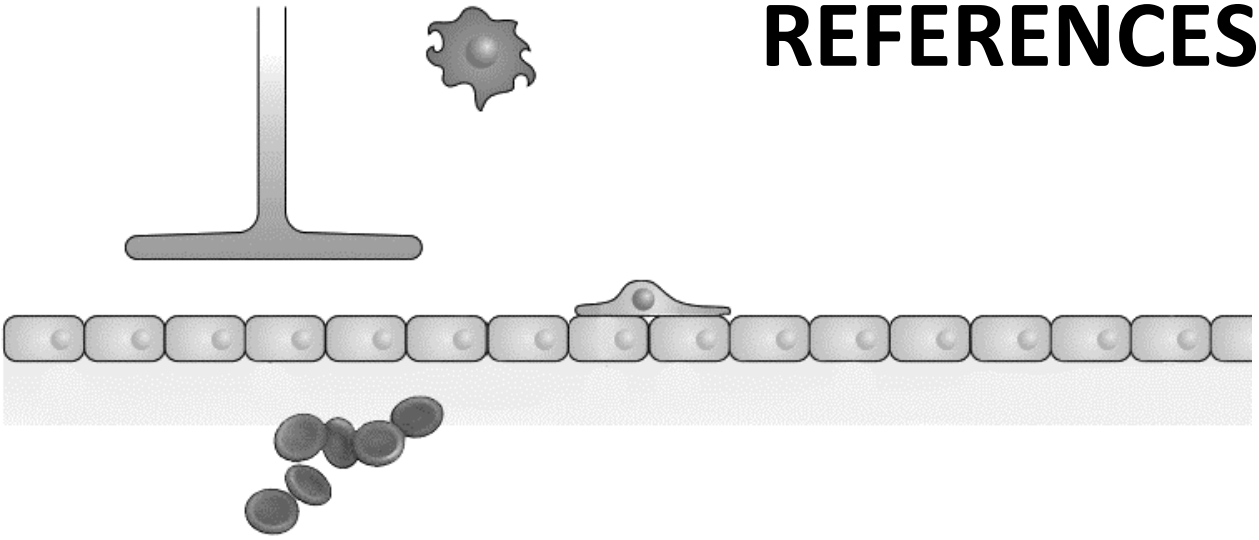

REFERENCES

[1] **HUGHES, J.P. ET AL.**, Principles of early drug discovery, Br. J. Pharmacol. 162: 6 (2011) 1239–1249.

[2] **SWINNEY, D.C.**, **ANTHONY, J.**, How were new medicines discovered?, Nat. Rev. Drug Discov. 10: 7 (2011) 507–519.

[3] **EDER, J. ET AL.**, The discovery of first-in-class drugs: origins and evolution., Nat. Rev. Drug Discov. 13: 8 (2014) 577–587.

[4] **PAUL, S.M. ET AL.**, How to improve R&D productivity: the pharmaceutical industry's grand challenge, Nat. Rev. Drug Discov. 9: 3 (2010) 203–214.

[5] **JONES, L.H.**, **BUNNAGE, M.E.**, Applications of chemogenomic library screening in drug discovery, Nat. Rev. Drug Discov. 16: 4 (2017) 285–296.

[6] **BLASS, B.E.**, Chapter 1. Drug discovery and development: an overview of modern methods and principles, in: M. Abou-Gharbia, L.H. Carnell (Eds.), Basic Princ. Drug Discov. Dev., Elsevier Inc., 2015: pp. 1–34.

[7] **WERMUTH, C.G.**, Chapter 7. Possible alternatives to high throughput screening, in: M.S. Chorghade (Ed.), Drug Discov. Dev., John Wiley & Sons, 2006: pp. 213-232.

[8] **BLEICHER, K.H. ET AL.**, Hit and lead generation: beyond high-throughput screening, Nat. Rev. Drug Discov. 2: 5 (2003) 369–378.

[9] **TERSTAPPEN, G.C. ET AL.**, Target deconvolution strategies in drug discovery, Nat Rev Drug Discov. 6: 11 (2007) 891–903.

[10] **ZHENG, W. ET AL.**, Phenotypic screens as a renewed approach for drug discovery, Drug Discov Today. 18: 21–22 (2013) 1067–1073.

[11] **KESERÜ, G.M.**, **MAKARA, G.M.**, The influence of lead discovery strategies on the properties of drug candidates, Nat. Rev. Drug Discov. 8: 3 (2009) 203–212.

[12] **MACARRON, R. ET AL.**, Impact of high-throughput screening in biomedical research, Nat. Rev. Drug Discov. 10: 3 (2011) 188–195.

[13] **PRITCHARD, J.F. ET AL.**, Making better drugs: decision gates in non-clinical drug development, Nat. Rev. Drug Discov. 2: 7 (2003) 542–553.

[14] **KHURANA, V. ET AL.**, Toward stem cell-based phenotypic screens for neurodegenerative diseases., Nat. Rev. Neurol. 11: 6 (2015) 339–350.

[**15**] **WAGNER, B.K.**, The resurgence of phenotypic screening in drug discovery and development, Expert Opin. Drug Discov. 11: 2 (2016) 121–125.

[**16**] **POWELL, D.J. ET AL.**, Chapter 1: Design and implementation of high-throughput screening assays, in: W.P. Janzen (Ed.), Mol. Biomethods Handb., Humana Press, 2016: pp. 1–32.

[**17**] **ZANELLA, F. ET AL.**, High content screening: seeing is believing, Trends Biotechnol. 28: 5 (2010) 237–245.

[**18**] **FRAIETTA, I.**, **GASPARRI, F.**, The development of high-content screening (HCS) technology and its importance to drug discovery, Expert Opin. Drug Discov. 11: 5 (2016) 501–514.

[**19**] **LEE, J.**, **BOGYO, M.**, Target deconvolution techniques in modern phenotypic profiling, Curr. Opin. Chem. Biol. 17: 1 (2013) 118–126.

[**20**] **MAHFOUZ, T.M.**, **CROSSGROVE, J.S.**, Chapter 9.1. Clinical trials and the Food and Drug Administration, in: C. Shayne (Ed.), Clin. Trials Handb., John Wiley & Sons, Inc, 2009: pp. 227–245.

[**21**] **TAN, S.-B.**, **MACHIN, D.**, Chapter 9.3. Phase II clinical trials, in: C.G. Shayne (Ed.), Clin. Trials Handb., John Wiley & Sons, Inc, 2009: pp. 255–279.

[**22**] **SHURBAJI, A. AL**, Chapter 27. Proof-of-principle/proof-of-concept trials in drug development, in: C.G. Shayne (Ed.), Clin. Trials Handb., John Wiley & Sons, Inc, 2009: pp. 1201–1218.

[**23**] **CHEN, C. ET AL.**, Chapter 5. Optimal cost-effective go no-go decisions in clinical development, in: W. He, J. Pinheiro, O.M. Kuznetsova (Eds.), Stat. Biol. Heal., Springer Science, 2014: pp. 91–115.

[**24**] **SCHMIDT, B.**, Proof of principle studies, Epilepsy Res. 68: 1 (2006) 48–52.

[**25**] **GROUP, B.D.W.**, Biomarkers and surrogate endpoints: preferred definitions and conceptual framework, Clin. Pharmacol. Ther. 69: 3 (2001) 89–95.

[**26**] **STRIMBU, K.**, **TAVEL, J. A**, What are biomarkers?, Curr Opin HIV AIDS. 5: 6 (2011) 463–466.

[**27**] **HURKO, O.**, **JONES, G.G.K.**, Valuation of biomarkers, Nat. Rev. Drug Discov. 10: 4 (2011) 253–254.

[**28**] **TOWNSEND, M.J.**, **ARRON, J.R.**, Reducing the risk of failure: biomarker-guided trial design, Nat. Rev. Drug Discov. 15: 8 (2016) 517–518.

[**29**] **SABA, N. ET AL.**, Chapter 9.4. Designing and conducting phase III studies, in: C.G. Shayne (Ed.), Clin. Trials Handb., John Wiley & Sons, Inc, 2009: pp. 279–303.

[**30**] **LOWENSTEIN, P.R.**, **CASTRO, M.G.**, Uncertainty in the translation of preclinical experiments to clinical trials. Why do most phase III clinical trials fail?, Curr. Gene Ther. 9: 5 (2009) 368–374.

[**31**] **HWANG, T.J. ET AL.**, Failure of investigational drugs in late-stage clinical development and publication of trial results, JAMA Intern. Med. 357: 21 (2016) 2109–2122.

[**32**] **HARRISON, R.K.**, Phase II and phase III failures: 2013–2015, Nat. Rev. Drug Discov. 15: 12 (2016) 817–818.

[**33**] **AVORN, J.**, **KESSELHEIM, A.S.**, The 21st Century Cures Act - will it take us back in time?, N. Engl. J. Med. 372: 26 (2015) 2473–2475.

[**34**] **MCCLELLAN, M.B.**, **SIGAL, E. V.**, The 21st Century Cures Act, N. Engl. J. Med. 373: 17 (2015) 1677–1678.

[**35**] **BAGAL, S.**, **BUNGAY, P.**, Restricting CNS penetration of drugs to minimise adverse events: role of drug transporters, Drug Discov. Today Technol. 12: (2014) 79–85.

[**36**] **DI, L.**, **KERNS, E.H.**, Chapter 1. Introduction and overview, in: L. Di, E.H. Kerns (Eds.), Blood-Brain Barrier Drug Discov., John Wiley & Sons, Inc, 2015: pp. 1–4.

[**37**] **BUNGAY, P. ET AL.**, Chapter 20. Designing peripheral drugs for minimal brain exposure, in: L. Di, E.H. Kerns (Eds.), Blood-Brain Barrier Drug Discov., John Wiley & Sons, Inc, 2015: pp. 446–462.

[**38**] **MORIMOTO, B.H. ET AL.**, Safety pharmacology in drug discovery and development, in: M.K. Pugsley, M.J. Curtis (Eds.), Handb. Exp. Pharmacol., Springer-Verlag Berlin Heidelberg, 2015: pp. 65–83.

[**39**] **CROWE, A.**, Chapter 21. Case studies of non-CNS drugs to minimize brain penetration - nonsedative antihistamines, in: L. Di, E.H. Kerns (Eds.), Blood-Brain Barrier Drug Discov., John Wiley & Sons, Inc, 2015: pp. 463–481.

[**40**] **HAMMARLUND-UDENAES, M.**, Chapter 5. Pharmacokinetic concepts in brain drug delivery, in: M. Hammarlund-Udenaes, E.C.M. de Lange, R.G. Thorne (Eds.), Drug Deliv. to Brain Physiol. Concepts, Methodol. Approaches, Springer-Verlag New York, New York, 2014: pp. 127–161.

[**41**] **DE LANGE, E.C.**, The mastermind approach to CNS drug therapy: translational prediction of human brain distribution, target site kinetics, and therapeutic effects., Fluids Barriers CNS. 10: 12 (2013) 1–16.

[**42**] **KASSEBAUM, N.J. ET AL.**, Global, regional, and national disability-adjusted life-years (DALYs) for 315 diseases and injuries and healthy life expectancy (HALE), 1990-2015: a systematic analysis for the Global Burden of Disease Study 2015, Lancet. 388: 10053 (2016) 1603–1658.

[**43**] **KAITIN, K.I.**, **DIMASI, J.A.**, Pharmaceutical innovation in the 21st century: new drug approvals in the first decade, 2000-2009., Clin. Pharmacol. Ther. 89: 2 (2011) 183–188.

[**44**] **KESSELHEIM, A.S. ET AL.**, Two decades of new drug development for central nervous system disorders, Nat. Rev. 14: 12 (2015) 1–2.

[**45**] **SCHWAB, M.E.**, **BUCHLI, A.D.**, Drug research: plug the real brain drain, Nature. 483: 7389 (2012) 267–268.

[**46**] **BUTLEN-DUCUING, F. ET AL.**, Challenges in drug development for central nervous system disorders: a European Medicines Agency perspective, Nat. Rev. Drug Discov. 15: 13 (2016) 813–814.

[**47**] **GOETGHEBEUR, P.J.**, **SWARTZ, J.E.**, True alignment of preclinical and clinical research to enhance success in CNS drug development: a review of the current evidence, J. Psychopharmacol. 30: 7 (2016) 586–594.

[**48**] **YOKLEY, B.H. ET AL.**, Role of academic drug discovery in the quest for new CNS therapeutics, ACS Chem. Neurosci. 8: 3 (2017) 429–431.

[**49**] **DE LANGE, E.C.M.**, **HAMMARLUND-UDENAES, M.**, Translational aspects of blood-brain barrier transport and central nervous system effects of drugs: from discovery to patients, Clin. Pharmacol. Ther. 97: 4 (2015) 380–394.

[**50**] **PANKEVICH, D.E. ET AL.**, Improving and accelerating drug development for nervous system disorders, Neuron. 84: 3 (2014) 546–553.

[**51**] **PALMER, A.M.**, **ALAVIJEH, M.S.**, Foundation review: translational CNS medicines research, Drug Discov. Today. 17: 19–20 (2012) 1068–1078.

[**52**] **ZHANG, M. ET AL.**, Phenotypic screens targeting neurodegenerative diseases, J. Biomol. Screen. 19: 1 (2014) 1–16.

[**53**] **HURKO, O.**, **RYAN, J.L.**, Translational research in central nervous system drug discovery, NeuroRx. 2: 4 (2005) 671–682.

[**54**] **CIPOLLA, M.J.**, The cerebral circulation, Morgan & Claypool Life Sciences, 2010.

[**55**] **ENGELHARDT, B.**, **SOROKIN, L.**, The blood-brain and the blood-cerebrospinal fluid barriers: Function and dysfunction, Semin. Immunopathol. 31: 4 (2009) 497–511.

[**56**] **STERN, L.**, **GAUTIER, R.**, Recherches sur le liquide céphalo-rachidien: les rapports entre le liquide céphalo-rachidien et la circulation sanguine, Arch. Int. Physiol. 17: 2 (1921) 138–192.

[**57**] **ABBOTT, N.J.**, Chapter 1. Anatomy and physiology of the blood–brain barriers, in: M. Hammarlund-Udenaes, E.C.M. de Lange, R.G. Thorne (Eds.), Drug Deliv. to Brain Physiol. Concepts, Methodol. Approaches, Springer-Verlag New York, 2014: pp. 3–21.

[**58**] **LIDDELOW, S.A.**, Fluids and barriers of the CNS: a historical viewpoint, Fluids Barriers CNS. 8: 2 (2011) 1–16.

[**59**] **WHISH, S. ET AL.**, The inner CSF-brain barrier: developmentally controlled access to the brain via intercellular junctions, Front. Neurosci. 9: 16 (2015) 1–15.

[**60**] **JOHANSON, C.E. ET AL.**, Chapter 4. The blood–cerebrospinal fluid Barrier: structure and functional significance, in: S. Nag (Ed.), Blood-Brain Other Neural Barriers Rev. Protoc., Humana Press, 2011: pp. 101–131.

[**61**] **ABBOTT, N.J.**, Blood-brain barrier structure and function and the challenges for CNS drug delivery, J. Inherit. Metab. Dis. 36: 3 (2013) 437–449.

[**62**] **DANDO, S.J. ET AL.**, Pathogens penetrating the central nervous system: infection pathways and the cellular and molecular mechanisms of invasion, Clin. Microbiol. Rev. 27: 4 (2014) 691–726.

[**63**] **KAUR, C. ET AL.**, The choroid plexus in healthy and diseased brain, J. Neuropathol. Exp. Neurol. 75: 3 (2016) 198–213.

[**64**] **LIN, J.H.**, CSF as a surrogate for assessing CNS exposure: an industrial perspective., Curr. Drug Metab. 9: 1 (2008) 46–59.

[**65**] **DAMKIER, H.H. ET AL.**, Cerebrospinal fluid secretion by the choroid plexus, Physiol. Rev. 93: 4 (2013) 1847–1892.

[**66**] **SPECTOR, R. ET AL.**, A balanced view of choroid plexus structure and function: focus on adult humans, Exp. Neurol. 267: (2015) 78–86.

[**67**] **ABBOTT, N.J.**, Prediction of blood-brain barrier permeation in drug discovery from in vivo, in vitro and in silico models, Drug Discov. Today Technol. 1: 4 (2004) 407–416.

[**68**] **JOHANSON, C.E. ET AL.**, Multiplicity of cerebrospinal fluid functions: new challenges in health and disease, Cerebrospinal Fluid Res. 5: 10 (2008) 1–32.

[**69**] **LUN, M.P. ET AL.**, Development and functions of the choroid plexus–cerebrospinal fluid system, Nat. Rev. Neurosci. 16: 8 (2015) 445–457.

[**70**] **DE LANGE, E.C.M.**, Chapter 14. PBPK modelling approach for prediction of human CNS drug brain distribution, in: L. Di, E.H. Kerns (Eds.), Blood-Brain Barrier Drug Discov., John Wiley & Sons, Inc, 2015: pp. 296–323.

[**71**] **KLAASSEN, C.D.**, **ALEKSUNES, L.M.**, Xenobiotic, bile acid, and cholesterol transporters: function and regulation, Pharmacol. Rev. 62: 1 (2010) 1–96.

[**72**] **STRAZIELLE, N.**, **GHERSI-EGEA, J.F.**, Efflux transporters in blood-brain interfaces of the developing brain, Front. Neurosci. 9: 21 (2015) 1–11.

[**73**] **GHERSI-EGEA, J.-F.**, **STRAZIELLE, N.**, Choroid plexus transporters for drugs and other xenobiotics., J. Drug Target. 10: 4 (2002) 353–357.

[**74**] **TACHIKAWA, M. ET AL.**, Chapter 2. Recent progress in blood–brain barrier and blood–CSF barrier transport research: pharmaceutical relevance for drug delivery to the brain, in: M. Hammarlund-Udenaes, E.C.M. de Lange, R.G. Thorne (Eds.), Drug Deliv. to Brain Physiol. Concepts, Methodol. Approaches, Springer-Verlag New York, 2014: pp. 23–62.

[**75**] **KAMAL, M.A. ET AL.**, Role and relevance of PEPT2 in drug disposition, dynamics, and toxicity, Drug Metab. Pharmacokinet. 23: 4 (2008) 236–242.

[**76**] **RAO, V. V ET AL.**, Choroid plexus epithelial expression of MDR1 P-glycoprotein and multidrug resistance-associated protein contribute to the blood-cerebrospinal-fluid drug-permeability barrier, Proc. Natl. Acad. Sci. U. S. A. 96: 7 (1999) 3900–3905.

[**77**] **GAZZIN, S. ET AL.**, Differential expression of the multidrug resistance-related proteins ABCb1 and ABCc1 between blood-brain interfaces, J. Comp. Neurol. 510: 5 (2008) 497–507.

[**78**] **KAUR, M.**, **BADHAN, R.K.S.**, Phytoestrogens modulate breast cancer resistance protein expression and function at the blood-cerebrospinal fluid barrier, J. Pharm. Pharm. Sci. 18: 2 (2015) 132–154.

[**79**] **SPECTOR, R. ET AL.**, A balanced view of the cerebrospinal fluid composition and functions: focus on adult humans, Exp. Neurol. 273: (2015) 57–68.

[**80**] **HEYWOOD, W.E. ET AL.**, Identification of novel CSF biomarkers for neurodegeneration and their validation by a high-throughput multiplexed targeted proteomic assay., Mol. Neurodegener. 10: 64 (2015) 1–16.

[**81**] **KIM, D. ET AL.**, Harnessing cerebrospinal fluid biomarkers in clinical trials for treating Alzheimer's and Parkinson's diseases: potential and challenges., J. Clin. Neurol. 12: 4 (2016) 381–392.

[**82**] **LEI, Y. ET AL.**, The brain interstitial system: anatomy, modeling, in vivo measurement, and applications, Prog. Neurobiol. (2016).

[**83**] **HAMMARLUND-UDENAES, M. ET AL.**, On the rate and extent of drug delivery to the brain, Pharm. Res. 25: 8 (2008) 1737–1750.

[**84**] **LORYAN, I. ET AL.**, Mechanistic understanding of brain drug disposition to optimize the selection of potential neurotherapeutics in drug discovery, Pharm. Res. 31: 8 (2014) 2203–2219.

[**85**] **DI, L. ET AL.**, Demystifying brain penetration in central nervous system drug discovery, J. Med. Chem. 56: 1 (2013) 2–12.

[**86**] **FRIDÉN, M. ET AL.**, Structure-brain exposure relationships in rat and human using a novel data set of unbound drug concentrations in brain interstitial and cerebrospinal fluids, J. Med. Chem. 52: 20 (2009) 6233–6243.

[**87**] **REICHEL, A.**, Chapter 2. Pharmacokinetics of CNS penetration, in: L. Di, E.H. Kerns (Eds.), Blood-Brain Barrier Drug Discov., John Wiley & Sons, Inc., 2015: pp. 7–41.

[**88**] **BALL, K. ET AL.**, Physiologically based pharmacokinetic modelling of drug penetration across the blood-brain barrier - towards a mechanistic IVIVE-based approach, AAPS J. 15: 4 (2013) 913–32.

[**89**] **DI, L. ET AL.**, Species independence in brain tissue binding using brain homogenates, Drug Metab. Dispos. 39: 7 (2011) 1270–1277.

[**90**] **LORYAN, I. ET AL.**, The brain slice method for studying drug distribution in the CNS., Fluids Barriers CNS. 10: 1 (2013) 1–9.

[**91**] **SUMMERFIELD, S.G.**, **DONG, K.C.**, In vitro, in vivo and in silico models of drug distribution into the brain, J. Pharmacokinet. Pharmacodyn. 40: 3 (2013) 301–314.

[**92**] **LORYAN, I.**, **HAMMARLUND-UDENAES, M.**, Chapter 10. Drug discovery methods for studying brain drug delivery and distribution, in: M. Hammarlund-Udenaes, E.C.M. de Lange, R.G. Thorne (Eds.), Drug Deliv. to Brain Physiol. Concepts, Methodol. Approaches, Springer-Verlag New York, 2014: pp. 127–161.

[**93**] **KALVASS, J.C.**, **MAURER, T.S.**, Influence of nonspecific brain and plasma binding on CNS exposure: implications for rational drug discovery, Biopharm. Drug Dispos. 23: 8 (2002) 327–338.

[**94**] **YAMAMOTO, Y. ET AL.**, A generic multi-compartmental CNS distribution model structure for 9 drugs allows prediction of human brain target site concentrations, Pharm. Res. 34: 2 (2017) 333–351.

[**95**] **FRIDÉN, M. ET AL.**, Measurement of unbound drug exposure in brain: modeling of pH partitioning explains diverging results between the brain slice and brain homogenate methods, Drug Metab. Dispos. 39: 3 (2011) 353–362.

[**96**] **ABBOTT, N.J. ET AL.**, Structure and function of the blood-brain barrier, Neurobiol. Dis. 37: 1 (2010) 13–25.

[**97**] **BERNACKI, J. ET AL.**, Physiology and pharmacological role of the blood-brain barrier, Pharmacol. Reports. 60: 5 (2008) 600–622.

[**98**] **HAWKINS, B.T.**, **DAVIS, T.P.**, The Blood-Brain Barrier / Neurovascular Unit in Health and Disease, Pharmacol. Rev. 57: 2 (2005) 173–185.

[**99**] **ABBOTT, N.J. ET AL.**, Astrocyte-endothelial interactions at the blood-brain barrier., Nat. Rev. Neurosci. 7: 1 (2006) 41–53.

[**100**] **PERSIDSKY, Y. ET AL.**, Blood-brain barrier: Structural components and function under physiologic and pathologic conditions, J. Neuroimmune Pharmacol. 1: 3 (2006) 223–236.

[**101**] **LECRUX, C.**, **HAMEL, E.**, The neurovascular unit in brain function and disease, Acta Physiol. 203: 1 (2011) 47–59.

[**102**] **BICKER, J. ET AL.**, Blood-brain barrier models and their relevance for a successful development of CNS drug delivery systems: a review, Eur. J. Pharm. Biopharm. 87: 3 (2014) 409–432.

[**103**] **WILHELM, I. ET AL.**, In vitro models of the blood-brain barrier, Acta Neurobiol. Exp. (Wars). 71: 1 (2011) 113–128.

[**104**] **CORREALE, J.**, **VILLA, A.**, Cellular elements of the blood-brain barrier, Neurochem. Res. 34: 12 (2009) 2067–2077.

[**105**] **WOLBURG, H. ET AL.**, Brain endothelial cells and the glio-vascular complex, Cell Tissue Res. 335: 1 (2009) 75–96.

[**106**] **RIBEIRO, M.M.B. ET AL.**, Translocating the blood-brain barrier using electrostatics, Front. Cell. Neurosci. 6: 44 (2012) 1–7.

[**107**] **PATEL, M.M. ET AL.**, Getting into the brain: approaches to enhance brain drug delivery, CNS Drugs. 23: 1 (2009) 35–58.

[**108**] **STRAZIELLE, N.**, **GHERSI-EGEA, J.F.**, Physiology of blood-brain interfaces in relation to brain disposition of small compounds and macromolecules, Mol. Pharm. 10: 5 (2013) 1473–1491.

[**109**] **DOBSON, P.D.**, **KELL, D.B.**, Carrier-mediated cellular uptake of pharmaceutical drugs: an exception or the rule?, Nat. Rev. Drug Discov. 7: 3 (2008) 205–220.

[**110**] **HERVÉ, F. ET AL.**, CNS delivery via adsorptive transcytosis., AAPS J. 10: 3 (2008) 455–472.

[**111**] **ARMULIK, A. ET AL.**, Pericytes and the blood–brain barrier: recent advances and implications for the delivery of CNS therapy, Ther. Deliv. 2: 4 (2011) 419–422.

[**112**] **DANEMAN, R.**, The blood-brain barrier in health and disease, Ann. Neurol. 72: 5 (2012) 648–672.

[**113**] **LÖSCHER, W.**, **POTSCHKA, H.**, Role of drug efflux transporters in the brain for drug disposition and treatment of brain diseases, Prog. Neurobiol. 76: 1 (2005) 22–76.

[**114**] **FORTUNA, A. ET AL.**, Evaluation of the permeability and P-glycoprotein efflux of carbamazepine and several derivatives across mouse small intestine by the Ussing chamber technique, Epilepsia. 53: 3 (2012) 529–538.

[**115**] **AGARWAL, S. ET AL.**, Breast cancer resistance protein and P-glycoprotein in brain cancer: two gatekeepers team up., Curr. Pharm. Des. 17: 26 (2011) 2793–2802.

[**116**] **UCHIDA, Y. ET AL.**, Quantitative targeted absolute proteomics of human blood-brain barrier transporters and receptors, J. Neurochem. 117: 2 (2011) 333–345.

[**117**] **SHAWAHNA, R. ET AL.**, Transcriptomic and quantitative proteomic analysis of transporters and drug metabolizing enzymes in freshly isolated human brain microvessels, Mol Pharm. 8: 4 (2011) 1332–1341.

[**118**] **NICOLAZZO, J. A ET AL.**, Methods to assess drug permeability across the blood-brain barrier., J. Pharm. Pharmacol. 58: 3 (2006) 281–293.

[**119**] **KOEHLER, R.C. ET AL.**, Astrocytes and the regulation of cerebral blood flow, Trends Neurosci. 32: 3 (2009) 160–169.

[**120**] **LIEBNER, S. ET AL.**, Current concepts of blood-brain barrier development, Int. J. Dev. Biol. 55: 4–5 (2011) 467–476.

[**121**] **SZU, J.I.**, **BINDER, D.K.**, The role of astrocytic aquaporin-4 in synaptic plasticity and learning and memory, Front. Integr. Neurosci. 10: 8 (2016) 1–16.

[**122**] **HELLSTRÖM, M. ET AL.**, Lack of pericytes leads to endothelial hyperplasia and abnormal vascular morphogenesis, J. Cell Biol. 152: 3 (2001) 543–553.

[**123**] **NAKAGAWA, S. ET AL.**, A new blood-brain barrier model using primary rat brain endothelial cells, pericytes and astrocytes, Neurochem. Int. 54: 3–4 (2009) 253–263.

[**124**] **WINKLER, E. A ET AL.**, Central nervous system pericytes in health and disease, Nat. Neurosci. 14: 11 (2011) 1398–1405.

[**125**] **GERHARDT, H.**, **BETSHOLTZ, C.**, Endothelial-pericyte interactions in angiogenesis, Cell Tissue Res. 314: 1 (2003) 15–23.

[**126**] **ARMULIK, A. ET AL.**, Pericytes regulate the blood-brain barrier., Nature. 468: 7323 (2010) 557–561.

[**127**] **BELL, R.D. ET AL.**, Pericytes control key neurovascular functions and neuronal phenotype in the adult brain and during brain aging, Neuron. 68: 3 (2010) 409–427.

[**128**] **QUAEGEBEUR, A. ET AL.**, Pericytes: blood-brain barrier safeguards against neurodegeneration?, Neuron. 68: 3 (2010) 321–323.

[**129**] **LANGE, S. ET AL.**, Brain pericyte plasticity as a potential drug target in CNS repair, Drug Discov. Today. 18: 9–10 (2013) 456–463.

[**130**] **CAI, W. ET AL.**, Pericytes in brain injury and repair after ischemic stroke, Transl. Stroke Res. 8: 2 (2017) 107–121.

[**131**] **ZENKER, D. ET AL.**, Human blood-derived macrophages enhance barrier function of cultured primary bovine and human brain capillary endothelial cells, J. Physiol. 551: Pt 3 (2003) 1023–1032.

[**132**] **DELI, M.A. ET AL.**, Permeability studies on in vitro blood-brain barrier models: Physiology, pathology, and pharmacology, Cell. Mol. Neurobiol. 25: 1 (2005) 59–127.

[**133**] **CESTELLI, A. ET AL.**, Functional feature of a novel model of blood brain barrier: Studies on permeation of test compounds, J. Control. Release. 76: 1–2 (2001) 139–147.

[**134**] **SCHIERA, G. ET AL.**, Synergistic effects of neurons and astrocytes on the differentiation of brain capillary endothelial cells in culture., J. Cell. Mol. Med. 7: 2 (2003) 165–170.

[**135**] **MCCONNELL, H.L. ET AL.**, The translational significance of the neurovascular unit, J. Biol. Chem. 292: 3 (2017) 762–770.

[**136**] **ZOBEL, K. ET AL.**, Blood-brain barrier properties in vitro depend on composition and assembly of endogenous extracellular matrices, Cell Tissue Res. 365: 2 (2016) 233–245.

[**137**] **SONG, I.**, **DITYATEV, A.**, Crosstalk between glia, extracellular matrix and neurons, Brain Res. Bull. (2017).

[**138**] **HARTMANN, C. ET AL.**, The impact of glia-derived extracellular matrices on the barrier function of cerebral endothelial cells: an in vitro study., Exp. Cell Res. 313: 7 (2007) 1318–1325.

[**139**] **BAETEN, K.M.**, **AKASSOGLOU, K.**, Extracellular matrix and matrix receptors in blood-Brain barrier formation and stroke, Dev. Neurobiol. 71: 11 (2011) 1018–1039.

[**140**] **OBERMEIER, B. ET AL.**, Development, maintenance and disruption of the blood-brain-barrier, Nat. Methods. 19: 12 (2013) 1584–1596.

[**141**] **ENGELHARDT, B.**, **LIEBNER, S.**, Novel insights into the development and maintenance of the blood-brain barrier, Cell Tissue Res. 355: 3 (2014) 687–699.

[**142**] **BLANCHETTE, M.**, **DANEMAN, R.**, Formation and maintenance of the BBB, Mech. Dev. 138: 1 (2015) 8–16.

[**143**] **DANEMAN, R. ET AL.**, Pericytes are required for blood–brain barrier integrity during embryogenesis, Nature. 468: 7323 (2010) 562–566.

[**144**] **CIPOLLA, M.J. ET AL.**, Cerebral vascular adaptation to pregnancy and its role in the neurological complications of eclampsia., J. Appl. Physiol. 110: 2 (2011) 329–339.

[**145**] **ROH, H.-T. ET AL.**, Effect of exercise intensity on neurotrophic factors and blood–brain barrier permeability induced by oxidative–nitrosative stress in male college students, Int. J. Sport Nutr. Exerc. Metab. 27:3 (2017) 239–246.

[**146**] **LEE, J.-M. ET AL.**, The ameliorative effects of exercise on cognitive impairment and white matter injury from blood-brain barrier disruption induced by chronic cerebral hypoperfusion in adolescent rats, Neurosci. Lett. 638: (2017) 83–89.

[**147**] **ERDŐ, F. ET AL.**, Age-associated physiological and pathological changes at the blood–brain barrier: a review, J. Cereb. Blood Flow Metab. 37: 1 (2017) 4–24.

[**148**] **NICOLAS, J.**, Chapter 4. Species differences and impact of disease state on BBB, in: L. Di, E.H. Kerns (Eds.), Blood–Brain Barrier Drug Discov., John Wiley & Sons, Inc., 2015: pp. 66–93.

[**149**] **COTRINA, M.L.**, **NEDERGAARD, M.**, Astrocytes in the aging brain, J. Neurosci. Res. 67: 1 (2002) 1–10.

[**150**] **DUNCOMBE, J. ET AL.**, Ageing causes prominent neurovascular dysfunction associated with loss of astrocytic contacts and gliosis, Neuropathol. Appl. Neurobiol. (2016).

[**151**] **POPESCU, B.O. ET AL.**, Blood-brain barrier alterations in ageing and dementia, J. Neurol. Sci. 283: 1–2 (2009) 99–106.

[**152**] **FARRALL, A.J.**, **WARDLAW, J.M.**, Blood-brain barrier: ageing and microvascular disease - systematic review and meta-analysis, Neurobiol. Aging. 30: 3 (2009) 337–352.

[**153**] **GORLÉ, N. ET AL.**, The effect of aging on brain barriers and the consequences for Alzheimer's disease development, Mamm. Genome. 27: 7–8 (2016) 407–420.

[**154**] **UENO, M. ET AL.**, Blood-brain barrier and blood-cerebrospinal fluid barrier in normal and pathological conditions, Brain Tumor Pathol. 33: 2 (2016) 89–96.

[**155**] **DESAI, B.S. ET AL.**, Blood-brain barrier pathology in Alzheimer's and Parkinson's disease: implications for drug therapy, Cell Transplant. 16: 32 (2007) 285–299.

[**156**] **JONKERS, N. ET AL.**, Benserazide decreases central AADC activity, extracellular dopamine levels and levodopa decarboxylation in striatum of the rat, J. Neural Transm. 108: 5 (2001) 559–570.

[**157**] **BARTELS, A.L. ET AL.**, Decreased blood-brain barrier P-glycoprotein function in the progression of Parkinson's disease, PSP and MSA, J. Neural Transm. 115: 7 (2008) 1001–1009.

[**158**] **KORTEKAAS, R. ET AL.**, Blood-brain barrier dysfunction in Parkinsonian midbrain in vivo, Ann. Neurol. 57: 2 (2005) 176–179.

[**159**] **WANG, N. ET AL.**, Iron chelation nanoparticles with delayed saturation as an effective therapy for Parkinson disease, Biomacromolecules. 18: 2 (2017) 461–474.

[**160**] **MARCHI, N. ET AL.**, Blood-brain barrier, bulk flow, and interstitial clearance in epilepsy, J. Neurosci. Methods. 260: (2016) 118–124.

[**161**] **VASILEVKO, V. ET AL.**, Aging and cerebrovascular dysfunction: contribution of hypertension, cerebral amyloid angiopathy, and immunotherapy, Ann. N. Y. Acad. Sci. 1207: (2010) 58–70.

[**162**] **ROSENBERG, G.A.**, Extracellular matrix inflammation in vascular cognitive impairment and dementia, Clin. Sci. 131: 6 (2017) 425–437.

[**163**] **MOHAMMADI, M.T.**, **DEHGHANI, G.A.**, Acute hypertension induces brain injury and blood-brain barrier disruption through reduction of claudins mRNA expression in rat, Pathol. Res. Pract. 210: 12 (2014) 985–990.

[**164**] **BIANCARDI, V.**, **STERN, J.**, Compromised blood-brain barrier permeability: novel mechanism by which circulating angiotensin II signals sympathoexcitatory centers during hypertension, J. Physiol. 594: 6 (2016) 1591–1600.

[**165**] **VILLAPOL, S.**, **SAAVEDRA, J.M.**, Neuroprotective effects of angiotensin receptor blockers, Am. J. Hypertens. 28: 3 (2015) 289–299.

[**166**] **MAMO, J.C.L. ET AL.**, Antihypertensive agents do not prevent blood–brain barrier dysfunction and cognitive deficits in dietary-induced obese mice, Int. J. Obes. 41:6 (2017) 926–934.

[**167**] **NIELSEN, P.A. ET AL.**, Models for predicting blood-brain barrier permeation, Drug Discov. Today. 16: 11–12 (2011) 472–475.

[**168**] **REICHEL, A. ET AL.**, An overview of in vitro techniques for blood-brain barrier studies, Methods Mol. Med. 89: (2003) 307–324.

[**169**] **LUNDQUIST, S. ET AL.**, Prediction of drug transport through the blood-brain barrier in vivo: a comparison between two in vitro cell models, Pharm. Res. 19: 7 (2002) 976–981.

[**170**] **LUNDQUIST, S.**, **RENFTEL, M.**, The use of in vitro cell culture models for mechanistic studies and as permeability screens for the blood-brain barrier in the pharmaceutical industry - background and current status in the drug discovery process, Vascul. Pharmacol. 38: 6 (2002) 355–364.

[**171**] **EYAL, S. ET AL.**, Drug interactions at the blood-brain barrier: fact or fantasy?, Pharmacol. Ther. 123: 1 (2009) 80–104.

[**172**] **LIU, R. ET AL.**, Targeting the neurovascular unit: Development of a new model and consideration for novel strategy for Alzheimer's disease, Brain Res. Bull. 86: 1–2 (2011) 13–21.

[**173**] **PRIETO, P. ET AL.**, Blood-brain barrier in vitro models and their application in toxicology. The report and recommendations of ECVAM Workshop 49, Altern. to Lab. Anim. 31: 1 (2004) 37–50.

[**174**] **DANIELS, B.P. ET AL.**, Immortalized human cerebral microvascular endothelial cells maintain the properties of primary cells in an in vitro model of immune migration across the blood brain barrier, J. Neurosci. Methods. 212: 1 (2013) 173–179.

[**175**] **KANSY, M. ET AL.**, Physicochemical high throughput screening: parallel artificial membrane permeation assay in the description of passive absorption processes, J. Med. Chem. 41: 7 (1998) 1007–1010.

[**176**] **DI, L. ET AL.**, Comparison of blood–brain barrier permeability assays: in situ brain perfusion, MDR1-MDCKII and PAMPA-BBB, J. Pharm. Sci. 98: 6 (2009) 1980–1991.

[**177**] **MENSCH, J. ET AL.**, Application of PAMPA-models to predict BBB permeability including efflux ratio, plasma protein binding and physicochemical parameters, Int. J. Pharm. 395: 1–2 (2010) 182–197.

[**178**] **DI, L. ET AL.**, High throughput artificial membrane permeability assay for blood-brain barrier, Eur. J. Med. Chem. 38: 3 (2003) 223–232.

[**179**] **MENSCH, J. ET AL.**, Evaluation of various PAMPA models to identify the most discriminating method for the prediction of BBB permeability, Eur. J. Pharm. Biopharm. 74: 3 (2010) 495–502.

[**180**] **RODRÍGUEZ-FRANCO, M.I. ET AL.**, Novel tacrine-melatonin hybrids as dual-acting drugs for alzheimer disease, with improved acetylcholinesterase inhibitory and antioxidant properties, J. Med. Chem. 49: 2 (2006) 459–462.

[**181**] **ARCE, M.P. ET AL.**, Neuroprotective and cholinergic properties of multifunctional glutamic acid derivatives for the treatment of Alzheimer's disease, J. Med. Chem. 52: 22 (2009) 7249–7257.

[**182**] **FERNÁNDEZ-BACHILLER, M.I. ET AL.**, Novel tacrine-8-hydroxyquinoline hybrids as multifunctional agents for the treatment of Alzheimers disease, with neuroprotective, cholinergic, antioxidant, and copper-complexing properties, J. Med. Chem. 53: 13 (2010) 4927–4937.

[**183**] **MARCO-CONTELLES, J. ET AL.**, Tacripyrines, the first tacrine-dihydropyridine hybrids, as multitarget-directed ligands for the treatment of Alzheimer's disease, J. Med. Chem. 52: 9 (2009) 2724–2732.

[**184**] **CAMPS, P. ET AL.**, Pyrano[3,2-c]quinoline-6-chlorotacrine hybrids as a novel family of acetylcholinesterase- and beta-amyloid-directed anti-Alzheimer compounds, J. Med. Chem. 52: 17 (2009) 5365–5379.

[**185**] **GONZÁLEZ-MUÑOZ, G.C. ET AL.**, Old phenothiazine and dibenzothiadiazepine derivatives for tomorrow's neuroprotective therapies against neurodegenerative diseases, Eur. J. Med. Chem. 45: 12 (2010) 6152–6158.

[**186**] **GONZÁLEZ-MUÑOZ, G.C. ET AL.**, N-acylaminophenothiazines: neuroprotective agents displaying multifunctional activities for a potential treatment of Alzheimer's disease, Eur. J. Med. Chem. 46: 6 (2011) 2224–2235.

[**187**] **FERNÁNDEZ-BACHILLER, M.I. ET AL.**, New tacrine-4-oxo-4H-chromene hybrids as multifunctional agents for the treatment of Alzheimer's disease, with cholinergic, antioxidant, and β-amyloid-reducing properties, J. Med. Chem. 55: 3 (2012) 1303–1317.

[**188**] **PÉREZ, D.I. ET AL.**, 5-Imino-1,2-4-thiadiazoles and quinazolines derivatives as glycogen synthase kinase 3β (GSK-3β) and phosphodiesterase 7 (PDE7) inhibitors: Determination of blood-brain barrier penetration and binding to human serum albumin, Eur. J. Pharm. Sci. 45: 5 (2012) 677–684.

[**189**] **GONZÁLEZ-LAFUENTE, L. ET AL.**, Benzothiazepine CGP37157 and its isosteric 2'-ethyl analogue provide neuroprotection and block cell calcium entry, ACS Chem. Neurosci. 3: 7 (2012) 519–529.

[**190**] **PAVON, F.J. ET AL.**, Antiobesity effects of the novel in vivo neutral cannabinoid receptor antagonist 5-(4-chlorophenyl)-1-(2,4-dichlorophenyl)-3-hexyl-1H-1,2,4-triazole - LH 21, Neuropharmacology. 51: 2 (2006) 358–366.

[**191**] **CHIOUA, M. ET AL.**, α-Aryl-N-alkyl nitrones, as potential agents for stroke treatment: synthesis, theoretical calculations, antioxidant, anti-inflammatory, neuroprotective, and brain−blood barrier permeability properties, J. Med. Chem. 55: 1 (2012) 153–168.

[**192**] **PATERNITI, I. ET AL.**, PDE 7 inhibitors: new potential drugs for the therapy of spinal cord injury, PLoS One. 6: 1 (2011) 1–15.

[**193**] **KÖNCZÖL, Á. ET AL.**, Applicability of a blood-brain barrier specific artificial membrane permeability assay at the early stage of natural product-based CNS drug discovery, J. Nat. Prod. 76: 4 (2013) 655–663.

[**194**] **MÜLLER, J. ET AL.**, BBB penetration-targeting physicochemical lead selection: ecdysteroids as chemo-sensitizers against CNS tumors, Eur. J. Pharm. Sci. 96: (2017) 571–577.

[**195**] **MÜLLER, J. ET AL.**, Tuning the predictive capacity of the PAMPA-BBB model, Pharm. Sci. 79: (2015) 53–60.

[**196**] **JHALA, D.D. ET AL.**, Optimization and validation of an in vitro model of the blood-brain barrier using artificial lipid membrane, J. Bioequivalence Bioavailab. 14 (2012) 10–14.

[**197**] **TSINMAN, O. ET AL.**, Physicochemical selectivity of the BBB microenvironment governing passive diffusion—matching with a porcine brain lipid extract artificial membrane permeability model, Pharm. Res. 28: 2 (2011) 337–363.

[**198**] **CARRARA, S. ET AL.**, Evaluation of in vitro brain penetration: optimized PAMPA and MDCKII-MDR1 assay comparison, Int. J. Pharm. 345: 1–2 (2007) 125–133.

[**199**] **AVDEEF, A. ET AL.**, PAMPA - A drug absorption in vitro model: 11. matching the in vivo unstirred water layer thickness by individual-well stirring in microtitre plates, Eur. J. Pharm. Sci. 22: 5 (2004) 365–374.

[**200**] **MENSCH, J. ET AL.**, In vivo, in vitro and in silico methods for small molecule transfer across the BBB, J. Pharm. Sci. 98: 12 (2009) 4429–4468.

[**201**] **PARDRIDGE, W.M.**, Introduction to the blood-brain barrier: methodology, biology and pathology, Cambridge University Press, 1998.

[**202**] **SIAKOTOS, A.N. ET AL.**, Isolation of highly purified human and bovine brain endothelial cells and nuclei and their phospholipid composition, Lipids. 4: 3 (1969) 234–239.

[**203**] **BENDAYAN, R. ET AL.**, Functional expression and localization of P-glycoprotein at the blood brain barrier, Microsc. Res. Tech. 57: 5 (2002) 365–380.

[**204**] **DEHOUCK, M.-P. ET AL.**, Drug transfer across the blood-brain barrier: comparison of in vitro and in vivo models., J. Neurochem. 58: 5 (1992) 1790–1797.

[**205**] **TÓTH, A.E. ET AL.**, Patented in vitro blood-brain barrier models in CNS drug discovery, Recent Pat. CNS Drug Discov. 6: 2 (2011) 107–118.

[**206**] **NAIK, P.**, **CUCULLO, L.**, In vitro blood-brain barrier models: current and perspective technologies, J. Pharm. Sci. 101: 4 (2012) 1337–1354.

[**207**] **PERRIÈRE, N. ET AL.**, A functional in vitro model of rat blood-brain barrier for molecular analysis of efflux transporters, Brain Res. 1150: 1 (2007) 1–13.

[**208**] **KUO, Y.-C.**, **LU, C.-H.**, Effect of human astrocytes on the characteristics of human brain-microvascular endothelial cells in the blood-brain barrier., Colloids Surf. B. Biointerfaces. 86: 1 (2011) 225–231.

[**209**] **MALINA, K.C.K. ET AL.**, Closing the gap between the in-vivo and in-vitro blood-brain barrier tightness, Brain Res. 1284: (2009) 12–21.

[**210**] **FRANKE, H. ET AL.**, Primary cultures of brain microvessel endothelial cells: a valid and flexible model to study drug transport through the blood-brain barrier in vitro, Brain Res. Protoc. 5: 3 (2000) 248–256.

[**211**] **CRONE, C.**, **OLESEN, S.P.**, Electrical resistance of brain microvascular endothelium, Brain Res. 241: 1 (1982) 49–55.

[**212**] **SMITH, Q.R.**, **RAPOPORT, S.I.**, Cerebrovascular permeability coefficients to sodium, potassium, and chloride, J. Neurochem. 46: 6 (1986) 1732–1742.

[**213**] **BUTT, A.M. ET AL.**, Electrical resistance across the blood-brain barrier in anaesthetized rats: a developmental study., J. Physiol. 429: (1990) 47–62.

[**214**] **GAILLARD, P.J. ET AL.**, Establishment and functional characterization of an in vitro model of the blood – brain barrier , comprising a co-culture of brain capillary endothelial cells and astrocytes, Eur. J. Pharm. Sci. 12: 3 (2001) 215–222.

[**215**] **PERRIÈRE, N. ET AL.**, Puromycin-based purification of rat brain capillary endothelial cell cultures. Effect on the expression of blood-brain barrier-specific properties, J. Neurochem. 93: 2 (2005) 279–289.

[**216**] **WUEST, D.M.**, **LEE, K.H.**, Optimization of endothelial cell growth in a murine in vitro blood-brain barrier model, Biotechnol. J. 7: 3 (2012) 409–417.

[**217**] **CULOT, M. ET AL.**, An in vitro blood-brain barrier model for high throughput (HTS) toxicological screening, Toxicol. Vitr. 22: 3 (2008) 799–811.

[**218**] **CANTRILL, C. A. ET AL.**, An immortalised astrocyte cell line maintains the in vivo phenotype of a primary porcine in vitro blood-brain barrier model, Brain Res. 1479: (2012) 17–30.

[**219**] **HELLINGER, É. ET AL.**, Comparison of brain capillary endothelial cell-based and epithelial (MDCK-MDR1, Caco-2, and VB-Caco-2) cell-based surrogate blood-brain barrier penetration models, Eur. J. Pharm. Biopharm. 82: 2 (2012) 340–351.

[**220**] **BOVERI, M. ET AL.**, Induction of blood-brain barrier properties in cultured brain capillary endothelial cells: Comparison between primary glial cells and C6 cell line, Glia. 51: 3 (2005) 187–198.

[**221**] **BICKEL, U.**, How to measure drug transport across the blood-brain barrier., NeuroRx. 2: 1 (2005) 15–26.

[**222**] **HELMS, H.C. ET AL.**, In vitro evidence for the brain glutamate efflux hypothesis: Brain endothelial cells cocultured with astrocytes display a polarized brain-to-blood transport of glutamate, Glia. 60: 6 (2012) 882–893.

[**223**] **KUSCH-PODDAR, M. ET AL.**, Evaluation of the immortalized human brain capillary endothelial cell line BB19 as a human cell culture model for the blood-brain barrier, Brain Res. 1064: 1–2 (2005) 21–31.

[**224**] **HAKKARAINEN, J.J. ET AL.**, Comparison of in vitro cell models in predicting in vivo brain entry of drugs, Int. J. Pharm. 402: 1–2 (2010) 27–36.

[**225**] **MILLER, D.W. ET AL.**, Evaluation of drug efflux transporter liabilities of darifenacin in cell culture models of the blood-brain and blood-ocular barriers, Neurourol. Urodyn. 30: 1 (2011) 1633–1638.

[**226**] **PATABENDIGE, A. ET AL.**, A detailed method for preparation of a functional and flexible blood-brain barrier model using porcine brain endothelial cells, Brain Res. 1521: (2013) 16–30.

[**227**] **PATABENDIGE, A. ET AL.**, Establishment of a simplified in vitro porcine blood-brain barrier model with high transendothelial electrical resistance, Brain Res. 1521: (2013) 1–15.

[**228**] **NITZ, T. ET AL.**, Serum-derived factors weaken the barrier properties of cultured porcine brain capillary endothelial cells in vitro., Brain Res. 981: 1–2 (2003) 30–40.

[**229**] **ZHANG, Y. ET AL.**, Porcine brain microvessel endothelial cells as an in vitro model to predict in vivo blood-brain barrier permeability., Drug Metab. Dispos. 34: 11 (2006) 1935–1943.

[**230**] **CALABRIA, A.R. ET AL.**, Puromycin-purified rat brain microvascular endothelial cell cultures exhibit improved barrier properties in response to glucocorticoid induction, J. Neurochem. 97: 4 (2006) 922–933.

[**231**] **LACOMBE, O. ET AL.**, In vitro primary human and animal cell-based blood-brain barrier models as a screening tool in drug discovery., Mol. Pharm. 8: 3 (2011) 651–663.

[**232**] **YANG, Z.-H. ET AL.**, An in vitro transport model for rapid screening and predicting the permeability of candidate compounds at blood-brain barrier, J. Asian Nat. Prod. Res. 13: 12 (2011) 1087–1097.

[**233**] **WATSON, P.M.D. ET AL.**, Modelling the endothelial blood-CNS barriers: a method for the production of robust in vitro models of the rat blood-brain barrier and blood-spinal cord barrier, BMC Neurosci. (2013) 14–59.

[**234**] **WEIDENFELLER, C. ET AL.**, Murine brain capillary endothelial cells exhibit improved barrier properties under the influence of hydrocortisone., Brain Res. 1053: 1–2 (2005) 162–174.

[**235**] **SCHROT, S. ET AL.**, Influence of hydrocortisone on the mechanical properties of the cerebral endothelium in vitro, Biophys. J. 89: 6 (2005) 3904–3910.

[**236**] **SHAYAN, G. ET AL.**, Murine in vitro model of the blood-brain barrier for evaluating drug transport, Eur. J. Pharm. Sci. 42: 1–2 (2011) 148–155.

[**237**] **TIGGES, U. ET AL.**, A novel and simple method for culturing pericytes from mouse brain, Microvasc. Res. 84: 1 (2012) 74–80.

[**238**] **KUO, Y.C.**, **SU, F.L.**, Transport of stavudine, delavirdine, and saquinavir across the blood-brain barrier by polybutylcyanoacrylate, methylmethacrylate-sulfopropylmethacrylate, and solid lipid nanoparticles, Int. J. Pharm. 340: 1–2 (2007) 143–152.

[**239**] **BERNAS, M. ET AL.**, Establishment of primary cultures of human brain microvascular endothelial cells: a new and simplified method to obtain cells for an in vitro model of the blood, Nat. Protoc. 5: 7 (2010) 1265–1272.

[**240**] **SMITH, M. ET AL.**, Primary porcine brain microvascular endothelial cells: biochemical and functional characterisation as a model for drug transport and targeting, J. Drug Target. 15: 4 (2007) 253–268.

[**241**] **ZHANG, Z. ET AL.**, Co-culture based blood-brain barrier in vitro model, a tissue engineering approach using immortalized cell lines for drug transport study, Appl. Biochem. Biotechnol. 163: 2 (2011) 278–295.

[**242**] **STEINER, O. ET AL.**, Comparison of immortalized bEnd5 and primary mouse brain microvascular endothelial cells as in vitro blood-brain barrier models for the study of T cell extravasation, J. Cereb. Blood Flow Metab. 31: 1 (2011) 315–327.

[**243**] **VU, K. ET AL.**, Immortalized human brain endothelial cell line HCMEC/D3 as a model of the blood-brain barrier facilitates in vitro studies of central nervous system infection by cryptococcus neoformans, Eukaryot. Cell. 8: 11 (2009) 1803–1807.

[**244**] **SOBUE, K. ET AL.**, Induction of blood-brain barrier properties in immortalized bovine brain endothelial cells by astrocytic factors, Neurosci. Res. 35: 2 (1999) 155–164.

[**245**] **NEUHAUS, W. ET AL.**, A novel flow based hollow-fiber blood-brain barrier in vitro model with immortalised cell line PBMEC/C1-2, J. Biotechnol. 125: 1 (2006) 127–141.

[**246**] **LAUER, R. ET AL.**, Development of an in vitro blood–brain barrier model based on immortalized porcine brain microvascular endothelial cells, Farm. 59: 2 (2004) 133–137.

[**247**] **TEIFEL, M.**, **FRIEDL, P.**, Establishment of the permanent microvascular endothelial cell line PBMEC/C1-2 from porcine brains, Exp. Cell Res. 228: 1 (1996) 50–57.

[**248**] **GOMES, P.**, **SOARES-DA-SILVA, P.**, Interaction between L-DOPA and 3-O-methyl-L-DOPA for transport in immortalised rat capillary cerebral endothelial cells, Neuropharmacology. 38: 9 (1999) 1371–1380.

[**249**] **ROUX, F.**, **COURAUD, P.-O.**, Rat brain endothelial cell lines for the study of blood-brain barrier permeability and transport functions, Cell. Mol. Neurobiol. 25: 1 (2005) 41–58.

[**250**] **GARBERG, P. ET AL.**, In vitro models for the blood-brain barrier, Toxicol. Vitr. 19: 3 (2005) 299–334.

[**251**] **YANG, T. ET AL.**, Evaluation of bEnd5 cell line as an in vitro model for the blood-brain barrier under normal and hypoxic/aglycemic condition, J. Pharm. Sci. 96: 12 (2007) 3196–3213.

[**252**] **LI, G. ET AL.**, Permeability of endothelial and astrocyte cocultures: In vitro Blood-brain barrier models for drug delivery studies, Ann. Biomed. Eng. 38: 8 (2010) 2499–2511.

[**253**] **BROWN, R.C. ET AL.**, Tight junction protein expression and barrier properties of immortalized mouse brain microvessel endothelial cells, Brain Res. 1130: 1 (2007) 17–30.

[**254**] **OMIDI, Y. ET AL.**, Evaluation of the immortalised mouse brain capillary endothelial cell line, b.End3, as an in vitro blood-brain barrier model for drug uptake and transport studies, Brain Res. 990: 1–2 (2003) 95–112.

[**255**] **GUO, J. ET AL.**, Estrogen-receptor-mediated protection of cerebral endothelial cell viability and mitochondrial function after ischemic insult in vitro, J. Cereb. Blood Flow Metab. 30: 3 (2010) 545–554.

[**256**] **BUREK, M. ET AL.**, Generation of an immortalized murine brain microvascular endothelial cell line as an in vitro blood brain barrier model, J. Vis. Exp. 66: e4022 (2012) 1–6.

[**257**] **WATANABE, T. ET AL.**, Paracellular barrier and tight junction protein expression in the immortalized brain endothelial cell lines bEND.3, bEND.5 and mouse brain endothelial cell 4, Biol. Pharm. Bull. 36: 3 (2013) 492–495.

[**258**] **URICH, E. ET AL.**, Transcriptional profiling of human brain endothelial cells reveals key properties crucial for predictive in vitro blood-brain barrier models, PLoS One. 7: 5 (2012) 1–16.

[**259**] **LU, J.**, A novel hypothesis of blood-brain barrier BBB development and in vitro BBB model: neural stem cell is the driver of BBB formation and maintenance, J. Exp. Integr. Med. 2: 1 (2012) 39–43.

[**260**] **WEKSLER, B.B. ET AL.**, Blood-brain barrier-specific properties of a human adult brain endothelial cell line, FASEB J. 19: 13 (2005) 1872–1874.

[**261**] **POLLER, B. ET AL.**, The human brain endothelial cell line hCMEC/D3 as a human blood-brain barrier model for drug transport studies, J. Neurochem. 107: 5 (2008) 1358–1368.

[**262**] **TAI, L.M. ET AL.**, Polarized P-glycoprotein expression by the immortalised human brain endothelial cell line, hCMEC/D3, restricts apical-to-basolateral permeability to rhodamine 123, Brain Res. 1292: (2009) 14–24.

[**263**] **DAUCHY, S. ET AL.**, Expression and transcriptional regulation of ABC transporters and cytochromes P450 in hCMEC/D3 human cerebral microvascular endothelial cells, Biochem. Pharmacol. 77: 5 (2009) 897–909.

[**264**] **SCHRADE, A. ET AL.**, Expression and localization of claudins-3 and -12 in transformed human brain endothelium, Fluids Barriers CNS. 9: 1 (2012) 1–5.

[**265**] **WEKSLER, B. ET AL.**, The hCMEC/D3 cell line as a model of the human blood brain barrier, Fluids Barriers CNS. 10: 1 (2013) 1–10.

[**266**] **KETABI-KIYANVASH, N. ET AL.**, NKIM-6, a new immortalized human brain capillary endothelial cell line with conserved endothelial characteristics, Cell Tissue Res. 328: 1 (2007) 19–29.

[**267**] **SANO, Y. ET AL.**, Establishment of a new conditionally immortalized human brain microvascular endothelial cell line retaining an in vivo blood-brain barrier function, J. Cell. Physiol. 225: 2 (2010) 519–528.

[**268**] **KAMIICHI, A. ET AL.**, Establishment of a new conditionally immortalized cell line from human brain microvascular endothelial cells: A promising tool for human blood-brain barrier studies, Brain Res. 1488: (2012) 113–122.

[**269**] **LIPPMANN, E.S. ET AL.**, Derivation of blood-brain barrier endothelial cells from human pluripotent stem cells, Nat. Biotechnol. 30: 8 (2012) 783–791.

[**270**] **LIPPMANN, E.S. ET AL.**, Modeling the blood-brain barrier using stem cell sources, Fluids Barriers CNS. 10: 1 (2013) 1–14.

[**271**] **DEMEUSE, P. ET AL.**, Compartmentalized coculture of rat brain endothelial cells and astrocytes : a syngenic model to study the blood-brain barrier, J. Neurosci. Methods. 121: 1 (2002) 21–31.

[**272**] **WUEST, D.M. ET AL.**, Membrane configuration optimization for a murine in vitro blood-brain barrier model, J. Neurosci. Methods. 212: 2 (2013) 211–221.

[**273**] **MA, S.H. ET AL.**, An endothelial and astrocyte co-culture model of the blood-brain barrier utilizing an ultra-thin, nanofabricated silicon nitride membrane, Lab Chip. 5: 1 (2005) 74–85.

[**274**] **HURWITZ, A.A. ET AL.**, Human fetal astrocytes induce the expression of blood-brain barrier specific proteins by autologous endothelial cells, Brain Res. 625: 2 (1993) 238–243.

[**275**] **TILLING, T. ET AL.**, Basement membrane proteins influence brain capillary endothelial barrier function in vitro, J. Neurochem. 71: 3 (1998) 1151–1157.

[**276**] **TILLING, T. ET AL.**, Expression and adhesive properties of basement membrane proteins in cerebral capillary endothelial cell cultures, Cell Tissue Res. 310: 1 (2002) 19–29.

[**277**] **LI, G. ET AL.**, A model for the blood-brain barrier permeability to water and small solutes, J. Biomech. 43: 11 (2010) 2133–2140.

[**278**] **RUBIN, L.L. ET AL.**, A cell culture model of the blood-brain barrier, J. Cell Biol. 115: 6 (1991) 1725–1735.

[**279**] **HASELOFF, R.F. ET AL.**, In search of the astrocytic factor(s) modulating blood-brain barrier functions in brain capillary endothelial cells in vitro, Cell. Mol. Neurobiol. 25: 1 (2005) 25–39.

[**280**] **SIDDHARTHAN, V. ET AL.**, Human astrocytes/astrocyte-conditioned medium and shear stress enhance the barrier properties of human brain microvascular endothelial cells, Brain Res. 1147: 1 (2007) 39–50.

[**281**] **WOLBURG, H. ET AL.**, Modulation of tight junction structure in blood-brain barrier endothelial cells. Effects of tissue culture, second messengers and cocultured astrocytes, J. Cell Sci. 107: Pt 5 (1994) 1347–1357.

[**282**] **HOHEISEL, D. ET AL.**, Hydrocortisone reinforces the blood-brain properties in a serum free cell culture system, Biochem. Biophys. Res. Commun. 247: 2 (1998) 312–315.

[**283**] **COLGAN, O.C. ET AL.**, Influence of basolateral condition on the regulation of brain microvascular endothelial tight junction properties and barrier function, Brain Res. 1193: (2008) 84–92.

[**284**] **FÖRSTER, C. ET AL.**, Occludin as direct target for glucocorticoid-induced improvement of blood-brain barrier properties in a murine in vitro system., J. Physiol. 565: Pt 2 (2005) 475–486.

[**285**] **FÖRSTER, C. ET AL.**, Differential effects of hydrocortisone and TNFalpha on tight junction proteins in an in vitro model of the human blood-brain barrier, J. Physiol. 586: 7 (2008) 1937–1949.

[**286**] **ARNDT, S. ET AL.**, Bioelectrical impedance assay to monitor changes in cell shape during apoptosis, Biosens. Bioelectron. 19: 6 (2004) 583–594.

[**287**] **CHAPPELL, D. ET AL.**, Hydrocortisone preserves the vascular barrier by protecting the endothelial glycocalyx, Anesthesiology. 107: 5 (2007) 776–784.

[**288**] **STANNESS, K. A ET AL.**, Morphological and functional characterization of an in vitro blood-brain barrier model, Brain Res. 771: 2 (1997) 329–342.

[**289**] **JANIGRO, D. ET AL.**, Dynamic modeling of the blood-brain barrier: a novel tool for studies of drug delivery to the brain, Pharm Sci Technolo Today. 2: 1 (1999) 7–12.

[**290**] **CUCULLO, L. ET AL.**, A new dynamic in vitro model for the multidimensional study of astocyte-endothelial cell interaction at the blood-brain barrier, Brain Res. 951: (2002) 243–254.

[**291**] **CUCULLO, L. ET AL.**, Immortalized human brain endothelial cells and flow-based vascular modeling: a marriage of convenience for rational neurovascular studies, J. Cereb. Blood Flow Metab. 28: 2 (2008) 312–328.

[**292**] **CUCULLO, L. ET AL.**, The role of shear stress in blood-brain barrier endothelial physiology, BMC Neurosci. 12: 40 (2011) 1–15.

[**293**] **SANTAGUIDA, S. ET AL.**, Side by side comparison between dynamic versus static models of blood-brain barrier in vitro: a permeability study, Brain Res. 1109: 1 (2006) 1–13.

[**294**] **CUCULLO, L. ET AL.**, A new dynamic in vitro modular capillaries-venules modular system: cerebrovascular physiology in a box, BMC Neurosci. 14: 18 (2013) 1–25.

[**295**] **BOOTH, R.**, **KIM, H.**, Characterization of a microfluidic in vitro model of the blood-brain barrier (μBBB), Lab Chip. 12: 10 (2012) 1784–1792.

[**296**] **PASTAN, I. ET AL.**, A retrovirus carrying an MDR1 cDNA confers multidrug resistance and polarized expression of P-glycoprotein in MDCK cells, Proc. Natl. Acad. Sci. U. S. A. 85: 12 (1988) 4486–4490.

[**297**] **KWATRA, D. ET AL.**, Interaction of gatifloxacin with efflux transporters: A possible mechanism for drug resistance, Int. J. Pharm. 395: 1–2 (2010) 114–121.

[**298**] **DURMUS, S. ET AL.**, P-glycoprotein (MDR1/ABCB1) and breast cancer resistance protein (BCRP/ABCG2) restrict brain accumulation of the JAK1/2 inhibitor, CYT387, Pharmacol. Res. 76: (2013) 9–16.

[**299**] **WANG, Q. ET AL.**, Evaluation of the MDR-MDCK cell line as a permeability screen for the blood-brain barrier, Int. J. Pharm. 288: 2 (2005) 349–359.

[**300**] **LOHMANN, C. ET AL.**, Predicting blood-brain barrier permeability of drugs: evaluation of different in vitro assays, J. Drug Target. 10: 4 (2002) 263–276.

[**301**] **HELLINGER, É. ET AL.**, Drug penetration model of vinblastine-treated Caco-2 cultures, Eur. J. Pharm. Sci. 41: 1 (2010) 96–106.

[**302**] **TAKAHASHI, K. ET AL.**, Spontaneous transformation and immortalization of human endothelial cells, Vitr. Cell. Dev. Biol. 26: 3 Pt 1 (1990) 265–274.

[**303**] **HURST, R.D.**, **FRITZ, I.B.**, Properties of an immortalised vascular endothelial/glioma cell co-culture model of the blood-brain barrier, J. Cell. Physiol. 167: 1 (1996) 81–88.

[**304**] **SCISM, J.L. ET AL.**, Evaluation of an in vitro coculture model for the blood-brain barrier: Comparison of human umbilical vein endothelial cells (ECV304) and rat glioma cells (C6) from two commercial sources, Vitr. Cell. Dev. Biol. - Anim. 35: 10 (1999) 580–592.

[**305**] **DIRKS, W.G. ET AL.**, ECV304 (endothelial) is really T24 (bladder carcinoma): Cell line cross-contamination at source, Vitr. Cell. Dev. Biol. - Anim. 35: 10 (1999) 558–559.

[**306**] **BROWN, J. ET AL.**, Critical evaluation of ECV304 as a human endothelial cell model defined by genetic analysis and functional responses: a comparison with the human bladder cancer derived epithelial cell line T24/83, Lab. Invest. 80: 1 (2000) 37–45.

[**307**] **NEUHAUS, W. ET AL.**, Validation of in vitro cell culture models of the blood-brain barrier: tightness characterization of two promising cell lines, J. Pharm. Sci. 97: 12 (2008) 5158–5175.

[**308**] **BARAR, J. ET AL.**, Barrier functionality and transport machineries of human ECV304 cells, Med. Sci. Monit. 16: 1 (2010) 52–60.

[**309**] **RODRIGUEZ-GAZTELUMENDI, A. ET AL.**, Comparison of the effects of nicotine upon the transcellular electrical resistance and sucrose permeability of human ECV304/rat C6 co-cultures and human Caco-2 cells, Toxicol. Lett. 207: 1 (2011) 1–6.

[**310**] **ALCENDOR, D.J. ET AL.**, Neurovascular unit on a chip: implications for translational applications, Stem Cell Res. Ther. 4: Suppl 1:S18 (2013) S18.

[**311**] **PALMIOTTI, C.A. ET AL.**, In vitro cerebrovascular modeling in the 21st century: current and prospective technologies, Pharm. Res. 31: 12 (2014) 3229–3250.

[**312**] **KILIC, O. ET AL.**, Brain-on-a-chip model enables analysis of human neuronal differentiation and chemotaxis, Lab Chip. 16: 21 (2016) 4152–4162.

[**313**] **HOVELL, C.M. ET AL.**, Microengineered vascular systems for drug development, J. Lab. Autom. 20: 3 (2015) 251–258.

[**314**] **SHAO, X. ET AL.**, Development of a blood-brain barrier model in a membrane-based microchip for characterization of drug permeability and cytotoxicity for drug screening, Anal. Chim. Acta. 934: (2016) 186–193.

[**315**] **ADRIANI, G. ET AL.**, A 3D neurovascular microfluidic model consisting of neurons, astrocytes and cerebral endothelial cells as blood-brain barrier, Lab Chip. 17: 3 (2017) 448–459.

[**316**] **HELM, M.W. VAN DER ET AL.**, Microfluidic organ-on-chip technology for blood-brain barrier research, Tissue Barriers. 4: 1 (2016) 1–13.

[**317**] **WANG, Y.I. ET AL.**, Microfluidic blood-brain barrier model provides in vivo-like barrier properties for drug permeability screening, Biotechnol. Bioeng. 114: 1 (2017) 184–194.

[**318**] **SELLGREN, K.L. ET AL.**, An optically transparent membrane supports shear stress studies in a three-dimensional microfluidic neurovascular unit model, Biomicrofluidics. 9: 6 (2015) 1–4.

[**319**] **BROWN, J.A. ET AL.**, Recreating blood-brain barrier physiology and structure on chip: a novel neurovascular microfluidic bioreactor, Biomicrofluidics. 9: 5 (2015) 1–15.

[**320**] **ACHYUTA, A.K.H. ET AL.**, A modular approach to create a neurovascular unit-on-a-chip, Lab Chip. 13: 4 (2013) 542–553.

[**321**] **GRIEP, L.M. ET AL.**, BBB on CHIP: Microfluidic platform to mechanically and biochemically modulate blood-brain barrier function, Biomed. Microdevices. 15: 1 (2013) 145–150.

[**322**] **YEON, J.H. ET AL.**, Reliable permeability assay system in a microfluidic device mimicking cerebral vasculatures, Biomed. Microdevices. 14: 6 (2012) 1141–1148.

[**323**] **JEFFREY, P.**, **SUMMERFIELD, S.**, Assessment of the blood-brain barrier in CNS drug discovery, Neurobiol. Dis. 37: 1 (2010) 33–37.

[**324**] **REICHEL, A.**, Addressing central nervous system (CNS) penetration in drug discovery: basics and implications of the evolving new concept, Chem. Biodivers. 6: 11 (2009) 2030–2049.

[**325**] **DI, L. ET AL.**, Strategies to assess blood – brain barrier penetration, Expert Opin. Drug Discov. 3: 6 (2008) 677–687.

[**326**] **PARDRIDGE, W.M.**, Holy grails and in vitro blood-brain barrier models, Drug Discov. Today. 9: 6 (2004) 258.

[**327**] **LIU, X. ET AL.**, Progress in brain penetration evaluation in drug discovery and development, J. Pharmacol. Exp. Ther. 325: 2 (2008) 349–356.

[**328**] **AVDEEF, A.**, How well can in vitro brain microcapillary endothelial cell models predict rodent in vivo blood-brain barrier permeability?, Eur. J. Pharm. Sci. 43: 3 (2011) 109–124.

[**329**] **OLDENDORF, W.H.**, Measurement of brain uptake of radiolabeled substances using a tritiated water internal standard, Brain Res. 24: 2 (1970) 372–376.

[**330**] **CECCHELLI, R. ET AL.**, Modelling of the blood-brain barrier in drug discovery and development, Nat. Rev. Drug Discov. 6: 8 (2007) 650–661.

[**331**] **PARDRIDGE, W.M.**, Transport of small molecules through the blood-brain biology and methodology barrier: biology and methodology, Adv. Drug Deliv. Rev. 15: 1–3 (1995) 5–36.

[**332**] **SMITH, Q.R.**, A review of blood-brain barrier transport techniques, Methods Mol. Med. 89: (2003) 193–208.

[**333**] **DE LANGE, E.C. ET AL.**, Methodological considerations of intracerebral microdialysis in pharmacokinetic studies on drug transport across the blood-brain barrier, Brain Res. Brain Res. Rev. 25: 1 (1997) 27–49.

[**334**] **DE LANGE, E.C.M. ET AL.**, Methodological issues in microdialysis sampling for pharmacokinetic studies, Adv. Drug Deliv. Rev. 45: 2–3 (2000) 125–148.

[**335**] **WESTERHOUT, J. ET AL.**, Preclinical prediction of human brain target site concentrations: considerations in extrapolating to the clinical setting, J. Pharm. Sci. 100: 9 (2011) 3577–3593.

[**336**] **KAKEE, A. ET AL.**, Brain efflux index as a novel method of analyzing efflux transport at the blood-brain barrier, J. Pharmacol. Exp. Ther. 277: 3 (1996) 1550–1559.

[**337**] **SHEN, D.D. ET AL.**, Principles and applicability of CSF sampling for the assessment of CNS drug delivery and pharmacodynamics, Adv. Drug Deliv. Rev. 56: 12 (2004) 1825–1857.

[**338**] **UPTON, R.N.**, Cerebral uptake of drugs in humans, Clin. Exp. Pharmacol. Physiol. 34: 8 (2007) 695–701.

[**339**] **SYVÄNEN, S. ET AL.**, Species differences in blood-brain barrier transport of three positron emission tomography radioligands with emphasis on P-glycoprotein transport, Drug Metab. Dispos. 37: 3 (2009) 635–643.

[**340**] **MABONDZO, A. ET AL.**, Validation of in vitro cell-based human blood-brain barrier model using clinical positron emission tomography radioligands to predict in vivo human brain penetration, Mol. Pharm. 7: 5 (2010) 1805–1815.

[**341**] **MAIRINGER, S. ET AL.**, The antiepileptic drug mephobarbital is not transported by P-glycoprotein or multidrug resistance protein 1 at the blood-brain barrier: a positron emission tomography study, Epilepsy Res. 100: 1–2 (2012) 93–103.

[**342**] **BANKSTAHL, J.P. ET AL.**, Tariquidar and elacridar are dose-dependently transported by P-glycoprotein and Bcrp at the blood-brain barrier: A small-animal positron emission tomography and in vitro study, Drug Metab. Dispos. 41: 4 (2013) 754–762.

[**343**] **SYVÄNEN, S.**, **ERIKSSON, J.**, Advances in PET imaging of P-glycoprotein function at the blood-brain barrier, ACS Chem. Neurosci. 4: 2 (2013) 225–237.

[**344**] **SPUCH, C.**, **NAVARRO, C.**, Liposomes for targeted delivery of active agents against neurodegenerative diseases (Alzheimer's disease and Parkinson's disease), J. Drug Deliv. 2011: (2011) 1–12.

[**345**] **SPUCH, C. ET AL.**, Advances in the treatment of neurodegenerative disorders employing nanoparticles, Recent Pat. Drug Deliv. Formul. 6: 1 (2012) 2–18.

[**346**] **KUO, Y.C.**, **LEE, C.L.**, Methylmethacrylate-sulfopropylmethacrylate nanoparticles with surface RMP-7 for targeting delivery of antiretroviral drugs across the blood-brain barrier, Colloids Surfaces B Biointerfaces. 90: 1 (2012) 75–82.

[**347**] **POTSCHKA, H.**, Role of CNS efflux drug transporters in antiepileptic drug delivery: overcoming CNS efflux drug transport, Adv. Drug Deliv. Rev. 64: 10 (2012) 943–952.

[**348**] **JUILLERAT-JEANNERET, L.**, The targeted delivery of cancer drugs across the blood-brain barrier: chemical modifications of drugs or drug-nanoparticles?, Drug Discov. Today. 13: 23–24 (2008) 1099–1106.

[**349**] **DILNAWAZ, F. ET AL.**, The transport of non-surfactant based paclitaxel loaded magnetic nanoparticles across the blood brain barrier in a rat model, Biomaterials. 33: 10 (2012) 2936–2951.

[**350**] **WONG, H.L. ET AL.**, Nanotechnological advances for the delivery of CNS therapeutics, Adv. Drug Deliv. Rev. 64: 7 (2012) 686–700.

[**351**] **CHEN, Y.**, **LIU, L.**, Modern methods for delivery of drugs across the blood-brain barrier, Adv. Drug Deliv. Rev. 64: 7 (2012) 640–665.

[**352**] **DELI, M.A.**, Potential use of tight junction modulators to reversibly open membranous barriers and improve drug delivery, Biochim. Biophys. Acta - Biomembr. 1788: 4 (2009) 892–910.

[**353**] **BURGESS, A.**, **HYNYNEN, K.**, Noninvasive and targeted drug delivery to the brain using focused ultrasound, ACS Chem. Neurosci. 4: 4 (2013) 519–526.

[**354**] **SCHERRMANN, J.M.**, Drug delivery to brain via the blood–brain barrier, Vascul. Pharmacol. 38: 6 (2002) 349–354.

[**355**] **GAILLARD, P.J. ET AL.**, Enhanced brain drug delivery: Safely crossing the blood-brain barrier, Drug Discov. Today Technol. 9: 2 (2012) e155–e160.

[**356**] **PARDRIDGE, W.M.**, Molecular Trojan horses for blood-brain barrier drug delivery, Curr. Opin. Pharmacol. 6: 5 (2006) 494–500.

[**357**] **OHTSUKI, S.**, **TERASAKI, T.**, Contribution of carrier-mediated transport systems to the blood-brain barrier as a supporting and protecting interface for the brain; importance for CNS drug discovery and development, Pharm. Res. 24: 9 (2007) 1745–1758.

[**358**] **LALATSA, A. ET AL.**, Chapter 5.50. Drug delivery across the blood-brain barrier, in: M. Moo-Young (Ed.), Compr. Biotechnol., Elsevier B.V., 2011: pp. 657–667.

[**359**] **KROL, S.**, Challenges in drug delivery to the brain: nature is against us, J. Control. Release. 164: 2 (2012) 145–155.

[**360**] **WOHLFART, S. ET AL.**, Transport of drugs across the blood-brain barrier by nanoparticles, J. Control. Release. 161: 2 (2012) 264–273.

[**361**] **KREUTER, J.**, Nanoparticulate systems for brain delivery of drugs, Adv. Drug Deliv. Rev. 64: SUPPL. (2012) 213–222.

[**362**] **REMPE, R. ET AL.**, Transport of poly(n-butylcyano-acrylate) nanoparticles across the blood-brain barrier in vitro and their influence on barrier integrity, Biochem. Biophys. Res. Commun. 406: 1 (2011) 64–69.

[**363**] **MALAKOUTIKHAH, M. ET AL.**, N-methyl phenylalanine-rich peptides as highly versatile blood-brain barrier shuttles, J. Med. Chem. 53: 6 (2010) 2354–2363.

[**364**] **BELHADJ, Z. ET AL.**, Design of Y-shaped targeting material for liposome-based multifunctional glioblastoma-targeted drug delivery, J. Control. Release. 255: (2017) 132–141.

[**365**] **GU, J. ET AL.**, Development of antibody-modified chitosan nanoparticles for the targeted delivery of siRNA across the blood-brain barrier as a strategy for inhibiting HIV replication in astrocytes, Drug Deliv. Transl. Res. 7: (2017) 497–506.

[**366**] **JIN, Q. ET AL.**, Edaravone-encapsulated agonistic micelles rescue ischemic brain tissue by tuning blood-brain barrier permeability, Theranostics. 7: 4 (2017) 884–898.

[**367**] **CHATURVEDI, M. ET AL.**, Tissue inhibitor of matrix metalloproteinases-1 loaded poly(lactic-co-glycolic acid) nanoparticles for delivery across the blood-brain barrier, Int. J. Nanomedicine. 9: 1 (2014) 575–588.

[**368**] **SALVATI, E. ET AL.**, Liposomes functionalized to overcome the blood-brain barrier and to target amyloid-β peptide: The chemical design affects the permeability across an in vitro model, Int. J. Nanomedicine. 8: (2013) 1749–1758.

[**369**] **SUN, Z. ET AL.**, Characterization of cellular uptake and toxicity of aminosilane-coated iron oxide nanoparticles with different charges in central nervous system-relevant cell culture models, Int. J. Nanomedicine. 8: (2013) 961–970.

[**370**] **HUANG, F.Y.J. ET AL.**, In vitro and in vivo evaluation of lactoferrin-conjugated liposomes as a novel carrier to improve the brain delivery, Int. J. Mol. Sci. 14: 2 (2013) 2862–2874.

[**371**] **HAO, Z.F. ET AL.**, Liposomes modified with P-aminophenyl-α-d-mannopyranoside: A carrier for targeting cerebral functional regions in mice, Eur. J. Pharm. Biopharm. 84: 3 (2013) 505–516.

[**372**] **TEOW, H.M. ET AL.**, Delivery of paclitaxel across cellular barriers using a dendrimer-based nanocarrier, Int. J. Pharm. 441: 1–2 (2013) 701–711.

[**373**] **KULKARNI, S. A**, **FENG, S.-S.**, Effects of particle size and surface modification on cellular uptake and biodistribution of polymeric nanoparticles for drug delivery, Pharm. Res. 30: 10 (2013) 2512–22.

[**374**] **XIA, H. ET AL.**, Penetratin-functionalized PEG-PLA nanoparticles for brain drug delivery, Int. J. Pharm. 436: 1–2 (2012) 840–850.

[**375**] **BOMMANA, M.M. ET AL.**, brain microdialysis to evaluate FITC-dextran encapsulated immunopegylated nanoparticles, Drug Deliv. 19: 6 (2012) 298–306.

[**376**] **LI, Y. ET AL.**, A dual-targeting nanocarrier based on poly(amidoamine) dendrimers conjugated with transferrin and tamoxifen for treating brain gliomas, Biomaterials. 33: 15 (2012) 3899–3908.

[**377**] **GAO, H. ET AL.**, Precise glioma targeting of and penetration by aptamer and peptide dual-functioned nanoparticles, Biomaterials. 33: 20 (2012) 5115–5123.

[**378**] **WAGNER, S. ET AL.**, Uptake mechanism of ApoE-modified nanoparticles on brain capillary endothelial cells as a blood-brain barrier model, PLoS One. 7: 3 (2012) 3–9.

[**379**] **ZENSI, A. ET AL.**, Albumin nanoparticles targeted with Apo E enter the CNS by transcytosis and are delivered to neurones, J. Control. Release. 137: 1 (2009) 78–86.

[**380**] **GUARNIERI, D. ET AL.**, Shuttle-mediated nanoparticle delivery to the blood-brain barrier, Small. 9: 6 (2013) 853–862.

[**381**] **LIEN, C.F. ET AL.**, In vitro assessment of alkylglyceryl-functionalized chitosan nanoparticles as permeating vectors for the blood-brain barrier, Biomacromolecules. 13: 4 (2012) 1067–1073.

[**382**] **GIL, E.S. ET AL.**, β‑cyclodextrin-poly(β-amino ester) nanoparticles for sustained drug delivery across the blood-brain barrier, Biomacromolecules. 13: 11 (2012) 3533–3541.

[**383**] **SHARMA, G. ET AL.**, Grafting of cell-penetrating peptide to receptor-targeted liposomes improves their transfection efficiency and transport across blood-brain barrier model, J. Pharm. Sci. 101: 7 (2012) 2468–2478.

[**384**] **XIE, Y.T. ET AL.**, Brain-targeting study of stearic acid-grafted chitosan micelle drug-delivery system, Int. J. Nanomedicine. 7: (2012) 3235–3244.

[**385**] **DAKWAR, G.R. ET AL.**, Delivery of proteins to the brain by bolaamphiphilic nano-sized vesicles, J. Control. Release. 160: 2 (2012) 315–321.

[**386**] **HEMMELMANN, M. ET AL.**, Amphiphilic HPMA-LMA copolymers increase the transport of rhodamine 123 across a BBB model without harming its barrier integrity, J. Control. Release. 163: 2 (2012) 170–177.

[**387**] **MONTENEGRO, L. ET AL.**, In vitro evaluation of idebenone-loaded solid lipid nanoparticles for drug delivery to the brain, Drug Dev. Ind. Pharm. 37: 6 (2011) 737–746.

[**388**] **HE, H. ET AL.**, PEGylated poly(amidoamine) dendrimer-based dual-targeting carrier for treating brain tumors, Biomaterials. 32: 2 (2011) 478–487.

[**389**] **RE, F. ET AL.**, Functionalization of liposomes with ApoE-derived peptides at different density affects cellular uptake and drug transport across a blood-brain barrier model, Nanomedicine Nanotechnology, Biol. Med. 7: 5 (2011) 551–559.

[**390**] **MARKOUTSA, E. ET AL.**, Uptake and permeability studies of BBB-targeting immunoliposomes using the hCMEC/D3 cell line, Eur. J. Pharm. Biopharm. 77: 2 (2011) 265–274.

[**391**] **KOFFIE, R.M. ET AL.**, Nanoparticles enhance brain delivery of blood-brain barrier-impermeable probes for in vivo optical and magnetic resonance imaging, Proc. Natl. Acad. Sci. 108: 46 (2011) 18837–18842.

[**392**] **GONG, W. ET AL.**, Improving efficiency of adriamycin crossing blood brain barrier by combination of thermosensitive liposomes and hyperthermia, Biol. Pharm. Bull. 34: 7 (2011) 1058–1064.

[**393**] **RAGNAILL, M.N. ET AL.**, Internal benchmarking of a human blood-brain barrier cell model for screening of nanoparticle uptake and transcytosis, Eur. J. Pharm. Biopharm. 77: 3 (2011) 360–367.

[**394**] **YING, X. ET AL.**, Dual-targeting daunorubicin liposomes improve the therapeutic efficacy of brain glioma in animals, J. Control. Release. 141: 2 (2010) 183–192.

[**395**] **HU, K. ET AL.**, Lactoferrin-conjugated PEG-PLA nanoparticles with improved brain delivery: in vitro and in vivo evaluations, J. Control. Release. 134: 1 (2009) 55–61.

[**396**] **DHANIKULA, R.S. ET AL.**, On the mechanism and dynamics of uptake and permeation of polyether-copolyester dendrimers across an in vitro blood-brain barrier model, J. Pharm. Sci. 28: 10 (2009) 3748–3760.

[**397**] **HOMBACH, J.**, **BERNKOP-SCHNÜRCH, A.**, Chitosan solutions and particles: Evaluation of their permeation enhancing potential on MDCK cells used as blood brain barrier model, Int. J. Pharm. 376: 1–2 (2009) 104–109.

[**398**] **GARCIA-GARCIA, E. ET AL.**, A relevant in vitro rat model for the evaluation of blood-brain barrier translocation of nanoparticles, Cell. Mol. Life Sci. 62: 12 (2005) 1400–1408.

[**399**] **LU, W. ET AL.**, Cationic albumin conjugated pegylated nanoparticle with its transcytosis ability and little toxicity against blood-brain barrier, Int. J. Pharm. 295: 1–2 (2005) 247–260.

[**400**] **GOETZ, C.G.**, The history of Parkinson's disease: early clinical descriptions and neurological therapies, Cold Spring Harb. Perspect. Med. 1: 1 (2011) 1–15.

[**401**] **DI STEFANO, A. ET AL.**, New drug delivery strategies for improved Parkinson's disease therapy, Expert Opin. Drug Deliv. 6: 4 (2009) 389–404.

[**402**] **TYSNES, O.-B.**, **STORSTEIN, A.**, Epidemiology of Parkinson's disease, J. Neural Transm. 124: 8 (2017) 901–905.

[**403**] **PRINGSHEIM, T. ET AL.**, The prevalence of Parkinson's disease: a systematic review and meta-analysis, Mov. Disord. 29: 13 (2014) 1583–1590.

[**404**] **POEWE, W. ET AL.**, Parkinson disease, Nat. Rev. Dis. Prim. 3: (2017) 1–21.

[**405**] **KURTIS, M.M.**, **MARTINEZ-MARTIN, P.**, Chapter 1. Parkinson's disease: symptoms, unmet needs and new therapeutic targets, in: A. Martinez, C. Gil (Eds.), Emerg. Drugs Targets Park. Dis., The Royal Society of Chemistry, 2013: pp. 3–25.

[**406**] **POSTUMA, R.B. ET AL.**, MDS clinical diagnostic criteria for Parkinson's disease, Mov. Disord. 30: 12 (2015) 1591–1601.

[**407**] **SHULMAN, J.M. ET AL.**, Parkinson's disease: genetics and pathogenesis, Annu. Rev. Pathol. Mech. Dis. 6: (2011) 193–224.

[**408**] **OERTEL, W.**, **SCHULZ, J.B.**, Current and experimental treatments of Parkinson disease: a guide for neuroscientists, J. Neurochem. 139: Suppl. 1 (2016) 325–337.

[**409**] **KAKKAR, A.K.**, **DAHIYA, N.**, Management of Parkinson's disease: current and future pharmacotherapy, Eur. J. Pharmacol. 750: (2015) 74–81.

[**410**] **HAUSER, R.A.**, Levodopa: past, present, and future, Eur. Neurol. 62: 1 (2009) 1–8.

[**411**] **ANNUS, Á.**, **VÉCSEI, L.**, Spotlight on opicapone as an adjunct to levodopa in Parkinson's disease : design, development and potential place in therapy, Drug Des. Devel. Ther. 11: (2017) 143–151.

[**412**] **KAGEYAMA, T. ET AL.**, The 4F2hc/LAT1 complex transports L-DOPA across the blood-brain barrier, Brain Res. 879: 1–2 (2000) 115–121.

[**413**] **GONÇALVES, D. ET AL.**, Bioanalytical chromatographic methods for the determination of catechol-O-methyltransferase inhibitors in rodents and human samples: a review, Anal. Chim. Acta. 710: (2012) 17–32.

[**414**] **PALMA, P.N. ET AL.**, Chapter 4. Catechol-O-methyltransferase inhibitors: present problems and relevance of the new ones, in: A. Martinez, C. Gil (Eds.), Emerg. Drugs Targets Park. Dis., Royal Society of Chemistry 2013, 2013: pp. 83–109.

[**415**] **BONIFÁCIO, M.J. ET AL.**, Catechol-O-methyltransferase and its inhibitors in Parkinson's disease, CNS Drug Rev. 13: 3 (2007) 352–379.

[**416**] **KISS, L.E.**, **SOARES-DA-SILVA, P.**, Medicinal chemistry of catechol-O-methyltransferase (COMT) inhibitors and their therapeutic utility, J. Med. Chem. 57: 21 (2014) 8692–8717.

[**417**] **MYÖHÄNEN, T.T.**, **MÄNNISTÖ, P.T.**, Distribution and functions of catechol-O-methyltransferase proteins. Do recent findings change the picture?, Int. Rev. Neurobiol. 95: C (2010) 29–47.

[**418**] **LOTTA, T. ET AL.**, Kinetics of human soluble and membrane-bound catechol-0-methyltransferase: a revised mechanism and description, Biochemistry. 34: 13 (1995) 4202–4210.

[**419**] **MANNISTO, P.T.**, **KAAKKOLA, S.**, Catechol-O-methyltransferase (COMT): biochemistry, molecular biology, pharmacology, and clinical efficacy of the new selective COMT inhibitors, Pharmacol. Rev. 51: 4 (1999) 593–628.

[**420**] **CHEN, J. ET AL.**, Orientation and cellular distribution of membrane-bound catechol-O-methyltransferase in cortical neurons: Implications for drug development, J. Biol. Chem. 286: 40 (2011) 34752–34760.

[**421**] **MYÖHÄNEN, T.T. ET AL.**, Distribution of catechol-O-methyltransferase (COMT) proteins and enzymatic activities in wild-type and soluble COMT deficient mice, J. Neurochem. 113: 6 (2010) 1632–1643.

[**422**] **SCHENDZIELORZ, N. ET AL.**, Catechol-O-methyltransferase (COMT) protein expression and activity after dopaminergic and noradrenergic lesions of the rat brain, PLoS One. 8: 4 (2013) 1–12.

[**423**] **DINGEMANSE, J.**, Catechol-O-methyltransferase inhibitors: clinical potential in the treatment of Parkinson's disease, Drug Dev. Res. 42: 1 (1997) 1–25.

[**424**] **BONIFÁCIO, M.J. ET AL.**, Kinetic inhibitory profile of BIA 3-202, a novel fast tight-binding, reversible and competitive catechol-O-methyltransferase inhibitor, Eur. J. Pharmacol. 460: 2–3 (2003) 163–170.

[**425**] **VIEIRA-COELHO, M.A.**, **SOARES-DA-SILVA, P.**, Effects of tolcapone upon soluble and membrane-bound brain and liver catechol-O-methyltransferase, Brain Res. 821: 1 (1999) 69–78.

[**426**] **LEARMONTH, D.A. ET AL.**, Synthesis of 1-(3,4-dihydroxy-5-nitrophenyl)-2-phenyl-ethanone and derivatives as potent and long-acting peripheral inhibitors of catechol-O-methyltransferase, J. Med. Chem. 45: 3 (2002) 685–695.

[**427**] **ALMEIDA, L.**, **SOARES-DA-SILVA, P.**, Pharmacokinetic and pharmacodynamic profiles of BIA 3-202, a novel catechol-O-methyltransferase (COMT) inhibitor, during multiple-dose administration to healthy subjects, J. Clin. Pharmacol. 43: 12 (2003) 1350–1360.

[**428**] **ZÜRCHER, G. ET AL.**, Ro 40-7592: inhibition of COMT in rat brain and extracerebral tissues., J. Neural Transm. Suppl 32 (1990) 375–380.

[**429**] **PARADA, A. ET AL.**, BIA 3-202, a novel catechol-O-methyltransferase inhibitor, enhances the availability of L-DOPA to the brain and reduces its O-methylation, Eur. J. Pharmacol. 420: 1 (2001) 27–32.

[**430**] **NISSINEN, E. ET AL.**, Biochemical and pharmacological properties of a peripherally acting catechol-O-methyltransferase inhibitor entacapone, Naunyn. Schmiedebergs. Arch. Pharmacol. 346: 3 (1992) 262–266.

[**431**] **KAAKKOLA, S. ET AL.**, Effect of a novel catechol-O-methyltransferase inhibitor, nitecapone, on the metabolism of L-Dopa in healthy volunteers, Clin. Neuropharmacol. 13: 5 (1990) 436–447.

[**432**] **KERÄNEN, T. ET AL.**, Inhibition of soluble catechol-O-methyltransferase and single-dose pharmacokinetics after oral and intravenous administration of entacapone, Eur. J. Clin. Pharmacol. 46: 2 (1994) 151–157.

[**433**] **ALMEIDA, L.**, **SOARES-DA-SILVA, P.**, Pharmacokinetics and pharmacodynamics of BIA 3-202, a novel COMT inhibitor, during first administration to humans, Drugs R D. 4: 4 (2003) 207–217.

[**434**] **JORGA, K.M. ET AL.**, Effect of liver impairment on the pharmacokinetics of tolcapone and its metabolites, Clin. Pharmacol. Ther. 63: 6 (1998) 646–654.

[**435**] **DINGEMANSE, J. ET AL.**, Pharmacokinetic-pharmacodynamic interaction between the COMT inhibitor tolcapone and single-dose levodopa, Br. J. Clin. Pharmacol. 40: 3 (1995) 253–262.

[**436**] **ALMEIDA, L. ET AL.**, Pharmacokinetics, pharmacodynamics and tolerability of opicapone, a novel catechol-O-methyltransferase inhibitor, in healthy subjects: prediction of slow enzyme-inhibitor complex dissociation of a short-living and very long-acting inhibitor, Clin. Pharmacokinet. 52: 2 (2013) 139–151.

[**437**] **KAAKKOLA, S.**, Clinical pharmacology, therapeutic use and potential of COMT inhibitors in Parkinson's disease, Drugs. 59: 6 (2000) 1233–1250.

[**438**] **BONIFÁCIO, M.J. ET AL.**, Pharmacological profile of opicapone, a third-generation nitrocatechol catechol-O-methyl transferase inhibitor, in the rat, Br. J. Pharmacol. 172: 7 (2015) 1739–1752.

[**439**] **KISS, L.E. ET AL.**, Efficient synthesis of 2-(trifluoromethyl) nicotinic acid derivatives from simple fluorinated precursors, Org. Lett. 10: 9 (2008) 1835–1837.

[**440**] **KISS, L.E. ET AL.**, Discovery of a long-acting, peripherally selective inhibitor of catechol- O-methyltransferase, J. Med. Chem. 53: 8 (2010) 3396–3411.

[**441**] **RODRIGUES, F.B.**, **FERREIRA, J.J.**, Opicapone for the treatment of Parkinson's disease, Expert Opin. Pharmacother. 18: 4 (2017) 445–453.

[**442**] **EMA**, Ongentys - Assessment report, EMA/343011/2016. (2016).

[**443**] **ROCHA, J.F. ET AL.**, Opicapone: a short lived and very long acting novel catechol-O-methyltransferase inhibitor following multiple dose administration in healthy subjects, Br. J. Clin. Pharmacol. 76: 5 (2013) 763–775.

[**444**] **BONIFÁCIO, M.J. ET AL.**, Brain and peripheral pharmacokinetics of levodopa in the cynomolgus monkey following administration of opicapone, a third generation nitrocatechol COMT inhibitor, Neuropharmacology. 77: (2014) 334–341.

[**445**] **ROCHA, J.-F. ET AL.**, Effect of opicapone multiple-dose regimens on levodopa pharmacokinetics, Br. J. Clin. Pharmacol. 83: 3 (2017) 540–553.

[**446**] **FERREIRA, J.J. ET AL.**, Effect of opicapone on levodopa pharmacokinetics, catechol-O-methyltransferase activity and motor fluctuations in patients with Parkinson's disease, Eur. J. Neurol. 22: 5 (2015) 815–825.

[**447**] **FERREIRA, J.J. ET AL.**, Opicapone as an adjunct to levodopa in patients with Parkinson's disease and end-of-dose motor fluctuations: A randomised, double-blind, controlled trial, Lancet Neurol. 15: 2 (2016) 154–165.

[**448**] **ROCHA, J.F. ET AL.**, Effect of opicapone and entacapone upon levodopa pharmacokinetics during three daily levodopa administrations, Eur. J. Clin. Pharmacol. 70: 9 (2014) 1059–1071.

[**449**] **GERLACH, M. ET AL.**, The central catechol-O-methyltransferase inhibitor tolcapone increases striatal hydroxyl radical production in L-DOPA/carbidopa treated rats, J. Neural Transm. 108: 2 (2001) 189–204.

[**450**] **ROBINSON, R.G. ET AL.**, Characterization of non-nitrocatechol pan and isoform specific catechol-O-methyltransferase inhibitors and substrates, ACS Chem. Neurosci. 3: 2 (2012) 129–140.

[**451**] **SILVA, T. ET AL.**, Development of blood-brain barrier permeable nitrocatechol-based catechol-O-methyltransferase inhibitors with reduced potential for hepatotoxicity, J. Med. Chem. 59: 16 (2016) 7584–7597.

[**452**] **BELIAEV, A. ET AL.**, Synthesis and biological evaluation of novel, peripherally selective chromanyl imidazolethione-based inhibitors of dopamine beta-hydroxylase, J. Med. Chem. 49: 3 (2006) 1191–1197.

[**453**] **ESLER, M.**, Pathophysiology of the human sympathetic nervous system in cardiovascular diseases: the transition from mechanisms to medical management, J. Appl. Physiol. 108: 2 (2010) 227–237.

[**454**] **SOROTA, S.**, The sympathetic nervous system as a target for the treatment of hypertension and cardiometabolic diseases, J. Cardiovasc. Pharmacol. 63: 5 (2014) 466–476.

[**455**] **GRASSI, G.**, **RAM, V.S.**, Evidence for a critical role of the sympathetic nervous system in hypertension, J. Am. Soc. Hypertens. 10: 5 (2016) 457–466.

[**456**] **ESLER, M.**, **KAYE, D.**, Measurement of sympathetic nervous system activity in heart failure: the role of norepinephrine kinetics, Heart Fail. Rev. 5: 1 (2000) 17–25.

[**457**] **ESLER, M.**, The sympathetic system and hypertension, Am. J. Hypertens. 13: 3 (2000) 99S–105S.

[**458**] **GRASSI, G.**, Assessment of sympathetic cardiovascular drive in human hypertension: achievements and perspectives, Hypertension. 54: 4 (2009) 690–697.

[**459**] **ESLER, M.**, The sympathetic nervous system through the ages: from Thomas Willis to resistant hypertension, Exp. Physiol. 96: 7 (2011) 611–22.

[**460**] **STANLEY, W.C. ET AL.**, Catecholamine modulatory effects of nepicastat (RS-25560-197), a novel, potent and selective inhibitor of dopamine β-hydroxylase, Br. J. Pharmacol. 121: 8 (1997) 1803–1809.

[**461**] **GRASSI, G. ET AL.**, Essential hypertension and the sympathetic nervous system, Neurol. Sci. 29: Suppl. 1 (2008) 33–36.

[**462**] **SCHLAICH, M.P.**, What we need to know about renal nerve ablation for treatment of hypertension and other states of sympathetic overactivity, Am. J. Physiol. - Ren. Physiol. 311: 6 (2016) F1267–F1270.

[**463**] **PFEFFER, M.A.**, **STEVENSON, L.W.**, Beta-adrenergic blockers and survival in heart failure, N. Engl. J. Med. 334: 21 (1996) 1396–1402.

[**464**] **ROCHA, J.F. ET AL.**, Single-dose tolerability, pharmacokinetics, and pharmacodynamics of etamicastat (BIA 5-453), a new dopamine beta-hydroxylase inhibitor, in healthy subjects, J. Clin. Pharmacol. 52: 2 (2012) 156–170.

[**465**] **ALMEIDA, L. ET AL.**, Etamicastat, a novel dopamine beta-hydroxylase inhibitor: tolerability, pharmacokinetics, and pharmacodynamics in patients with hypertension, Clin. Ther. 35: 12 (2013) 1983–1996.

[**466**] **BELIAEV, A. ET AL.**, Dopamine beta-monooxygenase: mechanism, substrates and inhibitors, Curr. Enzym. Inhib. 5: 1 (2009) 27–43.

[**467**] **VAZ-DA-SILVA, M. ET AL.**, Effect of food on the pharmacokinetic profile of etamicastat (BIA 5-453), Drugs R.D. 11: 2 (2011) 127–136.

[**468**] **SABBAH, H.N. ET AL.**, Effects of dopamine beta-hydroxylase inhibition with nepicastat on the progression of left ventricular dysfunction and remodeling in dogs with chronic heart failure, Circulation. 102: 1 (2000) 1990–1995.

[**469**] **NUNES, T. ET AL.**, Pharmacokinetics and tolerability of etamicastat following single and repeated administration in elderly versus young healthy male subjects: an open-label, single-center, parallel-group study, Clin. Ther. 33: 6 (2011) 776–791.

[**470**] **LOUREIRO, A.I. ET AL.**, Role of P-glycoprotein and permeability upon the brain distribution and pharmacodynamics of etamicastat: a comparison with nepicastat, Xenobiotica. 45: 9 (2015) 828–839.

[**471**] **LOUREIRO, A.I. ET AL.**, Etamicastat, a new dopamine beta-hydroxylase inhibitor, pharmacodynamics and metabolism in rat, Eur. J. Pharmacol. 740: (2014) 285–294.

[**472**] **IGREJA, B. ET AL.**, Blood pressure-decreasing effect of etamicastat alone and in combination with antihypertensive drugs in the spontaneously hypertensive rat, Hypertens. Res. 38: 1 (2014) 30–38.

[**473**] **PIRES, N.M. ET AL.**, Blood pressure decrease in spontaneously hypertensive rats folowing renal denervation or dopamine β-hydroxylase inhibition with etamicastat, Hypertens. Res. 38: 9 (2015) 605–612.

[**474**] **LOUREIRO, A.I. ET AL.**, Human disposition, metabolism and excretion of etamicastat, a reversible, peripherally selective dopamine beta-hydroxylase inhibitor, Br. J. Clin. Pharmacol. 77: 6 (2014) 1017–1026.

[**475**] **IGREJA, B. ET AL.**, Abstract 291: Antihypertensive effect of BIA 5-1058 a new selective peripheral dopamine beta-hydroxylase inhibitor, Hypertension. 60: A291 (2012) 1.

[**476**] **BONIFÁCIO, M.J. ET AL.**, Abstract 279P: BIA 5-1058 is a new noncompetitive dopamine-β-hydroxylase inhibitor, Br. Pharmacol. Soc. 10: 3 1.

[**477**] **IGREJA, B. ET AL.**, Abstract 532: BIA 5-1058, beyond blood pressure, improves cardiometabolism and decrease end-organ damage, Hypertension. 62: A532 (2013) 1.

[**478**] **MEGIDDO, I. ET AL.**, Health and economic benefits of public financing of epilepsy treatment in India: An agent-based simulation model, Epilepsia. 57: 3 (2016) 464–474.

[**479**] **FISHER, R.S. ET AL.**, ILAE Official Report: A practical clinical definition of epilepsy, Epilepsia. 55: 4 (2014) 475–482.

[**480**] **GUERRINI, R.**, **BARBA, C.**, Chapter 7. Classification, clinical symptoms, and syndromes, in: S. Shorvon, R. Guerrini, M. Cook, S.D. Lhatoo (Eds.), Oxford Textb. Epilepsy Epileptic Seizures, Oxford University Press, 2013: pp. 71–80.

[**481**] **FISHER, R.S.**, The new classification of seizures by the international league against epilepsy 2017, Curr. Neurol. Neurosci. Rep. 17: 6 (2017) 1–6.

[**482**] **WIEBE, S.**, **JETTE, N.**, Pharmacoresistance and the role of surgery in difficult to treat epilepsy, Nat. Rev. Neurol. 8: 12 (2012) 669–677.

[**483**] **GERLACH, A.C.**, **KRAJEWSKI, J.L.**, Antiepileptic drug discovery and development: what have we learned and where are we going?, Pharmaceuticals. 3: 9 (2010) 2884–2899.

[**484**] **BRODIE, M.J.**, Antiepileptic drug therapy the story so far, Seizure. 19: 10 (2010) 650–655.

[**485**] **FRENCH, J.A.**, **GAZZOLA, D.M.**, New generation antiepileptic drugs: what do they offer in terms of improved tolerability and safety?, Ther Adv Drug Saf. 2: 4 (2011) 141–158.

[**486**] **BRITTON, J.W.**, **CUNNINGHAM, J.**, Chapter 10. Antiepileptic drugs: pharmacology, epilepsy indications, and selection, in: G.D. Cascino, J.I. Sirven (Eds.), Adult Epilepsy, John Wiley & Sons, Inc., 2011: pp. 131–169.

[**487**] **BIALER, M.**, **WHITE, H.S.**, Key factors in the discovery and development of new antiepileptic drugs, Nat Rev Drug Discov. 9: 1 (2010) 68–82.

[**488**] **ALVES, G. ET AL.**, Disposition of eslicarbazepine acetate in the mouse after oral administration, Fundam. Clin. Pharmacol. 22: 5 (2008) 529–536.

[**489**] **BIALER, M.**, **ELGER, C.**, Chapter 33. Eslicarbazepine acetate, in: S. Shorvon, E. Perucca, J. Engel (Eds.), Treat. Epilepsy, John Wiley & Sons, Inc., 2016: pp. 447–460.

[**490**] **BIALER, M.**, **SOARES-DA-SILVA, P.**, Pharmacokinetics and drug interactions of eslicarbazepine acetate, Epilepsia. 53: 6 (2012) 935–946.

[**491**] **SOARES-DA-SILVA, P. ET AL.**, Eslicarbazepine acetate for the treatment of focal epilepsy: an update on its proposed mechanisms of action, Pharma Res. Perspect. 3: 2 (2015) 1–21.

[**492**] **ALMEIDA, L. ET AL.**, Single-dose and steady-state pharmacokinetics of eslicarbazepine acetate (BIA 2-093) in healthy elderly and young subjects, J. Clin. Pharmacol. 45: 9 (2005) 1062–1066.

[**493**] **ALVES, G. ET AL.**, Stereoselective disposition of S- and R-licarbazepine in mice, Chirality. 20: 6 (2008) 796–804.

[**494**] **FORTUNA, A. ET AL.**, Pharmacokinetics, brain distribution and plasma protein binding of carbamazepine and nine derivatives: New set of data for predictive in silico ADME models, Epilepsy Res. 107: 1–2 (2013) 37–50.

[**495**] **ALMEIDA, L. ET AL.**, Chapter 38. Eslicarbazepine acetate, in: S. Shorvon, E. Perucca, J. Engel (Eds.), Treat. Epilepsy, Blackwell Publishing, 2009: pp. 485–498.

[**496**] **REMY, S.**, **BECK, H.**, Molecular and cellular mechanisms of pharmacoresistance in epilepsy, Brain. 129: 1 (2006) 18–35.

[**497**] **DOESER, A. ET AL.**, Targeting pharmacoresistant epilepsy and epileptogenesis with a dual-purpose antiepileptic drug, Brain. 138: Pt 2 (2015) 371–387.

[**498**] **PARDRIDGE, W.M.**, The blood-brain barrier: bottleneck in brain drug development., NeuroRx. 2: 1 (2005) 3–14.

[**499**] **OTTAVIANI, G. ET AL.**, Parallel artificial membrane permeability assay: a new membrane for the fast prediction of passive human skin permeability, J. Med. Chem. 49: 13 (2006) 3948–3954.

[**500**] **SINKÓ, B. ET AL.**, Skin-PAMPA: a new method for fast prediction of skin penetration, Eur. J. Pharm. Sci. 45: 5 (2012) 698–707.

[**501**] **VUCICEVIC, J. ET AL.**, Prediction of blood–brain barrier permeation of a-adrenergic and imidazoline receptor ligands using PAMPA technique and quantitative-structure permeability relationship analysis, Eur. J. Pharm. Sci. 68: (2015) 94–105.

[**502**] **RANKOVIC, Z.**, CNS drug design: balancing physicochemical properties for optimal brain exposure, J. Med. Chem. 58: 6 (2015) 2584–2608.

[**503**] **ABBOTT, S.K. ET AL.**, An improved high-throughput lipid extraction method for the analysis of human brain lipids, Lipids. 48: 3 (2013) 307–318.

[**504**] **FOLCH, J. ET AL.**, A simple method for the isolation and purification of total lipids from animal tissues, J. Biol. Chem. 226: 1 (1957) 497–509.

[**505**] **MITCHELL, T.W.**, Tracking the glycerophospholipid distribution of docosahexaenoic acid by shotgun lipidomics, Methods Mol. Biol. 579: (2009) 19–31.

[**506**] **ROUSER, G. ET AL.**, Two dimensional thin layer chromatographic separation of polar lipids and determination of phospholipids by phosphorus analysis of spots, Lipids. 5: 5 (1970) 494–496.

[**507**] **FORTUNA, A. ET AL.**, Optimization of a parallel artificial membrane permeability assay for the fast and simultaneous prediction of human intestinal absorption and plasma protein binding of drug candidates: application to dibenz[b,f]azepine-5-carboxamide derivatives, J. Pharm. Sci. 101: 2 (2012) 530–540.

[**508**] **SUGANO, K. ET AL.**, High throughput prediction of oral absorption: improvement of the composition of the lipid solution used in parallel artificial membrane permeation assay, J. Biomol. Screen. 6: 3 (2001) 189–196.

[**509**] **GHOSE, A.K. ET AL.**, Knowledge-based, central nervous system (CNS) lead selection and lead optimization for CNS drug discovery, ACS Chem. Neurosci. 3: 1 (2012) 50–68.

[**510**] **KARELSON, M. ET AL.**, Correlation of blood-brain penetration and human serum albumin binding with theoretical descriptors, Arkivoc. 2008: 16 (2008) 38–60.

[**511**] **NAGPAL, K. ET AL.**, Drug targeting to brain: a systematic approach to study the factors, parameters and approaches for prediction of permeability of drugs across BBB, Expert Opin. Drug Deliv. 10: 7 (2013) 927–955.

[**512**] **PAJOUHESH, H.**, **LENZ, G.R.**, Medicinal chemical properties of successful central nervous system drugs, NeuroRx. 2: 4 (2005) 541–553.

[**513**] **WAGER, T.T. ET AL.**, Defining desirable central nervous system drug space through the alignment of molecular properties, in vitro ADME, and safety attributes, ACS Chem. Neurosci. 1: 6 (2010) 420–434.

[**514**] **WAGER, T.T. ET AL.**, Moving beyond rules: the development of a central nervous system multiparameter optimization (CNS MPO) approach to enable alignment of druglike properties, ACS Chem. Neurosci. 1: 6 (2010) 435–449.

[**515**] **BENET, L.Z. ET AL.**, BDDCS applied to over 900 drugs, AAPS J. 13: 4 (2011) 519–547.

[**516**] **ÖSTERBERG, T. ET AL.**, Chromatographic retention of drug molecules on immobilised liposomes prepared from egg phospholipids and from chemically pure phospholipids, Eur. J. Pharm. Sci. 12: 4 (2001) 427–439.

[**517**] **AVDEEF, A.**, Absorption and drug development: solubility, permeability, and charge state, first ed., John Wiley & Sons, Hoboken, New Jersey, 2003.

[**518**] **ROSE, K. ET AL.**, Modeling blood-brain barrier partitioning using the electrotopological state, J. Chem. Inf. Comput. Sci. 42: 3 (2002) 651–666.

[**519**] **CHEN, H. ET AL.**, Chapter 9. In silico tools for predicting brain exposure of drugs, in: L. Di, E.H. Kerns (Eds.), Blood–Brain Barrier Drug Discov., John Wiley & Sons, Inc., 2015: pp. 169–187.

[**520**] **MAHAR DOAN, K.M. ET AL.**, Passive permeability and P-glycoprotein-mediated efflux differentiate central nervous system (CNS) and non-CNS marketed drugs, J. Pharmacol. Exp. Ther. 303: 3 (2002) 1029–1037.

[**521**] **KERNS, E.H. ET AL.**, Combined application of parallel artificial membrane permeability assay and Caco-2 permeability assays in drug discovery, J. Pharm. Sci. 93: 6 (2004) 1440–1453.

[**522**] **REICHEL, A.**, The role of blood-brain barrier studies in the pharmaceutical industry, Curr. Drug Metab. 7: 2 (2006) 183–203.

[**523**] **HITCHCOCK, S.A.**, Structural modifications that alter the P-glycoprotein efflux properties of compounds, J. Med. Chem. 55: 11 (2012) 4877–4895.

[**524**] **KELDER, J. ET AL.**, Polar molecular surface as a dominating determinant for oral absorption and brain penetration of drugs, Pharm. Res. 16: 10 (1999) 1514–1519.

[**525**] **WATERBEEMD, H. VAN DE ET AL.**, Estimation of blood-brain barrier crossing of drugs using molecular size and shape, and H-bonding descriptors, J. Drug Target. 6: 2 (1998) 151–165.

[**526**] **WARING, M.J.**, Defining optimum lipophilicity and molecular weight ranges for drug candidates - molecular weight dependent lower log D limits based on permeability, Bioorganic Med. Chem. Lett. 19: 10 (2009) 2844–2851.

[**527**] **PALMER, A.M.**, **ALAVIJEH, M.S.**, Overview of experimental models of the blood-brain barrier in CNS drug discovery, Curr. Protoc. Pharmacol. 1: Suppl.62 (2013) 1–30.

[**528**] **CERAVOLO, R. ET AL.**, 18F-dopa PET evidence that tolcapone acts as a central COMT inhibitor in Parkinson's disease, Synapse. 43: 3 (2002) 201–207.

[**529**] **FORSBERG, M. ET AL.**, Pharmacokinetics and pharmacodynamics of entacapone and tolcapone after acute and repeated administration: a comparative study in the rat, J. Pharmacol. Exp. Ther. 304: 2 (2003) 498–506.

[**530**] **NAPOLITANO, A. ET AL.**, Effects of peripheral and central catechol-O-methyltransferase inhibition on striatal extracellular levels of dopamine: a microdialysis study in freely moving rats, Park. Relat. Disord. 9: 3 (2003) 145–150.

[**531**] **ZHAO, Y.H. ET AL.**, Predicting penetration across the blood-brain barrier from simple descriptors and fragmentation schemes, J. Chem. Inf. Model. 47: 1 (2007) 170–175.

[**532**] **LEARMONTH, D.A.**, **FREITAS, A.P.**, Chemical synthesis and characterization of conjugates of a novel catechol-O-methyltransferase inhibitor, Bioconjug. Chem. 13: 5 (2002) 1112–1118.

[**533**] **ASHRAF, T. ET AL.**, Chapter 3. Functional expression of drug transporters in glial cells: potential role on drug delivery to the CNS, in: T.P. Davis (Ed.), Pharmacol. Blood Brain Barrier Target. CNS Disord., Elsevier Inc., 2014: pp. 45–111.

[**534**] **SANCHEZ-COVARRUBIAS, L. ET AL.**, Transporters at CNS barrier sites: obstacles or opportunities for drug delivery?, Curr. Pharm. Des. 20: 10 (2014) 1422–1449.

[**535**] **LOSCHER, W. ET AL.**, Blood-brain barrier active efflux transporters: ATP-binding cassette gene family, NeuroRx. 2: 1 (2005) 86–98.

[**536**] **JULIANO, R.L.**, **LING, V.**, A surface glycoprotein modulating drug permeability in Chinese hamster ovary cell mutants, BBA - Biomembr. 455: 1 (1976) 152–162.

[**537**] **BUGDE, P. ET AL.**, The therapeutic potential of targeting ABC transporters to combat multi-drug resistance, Expert Opin. Ther. Targets. 21: 5 (2017) 511–530.

[**538**] **SHAROM, F.J.**, Complex interplay between the P-glycoprotein multidrug efflux pump and the membrane: its role in modulating protein function, Front. Oncol. 4: 41 (2014) 1–19.

[**539**] **HO, G.T. ET AL.**, Multidrug resistance 1 gene (P-glycoprotein 170): an important determinant in gastrointestinal disease?, Gut. 52: 5 (2003) 759–766.

[**540**] **PARDRIDGE, W.M. ET AL.**, Brain microvascular and astrocyte localization of P-glycoprotein, J. Neurochem. 68: 3 (1997) 1278–1285.

[**541**] **SCHLACHETZKI, F.**, **PARDRIDGE, W.M.**, P-glycoprotein and caveolin-1alpha in endothelium and astrocytes of primate brain, Neuroreport. 14: 16 (2003) 2041–2046.

[**542**] **VOLK, H. ET AL.**, Immunohistochemical localization of P-glycoprotein in rat brain and detection of its increased expression by seizures are sensitive to fixation and staining variables, J. Histochem. Cytochem. 53: 4 (2005) 517–531.

[**543**] **BEREZOWSKI, V. ET AL.**, Contribution of glial cells and pericytes to the mRNA profiles of P-glycoprotein and multidrug resistance-associated proteins in an in vitro model of the blood-brain barrier, Brain Res. 1018: 1 (2004) 1–9.

[**544**] **LEE, G. ET AL.**, Functional expression of P-glycoprotein in rat brain microglia, J. Pharmacol. Exp. Ther. 299: 1 (2001) 204–212.

[**545**] **RAJAGOPAL, A.**, **SIMON, S.M.**, Subcellular localization and activity of multidrug resistance proteins, Mol. Biol. Cell. 14: 8 (2003) 3389–3399.

[**546**] **CHEN, Z. ET AL.**, Mammalian drug efflux transporters of the ATP binding cassette (ABC) family in multidrug resistance: a review of the past decade, Cancer Lett. 370: 1 (2016) 153–164.

[**547**] **ALLER, S.G. ET AL.**, Structures of P-glycoproteins reveals a molecular basis for poly-specific drug binding, Science (80-.). 323: 5922 (2009) 1718–1722.

[**548**] **SCHINKEL, A.H.**, **JONKER, J.W.**, Mammalian drug efflux transporters of the ATP binding cassette (ABC) family: an overview, Adv. Drug Deliv. Rev. 55: 1 (2003) 3–29.

[**549**] **DOMICEVICA, L.**, **BIGGIN, P.C.**, Homology modelling of human P-glycoprotein, Biochem Soc Trans. 43: 5 (2015) 952–958.

[**550**] **CHEN, L. ET AL.**, Computational models for predicting substrates or inhibitors of P-glycoprotein, Drug Discov. Today. 17: 7–8 (2012) 343–351.

[**551**] **PADOWSKI, J.M.**, **POLLACK, G.M.**, Pharmacokinetic and pharmacodynamic implications of P-glycoprotein modulation, Methods Mol. Biol. 596: (2010) 359–384.

[**552**] **SHAPIRO, A.B.**, **LING, V.**, Positively Cooperative Sites for Drug Transport by P-Glycoprotein with Distinct Drug Specificities, Eur J Biochem. 250: 1 (1997) 130–137.

[**553**] **FERREIRA, R.J. ET AL.**, Molecular docking characterizes substrate-binding sites and efflux modulation mechanisms within P-glycoprotein, J. Chem. Inf. Model. 53: 7 (2013) 1747–1760.

[**554**] **SHAROM, F.J.**, The P-glycoprotein multidrug transporter, Essays Biochem. 50: 1 (2011) 161–178.

[**555**] **STAUD, F. ET AL.**, Expression and function of P-glycoprotein in normal tissues: effect on pharmacokinetics, Methods Mol. Biol. 596: (2010) 199–222.

[**556**] **VARMA, M.V.S. ET AL.**, P-glycoprotein inhibitors and their screening: a perspective from bioavailability enhancement, Pharmacol. Res. 48: 4 (2003) 347–359.

[**557**] **PALMEIRA, A. ET AL.**, Three decades of P-gp inhibitors: skimming through several generations and scaffolds, Curr Med Chem. 19: 13 (2012) 1946–2025.

[**558**] **FOOD AND DRUG ADMINISTRATION**, Guidance for industry: drug interaction studies - study design, data analysis, implications for dosing, and labeling recommendations, February (2012) 1–79.

[**559**] **GAMEIRO, M. ET AL.**, Cellular models and in vitro assays for the screening of modulators of P-gp, MRP1 and BCRP, Molecules. 22: 4 (2017) 1–48.

[**560**] **KWAK, J.O. ET AL.**, Selective inhibition of MDR1 (ABCB1) by HM30181 increases oral bioavailability and therapeutic efficacy of paclitaxel, Eur. J. Pharmacol. 627: 1–3 (2010) 92–98.

[**561**] **FOX, E.**, **BATES, S.E.**, Tariquidar (XR9576): a P-glycoprotein drug efflux pump inhibitor, Expert Rev. Anticancer Ther. 7: 4 (2007) 447–459.

[**562**] **SILVA, R. ET AL.**, Modulation of P-glycoprotein efflux pump: induction and activation as a therapeutic strategy, Pharmacol. Ther. 149: (2015) 1–123.

[**563**] **KANNAN, P. ET AL.**, The “specific” P-glycoprotein inhibitor tariquidar is also a substrate and an inhibitor for Breast Cancer Resistance Protein (BCRP/ABCG2), ACS Chem. Neurosci. 2: 2 (2011) 82–89.

[**564**] **WEIDNER, L.D. ET AL.**, Tariquidar is an inhibitor and not a substrate of human and mouse P-glycoprotein, Drug Metab. Dispos. 44: 2 (2016) 275–282.

[**565**] **BAUER, M. ET AL.**, Interaction of 11C-tariquidar and 11C-elacridar with P-glycoprotein and breast cancer resistance protein at the human blood-brain barrier, J. Nucl. Med. 54: 8 (2013) 1–19.

[**566**] **LI, X.Q. ET AL.**, Reversal of P-gp and BCRP-mediated MDR by tariquidar derivatives, Eur. J. Med. Chem. 101: (2015) 560–572.

[**567**] **SHEPARD, R.L. ET AL.**, Modulation of P-glycoprotein but not MRP1- or BCRP-mediated drug resistance by LY335979, Int. J. Cancer. 103: 1 (2003) 121–125.

[**568**] **DASH, R.P. ET AL.**, Therapeutic potential and utility of elacridar with respect to P-glycoprotein inhibition: an insight from the published in vitro, preclinical and clinical studies, Eur. J. Drug Metab. Pharmacokinet. (2017).

[**569**] **KRUIJTZER, C.M.F. ET AL.**, Increased oral bioavailability of topotecan in combination with the breast cancer resistance protein and P-glycoprotein inhibitor GF120918, J. Clin. Oncol. 20: 13 (2002) 2943–2950.

[**570**] **SANE, R. ET AL.**, Brain distribution and bioavailability of elacridar after different routes of administration in the mouse, Drug Metab. Dispos. 40: 8 (2012) 1612–1619.

[**571**] **TOURNIER, N. ET AL.**, Strategies to inhibit ABCB1- and ABCG2-mediated efflux transport of erlotinib at the blood–brain barrier: a PET study on non-human primates, J. Nucl. Med. 58: 1 (2017) 117–122.

[**572**] **WARD, K.W.**, **AZZARANO, L.M.**, Preclinical pharmacokinetic properties of the P-glycoprotein inhibitor GF120918A in the mouse, rat, dog, and monkey, J. Pharmacol. Exp. Ther. 310: 2 (2004) 703–709.

[**573**] **MONTESINOS, R.N. ET AL.**, Co-administration of P-glycoprotein modulators on loperamide pharmacokinetics and brain distribution, Drug Metab. Dispos. 42: 4 (2014) 700–706.

[**574**] **MONTESINOS, R.N. ET AL.**, Liposomes co-loaded with elacridar and tariquidar to modulate the P-glycoprotein at the blood-brain barrier, Mol. Pharm. 12: 11 (2015) 3829–3838.

[**575**] **REDDY, D.R. ET AL.**, Natural flavonoids silymarin and quercetin improve the brain distribution of co‐administered P‐gp substrate drugs, Springerplus. 5: 1 (2016) 1–9.

[**576**] **LIU, L. ET AL.**, Modulation of P-glycoprotein at the human blood-brain barrier by quinidine or rifampin treatment: A positron emission tomography imaging study, Drug Metab. Dispos. 43: 11 (2015) 1795–1804.

[**577**] **WOLKING, S. ET AL.**, Impact of genetic polymorphisms of ABCB1 (MDR1, P-glycoprotein) on drug disposition and potential clinical implications: update of the literature, Clin. Pharmacokinet. 54: 7 (2015) 709–735.

[**578**] **KALVASS, J.C. ET AL.**, Why clinical modulation of efflux transport at the human blood-brain barrier is unlikely: the ITC evidence-based position, Clin. Pharmacol. Ther. 94: 1 (2013) 80–94.

[**579**] **DOYLE, L.A. ET AL.**, A multidrug resistance transporter from human MCF-7 breast cancer cells, Proc Natl Acad Sci U S A. 95: 26 (1998) 15665–15670.

[**580**] **XIA, C.Q. ET AL.**, Breast cancer resistance protein in pharmacokinetics and drug-drug interactions, Expert Opin. Drug Metab. Toxicol. 1: 4 (2005) 595–611.

[**581**] **MAO, Q.**, **UNADKAT, J.D.**, Role of the breast cancer resistance protein (ABCG2) in drug transport, AAPS J. 7: 1 (2015) 118–133.

[**582**] **DOYLE, L.A.**, **ROSS, D.D.**, Multidrug resistance mediated by the breast cancer resistance protein BCRP (ABCG2), Oncogene. 22: 47 (2003) 7340–7358.

[**583**] **ZHANGLIN, N. ET AL.**, Structure and function of the human breast cancer resistance protein (BCRP/ABCG2), Curr. Drug Metab. 11: 7 (2010) 603–617.

[**584**] **HORSEY, A.J. ET AL.**, The multidrug transporter ABCG2: still more questions than answers, Biochem. Soc. Trans. 44: 3 (2016) 824–830.

[**585**] **ROSENBERG, M.F. ET AL.**, Three-dimensional structure of the human breast cancer resistance protein (BCRP/ABCG2) in an inward-facing conformation, Acta Crystallogr D Biol Crystallogr. 71: 8 (2015) 1725–1735.

[**586**] **ITO, K. ET AL.**, Quantitative membrane protein expression at the blood-brain barrier of adult and younger cynomolgus monkeys, J. Pharm. Sci. 200: 9 (2011) 3939–3950.

[**587**] **AGARWAL, S. ET AL.**, Quantitative proteomics of transporter expression in brain capillary endothelial cells isolated from P-glycoprotein (P-gp), breast cancer resistance protein (Bcrp), and P-gp/Bcrp knockout mice, Drug Metab. Dispos. 40: 6 (2012) 1164–1169.

[**588**] **JANI, M. ET AL.**, Structure and function of BCRP, a broad specificity transporter of xenobiotics and endobiotics, Arch. Toxicol. 88: 6 (2014) 1205–1248.

[**589**] **JONKER, J.W. ET AL.**, The breast cancer resistance protein BCRP (ABCG2) concentrates drugs and carcinogenic xenotoxins into milk, Nat. Med. 11: 2 (2005) 127–129.

[**590**] **VAN HERWAARDEN, A.E. ET AL.**, Multidrug transporter ABCG2/breast cancer resistance protein secretes riboflavin (vitamin B2) into milk, Mol. Cell. Biol. 27: 4 (2007) 1247–1253.

[**591**] **WIESE, M.**, BCRP/ABCG2 inhibitors: a patent review (2009 - present), Expert Opin. Ther. Pat. 25: 11 (2015) 1229–1237.

[**592**] **HASLAM, I.S. ET AL.**, Intestinal ciprofloxacin efflux: the role of breast cancer resistance protein (ABCG2), Drug Metab. Dispos. 39: 12 (2011) 2321–2328.

[**593**] **AN, G.**, **MORRIS, M.E.**, The sulfated conjugate of biochanin A is a substrate of breast cancer resistant protein (ABCG2), Biopharm. Drug Dispos. 32: 8 (2011) 446–457.

[**594**] **CLARK, R. ET AL.**, Multiple drug binding sites on the R482G isoform of the ABCG2 transporter, Br. J. Pharmacol. 149: 5 (2006) 506–515.

[**595**] **GIRI, N. ET AL.**, Substrate-dependent breast cancer resistance protein (Bcrp1/Abcg2)-mediated interactions: consideration of multiple binding sites in in vitro assay design, Drug Metab. Dispos. 37: 3 (2009) 560–570.

[**596**] **PEÑA-SOLÓRZANO, D. ET AL.**, ABCG2/BCRP: specific and nonspecific modulators, Med. Res. Rev. (2016) 1–64.

[**597**] **KÖHLER, S.C.**, **WIESE, M.**, HM30181 derivatives as novel potent and selective inhibitors of the breast cancer resistance protein (BCRP/ABCG2), J. Med. Chem. 58: 9 (2015) 3910–3921.

[**598**] **BARRERA, B. ET AL.**, The anthelmintic triclabendazole and its metabolites inhibit the membrane transporter ABCG2/BCRP, Antimicrob. Agents Chemother. 56: 7 (2012) 3535–3543.

[**599**] **WEIDNER, L.D. ET AL.**, The inhibitor Ko143 is not specific for ABCG2, J. Pharmacol. Exp. Ther. 354: 3 (2015) 384–393.

[**600**] **KÜHNLE, M. ET AL.**, Potent and selective inhibitors of breast cancer resistance protein (ABCG2) derived from the P-glycoprotein (ABCB1) modulator tariquidar, J. Med. Chem. 52: 4 (2009) 1190–1197.

[**601**] **HUANG, S.-M. ET AL.**, The International Transporter Consortium: a collaborative group of scientists from academia, industry, and the FDA, Clin. Pharmacol. Ther. 87: 1 (2010) 32–36.

[**602**] **GIACOMINI, K.M. ET AL.**, International Transporter Consortium commentary on clinically important transporter polymorphisms, Clin. Pharmacol. Ther. 94: 1 (2013) 23–26.

[**603**] **BAUER, M. ET AL.**, Pilot PET study to assess the functional interplay between ABCB1 and ABCG2 at the human blood–brain barrier, Clin. Pharmacol. Ther. 100: 2 (2016) 131–141.

[**604**] **REICHEL, A.**, Chapter 12. Integrated approach to optimizing CNS penetration in drug discovery: from the old to the new paradigm and assessment of drug–transporter interactions, in: M. Hammarlund-Udenaes, E.C.M. de Lange, R.G. Thorne (Eds.), Drug Deliv. to Brain Physiol. Concepts, Methodol. Approaches, Springer-Verlag New York, 2014: pp. 339–374.

[**605**] **EUROPEAN MEDICINES AGENCY**, Guideline on the investigation of drug interactions: CPMP/EWP/560/95/Rev. 1 Corr. 2**, June (2012) 1–59.

[**606**] **LEE, C.A. ET AL.**, Breast cancer resistance protein (ABCG2) in clinical pharmacokinetics and drug interactions: practical recommendations for clinical victim and perpetrator drug-drug interaction study design, Drug Metab. Dispos. 43: 4 (2015) 490–509.

[**607**] **SADEQUE, A.J.M. ET AL.**, Increased drug delivery to the brain by P-glycoprotein inhibition, Clin. Pharmacol. Ther. 68: 3 (2000) 231–237.

[**608**] **SASONGKO, L. ET AL.**, Imaging P-glycoprotein transport activity at the human blood-brain barrier with positron emission tomography, Clin. Pharmacol. Ther. 77: 6 (2005) 503–514.

[**609**] **MUZI, M. ET AL.**, Imaging of cyclosporine inhibition of P-glycoprotein activity using 11C-verapamil in the brain: studies of healthy humans, J. Nucl. Med. 50: 8 (2009) 1267–1275.

[**610**] **BROUWER, K.L.R. ET AL.**, In vitro methods to support transporter evaluation in drug discovery and development, Clin. Pharmacol. Ther. 94: 1 (2013) 95–112.

[**611**] **VOLPE, D.A.**, Transporter assays as useful in vitro tools in drug discovery and development, Expert Opin. Drug Discov. 11: 1 (2016) 91–103.

[**612**] **POIRIER, A. ET AL.**, The need for human breast cancer resistance protein substrate and inhibition evaluation in drug discovery and development: why, when, and how?, Drug Metab. Dispos. 42: 9 (2014) 1466–1477.

[**613**] **HERÉDI-SZABÓ, K. ET AL.**, A P-gp vesicular transport inhibition assay - optimization and validation for drug-drug interaction testing, Eur. J. Pharm. Sci. 49: 4 (2013) 773–781.

[**614**] **ELSBY, R. ET AL.**, Validation of membrane vesicle-based breast cancer resistance protein and multidrug resistance protein 2 assays to assess drug transport and the potential for drug-drug interaction to support regulatory submissions, Xenobiotica. 41: 9 (2011) 764–783.

[**615**] **IOJA, E. ET AL.**, Chapter 6. Membrane and dye efflux assays to detect and characterize the interaction of drugs with ABC transporters, in: K. Tihanyi, M. Vastag (Eds.), Solubility, Deliv. ADME Probl. Drugs Drug Candidates, Bentham Science Publishers, 2011: pp. 102–116.

[**616**] **FENG, B. ET AL.**, In vitro P-glycoprotein assays to predict the in vivo interactions of P-glycoprotein with drugs in the central nervous system, Drug Metab. Dispos. 36: 2 (2008) 268–275.

[**617**] **GIACOMINI, K.M. ET AL.**, Membrane transporters in drug development, Nat. Rev. Drug Discov. 9: 3 (2010) 215–236.

[**618**] **HAMMARLUND-UDENAES, M. ET AL.**, Preface, in: M. Hammarlund-Udenaes, E.C.M. de Lange, R.G. Thorne (Eds.), Drug Deliv. to Brain Physiol. Concepts, Methodol. Approaches, Springer-Verlag New York, 2014: pp. V–IX.

[**619**] **COLE, S. ET AL.**, Full efficacy with no CNS side-effects: unachievable panacea or reality? DMPK considerations in design of drugs with limited brain penetration, Xenobiotica. 42: 1 (2012) 11–27.

[**620**] **BART, J. ET AL.**, The distribution of drug-efflux pumps, P-gp, BCRP, MRP1 and MRP2, in the normal blood-testis barrier and in primary testicular tumours, Eur. J. Cancer. 40: 14 (2004) 2064–2070.

[**621**] **EDWARDS, J.E. ET AL.**, Role of P-glycoprotein in distribution of nelfinavir across the blood-mammary tissue barrier and blood-brain barrier, Antimicrob. Agents Chemother. 49: 4 (2005) 1626–1628.

[**622**] **MEISSNER, K. ET AL.**, The ATP-binding cassette transporter ABCG2 (BCRP), a marker for side population stem cells, is expressed in human heart, J. Histochem. Cytochem. 54: 2 (2006) 215–221.

[**623**] **RÖMERMANN, K. ET AL.**, The antiepileptic drug lamotrigine is a substrate of mouse and human breast cancer resistance protein (ABCG2), Neuropharmacology. 93: (2015) 7–14.

[**624**] **KAMIIE, J. ET AL.**, Quantitative atlas of membrane transporter proteins: Development and application of a highly sensitive simultaneous LC/MS/MS method combined with novel in-silico peptide selection criteria, Pharm. Res. 25: 6 (2008) 1469–1483.

[**625**] **BONIFÁCIO, M.J. ET AL.**, Characterization of the interaction of the novel antihypertensive etamicastat with human dopamine-β-hydroxylase: comparison with nepicastat, Eur. J. Pharmacol. 751: (2015) 50–58.

[**626**] **NAVARRO, C. ET AL.**, Influence of polyunsaturated fatty acids on cortisol transport through MDCK and MDCK-MDR1 cells as blood-brain barrier in vitro model, Eur. J. Pharm. Sci. 42: 3 (2011) 290–299.

[**627**] **CHEN, Z.-Z. ET AL.**, Influence of borneol and muscone on geniposide transport through MDCK and MDCK-MDR1 cells as blood-brain barrier in vitro model, Int. J. Pharm. 456: 1 (2013) 1–7.

[**628**] **HU, H.H. ET AL.**, Evaluation of blood-brain barrier and blood-cerebrospinal fluid barrier permeability of 2-phenoxy-indan-1-one derivatives using in vitro cell models, Int. J. Pharm. 460: 1–2 (2014) 101–107.

[**629**] **LI, Y. ET AL.**, Role of human breast cancer related protein versus P-glycoprotein as an efflux transporter for benzylpenicillin: potential importance at the blood-brain barrier, PLoS One. 11: 6 (2016) 1–13.

[**630**] **BRAUN, A. ET AL.**, Cell cultures as tools in biopharmacy, Eur. J. Pharm. Sci. 11: 2 (2000) 51–60.

[**631**] **QUAN, Y. ET AL.**, Expression profile of drug and nutrient absorption related genes in Madin-Darby Canine Kidney (MDCK) cells grown under differentiation conditions, Pharmaceutics. 4: 2 (2012) 314–333.

[**632**] **LI, L. ET AL.**, Cyclosporin A affects the bioavailability of ginkgolic acids via inhibition of P-gp and BCRP, Eur. J. Pharm. Biopharm. 88: 3 (2014) 759–767.

[**633**] **HUBATSCH, I. ET AL.**, Determination of drug permeability and prediction of drug absorption in Caco-2 monolayers, Nat. Protoc. 2: 9 (2007) 2111–2119.

[**634**] **GONÇALVES, D. ET AL.**, An HPLC-DAD method for the simultaneous quantification of opicapone (BIA 9-1067) and its active metabolite in human plasma, Analyst. 138: 8 (2013) 2463–2469.

[**635**] **GONÇALVES, D. ET AL.**, Development of a liquid chromatography assay for the determination of opicapone and BIA 9-1079 in rat matrices, Biomed. Chromatogr. 30: 3 (2016) 312–322.

[**636**] **WEISS, J.**, **HAEFELI, W.E.**, Evaluation of inhibitory potencies for compounds inhibiting P-glycoprotein but without maximum effects: f2 values, Drug Metab. Dispos. 34: 2 (2006) 203–207.

[**637**] **DUKES, J.D. ET AL.**, The MDCK variety pack: choosing the right strain, BMC Cell Biol. 12: 1 (2011) 1–4.

[**638**] **BALIMANE, P. V ET AL.**, Current industrial practices of assessing permeability and P-glycoprotein interaction, AAPS J. 8: 1 (2006) 1–13.

[**639**] **KRISHNA, G. ET AL.**, Permeability of lipophilic compounds in drug discovery using in-vitro human absorption model, Caco-2, Int. J. Pharm. 222: 1 (2001) 77–89.

[**640**] **TRAN, T.T. ET AL.**, Exact kinetic analysis of passive transport across a polarized confluent MDCK cell monolayer modeled as a single barrier, J. Pharm. Sci. 93: 8 (2004) 2108–2123.

[**641**] **PAVEK, P. ET AL.**, Human breast cancer resistance protein: interactions with steroid drugs, hormones, the dietary carcinogen 2-amino-1-methyl-6-phenylimidazo(4,5-b)pyridine, and transport of cimetidine, J. Pharmacol. Exp. Ther. 312: 1 (2005) 144–152.

[**642**] **URQUHART, B.L. ET AL.**, Breast cancer resistance protein (ABCG2) and drug disposition: intestinal expression, polymorphisms and sulfasalazine as an in vivo probe, Pharmacogenet Genomics. 18: 5 (2008) 439–448.

[**643**] **BICKER, J. ET AL.**, A new PAMPA model using an in-house brain lipid extract for screening the blood-brain barrier permeability of drug candidates, Int. J. Pharm. 501: 1–2 (2016) 102–111.

[**644**] **PARADA, A.**, **SOARES-DA-SILVA, P.**, BIA 3-202, a novel catechol-O-methyltransferase inhibitor, reduces the peripheral O-methylation of L-DOPA and enhances its availability to the brain, Pharmacology. 68: 1 (2003) 29–37.

[**645**] **WANG, C.**, **WILLIAMS, N.S.**, A mass balance approach for calculation of recovery and binding enables the use of ultrafiltration as a rapid method for measurement of plasma protein binding for even highly lipophilic compounds, J. Pharm. Biomed. Anal. 75: (2013) 112–117.

[**646**] **HAMMARLUND-UDENAES, M.**, Active-site concentrations of chemicals - are they a better predictor of effect than plasma/organ/tissue concentrations?, Basic Clin. Pharmacol. Toxicol. 106: 3 (2009) 215–220.

[**647**] **SUGANO, K. ET AL.**, Coexistence of passive and carrier-mediated processes in drug transport, Nat. Rev. Drug Discov. 9: 8 (2010) 597–614.

[**648**] **VIZSERÁLEK, G. ET AL.**, PAMPA study of the temperature effect on permeability, Eur. J. Pharm. Sci. 53: 1 (2014) 45–49.

[**649**] **KUSUHARA, H.**, **SUGIYAMA, Y.**, In vitro-in vivo extrapolation of transporter-mediated clearance in the liver and kidney, Drug Metab. Pharmacokinet. 24: 1 (2009) 37–52.

[**650**] **HOCHMAN, J.H. ET AL.**, Chapter 6. Establishment of P-glycoprotein structure-transport relationships to optimize CNS exposure in drug discovery, in: L. Di, E.H. Kerns (Eds.), Blood–Brain Barrier Drug Discov., John Wiley & Sons, Inc, 2015: pp. 113–124.

[**651**] **SRINIVASAN, B. ET AL.**, TEER measurement techniques for in vitro barrier model systems, J. Lab. Autom. 20: 2 (2015) 107–126.

[**652**] **AVDEEF, A. ET AL.**, Chapter 10. In vitro assays for assessing BBB permeability: artificial membrane and cell culture models, in: L. Di, E.H. Kerns (Eds.), Blood–Brain Barrier Drug Discov., John Wiley & Sons, Inc., 2015: pp. 188–237.

[**653**] **SOARES-DA-SILVA, P. ET AL.**, Catechol-O-methyltransferase inhibition in erythrocytes and liver by BIA 3-202 (1-[3,4-dibydroxy-5-nitrophenyl]-2-phenyl-ethanone), Pharmacol. Toxicol. 92: 6 (2003) 272–278.

[**654**] **FUNAKI, T. ET AL.**, The disposition of the tolcapone 3-O-methylated metabolite is affected by the route of administration, J. Pharm. Pharmacol. 46: 7 (1994) 571–574.

[**655**] **DIEHL, K.H. ET AL.**, A good practice guide to the administration of substances and removal of blood, including routes and volumes, J. Appl. Toxicol. 21: 1 (2001) 15–23.

[**656**] **STRICKLEY, R.G.**, Solubilizing excipients in oral and injectable formulations, Pharm. Res. 21: 2 (2004) 201–230.

[**657**] **MOTTU, F. ET AL.**, Organic solvents for pharmaceutical parenterals and embolic liquids: a review of toxicity data, PDA J. Pharm. Sci. Technol. 54: 6 (2000) 456–469.

[**658**] **LEE, Y.C. ET AL.**, An intravenous formulation decision tree for discovery compound formulation development, Int. J. Pharm. 253: 1–2 (2003) 111–119.

[**659**] **SMITH, Q.R.**, **SAMALA, R.**, Chapter 7. In situ and in vivo animal models, in: M. Hammarlund-Udenaes, E.C.M. de Lange, R.G. Thorne (Eds.), Drug Deliv. to Brain Physiol. Concepts, Methodol. Approaches, Springer-Verlag New York, 2014: pp. 199–211.

[**660**] **LONGHI, R. ET AL.**, Brain tissue binding of drugs: Evaluation and validation of solid supported porcine brain membrane vesicles (TRANSIL) as a novel high-throughput method, Drug Metab. Dispos. 39: 2 (2011) 312–321.

[**661**] **BOHNERT, T.**, **GAN, L.-S.**, Plasma protein binding: from discovery to development, J. Pharm. Sci. 102: 9 (2013) 2953–2994.

[**662**] **ILLAMOLA, S.M. ET AL.**, Determination of total and unbound concentrations of lopinavir in plasma using liquid chromatography-tandem mass spectrometry and ultrafiltration methods, J. Chromatogr. B. 965: (2014) 216–223.

[**663**] **THANABALASUNDARAM, G. ET AL.**, The impact of pericytes on the blood-brain barrier integrity depends critically on the pericyte differentiation stage, Int. J. Biochem. Cell Biol. 43: 9 (2011) 1284–1293.

[**664**] **BOBILYA, D.J.**, A model for transport studies of the blood–brain barrier, Methods Mol. Biol. 637: 1 (2010) 149–163.

[**665**] **NAKHLBAND, A.**, **OMIDI, Y.**, Barrier functionality of porcine and bovine brain capillary endothelial cells., Bioimpacts. 1: 3 (2011) 153–159.

[**666**] **JELIAZKOVA-MECHEVA, V. V.**, **BOBILYA, D.J.**, A porcine astrocyte/endothelial cell co-culture model of the blood-brain barrier, Brain Res. Protoc. 12: 2 (2003) 91–98.

[**667**] **SHAH, K.K. ET AL.**, In vitro models of the blood-brain barrier, Methods Mol. Biol. 814: (2012) 431–449.

[**668**] **CECCHELLI, R. ET AL.**, In vitro model for evaluating drug transport across the blood–brain barrier, Adv. Drug Deliv. Rev. 36: 2–3 (1999) 165–178.

[**669**] **HAMM, S. ET AL.**, Astrocyte mediated modulation of blood-brain barrier permeability does not correlate with a loss of tight junction proteins from the cellular contacts, Cell Tissue Res. 315: 2 (2004) 157–166.

[**670**] **VAN DER SANDT, I.C. ET AL.**, Assessment of active transport of HIV protease inhibitors in various cell lines and the in vitro blood-brain barrier, AIDS. 15: 4 (2001) 483–491.

[**671**] **DEHOUCK, M.P. ET AL.**, An easier, reproducible, and mass-production method to study the blood-brain barrier in vitro, J. Neurochem. 54: 5 (1990) 1798–1801.

[**672**] **DEHOUCK, M.P. ET AL.**, Drug transport to the brain: Comparison between in vitro and in vivo models of the blood-brain barrier, Eur. J. Pharm. Sci. 3: 6 (1995) 357–365.

[**673**] **XUE, Q. ET AL.**, A novel brain neurovascular unit model with neurons, astrocytes and microvascular endothelial cells of rat, Int. J. Biol. Sci. 9: 2 (2013) 174–189.

[**674**] **ABBOTT, N.J. ET AL.**, An improved in vitro blood-brain barrier model: rat brain endothelial cells co-cultured with astrocytes, Methods Mol. Biol. 814: (2012) 415–430.

[**675**] **XU, D.H. ET AL.**, Influence of P-glycoprotein on brucine transport at the in vitro blood-brain barrier, Eur. J. Pharmacol. 690: 1–3 (2012) 68–76.

[**676**] **HULTMAN, K. ET AL.**, Potentiating effect of endothelial cells on astrocytic plasminogen activator inhibitor type-1 gene expression in an in vitro model of the blood-brain barrier, Neuroscience. 166: 2 (2010) 408–415.

[**677**] **HANSSON, E. ET AL.**, μ-Opioid agonists inhibit the enhanced intracellular Ca2+ responses in inflammatory activated astrocytes co-cultured with brain endothelial cells, Neuroscience. 155: 4 (2008) 1237–1249.

[**678**] **SCHIERA, G. ET AL.**, Permeability properties of a three-cell type in vitro model of the blood-brain barrier, J. Cell. Mol. Med. 9: 2 (2005) 372–379.

[**679**] **HU, X. ET AL.**, In vitro study of the effects of angiostrongylus cantonensis larvae extracts on apoptosis and dysfunction in the blood-brain barrier (BBB), PLoS One. 7: 2 (2012) 1–7.

[**680**] **CIONI, C. ET AL.**, Expression of tight junction and drug efflux transporter proteins in an in vitro model of human blood-brain barrier, Front. Psychiatry. 3: 47 (2012) 1–8.

[**681**] **HATHERELL, K. ET AL.**, Development of a three-dimensional, all-human in vitro model of the blood-brain barrier using mono-, co-, and tri-cultivation Transwell models, J. Neurosci. Methods. 199: 2 (2011) 223–229.

[**682**] **CUCULLO, L. ET AL.**, Development of a humanized in vitro blood-brain barrier model to screen for brain penetration of antiepileptic drugs, Epilepsia. 48: 3 (2007) 505–516.

[**683**] **MEGARD, I. ET AL.**, A co-culture-based model of human blood – brain barrier: application to active transport of indinavir and in vivo – in vitro correlation, Brain Res. 927: (2002) 153–167.

[**684**] **FOOD AND DRUG ADMINISTRATION**, Guidance for industry: bioanalytical method validation, May (2001) 1–25.

[**685**] **EUROPEAN MEDICINES AGENCY**, Guideline on bioanalytical method validation: EMEA/CHMP/EWP/192217/2009 Rev.1 Corr.*, July (2011) 1–23.